Engineering of *Saccharomyces cerevisiae* for shikimate and malonyl-CoA pathway-derived precursor supply

Zur Erlangung des akademischen Grades eines

Dr.rer.nat

von der Fakultät Bio- und Chemieingenieurwesen
der Technischen Universität Dortmund
genehmigte Dissertation

vorgelegt von

M. Sc. Oliver Schiwy

aus

Emmerich am Rhein

Tag der mündlichen Prüfung: 20.06.2024

1. Gutachter: Prof. Dr. Dr. h. c. Oliver Kayser
2. Gutachter: Prof. Dr. Markus Nett

Dortmund 2024

Table of Content

Abstract

Many natural products are generated by polyketide and non-ribosomal peptide synthases (PKS and NRPS), which necessitates active acyl and peptide carry domains (ACP and PCP). This activation was enabled by the generation of two *Saccharomyces cerevisiae* CEN.PK2-1C variants (ST003 and ST004) harboring and functionally expressing a phosphopantetheinyl transferase (PPtase) $SFPp_{Bs}$ from *Bacillus subtilis*.

These strains serve as a foundation for further metabolic engineering approaches to enhance precursor provision. The glycolysis and malonyl-CoA pathway were successfully modified, leading to improved flux towards malonyl-CoA, as confirmed by a 3-hydroxypropionic acid (3-HP) detection method and subsequent NMR confirmation. Next, to implement the genes $acc1^{S659A,S686A,S1157A}$, *ald6, pdc1,* and $acs_{Se}{}^{L641P}$ for overexpression, the generated 3-HP titers were further improved by deleting *adh1* and implementing *tpi1*. Despite the encountered obstacles, the study successfully demonstrates the elevation of malonyl-CoA levels in yeast, yielding 3-HP titers of up to 249.66 mg L^{-1} in batch cultivations.

Using the initially generated PPtase strains as a basis, the genes for $ARO4p^{K229L}$, $ARO7p^{G141S}$, and $AroLp_{Ec}$, were integrated while simultaneously deleting *aro10* and *pdc5*. Making use of the tyrosine ammonia-lyase ($TALp_{Ha}$) enzyme from *Herpetosiphon aurantiacus* to generate p-coumaric acid (p-CA), the successful generated yeast strains demonstrated a modified shikimate pathway with elevated phenylalanine and tyrosine levels. Results revealed varying p-CA concentrations in different yeast strains, with ST004-based strains consistently outperforming ST003-based strains, resulting in p-CA concentration of up to 130.60 mg L^{-1} in batch cultivation. This highlighted, although successful, a notable discrepancy between the reported literature and this work, emphasizing the significant impact of cultivation conditions on yields for both pathways, as supported by existing literature.

Finally, malonyl-CoA pathway and shikimate pathway modifications were implemented in a single yeast strain (ST027), exhibiting initial 3-HP production with eventual p-CA production at slightly higher levels than compared to solely shikimate pathway-modified strain (ST008). This suggests a potential synergistic effect between both pathways, supporting increased tyrosine production. The present thesis resulted in the optimized strains with the necessity for cultivation optimization attempts, ultimately further increasing production titers of compounds harnessing precursors from both pathways, as for instance, cryptophycins, resveratrol, or maybe aromatic phytocanabinoids.

Zusammenfassung

Viele Naturstoffe werden durch Polyketid- und nicht-ribosomale Peptidsynthasen (PKS und NRPS) erzeugt, wofür aktive Acyl- und Peptidträgerdomänen (ACP und PCP) erforderlich sind. Um diese Aktivierung zu ermöglichen, wurden zwei Varianten von *Saccharomyces cerevisiae* CEN.PK2-1C (ST003 und ST004) erzeugt, die eine Phosphopantetheinyltransferase (PPtase) $SFPp_{Bs}$ aus *Bacillus subtilis* beherbergen und funktionell exprimieren.

Diese Stämme dienen als Grundlage für weitere metabolische Engineering-Ansätze, um die Bereitstellung von Vorstufen zu verbessern. Die Glykolyse und der Malonyl-CoA-Weg wurden erfolgreich modifiziert, was zu einem verbesserten Fluss in Richtung Malonyl-CoA führte, wie durch eine 3-Hydroxypropionsäure (3-HP)-Detektionsmethode und eine anschließende NMR-Messung bestätigt wurde. Um die Gene $acc1^{S659A,S686A,S1157A}$, *ald6, pdc1* und $acs_{Se}{}^{L641P}$ für eine Überexpression zu implementieren, wurden die erzeugten 3-HP-Titer durch Deletion von *adh1* und Implementierung von *tpi1* weiter verbessert. Trotz der aufgetretenen Hindernisse zeigt diese Arbeit erfolgreich die Erhöhung des Malonyl-CoA-Gehalts in Hefe, wobei 3-HP-Titer von bis zu 249.66 mg L-1 in Batch-Kulturen erzielt wurden.

Unter Verwendung der ursprünglich erzeugten PPtase-Stämme als Grundlage wurden die Gene für $ARO4p^{K229L}$, $ARO7p^{G141S}$ und $AroLp_{Ec}$ integriert und gleichzeitig *aro10* und *pdc5* deletiert. Unter Verwendung des Enzyms Tyrosin-Ammoniak-Lyase ($TALp_{Ha}$) aus *Herpetosiphon aurantiacus* zur Erzeugung von p-Cumarinsäure (p-CA) zeigten die erfolgreich erzeugten Hefestämme einen modifizierten Shikimat-Weg mit erhöhten Phenylalanin- und Tyrosinwerten. Die Ergebnisse zeigten unterschiedliche p-CA-Konzentrationen in den verschiedenen Hefestämmen, wobei ST004-basierte Stämme durchweg besser abschnitten als ST003-basierte Stämme, was zu einer p-CA-Konzentration von bis zu 130.60 mg L-1 in Batch-Kulturen führte. Damit wurde, obwohl erfolgreich, eine bemerkenswerte Diskrepanz zwischen der Literatur und dieser Arbeit hervorgehoben, die den signifikanten Einfluss der Kultivierungsbedingungen auf die Ausbeute für beide Stoffwechselwege unterstreicht, wie dies auch in der vorhandenen Literatur bestätigt wird.

Schließlich wurden diese Modifikationen in einen einzigen Hefestamm (ST027) implementiert, der eine anfängliche 3-HP-Produktion mit einer späteren p-CA-Produktion auf etwas höherem Niveau aufwies als die ausschließlich über den Shikimat-Weg modifizierten Stämme (ST008). Dies deutet auf einen potenziellen Synergieeffekt zwischen beiden Stoffwechselwegen hin, der eine erhöhte Tyrosinproduktion unterstützt. Die vorliegende Arbeit führte zu optimierten Stämmen mit der Notwendigkeit von Optimierungsversuchen bei der Kultivierung, um letztlich die Produktionstiter von Verbindungen zu erhöhen, die Vorstufen aus beiden Stoffwechselwegen nutzen, wie z. B. Cryptophycine, Resveratrol oder möglicherweise aromatische Phytocannabinoide.

.

Chapter I Introduction

1.1 Natural Products

The term natural product (NP) describes a molecule produced by a living organism and is found in nature. [1] NPs originate from bacteria, fungi, plants, and marine organisms and represent a large family of diverse molecules with a wide range of biological activities and are extensively used in medicine and agriculture. [1–4] The treatment of diseases has been a central part of human life since human existence, especially highlighted by the fact that the earliest record of humans using NP dates to around 2600 BC. Since then, traditional medicine has mainly relied on plant-derived substances like essential oils to treat colds and parasitic infections. [1]

The importance of NP is evident; a widely accepted perspective among scientists is, that NPs harbour a great potential for developing new pharmaceuticals. A recent review by Newmann and Cragg shows that 42 % of all new drugs till 2019 are NPs or NP derivatives. If NP mimics and synthetic compounds containing the active pharmacophore of NPs are also included, nearly two third of all approved drugs are based on NPs. [4] The approved drugs show activities against bacteria, fungi, viruses, parasites, cancer, and many more. [4–8]

Since living organisms produce a wide variety of molecules, they can be categorized into primary and secondary metabolites. While primary metabolites, like DNA, RNA, proteins, and sugars, are vital for live, secondary metabolites are not. Products from the primary metabolism are mostly excluded from the definition as NPs. They are produced as secondary metabolites by bacteria, fungi, and plants and come together with benefits for the host organism. Such compounds offer the host an advantage in its natural environment by promoting defence mechanisms, conferring anti-microbial properties, and facilitating communication with other organisms. [9–12]

NPs are a chemically diverse group of complex molecules with a wide range of molecular weights, stereo-specific centers, higher H-bond acceptors and donors, and higher rigidity than synthetic compounds. This complexity presumably shows their evolutionary optimized structures, which often serve a particular purpose in their host and are now exploited for their biological activity in medicine. [2,13]

In general, NPs can be classified into four substance classes, namely terpenoids, phenylpropanoids, alkaloids and polyketides. [14]

1.1.1 Terpenoids

Terpenoids, also called isoprenoids, are the most comprehensive class of NPs consisting of more than 40,000 to 60,000 known compounds (depending on which source) with differing functional groups. [14,15] The hydrocarbon skeleton of all terpenoids is generated from two universal C_5 building blocks, called isopentenyl diphosphate (IPP) and dimethylallyl diphosphate (DMAPP), whereby the resulting higher terpenes are classified into mono- (C_{10}), sesqui- (C_{15}), di- (C_{20}), tri-(C_{30}) and tetra-terpenes (C_{40}). Further, terpenoids are derived from terpenes by the addition of functional groups, usually with oxygen atoms forming oxygenated derivatives. [16,17]

In nature, IPP and DMAPP are synthesized from two separate, non-homologous pathways: The mevalonate pathway (MVA pathway) and the later discovered non-mevalonate pathway, also known as MEP pathway (2-C-methyl-d-erythritol-4-phosphate) or DXP pathway, named after the 1-deoxyxylulose-5-phosphate intermediate. [18,19] Many organisms produce IPP and DMAPP exclusively through one of the two pathways. Archaea, fungi, and eukaryotes employ the MVA pathway, while bacteria and algae utilize the MEP pathway. Plants are the only organisms capable of performing both pathways in separate compartments of their cells: the MVA pathway occurs in the cytoplasm, while the MEP pathway takes place in the plastids. [19–21]

The most famous terpenoid representatives are most likely the antimalaria drug artemisinin and the anti-cancer drug taxol, also known as paclitaxel (Figure 1). [6,8,14,22–24] Both molecules undergo biosynthesis through additional tailoring reactions from their respective precursors: baccatin III in the case of taxol and amorphadiene for artemisinin. However, these precursors are initially constructed through head-to-tail chain elongation of IPP and DMAPP creating geranylgeranyl diphosphate or farnesyl diphosphate, followed by cyclization reactions and the addition of functional groups. Significantly, the common starting point for biosynthesis across all terpenes traces back to the generation of IPP and DMAPP from glyceraldehyde-3-phosphate (G3P), pyruvate (Pyr), and acetyl-CoA. These initial compounds, sourced, for instance, from glycolysis and subsequent pathway steps, set the foundation for the exemplary biosynthetic pathways described above (Figure 1).

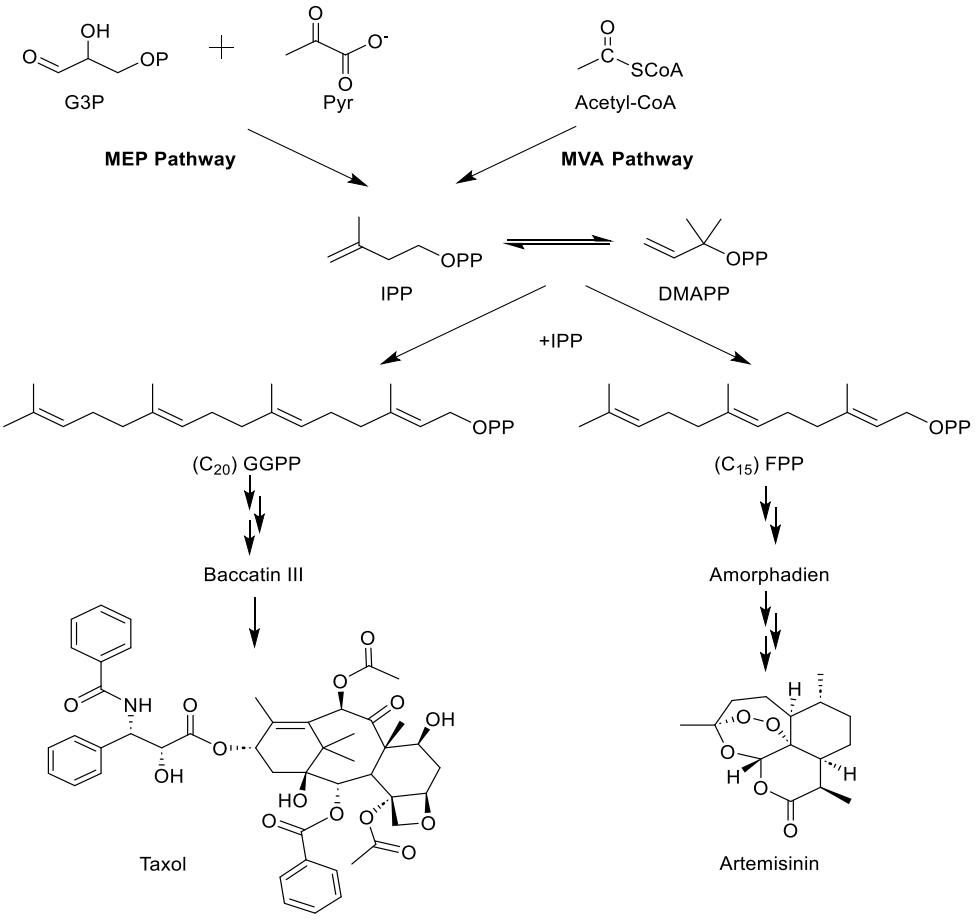

Figure 1: Most relevant isoprenoid biosynthesis steps for terpenoid biosynthesis on taxol and artemisinin. Isoprenoids are generated from the two major pathways, the MVA and MEP pathway. Both pathways produce IPP and DMAP, whereas the MEP pathway is started via condensation of glyceraldehyde-3-phosphate (G3P) and pyruvate (Pyr), while the MVA pathway is initiated via condensing three acetyl-CoA molecules. The terpene carbohydrate chain of the higher terpenes is generated by successive head-to-tail chain elongation reactions with IPP and DMAPP as starting molecules, to e.g., farnesyl diphosphate (FPP) and geranylgeranyl diphosphate (GGPP), both early intermediates of artemisinin and taxol. Subsequent biosynthetic steps lead via amorphadien to artemisinin and via baccatin III to taxol. [6,19,25]

1.1.2 Phenylpropanoids/Flavonoids and Alkaloids

Phenylpropanoids and alkaloids are among the more than 200,000 secondary metabolites identified and documented in plants. These compounds play various roles. They influece influencing growth, development, reproduction, defence mechanisms, and responses to environmental stimuli. [26–28] Derived from chorismate-derived aromatic compounds, phenylpropanoids and alkaloids share a common biosynthetic origin. While alkaloids include at least one nitrogen atom and extend beyond aromatic structures, their diverse structural nature complicates straightforward classification. Nevertheless, common classification strategies involve structurally related features and heterocyclic ring structures. Alternatively, some categorize them based on their origin, spectroscopic attributes, or biosynthetic pathways. [28,29] Alkaloids themselves can be categorized into four classes: amino acid derivatives (e.g., ornithine, lysine, anthranilic acid, tyrosine, and tryptophan), purine derivatives

(e.g., zanthine and caffeine), aminated terpenes (e.g., aconitine and solanine), and polyketides (e.g., coniine and the coccinellines). [30]

Chorismate is the end product of the shikimate pathway and acts as the primary metabolite for amino acid synthesis, acting as precursors for phenylpropanoids and alkaloids. As can be taken from Figure 2 aromatic amino acids – tyrosine (a precursor of isoquinoline alkaloids), phenylalanine (a precursor of phenylpropanoids), and tryptophan (a precursor of indole alkaloids) – are derived from the shikimate pathway and play vital roles as essential building blocks for proteins. [27,28,31] Pathways arising from the production of aromatic amino acids are present in bacteria, fungi, and plants but notably absent in many animals. Consequently, certain derivatives originating from aromatic amino acids become essential nutrients in human and animal diets. Furthermore, alkaloids and phenylpropanoids exhibit notable pharmacological and biological activities, making them particularly interesting for applications in pharmacology and nutrition. Prominent phenylpropanoids include flavonoids and stilbenes, such as resveratrol and naringenin, recognized for their antioxidant, antiallergic, antibacterial, anticancer, and hepatoprotective properties. [27,31–35] Similarly, well-known alkaloids encompass the anaesthetic morphine (derived from tyrosine), the anti-cancer drugs vincristine/vinblastine (derived from tryptophan), and nicotine (depicted in Figure 2). [29,30] Similarly to the previously shown terpene biosynthesis pathway (Chapter 1.1.1), phenylpropanoids and alkaloids originate from primary metabolic pathway, the glycolysis and pentose phosphate pathway. The combination of phosphoenolpyruvate (PEP) and D-erythrose-4-phophate (E4P) marks the start of the shikimate and subsequent aromatic amino acid pathway with their derivatives (Figure 2).

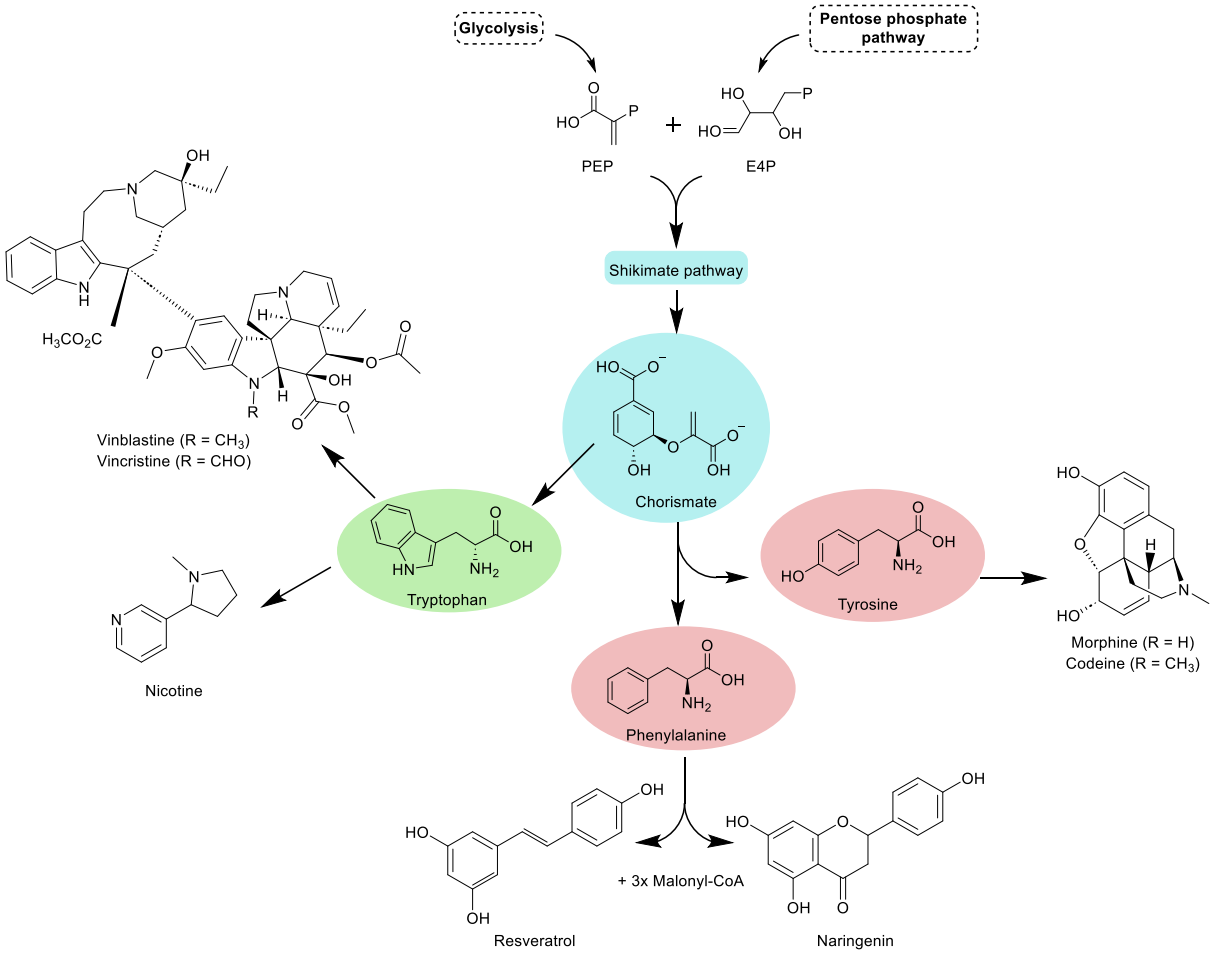

Figure 2: Phenylpropanoid biosynthesis overview, illustrated through examples such as resveratrol and naringenin, and the alkaloid biosynthesis overview, demonstrated with examples like vinblastine/vincristine, nicotine, and morphine/codeine. Phosphoenolpyruvate (PEP) and D-erythrose-4-phophate (E4P) are provided by the glycolysis and the pentose phosphate pathway, supplying educts for the shikimate pathway producing chorismate. Chorismate is converted to tyrosine, phenylalanine, and tryptophan as the origin for phenylpropanoids and alkaloids. Colors for tyrosine, phenylalanine, and tryptophan indicate that phenylalanine and tyrosine are formed from prephenate (not shown), unlike tryptophan. Resveratrol and naringenin are formed with additional three malonyl-CoA units. [28,29,31]

1.1.3 Polyketide

Polyketides, akin to alkaloids, represent a highly diverse class of natural products characterized by extensive structural variation, providing various functionalities. This structural diversity arises from reduction, aromatization, cyclization, and other tailoring reactions on a hydrocarbon skeleton predominantly synthesized from β-keto groups. The resulting compounds encompass polyenes, polyethers, macrolides, phenolic, and polycyclic aromatic substances. [36–38] The polyketide formation follows a process similar to fatty acid biosynthesis, involving consecutive Claisen condensation reactions of malonyl-CoA with acyl-thioester units, resulting in continuous chain elongation reactions. In each elongation step, the chain grows by approximately two carbon atoms, accompanied by the release of one CO_2 molecule due to decarboxylation. [39] This biosynthetic process is facilitated by polyketide synthases (PKS), which can be classified into three types based on their biosynthetic

mechanisms and structures. Type I PKSs are multifunctional complexes with multiple domains, further categorized into iterative complexes that reuse domains or modular complexes catalyzing chain elongation in different domains. Conversely, Type II PKSs consist of monofunctional enzymes operating in a repetitive manner, ultimately generating aromatic compounds after the final cyclization reaction. Both type I and type II PKS share three fundamental domains: the acyltransferase (AT), responsible for loading starter and extender acyl units; the acyl carrier protein (ACP), used as a docking station for the extender units and growing acyl chain; and lastly the ketosynthase (KS), catalyzing the condensation reaction of the starter/growing unit to the extender. The earlier mentioned diversity of the polyketides is then introduced through additional reducing domains like the β–keto reductase (KR), the dehydratase (DH), and the enol reductase (ER). [36,37] Type III PKS, on the other hand, are much smaller and less complex than type I and type II PKS but are the most widespread type of PKS. They consist of homodimeric ketosynthases, which use free coenzyme A for the thio-linkage of the substrates instead of ACP, used by type I and type II PKS. Another difference is the promiscuity towards the starter units because type III PKSs use aliphatic CoA units, like acetyl-CoA and malonyl-CoA, as well as aromatic CoA units, like coumaroyl-CoA. [38,39]

Analogous to the other NP classes, polyketides have bioactive properties like antibiotic, immunosuppressive, and anti-inflammatory, which make them attractive candidates for pharmacological applications in human medicine. [4] Examples of such pharmacological uses are the antibiotics tetracycline, rapamycin, which suppress the immune response and lovastatin, which lowers the cholesterol level. [2,40–43] The core backbone of this compounds is derived from intermediates originating from the glycolysis and downstream pathways, including the shikimate pathway and malonyl-CoA biosynthesis. Through a series of post-modification steps, the ultimate compounds – tetracycline, rapamycin, and lovastatin – are produced. Notably, malonyl-CoA serves as a precursor for all the illustrated bioactive polyketides (Figure 3).

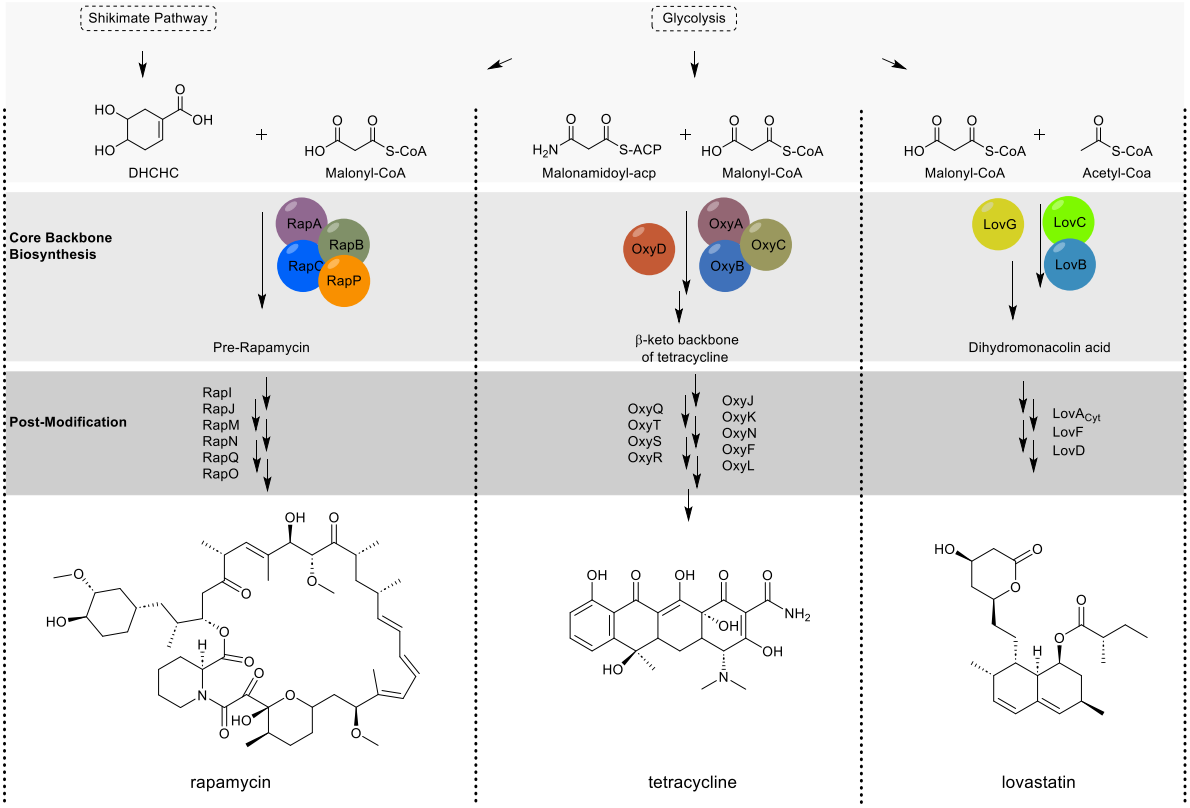

Figure 3: Brief overview of rapamycin (left), tetracycline (middle), and lovastatin (right) biosynthesis, the precursors that are involved, as well as the enzyme facilitating the reactions. Rapamycin: The core polyketide chain is formed by the type I modular PKS system of RapA, RapB, and RapC using 4,5-dihydrocyclohex-1-ene-carboxylic acid (DHCHC) as a starter unit, which is derived from chorismate by RapK (not shown). Pre-rapamycin is condensed with pipecolate through RapP and subsequent cyclization reaction (not shown). The genes *rapI, rapJ, rapM, rapN, rapQ*, and *rapO* encode for post-modification enzymes that produce rapamycin through O-methylation, hydroxylation, and oxidation. **Tetracycline:** The main β-keto backbone is iteratively formed through a condensation of 8 malonyl-CoA units with a malonamidoyl starter unit by the PKS enzymes OxyA, OxyB, OxyC, and OxyD. OxyD is an amidotransferase homolog that is responsible for the incorporation of malonamyl. Post-modification genes *oxyJ, oxyK, oxyN, oxyF, oxyL, oxyQ, oxyT, oxyS,* and *oxyR* successively built tetracycline through reduction, cyclization, methylation, hydroxylation, and amidation. **Lovastatin:** Lovastatin is synthesized via the intermediate dihydromonacolin acid from malonyl-CoA and acytyl-CoA by the enzymes LovB, LovC, and LovG. Successive post modifications via LovA$_{Cyt}$, LovF, and LovD generate Lovastatin by dehydration, hydroxylation, and the linkage of methylbutyryl-CoA (not shown). Source and modified according to [36,40–45].

As discussed above, natural products harbour great potential. They are of high interest to the pharmaceutical industry, especially due to their biological activities like anticancer, anti-viral, anti-inflammatory, anti-microbial, and properties as neuroprotective antioxidants or as nutraceuticals for diabetes treatment and also other industrial uses e.g. in biofuels.[1,3,19,46–49]

In our modern society, the demand for natural products is rising increasingly, especially with rising worries regarding global warming, the recent energy crisis involving fossil fuels and the uprising of many antibiotic-resistant microorganisms. [50] This high demand for NPs leads to a need for high quantities of NPs for such use cases, but in nature, NP occur in relatively low quantities in their native host organism. This is especially true in comparison with their respective primary metabolites. Therefore, the direct isolation is not environmentally friendly, sustainable, or economical. This can be impressively seen for taxol (paclitaxel) (Figure 1),

which was initially extracted from the bark of *Taxus brevifolia* (pacific yew). The yield of this extraction was only 0.01 % of the dry mass (approximately 300 mg/tree), meaning that up to four trees were needed to treat one patient, highlighting that the demand cannot be covered from natural sources. [8,51] An alternative is the chemical or combinatorial synthesis of NP, a critical approach to generating NPs. However, due to their complex structure, stereochemistry, and reliance on fossil resources, this is still very laborious, impractical, and not environmentally sustainable. [14] Therefore, another promising alternative is the metabolic engineering (Chapter 1.2) of different microbial organisms for the directed production of the compound of interest, ideally using renewable feedstock.

1.2 Metabolic engineering

Metabolic engineering developed to address the limitations of natural cellular processes for specific applications, particularly those of interest to humans. Natural metabolic pathways in cells are not inherently designed to produce compounds at levels suitable for industrial or therapeutic purposes. The traditional processes of cells may not yield desired products in the necessary quantities or with the desired characteristics. [52] Metabolic engineering emerged as a response to these challenges, aiming to optimize cellular metabolism for the efficient production of specific compounds. The field initially employed molecular biological methods and later incorporated analytical techniques and cloning methods. The ability to modify the genetic makeup of microorganisms has allowed scientists to enhance or expand natural metabolic pathways, creating new opportunities to produce valuable substances. One of the key milestones in the development of metabolic engineering was the successful transformation of *Escherichia coli* with a recombinant plasmid in 1973. [53,54] This achievement laid the foundation for future biotechnological processes and academic research, demonstrating the potential to modify organisms for specific purposes, including the insulin biosynthesis in *E. coli* or the complete biosynthesis of artemisinic acid in *Saccharomyces cerevisiae*. [6,7,55] As metabolic engineering progressed, advancements in genetic tools, analytical capabilities, and the understanding of metabolic networks allowed for more sophisticated and targeted modifications. According to Bailey, metabolic engineering utilizes the improvement of cellular activities through manipulating enzymes, the transport, and regulatory functions in cells with the help of recombinatorial DNA techniques. [52] The iterative process involves three steps: analysing metabolism and genetic functions, designing changes, and genetically modifying the organism. This cyclic approach ideally repeats itself until the yield or productivity is enhanced, with the ultimate goal of implementing new or improved industrial processes.

Nielsen categorized metabolic engineering into seven types: (1) heterologous protein production (e.g., pharmaceutical products: hormones, antibodies, vaccines), (2) diversification

of the substrate tolerance (including more efficient conversion of raw material and the prevention of by-product formation), (3) implementation of new pathways for the synthesis of new products or (4) the degradation of xenobiotics (extension of existing pathways with heterologous enzymes or even integrating new pathways), (5) process improvement through engineering of the cellular physiology (tolerance to low O_2 or high concentrations of glucose), (6) reduction or eliminating of by-product formation and (7) improvement of yield or productivity. [53] In summary, metabolic engineering is the enhancement or extension of a natural system, primarily aimed at producing a specific product from the cell's metabolism or of heterologous origin. Various strategies can be applied to modify the metabolism. This involves enhancing and expanding processes by increasing precursor and co-factor provision, eliminating competing pathways and bottlenecks, and overexpressing enzymes while enhancing their specificity (Figure 4). [56]

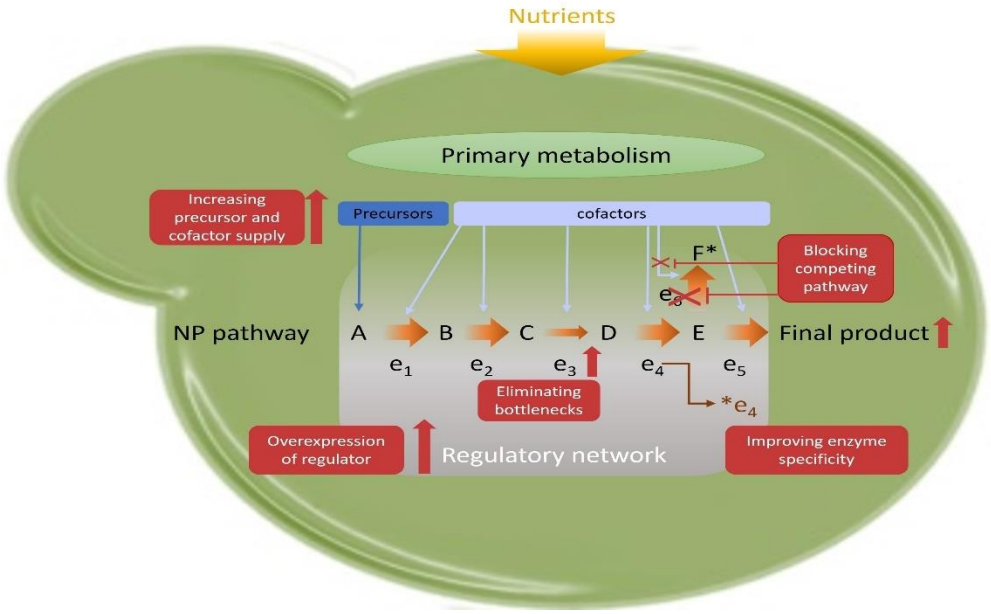

Figure 4: Generalised overview of various metabolic engineering strategies for final product production and titer improvements. Capital letters A-F represent the respective intermediates and e_1-e_6 represent the corresponding pathway enzymes. Modified according to Pickens et al., 2011 [56]

The advent of computer-based tools encompassing genomics, transcriptomics, proteomics, and other disciplines, collectively categorized as omics/multiomics, as well as genome mining (with and without integrated omics data), metabolic pathway design, genome-scale modelling (with and without integrated omics data), identification of overexpression and knockout targets, and enzyme engineering, empowers researchers to analyse, design, and predict metabolic networks and the implemented modifications. These in silico tools, coupled with advanced genetic techniques for host organism modifications – such as DNA assembly methods like BioBrick, Golden Gate, and Gibson assembly, alongside USER (Uracil specific excision reagent) cloning, chromosome and enzyme engineering methods (e.g., site-specific integration, MAGE - Multiplex automated genome engineering, CRISPR/Cas technologies),

and de novo enzyme design, biosensors, among others – alongside the continuously expanding data volumes, are poised to enhance metabolic engineering strategies and reduce the need for unnecessary trial-and-error experiments. [57] However, it is not only the tools for modification that matter; the intended target is equally crucial. *Escherichia coli* and *Saccharomyces cerevisiae* are the most widely utilized organisms for bio-based product production, benefiting from well-developed engineering tools. These organisms have been instrumental in advancing the understanding of metabolism and physiology in conjunction with the development of the aforementioned tools. [57]

1.3 *Saccharomyces cerevisiae* as a host organism

In addition to *E. coli, S. cerevisiae*, commonly known as baker's yeast, stands out as one of the most significant and extensively employed organisms in both industrial and academic settings. This is underscored by the milestone of transforming yeast cells as early as 1978. [58] The designation of *S. cerevisiae* as a GRAS (generally regarded as safe) organism, coupled with its capacity for high-density fermentation, robustness in harsh environmental conditions, high tolerance to inhibitory compounds, and ease of cultivation and genetic control, has increasingly made it an attractive choice for biotechnological applications. [59] The relative ease with which the cell can be manipulated and transformed with exogenous DNA through the extremely effective homologous recombination mechanism made it a go-to candidate for producing many valuable compounds and proteins naturally not occurring in yeast. Well-known examples, as mentioned before (Chapter 1.1.1,Chapter 1.1.2 and Chapter 1.2) are insulin [55], a precursor of the anti-malaria drug artemisinin, artemisinic acid [6], and resveratrol [35]. Other noteworthy compounds of significance, particularly in the context of the ongoing legalization discussion, are cannabinoids. [60,61] The growing interest in yeast as a versatile platform for bioproduction is the outcome of numerous techniques developed over the years, often aligned with the production of heterologous compounds. Genomic engineering of baker's yeast has been facilitated by reliable chromosomal alteration techniques like long terminal repeat cloning [62,63] and CRISPR/Cas9 [64,65], utilizing homologous recombination for straightforward modification. The continuously expanding "toolbox" for DNA assembly and protein expression in yeast, [63,66–68] based on methods like USER [69], Golden gate [70], and Gibson [71], enables the addition of new "parts" for customizable and rapid pathway modifications. These advancements position *S. cerevisiae* as a perfect chassis for NP production, where biosynthesis genes can be introduced via genetic information and the NPs can be assembled based on already present, high titers of precursor molecules needed for their *in vivo* production.

Over the years, yeast was engineered to produce various secondary metabolites based on different pathways. [72–76] To capitalize on the collective expertise in yeast engineering,

the next step in yeast cell factory utilization involves combining those engineering efforts and creating a yeast platform strain that provides precursor molecules at sufficient levels.

The following chapters will focus on the glycolysis, the glycolysis-derived compounds malonyl- and acetyl-CoA and the shikimate pathway.

1.4 Glycolysis and Malonyl-CoA

Glycolysis is the universal metabolic pathway in nearly all living cells and was already completely enlightened in 1940. It is often termed as Embden-Meyerhof-Parnas pathway in honor of its initial discoverers, who significantly participated in clarifying the pathway. Glucose, as a central energy source, is oxidized while passing through the pathway, generating the building blocks for subsequent anabolic metabolites and the energy needed for cellular processes, hence its position as the essential organic fuel for microbes, animals, and plants.

The glycolysis forms two pyruvate molecules from only one molecule of glucose, yielding a total net of two adenosine triphosphate (ATP) and two reduced nicotinamide adenine dinucleotide (NADH) molecules as energy (Figure 5). [77,78]

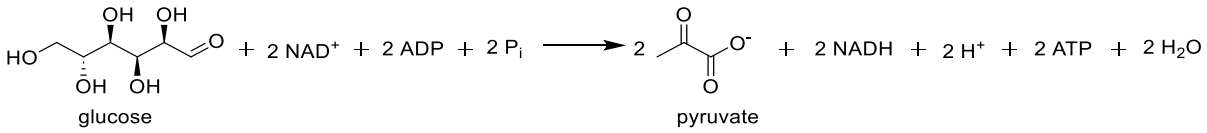

Figure 5: Net glycolysis reaction for the formation of two pyruvate molecules from glucose. NAD: nicotinamide adenine dinucleotide, ADP: adenosine diphosphate, P_i: phosphate, NADH: reduced nicotinamide adenine dinucleotide, H^+: proton, ATP: adenosine triphosphate, H_2O: water.

The glycolysis from glucose to pyruvate consists of a series of ten sequential enzymatic reactions (Figure 6). From this sequence, intermediates divert into the glycogenesis, pentose phosphate pathway, and shikimate pathway; there are also three irreversible reaction steps along the pyruvate formation path. Since this work will primarily focus on *S. cerevisiae* or yeast, the following description will concentrate on the enzymes involved in the yeast glycolysis. As mentioned before, there are ten reaction steps to form pyruvate, and eight are facilitated via paralogs. [79]

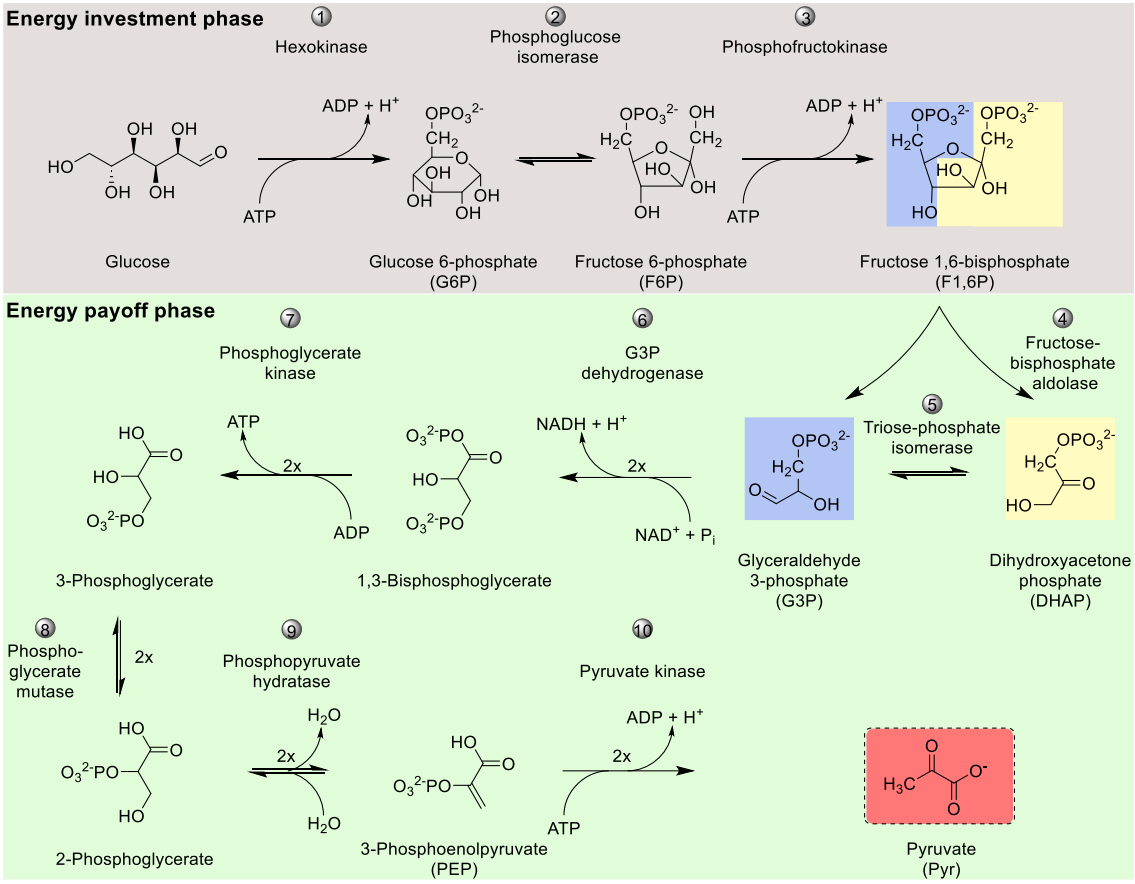

Figure 6: Overview over the ten enzymatic reaction steps of the glycolysis starting from glucose, yielding pyruvate. The energy investment phase is highlighted in grey, while the energy payoff phase is colored in green. The split of F1,6P is underlined through the colors blue for G3P as the product and yellow for DHAP. Pyruvate, the final product of the glycolysis, is highlighted separately in red.

In the initial step, a hexokinase transfers a phosphate group (P_i) from ATP to the C-6 position of the glucose molecule, resulting in the formation of glucose-6-phosphate (G6P). In yeast, this reaction is carried out by enzymes coded by *hkx1* and *hkx2*. [80] Subsequently, in the next two steps, G6P is converted to fructose-6-phosphate (F6P) and, with an additional phosphate from ATP, to fructose-1,6-phosphate (F1,6P), facilitated by G6P isomerase encoded by *pgi1* and phosphofructokinases encoded by *pfk1* and *pfk2*. [81,82] Following these steps, the double-phosphorylated hexose sugar undergoes cleavage into two triose sugars, dihydroxyacetone phosphate (DHAP) and glyceraldehyde 3-phosphate (G3P), catalyzed by the enzyme fructose-bisphosphate aldolase (*fba1* in yeast). [81–83] It is noteworthy that DHAP cannot further participate in glycolysis unless it is converted to G3P, a reaction facilitated by triose-phosphate-isomerase (*tpi1).* [81,84] This phase can be considered as an energy investment phase, activating the sugar through the transfer of P_i from two invested ATPs. From this point onward, the reactions generate valuable energy. The two resulting G3Ps, in turn, undergo a series of phosphorylation (glyceraldehyde-3-phosphate dehydrogenase coded by *tdh1-3*), transfer (phosphoglycerate kinase coded by *pgk1*), mutase (2,3-bisphosphoglycerate-dependent phosphoglycerate mutase coded by *gpm1-3*) and hydratase (phosphopyruvate hydratase coded by *eno1-2*) reactions to yield phosphoenolpyruvate (PEP), accompanied by

inorganic phosphate and NAD^+ generating two NADH and two ATP. The intermediates follow the order of 1,3-bisphosphoglycerate, 3-phosphoglycerate, 2-phosphoglycerate, and PEP. The final enzymatic step in the glycolysis is the formation of two pyruvate molecules from PEP, accomplished by the pyruvate kinase (*pyk2* and *cdc19*). [81,82,85–88] Pyruvate, as the product of the glycolysis, now acts as an intermediate for several different reactions. The above-described glycolysis is depicted in Figure 6.

The glycolysis can occur either aerobically or anaerobically. Under aerobic conditions, pyruvate is formed, while under anaerobic conditions, such as in muscle cells, lactate is produced through lactic acid fermentation. Until pyruvate is formed, the pathway operates without requiring oxygen. [77,78] When considering yeast as a potential production strain under anaerobic conditions, cells generate ethanol through alcoholic fermentation. [81,82] Upon pyruvate formation under aerobic conditions, it is transferred to the mitochondria and undergoes complete oxidation in the citric acid cycle yielding CO_2 and significantly more energy than from glycolysis alone. Lactate, formed in the absence of oxygen in the cytosol, is produced through lactate dehydrogenase (muscle cells). [89] Despite yeast's ability to metabolize glucose in the presence of oxygen, it exhibits a preference for alcoholic fermentation. This preference persists even when aerobic metabolism is viable. However, in the presence of excess glucose, cells shift to the fermentation reaction, producing ethanol (unlike lactate in muscle cells) through two additional enzymatic steps. This phenomenon is known as the Crabtree effect. [82,90]

In conditions of low oxygen or high glucose concentrations, yeast transforms pyruvate into ethanol. This process unfolds in the cytosol, where pyruvate undergoes decarboxylation to produce acetaldehyde through the enzyme pyruvate decarboxylase (*pdc1, 5,* and *6*), releasing CO_2 for each pyruvate molecule. [91,92] The final step in ethanol formation has a drawback: the reversible reaction catalyzed by the alcohol dehydrogenase (*adh1-5*) converts acetaldehyde to ethanol, but each reduction to ethanol consumes one NADH energy equivalent. Consequently, the glycolysis only produces two ATP in total. *S. cerevisiae* compensates for this low energy yield through a high flux, processing 20-25 mmol ethanol per gram dry weight per hour. [79,92] Once all glucose is depleted, yeast cells can shift their metabolism to consume ethanol, regaining the invested energy and producing acetaldehyde. Acetaldehyde, derived either from ethanol or directly from pyruvate, can then be further converted to acetate using the aldehyde dehydrogenase again (*ald2-6*) generating one NADH or NADPH. Acetate now is the precursor to one of the key metabolites in the metabolic network of yeast, acetyl-CoA produced by acetyl-CoA synthase (*acs1,2*). This process involves combining acetate and coenzyme A while consuming one ATP. Acetyl-CoA is present in at least four cellular compartments, the cytosol, in mitochondria, the peroxisome and nucleus (Figure 7). [92]

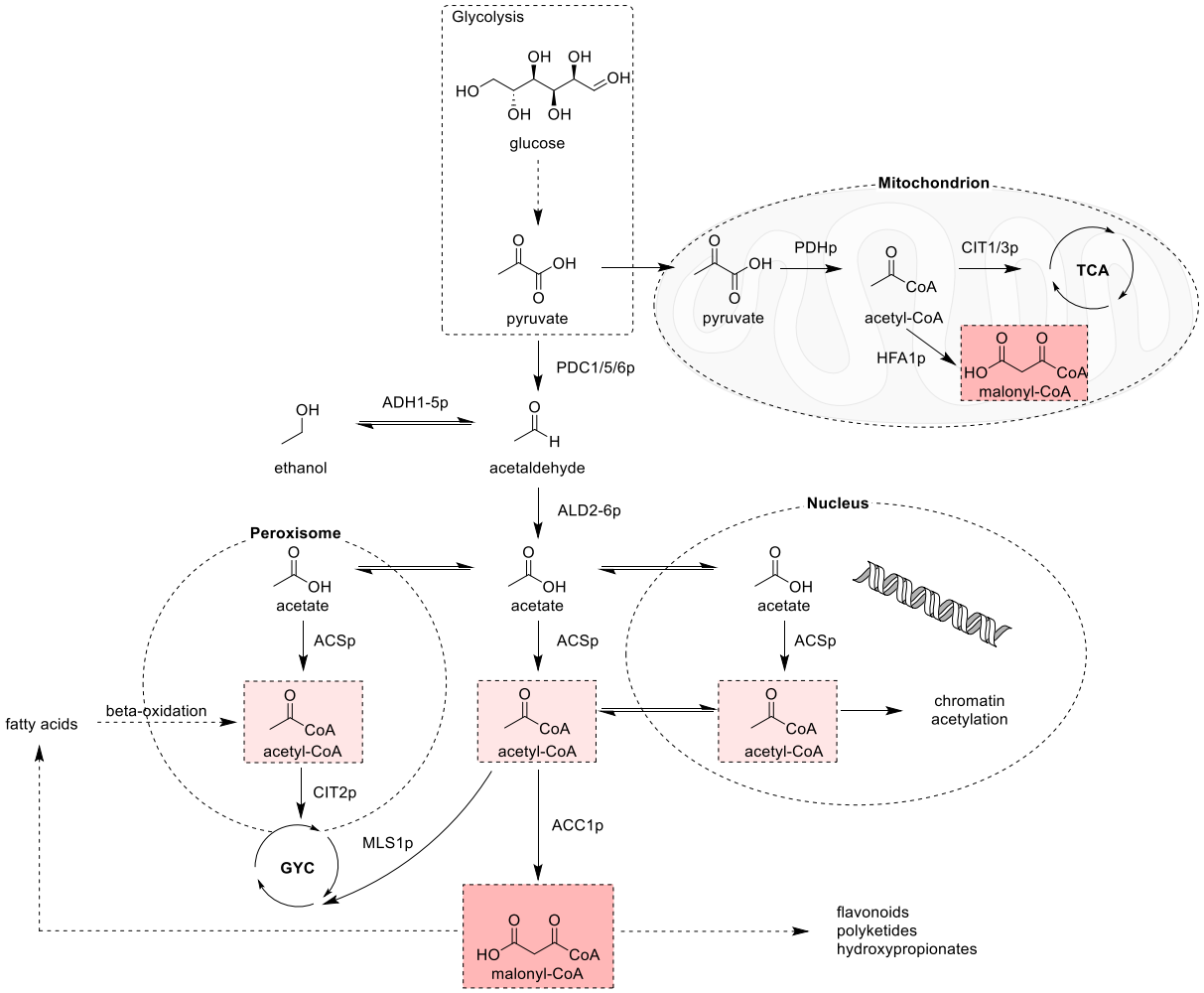

Figure 7: Acetyl- and Malonyl-CoA pathway with the different compartments involved. The key intermediates Acetyl-CoA and Malonyl-CoA are highlighted in red. TCA: tricarboxylic acid cycle, GYC: glyoxylate cycle, PDHp: pyruvate dehydrogenase complex, PDC1/5/6p: pyruvate decarboxylase, ADH1-5p: alcohol dehydrogenase, ALD2-6p: aldehyde dehydrogenase, ACSp: acetyl-CoA synthase, ACC1p: acetyl-CoA carboxylase, HFA1p: mitochondrial acetyl-coenzyme A carboxylase, CIT1/2/3p: citrate synthase, MLS1p: malate synthase. Modified according to [92].

As mentioned earlier, glycolysis serves as the central metabolic pathway, with various intermediates branching off toward different pathways responsible for amino acid and fatty acid synthesis. Cytosolic Acetyl-CoA, generated from acetate is the main precursor and building block of fatty acids biosynthesis. [93,94] Despite its presence in various compartments, the transport of acetyl-CoA between these compartments is not possible. [95] Acetyl-CoA is formed from acetate with the assistance of the acetyl-CoA synthase, which operates in the cytosol, peroxisome, and nucleus. In the nucleus, acetyl-CoA is utilized for chromatin acetylation, while in the peroxisome, it contributes to the glyoxylate cycle (GYC) as a substrate. The addition of acetyl-CoA to the GYC also occurs through the β-oxidation of fatty acids in the peroxisome. The transfer to the GYC is enabled by the citrate synthase (*cit2*) in conjunction with oxaloacetate. [92,96] Furthermore, the condensation reaction of acetyl-CoA with glyoxylate catalyzed by the malate synthase (*mls1*) also directs acetyl-CoA into the GYC. This cycle shares many identical steps with the tricarboxylic acid (TCA) cycle. While the majority of acetyl-CoA inside the mitochondria enters the TCA cycle, before that however, pyruvate is

transferred to the mitochondria and is converted into acetyl-CoA, CO_2, and NADH by the pyruvate dehydrogenase complex (*pdh*), one of the largest and most complex enzymes. The PDHp consists of a pyruvate dehydrogenase (PDA1 and PDB1), a dihydrolipoamide acetyltransferase (LAT1), a dihydrolipoamide dehydrogenase (LPD1), and a pyruvate dehydrogenase complex component X (PDX1). Subsequently, acetyl-CoA enters the TCA cycle, similar to the GYC, condensed with oxaloacetate as citric acid, catalyzed via the citric acid synthase encoded by *cit1* and *cit3*. [92,94,97,98]

Apart from acetyl-CoA as a key intermediate, malonyl-CoA is another valuable intermediate directly derived from acetyl-CoA. It is the cytosol-based precursor to the fatty acid biosynthesis, marking the first step in this anabolic pathway. This first reaction occurs under the acetyl-CoA carboxylase's catalysis (*acc1* or *fas3*). [92,99] However, this also highlights the rate-limiting step, and its expression is controlled by factors like Ino2p and Ino4p, as well as Opi1p and Snf1p. [92,100–102] Another isoform of the ACC1p is mainly found in mitochondria and encoded by *hfa1*. [92,103] As discussed in the previous chapters (Chapters 1.1.2 and Chapter 1.1.3), malonyl-CoA is not only a precursor for fatty acid synthesis but also serves as a starting point for the production of various valuable compounds, including flavonoids, polyketides, and hydroxypropionates. [102,104,105]

1.4.1 Malonyl-CoA and strategies for its increase

In the Chapters 1.2 and 1.3, the importance of *S. cerevisiae* in metabolic engineering efforts and in general as a host organism to produce valuable chemicals through different modification strategies was illustrated. As for this work, this chapter will focus on modifications already used in the literature to increase titers of malonyl-CoA and, as a direct precursor, of acetyl-CoA in *S. cerevisiae*.

Many studies investigated the metabolic pathway manipulation to increase the key intermediate malonyl-CoA, as it serves as the precursor molecule for various high-value compounds. Among these products are 3-hydroxypropionic acid (3-HP) [76,101,106–110], products derived from fatty acids (free fatty acids [93,111–113], fatty alcohols [114], fatty acid ethyl esters [101,115]), and plant derived flavonoids naringenin [116], kaempferol [117], and resveratrol [35,118]).

Malonyl-CoA is a derivative of malonic acid, covalently linked to coenzyme A through a thioester bond (Figure 7). The direct formation of malonyl-CoA from acetyl-CoA occurs in an ATP-dependent carboxylation reaction. This reaction is catalyzed by acetyl-CoA carboxylase ACC1p in the cytosol and by HFA1p in mitochondria (Chapter 1.4). The ACC1p is responsible for the initial reaction in the fatty acid biosynthesis and represents the rate-limiting step. [93] However, when enhancing malonyl-CoA production, it is important to note that its

concentration is kept at low levels during growth, making it challenging to improve the production of derived product. [106] To address this, it's crucial to consider the biotin-dependent carboxylase ACC1p, as its activity relies heavily on biotinylation, biotin concentration, and transcriptional regulation through Ino2p and Ino4p (positive regulators) and Opi1p (a negative regulator). [119,120] Additionally, posttranscriptional modifications, a pivotal aspect of signal transduction and gene regulation, are responsible for ACC1p regulation. By this means, the phosphorylation via the protein kinase SNF1p is essential. [101,121,122]

One strategy is overexpressing the native endogenous ACC1p with strong promotors or a heterologous carboxylase (ACC from *Lipomyces starkeyi*). However, the results suggested that simple overexpression of native and heterologous ACC1p did not significantly increase the production of malonyl-CoA-derived products. [93,101,123,124] In addition, results suggest that the overexpression causes impaired growth in yeast (up to one-third reduction in final OD_{600}). [117,124] Since ACC1p undergoes regulation by SNF1p through phosphorylation, studies investigating the deregulation of ACC1p for the enhanced production of malonyl-CoA-dependent products and revealed that mutations at phosphorylation sites Ser1157 and Ser659 alleviate SNF1p regulation of ACC1p. [101,122,124] These two mutations in ACC1p were subsequently employed in numerous studies focused on converting acetyl-CoA to malonyl-CoA. For instance, the double ACC1p mutant increased the production of fatty acids 3-fold (15.8 mg/L) and of 3-HP 6-fold (279 mg/L). [101] Combining these mutations with further modifications resulted in an increased production of various target compounds, including fatty acid-derived products, resveratrol (+30%), and 3-HP. [35,76,109,118,125] A study from Chen and coworkers using a malonyl-CoA sensitive biosensor confirmed the ACC1p deregulation with the introduction of the widely used S1157A and S659A mutations and identified an additional phosphorylation site, Ser686, that further increased ACC1 activity by approximately 15-20 % when tested for 3-HP production. [126] Moreover, Li and coworkers, during the development of the malonyl-CoA sensitive biosensor, discovered an additional enhancement in product titer by overexpressing TPIp, resulting in a 120% increase in 3-HP titers. [127]

Over the years, various strategies employing different combinations of up- or downstream pathway modifications leading to cytosolic malonyl-CoA have emerged in numerous studies. The primary focus of this route often revolves around ACC1p, with additional flux-directing actions. One such strategy is commonly referred to as the pyruvate dehydrogenase bypass. It starts with the pyruvate decarboxylase PDC1p and proceeds with the aldehyde dehydrogenase ALD6p and a heterologous acetyl-CoA synthase from *Salmonella enterica* ACS_{Se}p (Figure 8). [128,129] The goal is to direct the carbon flux from acetaldehyde towards acetate and the ACS_{Se}p due to the low Michaelis-Menten constant K_m of the aldehyde dehydrogenase (*ald6*) for acetaldehyde compared to the alcohol dehydrogenase (*adh1-5*). [130] The ADHp has a 2-fold higher K_m-value for acetaldehyde than

ALD6, meaning that by introducing the modifications pulling the carbon flux from the consistently highly expressed PDCp (pyruvate decarboxylase) and direct it to malonyl-CoA, the flux to ethanol through the ADHp (alcohol dehydrogenase) is decreased. [94,128,130] The introduction of the post-translationally deregulated acetyl-CoA synthase from *S. enterica* (acs_{se}), where the substitution of proline at position 641 for leucine prevents the inactivating acetylation and maintains its activity, further concentrates the flux for acetyl-CoA formation. [128,131] Some studies have employed this or parts of this upstream flux-pulling modification strategy with additional overexpressions or deletions. The study by de Jong and coworkers used the overexpression of the genes *adh2, ald6,* acs_{se}^{L641P}*,* $acc1^{S1157A,S659A}$ together with deletions impairing storage lipid formation and β-oxidation yielding 4.4 mg/L fatty acid ethyl esters. [125] With multicopy integration of $ACC1^{S1157A,S659A}$, and an increased NADPH supply, Kildegaard and coworker were able to create a strain producing up to 9.8 g/L 3-HP in carbon-limited fed-batch cultivation at pH 5. [76] Shiba and coworkers produced up to 120 mg/L of amorphadiene, while Duan and coworkers could produce up to 66.29 mg/L of kaempferol employing this strategy. [117,128] Other studies using acetyl-CoA as the key intermediate also employed this strategy successfully producing ethyl acetate, polyhydroxybutyrate, n-butanol, while adding different additional modifications like impairing or inactivating glycerol (deleting *gpd1* and *gpd2*) and ethanol (deleting *adh* genes) production as well as reducing the drainage of acetyl-CoA through the GYC (deleting *mls1* and *cit2*). [132–135] This enhances the availability of cytosolic acetyl-CoA.

Further exploration of the literature reveals more strategies to increase cytosolic acetyl-CoA, such as recovering acetyl-CoA after its conversion to other intermediates or redirecting the carbon flux through other pathways, like the pentose phosphate pathway (PPP) towards increased acetyl-CoA supply. Utilizing an elevated flux through the PPP, Yu and coworker employed the overexpression of the genes *zwf1* (glucose-6-phosphate dehydrogenase)*, gnd1* (phosphogluconate dehydrogenase)*, tkl1* (transketolase)*, tal1* (transaldolase) and the down-regulation of *pgi1* (phosphoglucose isomerase) to increase NADPH energy supply and yield an improved free fatty acid production of 28 %. [136] A similar strategy, but with the addition of the xylulose-5-phosphate specific phosphoketolase (xPKp, from *Leuconostoc mesenteroides*) and phosphotransacetylase (PTAp, from *C. kluyveri*) directly produced acetyl-CoA from the PPP with the benefit of the increased energy yield and without carbon loss. With that strategy, Qin and coworkers were able to yield a 41.9 % higher 3-HP and reduced glycerol production. [109] An earlier comparable approach led to an 1.7-fold increase in free fatty acid production. [115] Lian and coworkers investigated the actetyl-CoA recovery from citrate using the ATP-dependent citrate lyase (ACLp) from the oleaginous yeast *Yarrow lipolytica* and increased the n-butanol production 3-fold. [134] However, Rodriguez and coworkers demonstrated that the ACLp from *Aspergillus nidulans* performed approximately one order of

magnitude better than that of *Y. lipolytica*. [137] Furthermore, an interesting strategy to prevent ATP loss and acetate build-up was shown by bypassing the native cytosolic ALD-ACS pathway by introducing a heterologous acetylating acetaldehyde dehydrogenase (A-ALDp). By implementing this approach, Kozak and co-workers could show the successful substitution of the ALD-ACS pathway, deleting only one gene (*ald6, acs*) or both *ald6* and *acs*. However, they observed reduced growth in the modified strains, attributing it to the accumulation of toxic acetaldehyde within the cells. [138,139] Applying a comparable method involved introducing a modified multifunctional oxidoreductase, *adhE,* from *E. coli*, now serving as an A-ALD (*adhE*$^{A267T/E568K/R577S}$) together with the deletion of *ald6* led to an n-butanol titer of around 633.92 mg/L. However, this worked best when combined with increased coenzyme A supply through additional modification of the native CoA pathway. [140]

A summary of the mentioned modifications and their position in the pathways can be found in Figure 8.

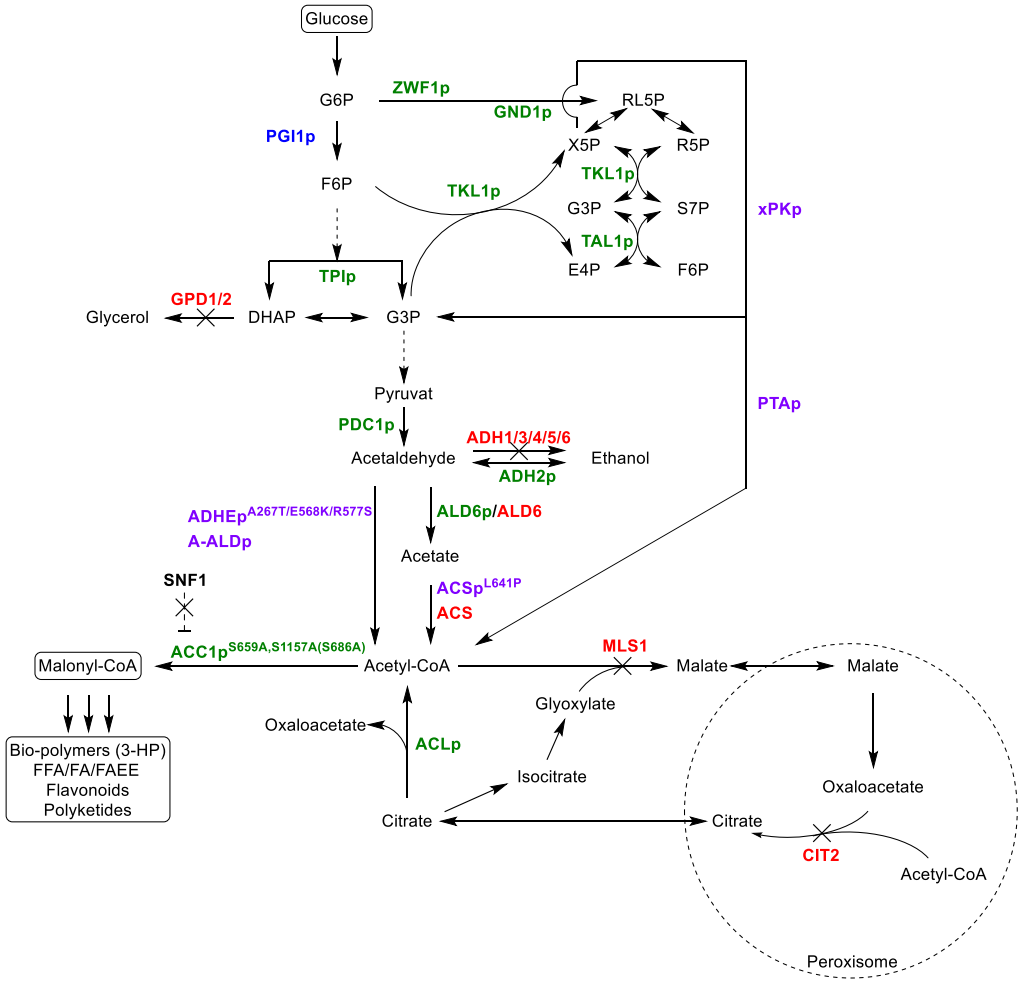

Figure 8: Summary of common metabolic modifications increasing malonyl-CoA and acetyl-CoA provision for subsequent 3-HP, fatty acid-derived products (FFA/FA/FAEE), flavonoid, and polyketide production used in literature. Enzymes used for endogenous overexpression are shown in green, heterologous overexpressions in purple, deleted genes in red, and downregulated enzymes in blue. G6P: glucose-6-phosphate, F6P; fructose-6phosphate, G3P: glyceraldehydes-3-phosphate, DHAP: dihydroxyacetone phosphate, RL5P: ribulose-5-phosphate, X5P: xylulose-5-phosphate, R5P: ribose-5-phosphate, S7P: sedoheptulose-7-phosphate, E4P: erythrose-4-phosphate, FFA: free fatty acids, FA: fatty alcohols, FAEE: fatty acid ethyl ester.

Upon revisiting yeast metabolism, it becomes evident that crucial metabolites for the production of heterologous compounds go beyond malonyl-CoA or acetyl-CoA. As highlighted in Chapters 1.1.2 and 1.1.3, NPs such as resveratrol, naringenin, and rapamycin (Figure 2 and Figure 3) also need compounds derived from other pathways for their generation, including the shikimate pathway and the subsequent aromatic amino acid biosynthesis.

1.5 Shikimate Pathway

The shikimate pathway is a seven-enzyme catalyzed pathway with chorismate as the final product, also representing the pivotal common intermediate for the three aromatic amino acids (AAA): tyrosine, phenylalanine, and tryptophan. In this central anabolic metabolism, the AAAs are synthesized through the condensation of PEP and erythrose-4-phosphate (E4P) derived from the glycolysis and the pentose phosphate pathway, respectively. Notably, the shikimate pathway is exclusive to plants and microorganisms. [72,141,142] Animals rely on obtaining AAAs from their diet due to their inability to *de novo* synthesize them, despite their capacity to convert phenylalanine and tyrosine through hydroxylation. [142,143]

The initial reaction for the shikimate pathway is catalyzed by the 3-deoxy-d-arabino-heptulosonate-7-phosphate (DAHP) synthase. This reaction involves the combination of PEP and E4P to produce DAHP, and in yeast, it is carried out by two isoenzymes encoded by *aro3* and *aro4*. Both enzymes are subject to feedback regulation by tyrosine (ARO4p) and phenylalanine (ARO3p). [141,144,145] Subsequently, a single large pentafunctional enzyme encoded by the *aro1* gene facilitates the next five crucial steps in the pathway. This enzyme oversees the successive transformations of DAHP into 3-dehydroquinic acid (DHQ), 3-dehydroshikimate (DHS), shikimate, and shikimate-3-phosphate, combining the DHQ synthase, DHQ dehydratase, shikimate dehydrogenase, and shikimate kinase activities within one single enzyme, consuming NADPH and ATP along the way. The final ARO1p catalyzed reaction involves the condensation of shikimate-3-phosphate with an additional PEP molecule, resulting in the formation of 3-enolpyruvyl-shikimate 5-phosphate (EPSP) through EPSP synthase activity. The pathway culminates in chorismate as the ultimate product facilitated through the chorismate synthase, encoded by the *aro2* gene. This last enzymatic step removes a phosphate group, introducing a double bound to EPSP, yielding chorismate (Figure 9). [141,142,146]

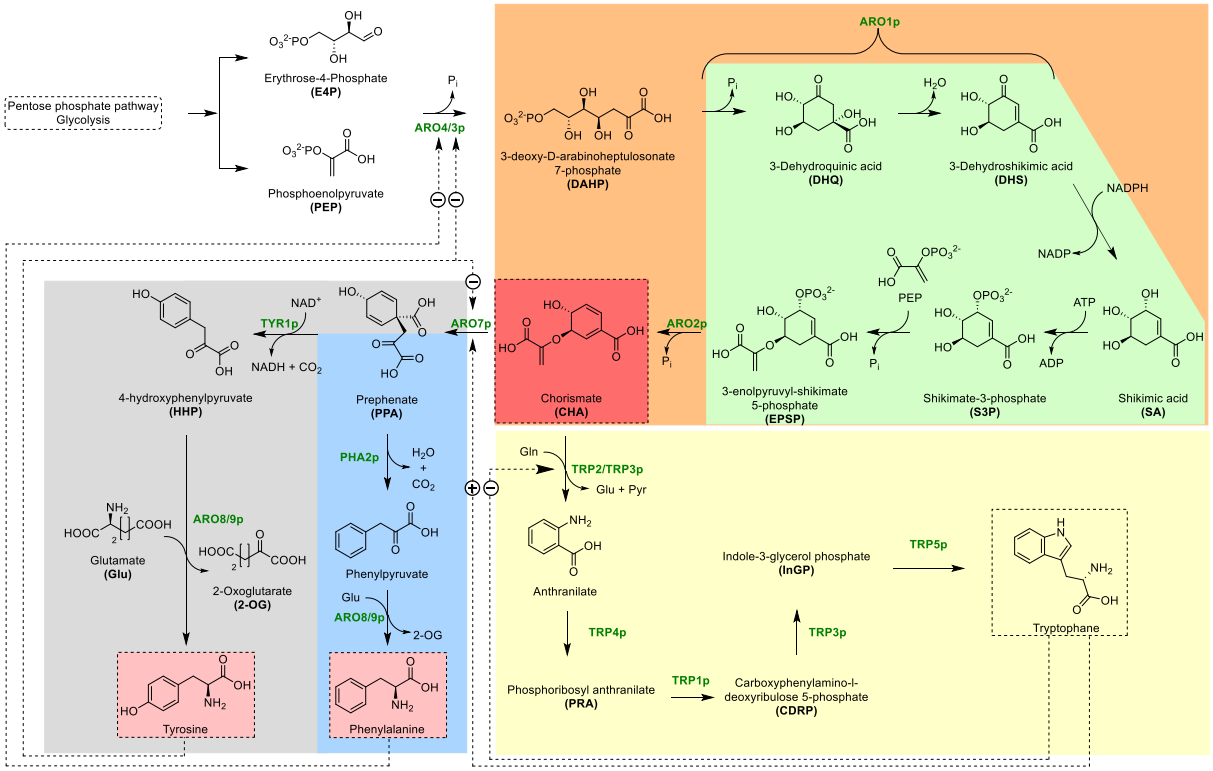

Figure 9: Overview of the shikimate pathway yielding chorismate and the AAA biosynthesis of tyrosine, phenylalanine, and tryptophan. The shikimate pathway is highlighted in orange, with the five ARO1p-catalyzed reactions in green. The tyrosine and phenylalanine branches are colored grey and blue, respectively. The tryptophan branch is highlighted in yellow. Chorismate as the central intermediate and final product of the shikimate pathway, and the relevant amino acids phenylalanine and tyrosine are shown in red. Dashed lines indicate regulatory actions of the biosynthesis products, minus indicates feedback inhibitions, plus indicates activations. ARO4/3p: 3-deoxy-d-arabino-heptulosonate-7-phosphate (DAHP) synthase, ARO1p: pentafunctional arom protein, ARO2p: chorismate synthase, ARO7p: chorismate (CHA) mutase, TYR1p: prephenate dehydrogenase, PHA2p: prephenate dehydratase, ARO8/9p: aromatic aminotransferase, TRP2/TRP3p: anthranilate synthase complex, TRP4p: phosphoribosyltransferase, TRP1p: phosphoribosyl anthranilate (PRA) Isomerase, TRP3p: indole-3-glycerol phosphate synthase (InGP) synthase, TRP5p: tryptophan synthase, Glu: glutamate, 2-OG: 2-oxoglutarate, Gln: glutamine, Pyr: pyruvat.

Now, proceeding from chorismate, the intermediates for the aromatic amino acids (AAAs) diverge into the phenylalanine-tyrosine and tryptophan branches (Figure 9). For tryptophan, chorismate undergoes a conversion to anthranilate catalyzed by the anthranilate synthase complex, comprising TRP2p and TRP3p. This complex transfers an amino group from glutamate to chorismate, with feedback inhibition directly regulated by tryptophan. Subsequently, the monofunctional enzyme phosphoribosyltransferase (*trp4*) converts anthranilate to phosphoribosyl anthranilate (PRA). The PRA isomerase (*trp1*) then irreversible forms carboxyphenylamino-l-deoxyribulose 5-phosphate (CDRP), and the indole-3-glycerol phosphate synthase (InGP) synthase (*trp3*) decarboxylates CDRP, ultimately yielding InGP by closing the second ring. Finally, the tryptophan synthase (*trp5*) combines InGP with serine, resulting in the production of tryptophan (Figure 9). In *S. cerevisiae,* these enzymes are encoded by the genes *trp1-5*. [142] Compounds derived from tryptophan include vinblastine/vincristine and nicotine, as detailed in Chapter 1.1.2 and Figure 2.

The other two aromatic amino acids, phenylalanine and tyrosine, also derive from chorismate. The initial shared step in this branch is catalyzed by chorismate (CHA) mutase, which induces an intramolecular rearrangement leading to prephenate. The CHA mutase is encoded by the gene *aro7* and is negatively feedback-regulated by tyrosine, an end product of this branch. This inhibition guides the flux, directing it toward tryptophan production when tyrosine concentrations are high, and strongly activating ARO7p when tryptophan concentrations are elevated, redirecting the flux toward the phenylalanine and tyrosine branches. [147] Prephenate serves as the last common intermediate for phenylalanine and tyrosine. The carbon flux diverges toward phenylpyruvate for phenylalanine and 4-hydroxyphenylpyruvate for tyrosine. Both reactions in yeast are catalyzed by the prephenate dehydratase *pha2* and the prephenate dehydrogenase *tyr1*, releasing one CO_2 for each reaction. On the tyrosine side, one NADPH is generated. [142] The final step for both branches involves the reversible reaction catalyzed by the aromatic aminotransferase. This transferase transfers an amino group from glutamate onto phenylpyruvate and hydroxyphenylpyruvate, generating tyrosine and phenylalanine, with 2-oxogluterate as a by-product. In this reaction, glutamate, phenylalanine, tyrosine, and tryptophan can all serve as amino donors, while phenylpyruvate, hydroxyphenylpyruvate, 2-oxoglutarate, and pyruvate act as amino acceptors. ARO8p is responsible for conducting this reaction. ARO9p, alongside ARO8p, can contribute to phenylalanine and tyrosine formation, with its primary role in the catabolic degradation of tryptophan. Nonetheless, it has been demonstrated that ARO9p can sustain the biosynthesis of phenylalanine and tyrosine in Δ*aro8* deletion mutants by transferring amino groups from alanine onto phenylpyruvate or 4-hydroxyphenylpyruvate, releasing pyruvate as a byproduct. [148–150] In Chapter 1.1.2 and Figure 2, these two amino acids are described to be further utilized in the generation of resveratrol, naringenin, codeine, and morphine.

1.5.1 Engineering efforts for shikimate pathway derived products

As in Chapter 1.4.1 for malonyl-CoA, this chapter will also focus on common and already used modifications introduced to the host organism *S. cerevisiae* for heterologous compound productions based on the shikimate pathway and AAA biosynthesis. The focus will mainly lie on the phenylalanine and tyrosine branches.

Small molecules with aromatic structures hold special significance in biotechnology, particularly as precursors for various compounds such as p-coumaric acid [151–154], caffeic acid [155,156], rosmarinic acid [157], and reticuline [158,159]. Furthermore, previously mentioned compounds (Chapter 1.4.1), like resveratrol [31,35,118], naringenin [27,116,160], and kaempferol [117] rely on shikimate pathway- and AAA-derived precursors for their biosynthesis, as well as many more. [72,161]

In numerous studies within this domain, *S. cerevisiae* is frequently chosen as the host for producing these secondary metabolites. This preference stems from the involvement of P450 enzymes in their biosynthesis, which, due to their challenging expression at high levels, makes the eukaryote *S. cerevisiae* one of the primary and most effective choices for heterologous expression of eukaryotic P450s [162]. Furthermore, yeast is generally considered a suitable candidate as a production host and platform organism for various biological molecules (Chapter 1.3).

When exploring the literature for modifications in the shikimate pathway and compounds derived from AAA, strategies to enhance AAA production have been extensively studied. Similar to the approach for malonyl-CoA provision (Chapter 1.4.1), several common strategies have been implemented with distinct modification patterns. A prevalent tactic for the shikimate pathway involves alleviating the feedback inhibition of DAHP synthase, primarily ARO4p, and chorismate mutase, Aro7p. Introducing a single lysine-to-leucine mutation at position 229 for ARO4p (ARO4p^{K229L}) and a serine-to-glycine mutation at position 141 for ARO7p (ARO7p^{G141S}) increasing the flux through the shikimate and subsequent AAA biosynthesis pathway by approximately 4.5-fold. [163] However, overexpressing the feedback-resistant DAHP synthase ARO4p led to shikimate accumulation, revealing a bottleneck in the catalyzed reaction of the pentafunctional enzyme ARO1p. [163] Therefore, testing the overexpression of several heterologous monofunctional enzymes from *E. coli*, each catalysing only one of the reaction of ARO1p, including the dehydroquinate synthase (*aroB*$_{Ec}$), the shikimate dehydrogenase (*ydiB*$_{Ec}$), the EPSP synthase (a*roA*$_{Ec}$), and the shikimate kinase (*aroL*$_{Ec}$) successfully increased target compound production. Notably, AroLp$_{Ec}$ stood out, increasing the flux by converting shikimate, supporting the shikimate intermediate accumulation observation, and alleviating the identified bottleneck. [151,163]

Additionally, preventing the degradation of AAA is another effective strategy. Deleting thiamine-pyrophosphate-dependent 2-oxo-acid decarboxylases *pdc5, pdc6,* and *aro10*, thus preventing phenylpyruvate from decarboxylation and flux through the Ehrlich pathway, resulted in a 40-fold increase in extracellular naringenin concentration. [160] Combining overexpressing ARO4p^{K229L}, ARO7p^{G141S}, AroLp$_{Ec}$, and the deletion of *aro10* and *pdc5* resulted in the highest p-coumaric acid titer of almost 2 g/L (1.93 g/L), outperforming simply overexpressing ARO1p and ARO2p (chorismate synthase). [151] This engineering strategy is a widely employed and a successful approach in the literature, achieving up to 12.5 g/L p-coumaric acid with additional modifications. [153,157]

Many studies centered around this strategy have produced different compounds with various additions to the modification pattern detailed above. For example, Zhou and colleagues replaced ARO3 with the feedback-resistant ARO4p^{K229L} and achieved caffeic acid titers of up

to 769.3 mg/L in shake-flasks. [155] While the deletion of ARO3p worked for caffeic acid, Bisquert and coworkers increased hydroxytyrosol production by overexpressing different combinations of ARO3p, ARO3p^{K222L}, and ARO10 with the abovementioned modifications, leading to 375 mg/L hydroxytyrosol. However, they found that the overexpression of native ARO3p worked best in combination with the modifications ARO4p^{K229L}, ARO7p^{G141S}, and ARO10. [164]

In a separate study, the naringenin titer significantly increased by knocking out PHA2p, impairing the flux towards phenylalanine. [32,165] With the downregulation of PHA2p Lyu and coworkers similarly demonstrated the advantageous impact for naringenin production. [116] Despite the commonly held belief that E4P serves as a bottleneck in AAA-derived compound biosynthesis, the introduction of the heterologous phosphoketolase (*xfpk*$_{Bb}$) from *Bifidobacterium breve*, to enhance flux from glycolysis directly towards E4P, aiming to increase its supply, resulted in a reduction in naringenin titer. [32,165] This contradicts the beneficial effects of the same phosphoketolase in other successful metabolic engineering approaches. [153,165]

Unlike the direct E4P increase detailed before, the redirection of flux from glycolysis through the PPP to increase E4P supply and through the glycolysis to increase PEP production has also been studied. Several studies increased the production of compounds such as shikimic acid, muconic acid and tyrosine by overexpressing the gene *eno2* to increase PEP and *tal1* for E4P, as well as *rki1* and *tkl1* to increase flux through the PPP. [152,166,167] Mao and coworkers increased and redirected the flux for PEP and E4P with an additional overexpression of TYR1p increasing p-coumaric acid production by 12.5-fold compared to the wildtype strain. [152]

With an extra deletion of the transcription factor *ric1*, which negatively controls the ARO genes, and the addition of mutated ARO1p, while knocking out the native one, Suastegui and coworkers increased shikimic acid production up to 2.5 g/L. [166] However, they stated that the overexpression of *tal1* actually decreased product titers, which could explain the low p-coumaric acid yields (21.3 mg/L) described by Mao, utilizing TAL1p overexpression. [152] Using a similar approach, Leavitt and coworkers produced up to 2.1 g/L muconic acid, deleting *zwf1* and *aro1* with simultaneous overexpression of a truncated ARO1p, while complementing the growth ability of the modified strain with *aroE*$_{Ec}$. [167] Despite TKL1p overexpression proving to be beneficial [166,167], Liu and coworkers could not increase the product titer using TKL1p overexpression. [153] Further deletion strategies like knocking out ARO7p and TRP3p could achieve up to 2.9 g/L p-hydroxybenzoic acid. [168]

The following Figure 10 summarizes the mentioned modifications. However, all these manipulations must be viewed in their respective context and target compound production strategies.

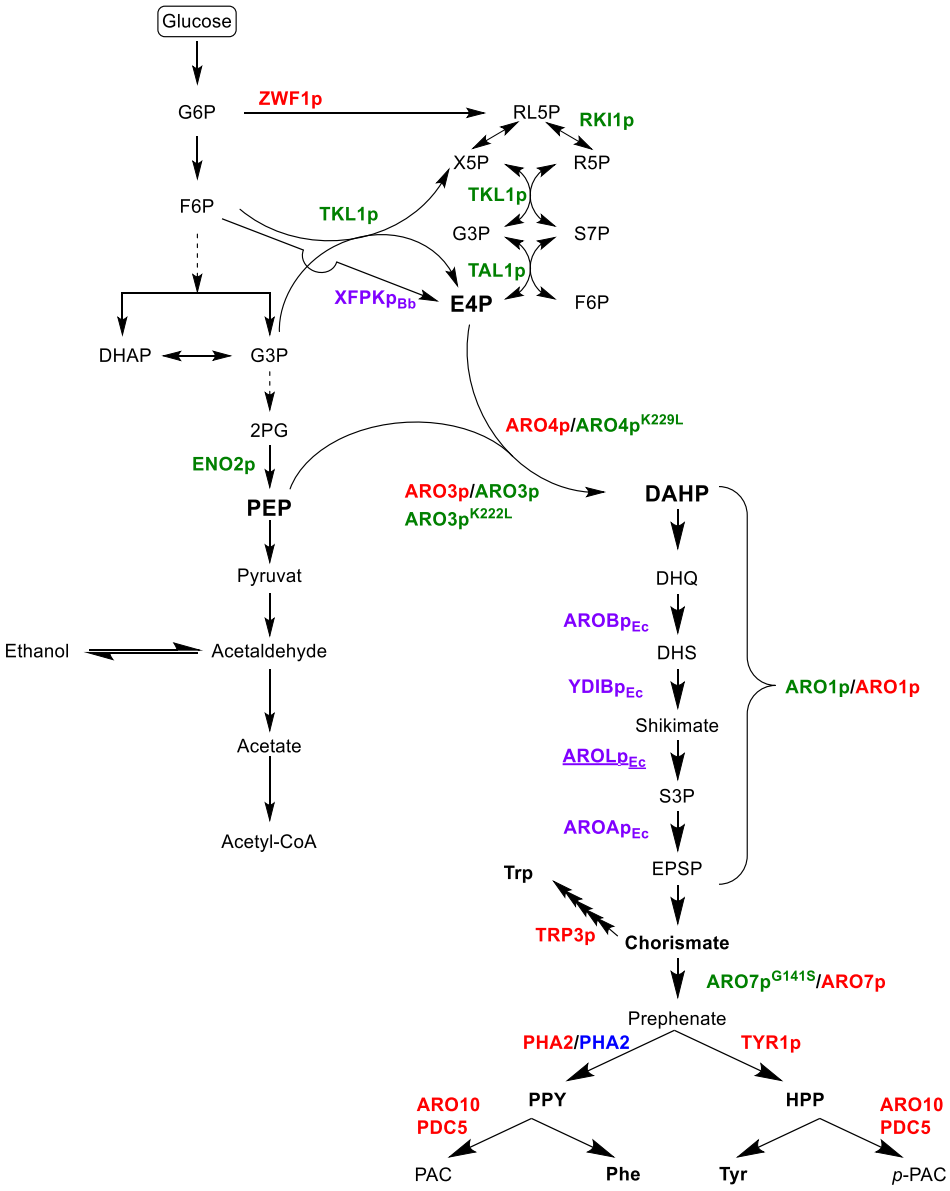

Figure 10: Summary of the modifications that increased their respective target compound production derived from the shikimate and PP pathway found in the literature. Overexpressed enzymes are shown in green, and heterologous enzymes in purple. Red indicates knockouts, while blue indicates downregulation. DHAP: 3-deoxy-D-arabino-heptulosonic acid 7-phosphate, DHQ: 3-dehydroquinate, DHS: 3-dehydro-shikimate, S3P: shikimate-3-phosphate, EPSP: 5-enolpyr- uvylshikimate-3-phosphate, PPY: phenylpyruvate, HPP: para-hydroxy-phenylpyruvate, PAC: phenylacetaldehyde, PHE: phenylalanine, TYR: tyrosine, *p*-PAC: para-hydroxy-acetaldehyde, Aro3/4: 3-deoxy-D-arabino-heptulosonate-7-phosphate (DAHP) synthase, Aro1: pentafunctional AROM complex, Aro2: bifunctional chorismate synthase and flavin reductase, Aro7: chorismate mutase, Pha2: prephenate dehydratase, Tyr1: prephenate dehydrogenase, ARO8: aromatic aminotransferase I, Aro9: aromatic aminotransferase II, TAL: tyrosine ammonia-lyase, Aro10: phenylpyruvate decarboxylase, Pdc5: pyruvate decarboxylase.

1.6 Cryptophycin a potent Macrolide Derived from a mixed PKS/NRPS

With metabolic engineering and the already evaluated pathway modifications presented in the previous chapters (chapter 1.2 to 1.5) a promising candidate for heterologous production in yeast could be cryptophycin. This class of macrolide molecules was first discovered in 1990 through the screening of cultured algae, where cryptophycins initially demonstrated antifungal properties. The name cryptophycin arose from the activity against filamentous fungi and yeast of the genus *Cryptococcus*. [171] While cryptophycin initially was discovered in the cyanobacteria *Nostoc* sp. ATCC 53789, subsequent findings revealed the production of cryptophycin by *Nostoc* sp. GSV 224, and marine sponges as well. [172,173] In the aforementioned blue-green algae alone, more than 25 derivatives of cryptophycins are generated, with cryptophycin 1 being the predominant representative. [174] This group of macrocyclic depsipeptides consists of four units, including a phenyl-octenoic acid (unit A), two amino acids, methyl-D-tyrosine (unit B) and (methyl) β-alanine (unit C), and L-leucic acid (unit D), linked in a cyclic ABCD sequence (Figure 11).

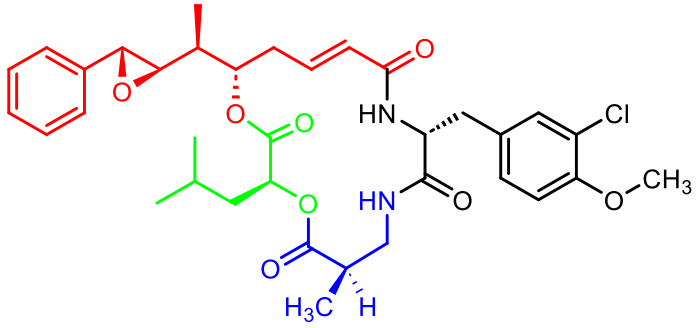

Figure 11: Chemical structure of cryptophycin 1 with differently colored units. Unit A is highlighted in red and consists of the starter unit (cinnamic acid derived) and the malonyl-CoA derived units (red), unit B is shown in black and is signified by tyrosine, unit C is highlighted in blue and consists of β-alanine, and lastly the unit D in green is derived from leucine.

Cryptophycins exhibit potent cytotoxicity and hold promising potential as antiproliferative agents for chemotherapy. Preclinical trials have demonstrated their high efficacy against various tumors and their effectiveness in studies focused on targeted drug delivery to multidrug-resistant cancer cell lines, displaying cytotoxic activity in the subnanomolar range. [175–177] The IC_{50} values of cryptophycin 1 against different tumor cell lines are in the low picomolar range. It acts as a tubulin-destabilizing agent and interferes with microtubule dynamics by inducing conformational changes upon binding, preventing the polymerization of microtubules. The disrupted microtubule dynamics ultimately lead to caspase 3 activation and phosphorylated BcL2-induced apoptosis. [178]

The biosynthesis of cryptophycin in the native cyanobacteria is generated by a mixed PKS/non-ribosomal peptide synthase (NRPS) gene cluster. NRPS, akin to PKS (Chapter 1.1.3), are multi-domain megasynthases that biosynthesize compounds similarly to

PKS. Each module comprises domains that facilitate various tasks required to elongate and modify the compound skeleton. Comparing these domains to those of PKS, the adenylation domain corresponds to the AT domain. Its role is substrate recognition and loading onto the peptide carrier domain (PCP), which transports the growing chain to the condensation (C) domain. These two domains correspond to the ACP and KS domains in PKS, respectively. The distinction is in the elongation reaction and the substrate used; PKS incorporates acyl-CoA units, whereas NRPS utilizes amino acids. The elongation reaction conducted through the C domain leads to amide or ester bond formation, unlike the C-C bond formation of PKSs. A TE domain eventually terminates the assembly-elongation reaction, releasing either a linear or a macrocyclic peptide. Additional tailoring domains such as methyltransferases (MT), KR domains, or epimerases (E) introduce further modifications to the peptide chain. The modular assembly of PKS and NRPS can also be mixed, as illustrated in the biosynthesis of cryptophycin (Figure 12). The first modules, consisting of PKS modules, initially synthesize a carbon skeleton using three malonyl-CoA units with a presumed *trans*-cinnamic acid starter, handing the intermediate over to the NRPS, which sequentially adds tyrosine, β-alanine, and leucine (Figure 12). [36,174]

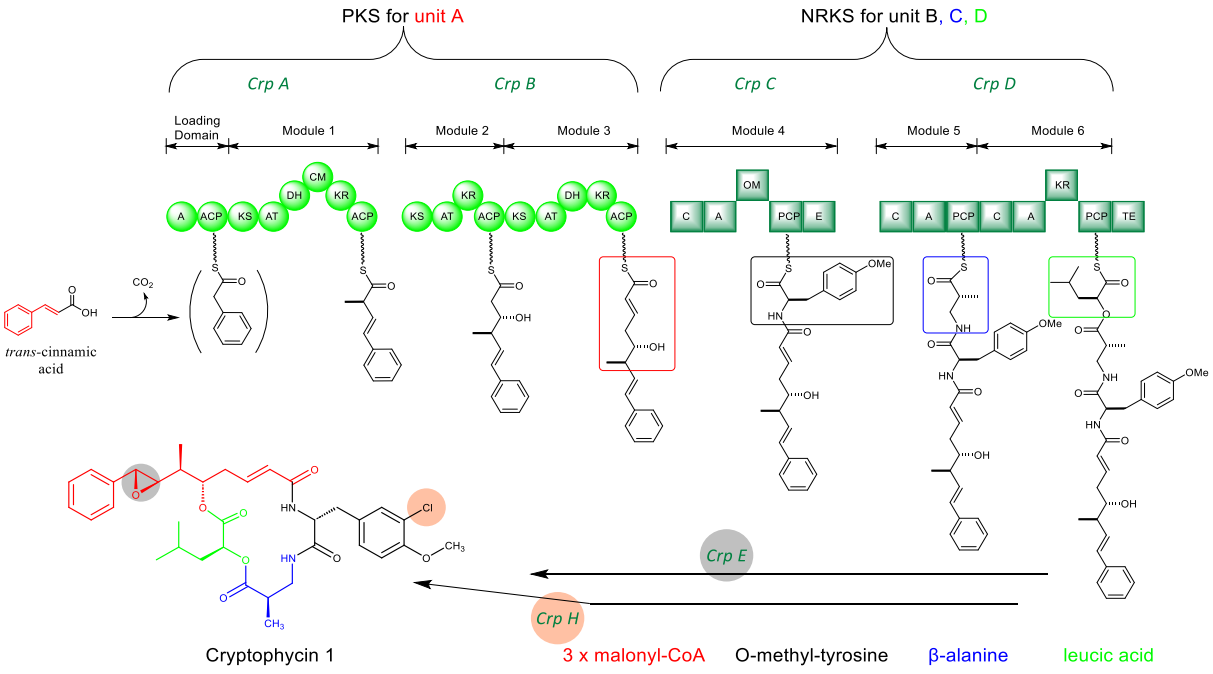

Figure 12: Proposed biosynthesis of cryptophycin 1 from cyanobacteria by Magarvey et al., 2006. The PKS/NRPS multienzyme complex is encoded by *crpA-D*, with *crpA* and *crpB* featuring loading modules and modules 1-3 (depicted by green spheres) representing the PKS, while modules 4-6 (encoded by *crpC-D*) signify the NRPS (represented by green squares). *Trans*-cinnamic acid is suggested as the presumed starter for biosynthesis, and the colored squares highlight the extender units derived from malonyl-CoA (red), tyrosine (black), β-alanine (blue), and leucine (green). The end product, exemplified by cryptophycin 1, requires additional tailoring enzymes for its epoxide (*crpE*, epoxidase) and chloride (*crpH*, hologenase) functionalization. AT, acyltransferase domain; KS, ketosynthase domain; CM, C-methyltransferase domain; DH, dehydratase domain; KR, ketoreductase domain; ACP, acyl carrier protein; A, adenylation domain; C, condensation domain; PCP, peptidyl carrier protein; OM, O-methyltransferase domain; E, epimerase; TE, thioesterase domain. The figure has been modified and extended according to Magarvey et al., 2006. [174]

1.7 Scope of the Thesis

Metabolic engineering is a captivating scientific domain offering the means to modify microbial metabolism. As elucidated in earlier discussions, this manipulation can be executed through diverse methods and tools tailored to the selected host organism. [57] This can be achieved by different means and with different tools for the dedicated organism selected as a host, as shown earlier. [62–68,70,71] The targeted production of NPs with diverse applications in today's modern world is especially intriguing. Fulfilling this demand often encounters obstacles presented by costly, intricate, and potentially hazardous extraction methods. These problems can potentially be overcome by applying metabolic engineering approaches to modify well-established and safe organisms, such as *S. cerevisiae*, as demonstrated in the preceding chapter. [59,72,113,169,170] Leveraging these organisms enables the circumvention of expensive, complex, and harmful NP production processes, leading to the high-yield fermentation of modified organisms for the targeted production of NPs, as successfully exemplified in the existing literature. [6,19,31,55]

The first aim of this thesis, as part of a “Bundesministerium für Bildung und Förderung” funded project, is the establishment of a foundational yeast strain for the production of heterologous compounds generated by PKS and non-ribosomal peptide synthase (NRPS), enabling their respective activation, after expression. These megasynthases employ the utilization of precursors of different metabolic pathways, namely the glycolysis and subsequent malonyl-CoA pathway, as well as the shikimate pathway with its following AAA biosynthesis. Therefore, the second aim of the present thesis is the creation of strains with elevated precursor levels of malonyl-CoA, phenylalanine, and tyrosine, the products of the involved pathways.

As demonstrated in the introduction, NPs play a pivotal role in various fields of everyday life often necessitating the combined supply of precursors derived from two metabolic pathways, the malonyl-CoA pathway and AAA biosynthesis, with their preceding glycolysis and shikimate pathway, respectively. This work's third and overall aim is to combine the PKS/NRPS activating strain with the increased precursor provision (malonyl-CoA, phenylalanine, and tyrosine) to create a yeast platform or chassis. The generated platform strain aims to enable the seamless production of any NP that requires these specific precursors within a single yeast strain.

Chapter II Results and Discussion

The chapter “Results and Discussion” is divided into four subchapters accounting for the different work packages

2.1 Part 1 – Phosphopantetheinyl transferase genome integration

2.2 Part 2 – Modulation of malonyl-CoA provision

2.3 Part 3 – Engineering the shikimate pathway

2.4 Part 4 – Combining malonyl-CoA and shikimate pathway modifications

2.1 Part 1 – Phosphopantetheinyl transferase genome integration

As part of a “Bundesministerium für Bildung und Förderung” (BMBF) funded project, the first task in this dissertation involved the integration of a phosphopantetheinyl transferase into the genome of the yeast strain CEN.PK2-1C (Table 6). The objective of this project was the heterologous biosynthesis of the bioactive compound cryptophycin (Figure 11), using yeast as a host.

For this the BMBF-funded project aimed for the functional reconstitution of the PKS/NRPS biosynthesis cluster (Figure 12). This includes the conversion of ACP and PCP domains into their active *holo*-form. Activating these carrier protein domains involves using a phosphopantetheinyl transferase (PPTase). These enzymes, dependent on Mg^{2+}, transfer a phosphopantetheine moiety from coenzyme A onto a conserved serine residue on the ACP and PCP (Figure 13). With this phosphopantetheinyl group, the enzyme complex can bind and transport the growing polyketide/non-ribosomal peptide chain through a thioester group. [179,180]

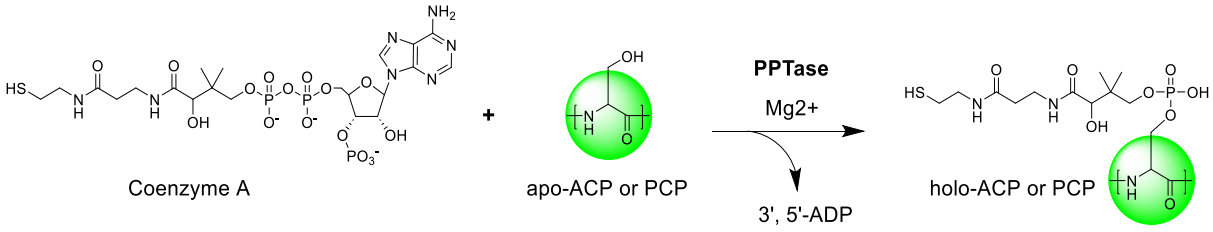

Figure 13: Reaction catalyzed by PPtases. The PPTase transfers a 4’-phosphopantetheine moiety onto an ACP or PCP of PKS/NRPS, converting them from the inactive *apo*- to the active *holo*-form. Figure modified according to Mootz et al., 2002. [180]

Since *S. cerevisiae* does not naturally produce polyketides or other non-ribosomal peptides, introducing a PPTase into yeast cells becomes necessary. To fulfill this requirement, the PPTase selected originates from *Bacillus subtilis*, specifically its sfp_{Bs} PPTase, which has previously demonstrated activity with appropriate promiscuity towards different ACPs and PCPs. [180] Therefore, this PPTase was chosen for implementation into the CEN.PK2-1C yeast genome (Table 6).

2.1.1 CRISPR/Cas9 based integration into *S. cerevisiae* genome

To achieve the stable integration of the sfp_{Bs} PPTase gene from *B. subtillis* into the targeted yeast genome, the CRISPR/Cas9 editing method was selected, as detailed in Apel et al., 2017. [68]

Apel and colleagues utilized the Cas9 endonuclease from *Streptococcus pyogenes*, which has an NGG PAM sequence, and a single “crRNA” termed single-guide RNA (sgRNA), where trac- and crRNA are fused together while still retaining the Cas9 DNA specific cleavage

ability. They provide 23 pre-characterized integration sites with Cas9-sgRNA targeting plasmids. [68]

In order to integrate the PPTase, an integration cassette consisting of a promotor, gene, and terminator for *sfp*$_{Bs}$ integration was prepared using the polymerase chain reaction (PCR, Chapter 4.6.3) and the Gibson assembly (Chapter 4.6.7.1). The integration site chosen for *sfp*$_{Bs}$ was 720a, as described in Apel el al., 2017, on chromosome VII near the centromere. The integration cassette, along with flanking regions containing homologous DNA sequences to the integration site 720a for homologous integration, was introduced into the yeast cells (Chapter 4.7.4). Additionally, a pCutX plasmid was included in the process. This pCutX plasmid is necessary as it carries the genetic information for the Cas9 protein and the sgRNA, collectively facilitating the double-strand break at the desired position. The whole procedure is outlined in Figure 14.

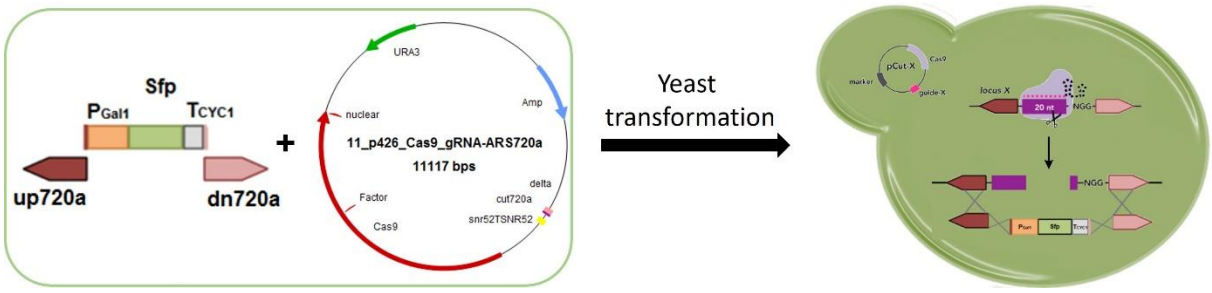

Figure 14: Scheme of the *sfp*$_{Bs}$ integration process using CRISPR/Cas9 and yeast cell transformation. Initially, the integration cassette and homologous segments designed for integration at position 720a were prepared. Subsequently, these components, along with the plasmid (depicted as pCut-X) containing the SgRNA and Cas9 sequences, were utilized for yeast cell transformation. Inside the cells, the protein Cas9 is expressed and the sgRNA is transcribed, binding to the target sequence adjacent to the NGG PAM sequence. This results in DNA cleavage, and the yeast's homologous recombination system aids in repairing the DNA using the homologous flanking regions and the *sfp*$_{Bs}$ integration cassette, thereby integrating the same into the genome. The figure has been modified and extended according to Apel et al., 2017. [68]

Following the successful PCR amplification of the *sfp*$_{Bs}$ gene fragments and the pDionysosGlcRepfree target vector (Supplements 1.1, Chapter 4.6.3) and their subsequent purification (Chapter 4.6.5.1ii), the two fragments were merged using a Gibson reaction (Chapter 4.6.7.1, Figure 15). The resulting construct was used for the transformation of *E. coli* DH5α cells (Chapter 4.7.2).

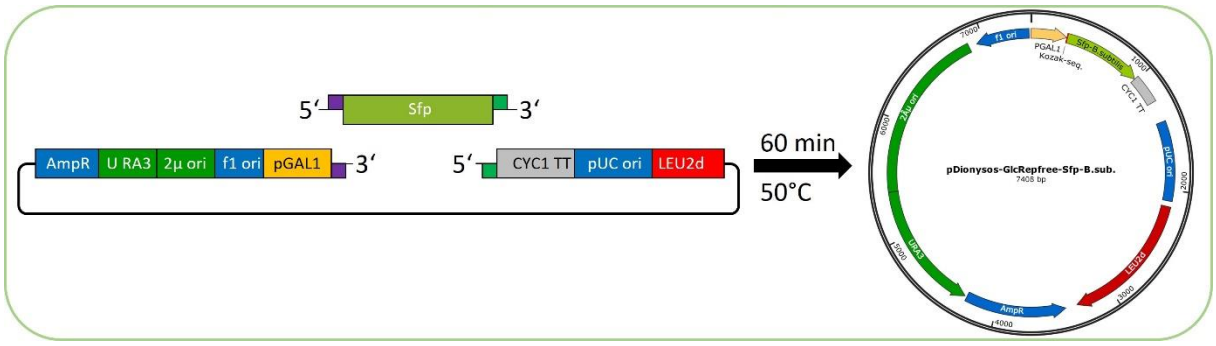

Figure 15: Scheme of the Gibson assembly shown for the *sfp*$_{Bs}$ integration cassette assembly as an example, representative for all other Gibson assemblies.

Validation of the success of the Gibson reaction and transformation was carried out by colony PCR (chapter 4.6.3.4), using a small portion of the grown colony as the DNA template. The results of the colony PCR are illustrated in Figure S49 in the Supplements 1.1. This process, including sequencing (Chapter 4.6.8) represents the standard approach when new plasmids were constructed.

The construction of the *sfp*$_{Bs}$ plasmid aimed to establish the *sfp*$_{Bs}$ integration cassette for convenient availability at any time. PCR amplifications (Chapter 4.6.3.1) of the integration cassette and the homologous flanking regions of the integration sites 720a were performed to generate the DNA required for subsequent transformation. This transformation (Chapter 4.7.4) was performed after purifying the DNA from the PCRs (Chapter 4.6.5.1ii). The fragments (*sfp*$_{Bs}$-cassette and 720a flanking regions) were introduced along with the pCutX-720a plasmid. The integration process is depicted in Figure 14. Similar to the previous *E. coli* colony PCR, yeast cells underwent testing for positive colonies via PCR (Chapter 4.6.3.5 and Supplements 1.2i, Figure S50).

Positive colonies were then regenerated on 5-fluoroorotic acid (5-FOA) selection plates to eliminate the p-CutX-720a plasmid from the cells. This selection leverages the toxicity of 5-FOA for cells possessing a functional URA3 gene, as outlined by previous research. [182] An example of this selection is presented in the Supplements 1.2i, Figure S51.

The final validation of the integration involved a conclusive PCR (Chapter 4.6.3.1) and sequencing (Chapter 4.6.8) of the isolated genomic yeast DNA (Chapter 4.6.5.1iii). This validation process represents the standard procedure for yeast genome modification used here.

The results confirmed successful integration (Figure 16) without mutations in the sequence (Figure S52). This indicates the successful and accurate integration of the *sfp*$_{Bs}$-cassette at position 720a on chromosome VII. Table S43 displays the newly constructed strains. Two strains were constructed, with one strain being glucose deregulated through a

Mig1p binding-site deletion in the *gal4* gene, decreasing the repressing impact of glucose. [183–185]

Figure 16: Agarose gel of the PCR with the genomic DNA as template as a final validation of the *sfp* integration. The red boxes highlight the correct fragment sizes. The numbers show the colony numbers. L: *GeneRuler™ 1 kb DNA Ladder Plus* from Thermo Fischer Scientific

2.1.2 CRISPR/Cas9 mediated *lys5* knockout – PPTase functionality test

While confirming the correct integration of the PPTase into the yeast genome is a crucial step, this does not guarantee its functional expression or expression at all. To address this, a functionality test was conducted by creating a *lys5* knockout mutant utilizing CRISPR/Cas9. The *lys5* gene encodes a PPTase responsible for activating the Lys2 enzyme, converting it to its active *holo*-form, akin to the $SFPp_{Bs}$ reaction from *B. subtilis.* [186] The interaction between Lys2p and Lys5p is a pivotal step in lysine biosynthesis in yeast cells (Figure 17). The premise of the functionality test is that $SFPp_{Bs}$ can complement the *lys5* knockout mutation and is able to activate the Lys2 enzyme activity, reinstating the lysine biosynthesis. This has been successfully demonstrated in prior literature. [180]

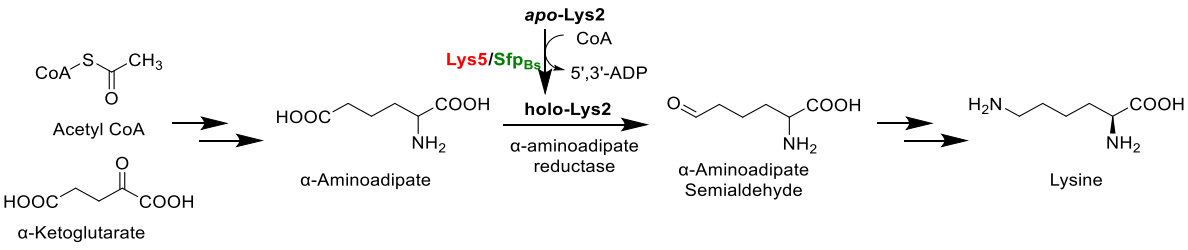

Figure 17: Lysine biosynthesis with a deleted *lys5* gene (red) and heterologous expressed $SFPp_{Bs}$ converting *apo*-Lys2 to *holo*-Lys2 complementing the biosynthetic route.

To perform the *lys5* knockout, a gRNA is needed, targeting the *lys5* gene. Together with the Cas9 endonuclease, a double-strand break is induced to trigger the yeast DNA repair system. Through the addition of oligonucleotides homologous to the double-strand break sequence position, the cells use this altered sequence for the DNA repair, thus introducing a point mutation and an additional stop codon to the *lys5* gene, preventing the expression of Lys5p.

With overlapping primers (Table 8), the gRNA of the pCutX720a plasmid was exchanged (Chapter 4.6.3.1), creating the pCutX-Lys5-knockout plasmid (Supplements 1.1). A two-step PCR was conducted, with 18 cycles at the temperature of one oligonucleotide and 18 cycles at the temperature of the second oligonucleotide in the second step. Subsequently, *DpnI* digestion (Chapter 4.6.4.1), transformation of *E. coli* (Chapter 4.7.2), and plasmid isolation (Chapter 4.6.5.1i) to obtain sufficient quantities of the plasmid were carried out. The oligonucleotide strands needed for the homologous recombination after the induced double-strand break were ordered, introducing a “taaa” sequence disrupting the *lys5* gene (Table 8). Following denaturation of the oligonucleotides for homologous recombination (5 min at 99 °C, with slow renaturation by cooling to room temperature), a double-stranded DNA sequence was created. This DNA strand was used together with the new pCutX-Lys5-knockout plasmid for the transformation of yeast cells (Chapter 4.7.4). A yeast strain harbouring the sfp_{Bs}-cassete (ST003) and a strain without it (Table 6) were used for transformation. The success of this knockout was determined via sequencing (Chapter 4.6.8) after genomic DNA isolation (Chapter 4.6.5.1iii) and PCR (Chapter 4.6.3.1). The sequencing results (Supplements 1.2ii, Figure S53) confirmed the successful integration of the "taaa" mutation.

This genomic alteration marks the initial step in validating the functionality of the PPTase $SFPp_{Bs}$. An activity assay was conducted to test the ability of $SFPp_{Bs}$ to restore lysine biosynthesis by plating the cells on yeast nitrogen base (YNB) agar plates without lysine, uracil, and leucine. The expression of $SFPp_{Bs}$ was further induced by adding 0.5 % galactose to the plates. As shown in Figure 18, the assembled $SFPp_{Bs}$ integration cassette successfully works, and $SFPp_{Bs}$ can restore lysine biosynthesis disrupted by the *lys5* knockout. Cells lacking information for the $SFPp_{Bs}$ PPTase were unable to grow on plates without lysine (Figure 18, A and B). In contrast, those transformed with sfp_{Bs} information, either on a plasmid (C) or integrated into the genome (D), were able to grow in lysine-deficient plates.

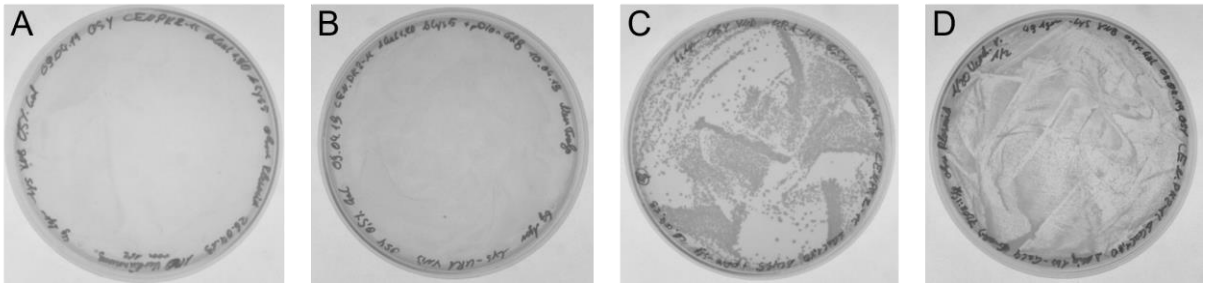

Figure 18: Selective YNB agar plates for $SFPp_{Bs}$ activity assay using *lys5* knockout yeast cells. A: CEN.PK2-1C *Δlys5* without sfp_{Bs} on -lysine YNB agar selection plate, B: CEN.PK2-1C *Δlys5* with empty pDionysos-GlcRepfree plasmid on -lysine, -uracil YNB agar selection plate, C: CEN.PK2-1C *Δlys5* with sfp_{Bs} on the plasmid pDionysos-Sfp_{Bs} on -lysine, -uracil YNB agar selection plate, D: CEN.PK2-1C *Δlys5* 720aΔ::sfp_{Bs} without plasmids on -lysine YNB agar selection plate.

This result was further confirmed by RNA isolation. Yeast cells were cultivated with and without 0.5 % galactose (Chapter 4.7.5), total RNA was isolated (Chapter 4.6.5.1iv), reverse

transcribed (Chapter 4.6.3.2), amplified (Chapter 4.6.3.1), and analysed (Chapter 4.6.1) using the housekeeping gene acetyl-CoA synthase (*acs*) as a reference. Figure 19 demonstrates the successful *sfp*$_{Bs}$ transcription in the manipulated yeast cells, with Figure S54 (Supplements 1.2ii) proving the galactose inducibility of the integrated cassette.

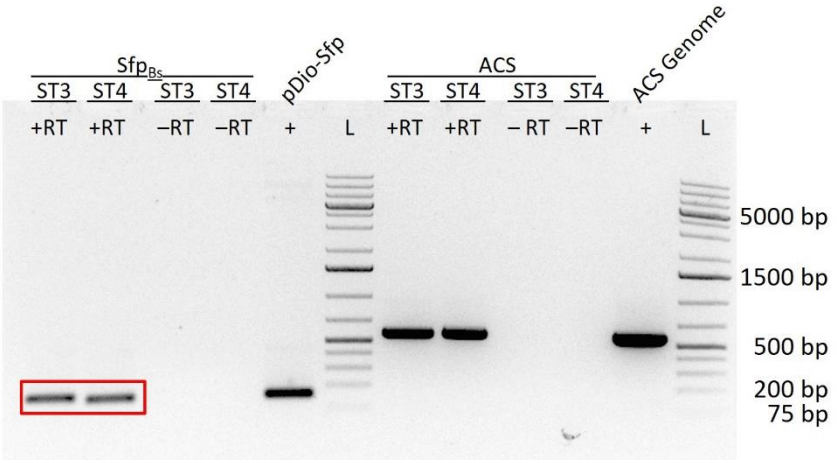

Figure 19: Agarose gel showing the *sfp*$_{Bs}$ and *acs* PCR after RNA isolation. The red box indicates the s*fp*$_{Bs}$ gene fragments amplified from cDNA, reverse transcribed from the RNA isolation, confirming the PPTase transcription from the integration cassette. The housekeeping gene *acs* was successfully amplified, indicating the successful RNA isolation and reverse transcription. The negative controls are shown in the empty lanes (-RT), while the positive controls are shown with the fragments generated from the pDionysos-*Sfp*$_{Bs}$ plasmid (pDio-Sfp) and the *acs* sequence from the yeast genome. ST3/ST4: yeast strains harboring the 720aΔ::*sfp*$_{Bs}$ modification (Table S43), +RT: RNA reverse transcription with reverse transcriptase, -RT: RNA reverse transcription without reverse transcriptase, L: GeneRuler™ 1 kb DNA Ladder Plus, Thermo Scientific.

The results of the PPTase activity assay and the RNA isolation confirm that the *sfp*$_{Bs}$ integration cassette is transcribed and expressed in the transformed yeast cells. This indicates that the PPTase is able to convert the cryptophycin ACP and PCP to their active *holo*-forms (Chapter 2.1) when the PKS/NRPS gene cluster is expressed in yeast cells bearing *sfp*$_{Bs}$. This can also be extended to other PKS and NRPS gene clusters biosynthesizing different NPs.

2.2 Part 2 – Modulation of malonyl-CoA provision

The malonyl-CoA level in yeast is kept at a low level due to the strong regulation of fatty acid biosynthesis. Thus, a metabolism modification to increase the malonyl-CoA supply is essential. [120,187] As shown in the introduction and the previous chapter (Chapter 2.1), malonyl-CoA plays an essential role in the biosynthesis of many NPs. Therefore, this work aimed to generate an intermediate yeast strain with increased cytosolic malonyl-CoA levels for further modification and modulation in later chapters (Chapter 2.4).

Malonyl-CoA is formed in a key reaction by ACC1 (acetyl-CoA carboxylase 1) from acetyl-CoA, which in turn is derived from glycolysis, with glucose as the starting material (Figure 20). The regulation of ACC1p involves various factors, including phosphorylation by the protein kinase SNF1. This regulation can be mitigated by the three mutations depicted in Figure 20, as discussed in Chapter 1.4.1. [121,126,188]

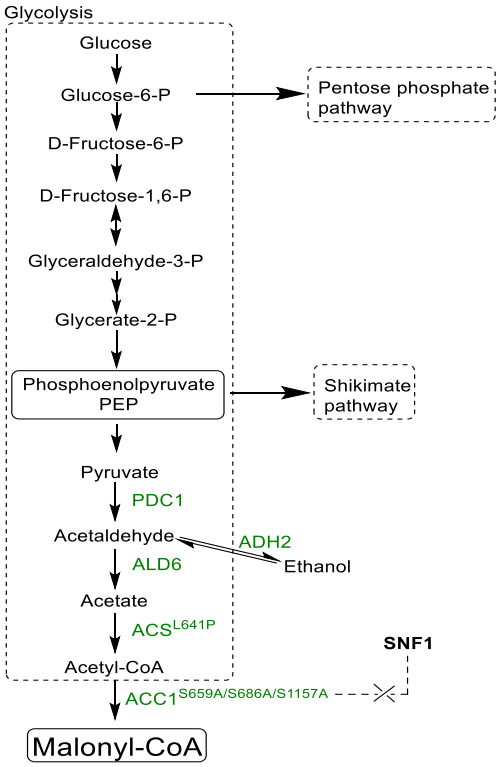

Figure 20: Overview of malonyl-CoA biosynthesis. Additional branch points to pentose phosphate and shikimate pathways originating from glycolysis are highlighted. Targeted modifications through overexpression are depicted in green. Furthermore, the figure illustrates the critical bottleneck in malonyl-CoA production, featuring the mutated and SNF1 deregulated *acc1* mutant. PDC1: pyruvate decarboxylase; ALD6: aldehyde dehydrogenase; ACS: acetyl-CoA synthase; ADH2: alcohol dehydrogenase 2; ACC1: acetyl-CoA carboxylase.

2.2.1 Outline of planned malonyl-CoA pathway modification

Following an extensive literature review, as detailed in Chapter 1.4.1, a list of modifications aimed at elevating cytosolic malonyl-CoA level was compiled in Table 1.

Table 1: Summary of planned modifications to increase the cytosolic malonyl-CoA level in yeast. The table outlines the proposed steps detailing which genes are modified and specifies the nature of the planned modifications. Additionally, the table includes information on the respective sources of these modifications.

Step	Modification	Enzyme	Gene	Source
1	Overexpression	Acetyl-CoA carboxylase	*acc1*^{S659A,S686A,S1157A}	Chen et al., 2018 [126] Kildegaard et al., 2016 [76]
		Aldehyde dehydrogenase	*ald6*	Kildegaard et al., 2016 [76]
		Pyruvate decarboxylase 1	*pdc1*	
	Heterologous overexpression	Acetyl-CoA synthase	*acs*^{L641P} *(Salmonella enterica)*	
2	Overexpression	Alcohol dehydrogenase 2	*adh2*	De Jong et al., 2015 Click here to enter
3		Triose-phosphate isomerase 1	*tpi1*	Li et al., 2015 [127]

Step	Modification	Enzyme	Gene	Source
4	Deletion	Glycerol-3-phosphate dehydrogenase	*gpd1*	A. Ghosh et al., 2016 [135]

Chapter 1.4.1 previously delineated strategies employed in the literature to increase malonyl-CoA supply in yeast, involving a combination of overexpressing heterologous or endogenous genes and employing deletion or downregulation approaches. Based on this research, the decision was made to commence with the modifications described by Kildegaard et al., 2016, given that their study yielded the highest titers of malonyl-CoA-derived products as of the start of this thesis. [76] This involved overexpressing the genes *pdc1, ald6,* acs_{Se}^{L641P} (*S. enterica*), and the triple mutated *acc1*, directing flux towards malonyl-CoA to overcome the bottleneck between acetyl-CoA and malonyl-CoA (Figure 21). Notably, the triple-mutated *acc1* is an addition to the modifications conducted by Kildegaard and colleagues, who only utilized the double mutant in their study (Chapter 1.4.1). [126] The additional mutation was reported by Chen and coworkers [126], as discussed in Chapter 1.4.1. Subsequent modifications, such as the isomerase TPI1p overexpression and *gpd1* deletion, were planned to be introduced incrementally to drive flux toward malonyl-CoA further. [127,135] The procedural details and the respective steps are outlined in Table 1 and are reiterated for clarity in Figure 21.

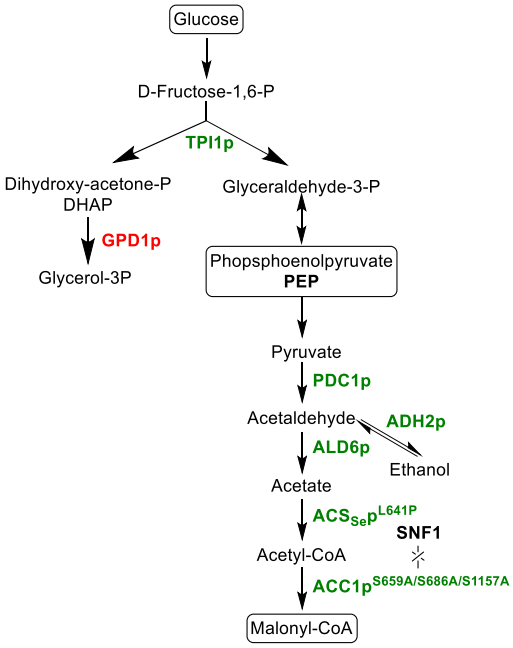

Figure 21: Overview of the metabolic pathway incorporating all modifications outlined in Table 1. Overexpressed genes are visually highlighted in green, while deletions are represented in red. Key compounds are framed for emphasis, including glucose as the initial substrate, PEP as one of the starting materials for the shikimate pathway, and malonyl-CoA as the target product. The non-regulated *acc1* mutant is specifically highlighted by the presence of SNF1. PDC1p: pyruvate decarboxylase; ALD6p: aldehyde dehydrogenase; $ACS_{Se}p$: acetyl-CoA synthase; ADH2p: alcohol dehydrogenase 2; ACC1p: acetyl-CoA carboxylase; TPI1p: triose-phosphate-isomerase; GPD1p: glycerol-3-phosphate dehydrogenase.

All the genes designated for overexpression are intended to be integrated into the yeast genome as a cassette with a promoter and terminator, utilizing CRISPR/Cas9 and simple

homologous recombination to establish a stable genomic integration. However, plasmid construction with the required integration cassettes was necessary before this integration.

2.2.2 Initial plasmid assembly for target gene integrations

To commence, yeast-specific genes (*ald6, pdc1, acc1,* and *adh2*) involved in the initial two steps (Table 1) were directly amplified from the CEN.PK2-1C genome. The *acs* gene, originating from *S. enterica*, was ordered as a codon-optimized DNA string from ThermoFisher Scientific to enhance expression in yeast, accounting for different tRNA usage. The codon usage was modified using the gcua – graphical codon usage analyzer online tool, comparing the codon tables of *S. cerevisiae* and *S. enterica* and the codon usage of *S. enterica* for ACSp. [189] This adaptation aimed to mimic the intrinsic codon usage pattern of *S. enterica* in yeast, considering potential variations in translation speed at certain rarer codon usage points, providing the enzyme adequate time for proper folding within its host organism.

To ensure concise and strong expression cassettes, two approaches were considered. Firstly, distinct promoter-terminator combinations were employed to provide selected genes with an additional expression boost at crucial biosynthesis steps. The planned combinations of promoters and terminators are detailed in Table 2. Secondly, synthetic terminators (tsynth 7, 8, 19) were employed to maintain cassette brevity, while expression-enhancing terminators (tCPS1, tHis5), previously documented in the literature, were incorporated for added expression efficacy. [190,191] Promotors were selected based on their strength, as described by Lee et al., 2015. [67]

Table 2: Combination of promoters and terminators with their respective genes to modify malonyl-CoA metabolism.

Promotor	Gene	Terminator
pRPL18B	ALD6	tsynth 8
pTDH3	ACC1 (S659A,S686A,S1157A)	tCPS1
pHHF1	ACS (L641P) [*Salmonella enterica*]	tsynth19
pPGK1	PDC1	tsynth7
pTEF1	ADH2	tHIS5

All necessary DNA fragments for plasmid construction were obtained through PCR amplification (Chapter 4.6.3.1), followed by purification (Chapter 4.6.5.1ii). Subsequently, these fragments were assembled by a Gibson assembly reaction (Chapter 4.6.7.1) and then used for *E. coli* transformation for amplification (Chapter 4.6.2), plasmid isolation (Chapter 4.6.2), and sequence verification by sequencing procedures (Chapter 4.6.8).

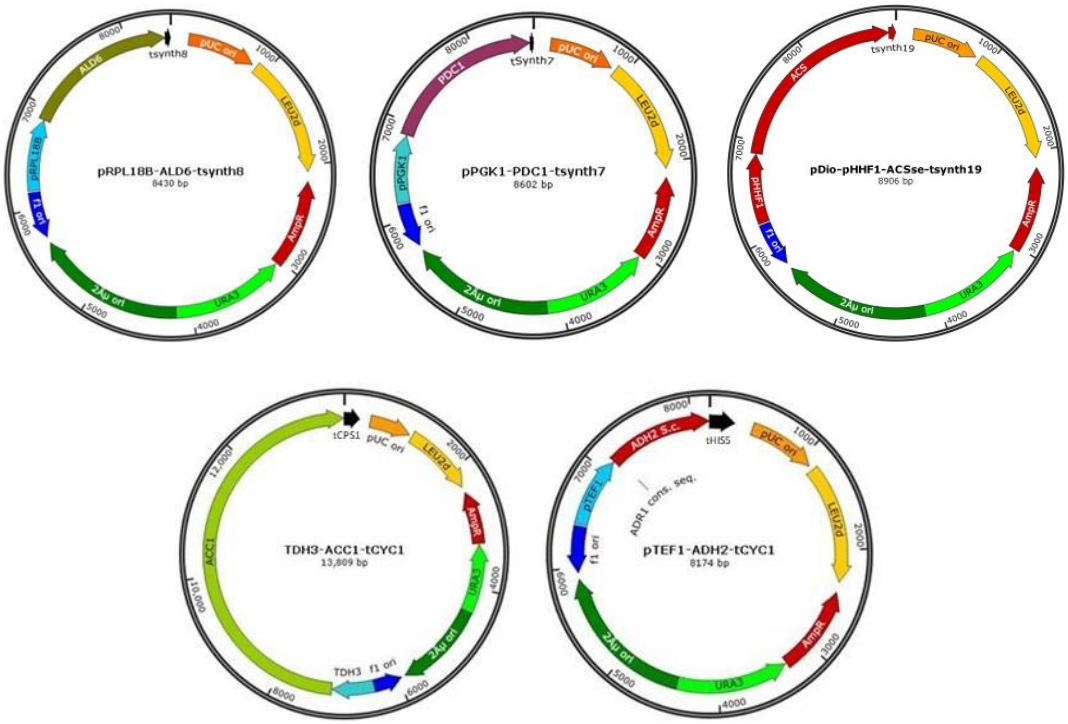

Figure 22: Plasmids to be constructed for the integration cassettes for the malonyl-CoA level manipulation.

The envisioned strategy for visualizing the effects of the aforementioned integrations involved utilizing a malonyl-CoA biosensor, previously described in the literature. [126,192] This biosensor was developed based on the *B. subtilis* transcription factor FapR. The FapR protein acts as a repressor protein, binding to the operator sequence *fapO* (Figure 23), located downstream of the promoter. This arrangement hinders the transcription of the reporter protein, GFP (Green fluorescence protein), when the repressor protein FapR is bound. This biosensor's advantage and unique feature is its direct use of malonyl-CoA as a substrate for signal development, eliminating the need for prior conversion. When malonyl-CoA binds to the FapR repressor protein, the FapR protein detaches from the *fapO* sequence, enabling the transcription of GFP for signal development (Figure 23).

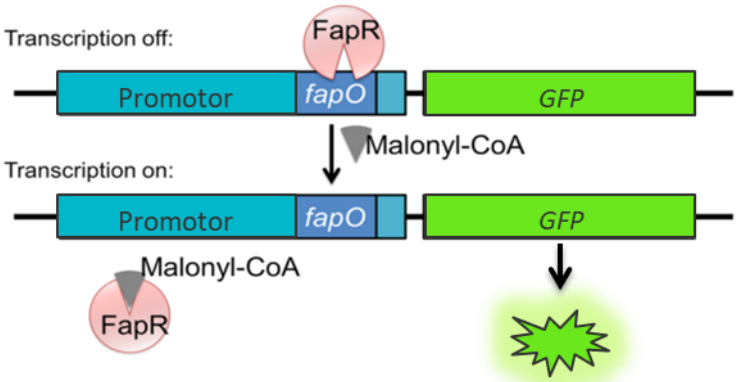

Figure 23: Operation principle of the malonyl-CoA biosensor. The *gfp* transcription is prevented upon binding of the FapR repressor protein to its *fapO* binding sequence. The *gfp* transcription is possible when malonyl-CoA (grey triangle) binds to FapR, preventing it from further binding.

The biosensor construction necessitates two plasmids: one carrying the promoter with the *fapO* and the *gfp* sequence. The other plasmid facilitates the expression of the FapR protein. The biosensor variant by Chen et al., 2018 was chosen, because of the detailed description of the biosensor construction. [126] For this purpose, a hybrid promoter consisting of a TEF1-UAS and a *Gal1-core* sequence was constructed. The *fapO* sequence was positioned 7 bp downstream of the TATA box and placed upstream of the GFP protein, followed by the tCYC1 terminator (Figure 24). All fragments for this plasmid were amplified by PCR (Chapter 4.6.3.1) and underwent purification (Chapter 4.6.5.1ii). The construction process utilized the yeast's any-gene-any-plasmid (AGAP) cloning method, harnessing the cells' homologous recombination abilities to merge fragments by overlapping DNA sequences after a simple yeast transformation (Chapter 4.7.4). [193]

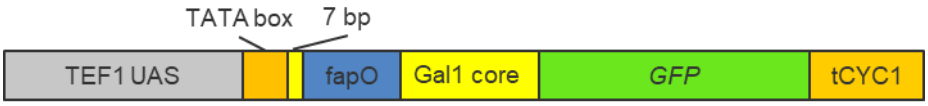

Figure 24: Structure of the hybrid promotor controlling the GFPp expression.

However, before concluding the work on the aforementioned plan, an opportunity arose to acquire all the genes with a ready-to-use integration system. Notably, this included genes and plasmids for manipulating subsequent genes in the shikimate pathway, offering the potential for substantial time savings in generating the modified yeast strains.

2.2.3 Implementing the EasyClone system for malonyl-CoA elevation

The approach to elevate cytosolic malonyl-CoA levels, as discussed in Chapter 2.2.1, was chosen based on the authors' success in achieving high yields of 3-HP directly derived from malonyl-CoA. [76] In their study, Kildegaard and colleagues employed the EasyClone method, a previously established technique for efficient genetic engineering that allows repetitive cycles of simultaneous stable integration into the yeast genome. This method involves a set of pre-assembled plasmids designed to seamlessly integrate cassettes into 14 pre-characterized integration sites on chromosomes X, XI, and XII (Figure 25). This system also enables the eventual removal of the used selection markers via Cre/*loxP* excision, allowing for the reuse of these markers if needed. [62,63] Together with rapid DNA modification techniques like PCR (Chapter 4.6.3) and assembly methods such as Gibson assembly (Chapter 4.6.7.1), they hold the potential to accelerate the strain construction process substantially.

The EasyClone system was generously provided by Irina Borodina from the Technical University of Denmark (DTU), who is part of the same research group that conducted the study by Kildegaard et al., 2016. These plasmids already contained the selected genes for elevating

malonyl-CoA levels (genes of steps one and two, Table 1), along with the genes for the planned shikimate pathway modifications and their respective reporter system (Chapter 2.3). Consequently, the initially outlined procedure described in the preceding Chapter 2.2.2 was temporarily put on hold and proceeded with the genes and plasmids provided by Irina Borodina (DTU, Table 3).

Table 3: Plasmids provided by DTU for malonyl-CoA level modifications, detailing the included genes, targeted integration sites, selection markers, and any unique features that the plasmids may possess. Only plasmids with genes associated with malonyl-CoA level optimization are shown.

Gene	Plasmid	Integration site	Marker	Specials
1. ACC1^{S659A,S1157A}	p0343	pX-2-loxP	KlURA3	CaMCR
ALD6	p0380	pX-3-loxP	KlLEU2	
PDC1	p0382	pX-4-loxP	SpHis5	
ACSse^{L641P}	p0380	pX-3-loxP	KlLEU2	
2. ACC1^{S659A,S1157A}	p0376	pTY4-loxP	KlURA3	CaMCR
3. ACC1^{S659A,S1157A}	p0474	pTY4-no loxP	KlURA3	CaMCR

The EasyClone system uses pre-assembled plasmids containing up to two integration cassettes in opposing orientations and a *loxP*-encased selection marker. These components are flanked by pre-characterized integration sequences, facilitating integration into the selected sites on chromosomes X, XI, and XII, as illustrated in Figure 25.

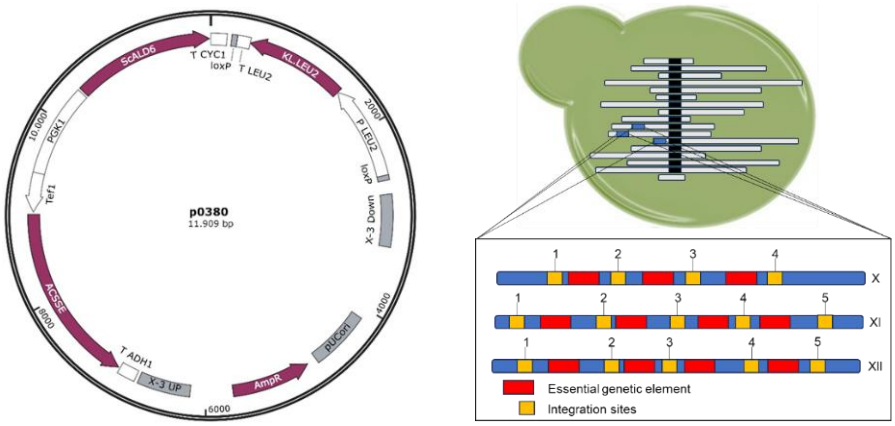

Figure 25: Integration plasmid p380 (left) and integration sites arranged on chromosomes X, XI, and XII (right). The genes *ald2, acs$_{Se}$*, and *leu2$_{Kl}$* on plasmid p380 are flanked by the integration sequences (X-3 UP and Down, grey) for the integration into integration site 3 on chromosome X. The placement of all integration sites (depicted as yellow boxes) is interspersed with essential genetic elements crucial for growth (depicted as red boxes). Adapted and modified according to Jensen et al., 2014. [63]

Since the system leverages homologous yeast recombination, plasmids are introduced into the cell by standard yeast cell transformation (Chapter 4.7.4). However, enzymatic digestion (Chapter 4.6.4.2) is applied to linearize the plasmids before transformation. This step necessitates the provision of plasmids in substantial quantities. To meet this requirement, a high-yield plasmid isolation protocol was established using alkali lysis (Chapter 4.6.5.2) and

plasmid precipitation (Chapter 4.6.5.3). This protocol yielded a plasmid DNA concentration approximately an order of magnitude higher than that achieved with the plasmid isolation kit (Chapter 4.6.5.1), even when isolated from the same amount of cell suspension.

2.2.4 Mutated *acc1* and malonyl-CoA reductase (MCR) read-out system

To incorporate the modifications (detailed in Table 3), the acetyl-CoA carboxylase 1 (*acc1*) gene was initially subjected to site-directed mutagenesis (Chapter 4.6.3.3), introducing the third mutation identified by Chen and colleagues. [126] This resulted in the generation of plasmids p0343*, p0376*, and p0474*, each carrying the new *acc1*^{S659A,S686A,S1157A}. The sequencing results are depicted in Figure S55 (Supplements 1.2iii).

Initially, the plan involved monitoring the modification progress and success using the malonyl-CoA biosensor. However, the use of malonyl-CoA reductase (*mcr*$_{Ca}$) from *Chloroflexus aurantiacus,* as employed in prior studies, allowed for direct detection of the malonyl-CoA conversion product 3-HP through high-performance liquid chromatography (HPLC). [76,194] The HPLC detection protocol from the literature could be seamlessly adapted, given its high resemblance to the sugar detection protocol used on the established and solely for this purpose intended HPLC device (Agilent, Chapter 4.10.1.2). As the *mcr* expression cassette was included on the *acc1* containing plasmids, the detection and production of 3-HP could be directly employed. The reductase directly converts malonyl-CoA to 3-HP in a two-step reaction, utilizing nicotinamide adenine dinucleotide phosphate (NADPH, Figure 26). This reaction requires two molecules of NADPH for each 3-HP and specifically requires NADPH over NADH. [195]

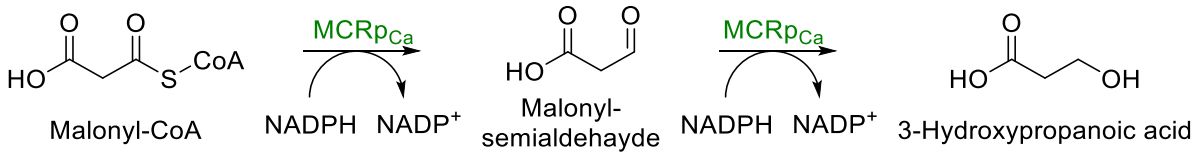

Figure 26: Malonyl-CoA reductase catalyzed reaction converting malonyl-CoA via malonyl-semialdehyde to 3-HP (3-hydroxypropionic acid) consuming two NADPH for the reduction reactions.

The utilization of the malonyl-CoA reductase (*mcr*$_{Ca}$) gene and its associated reaction is solely necessary for monitoring progress during strain construction and is not meant for the final strain with elevated cytosolic malonyl-CoA levels. Consequently, the *mcr*$_{Ca}$ expression cassette is excised from the *acc1* integration plasmid and instead subcloned into a new episomal plasmid designed for MCRp$_{Ca}$ expression (pCaMCR-TRP1, Supplements 1.1). This modification allows for expression from a high-copy-number plasmid featuring a 2µ origin of replication, offering the advantage of plasmid removal from the cell instead of removing the *mcr*$_{Ca}$ cassette from the genome.

Therefore, the expression of $MCRp_{Ca}$ and, consequently, the malonyl-CoA reporter system from an episomal plasmid was assessed. Strains ST003 and ST004 (Table S43) were used for transformation with the created *mcr*$_{Ca}$ readout plasmid (Chapter 4.7.4), and the resulting colonies were cultivated and tested for 3-HP (Chapter 4.10.1.2) production. The HPLC method for 3-HP detection was derived from Kildegaard and coworkers. [194] The column temperature and the column itself, although both, the column used here and in the reported protocol, were specifically recommended for carbohydrate analysis. [196,197] Nonetheless, the protocol was initially tested, measuring a serial dilution of standards for 3-HP quantification as well as other relevant metabolites (Chapter 4.10.1.2). This process of measuring a serious of standards was included in every measuring sequence. An illustrative example can be found in Supplements 1.2iii.

Upon cultivation of the generated strains ST018 (ST003 + pCaMCR-TRP1) and ST019 (ST004 + pCaMCR-TRP1), it became evident that the episomal expression of $MCRp_{Ca}$ did not yield any 3-HP, at least not without any additional modifications (Figure 27). Both strains display comparable amounts of residual glucose, consumed over the curse of cultivation, and comparable concentrations of generated pyruvate, glycerol, and acetate, as illustrated in Figure 27. The cultivation conditions involved batch cultivation with a duration of 72 h in YNB SC-medium, oriented to the duration and medium stated in the reference literature.

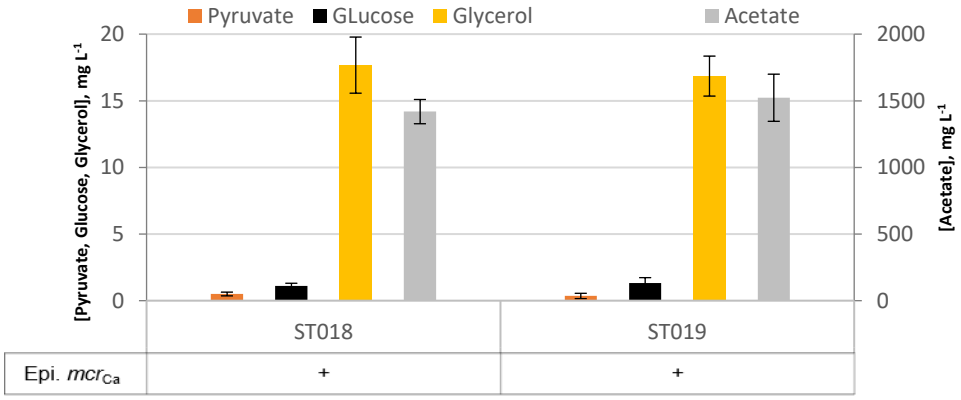

Figure 27: HPLC results of ST018 and ST019 showing the measured levels of residual glucose and the generated concentrations of pyruvate, glycerol, and acetate with missing 3-HP yields. Signals were detected with HPLC-UV at 210 nm for pyruvate (orange) and acetate (grey) and with HPLC-RI for glucose (black) and glycerol (yellow).

The subsequent logical step was to implement the targeted modifications outlined in Table 1 in a sequential manner. Therefore, the process commenced with the sole integration of the triple-mutated *acc1**** (p0343-acc1***, Table 7) and the combination of *acc1****-*mcr*$_{Ca}$ (plasmid p0343*, Table 7), as well the multicopy TY4 integration of the *acc1****-*mcr*$_{Ca}$ combination (plasmid p0474*, Table 7). This multicopy integration utilized transposable elements, DNA sequences capable of relocating to new sites in the genome, a phenomenon observed in yeast. Yeast possesses five families of TY elements denoted TY1-TY5, falling

within the subclass of retrotransposons known as Class-I elements. [198] These elements transpose via a copy-paste mechanism involving an RNA intermediate and are characterized by two long terminal repeats (LTRs) flanking the open reading frame. [199–201]

As illustrated with the strains ST018 and ST019 (Figure 27), single integrations into the genome of ST018 and ST019 with solely *acc1**** (p0343-acc1***) and into ST003 and ST004 with both *acc1**** and mcr_{Ca}, (p0343*-*acc1****-mcr_{Ca}) did not result in detectable 3-HP upon selection and cultivation. However, the TY4 multicopy integration experiment presented different results compared to Figure 27 (Figure 28).

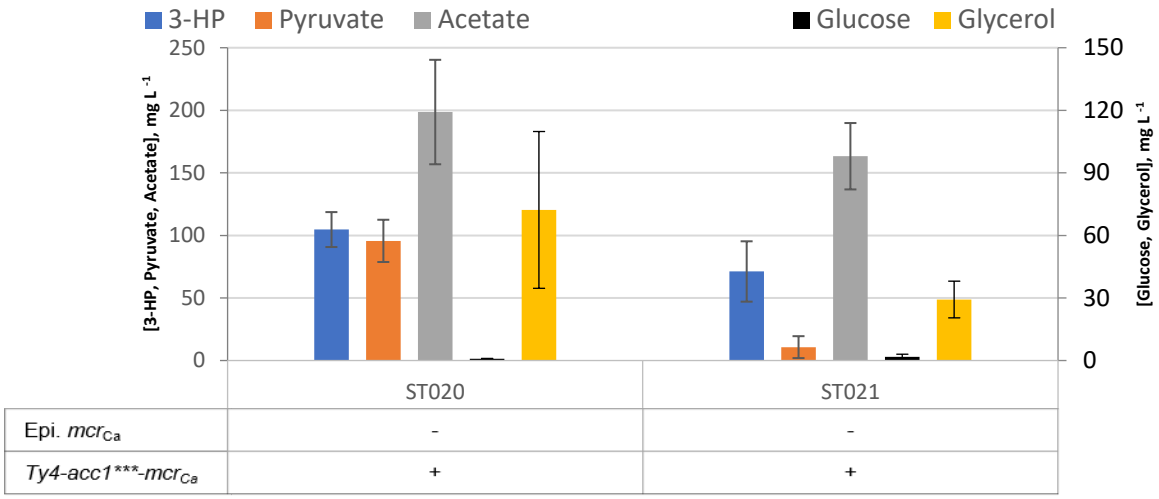

Figure 28: HPLC results of the multicopy integration of *acc1*-*mcr_{Ca} into the genome of yeast strains ST003 and ST004, resulting in strains ST020 and ST021.** Signals were detected with HPLC-UV at 210 nm for 3-HP (blue), pyruvate (orange), and acetate (grey) and with HPLC-RI for glucose (black) and glycerol (yellow).

The engineered strains ST020 and ST021 demonstrated successful production of 3-HP. ST020 achieved an average yield of 104.67±13.95 mg L^{-1} 3-HP, while ST021 produced an average of 71.16±24.13 mg L^{-1} 3-HP. However, as the figure above shows, the 3-HP yield exhibited relatively high fluctuations from cultivation to cultivation, reflecting distinct growth patterns. Individual cultivations reached 242.85 mg L^{-1} (ST020) and 202.87 mg L^{-1} (ST021). The TY4 integration appears to compromise the growth capacity of the engineered strains. Although the growth remains lower than that of the basis strains (ST003 and ST004), the 3-HP production exhibits prominent peaks, as mentioned earlier. This peak in 3-HP production could be observed through a short assessment conducted every 24 h, evaluating 3-HP production illustrated in Figure 29 below. The figure demonstrates that 3-HP production starts relatively early during yeast cultivation, showing a robust linear correlation with cultivation time.

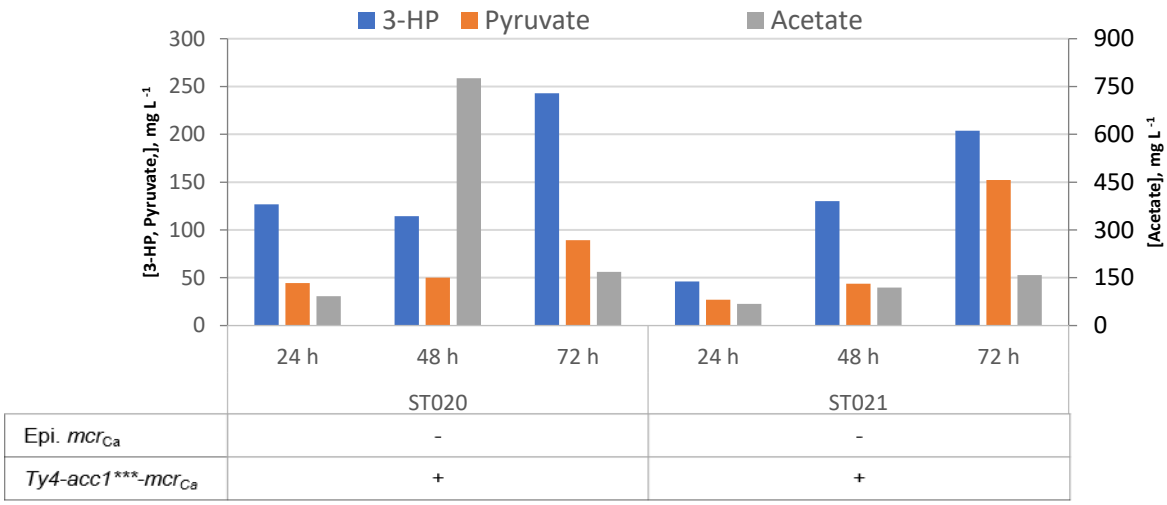

Figure 29: 3-HP production over time at sampling points after 24 h, 48 h, and 72 h for the strains ST020 and ST021. Results represent quick single-sample testing. Signals were detected with HPLC-UV at 210 nm for 3-HP (blue), pyruvate (orange), and acetate (grey).

The decline in 3-HP concentration after 48 h for ST020 could potentially be attributed to 3-HP degradation, although this remains speculative. Hence, the ST021 does not exhibit such a decline. Additional sampling would be necessary to confirm and delve further into this matter since 3-HP degradation is not addressed in the referenced literature thus far. [76,194] However, recent reports suggest that 3-HP can undergo catabolism in various production strains. [202–204] Upon glucose depletion, studies by Yang, Liu, and coworkers reported 3-HP degradation through a one-step dehydrogenase conversion of 3-HP to acetyl-CoA in *Methylobacterium extorquens*, degradation involving the branch amino acid degradation pathway, and oxidative degradation via ALD6 in *Rhodosporidium toruloides*. [202–204] Therefore, it is conceivable that 3-HP could also be degraded in *S. cerevisiae*, particularly when accumulated within the cell, due to its low pKa value of 4.5, keeping it in its dissociated state because of the nearly neutral pH of the cytoplasm. [205–207] Thus, hindering simple diffusion of 3-HP out of the cell in its neutral state, potentially leading to cytoplasmic acidification, which is toxic to the cell. [208] This could furthermore offer an explanation for impaired growth (Supplements 1.2iii) and also suggest a potential mechanism for preventing such acidification.

Notably, recent findings indicate that *S. cerevisiae* is capable of degrading 3-HP through its malonyl semialdehyde intermediate with the deletion of the gamma-aminobutyrate (GABA) transaminase *uga1*, resulting in increased 3-HP production. [206] This degradation appears to occur only after glucose depletion, with some studies indicating it does not happen earlier than after 96 hours of cultivation. [202,203] This suggests that with a constant glucose supply or shorter cultivation periods, degradation should not be an issue, as observed in this study.

Nevertheless, from the results shown in Figure 28 and Figure 29, it becomes evident that a bottleneck may exist in acetate conversion when smaller amounts of 3-HP are detected. The acetate concentration remains relatively high in the 48-hour sample (ST020) compared to other samples (Figure 29). Therefore, modifications upstream of acetyl-CoA were introduced (Chapter 2.2.5).

2.2.5 Introducing upstream modifications for increased malonyl-CoA provision

The same yeast cell manipulation procedure performed in the previous chapter was replicated in this section. However, the detailed explanation of the procedure was omitted from the preceding discussion. For this reason, a brief description will be provided here (Figure 30).

The plasmids must first be linearized before being used for yeast cell transformation. All plasmids intended for transformation were cleaved using the endonuclease *Not*I (Chapter 4.6.4.2, Table 21). The linearization is visualized and verified via agarose gel in Figure S60 (Supplements 1.2iv). Once all expression cassettes were prepared, the genetic material was introduced into the yeast cells through standard yeast cell transformation (Chapter 4.7.4). The progress and success of these integration experiments were assessed by observing colony growth under the selection pressure associated with the plasmid and integration cassette, followed by deep-well cultivation using 48-well FlowerPlates and the Biolector system (M2P labs GmbH, Germany, Chapter 4.7.5.1). After 72 hours of cultivation, the supernatant was collected and analyzed using HPLC (Chapters 4.10.1). The workflow is summarized in Figure 30.

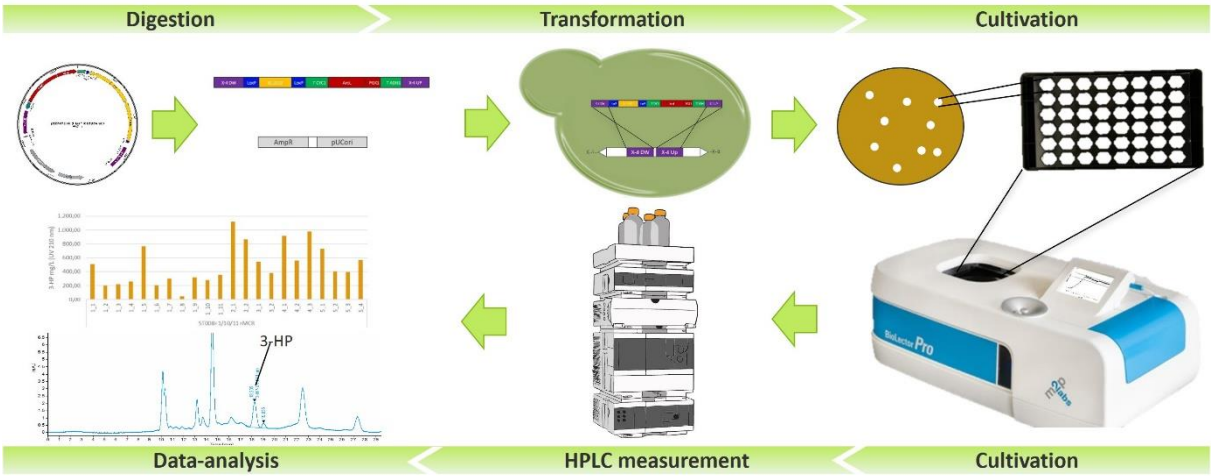

Figure 30: Visualization of the iterative and repetitive work cycle involving yeast cell transformation, selection, cultivation, and analysis of the modification success. Digestion: linearization of the integration plasmid; Transformation: yeast cell transformation and homologous recombination event for genome modification; Cultivation: selection of modified and growing yeast cells for cultivation in the 48-well-FlowerPlate using the Biolector system (M2P labs GmbH, Germany) for parallelization; HPLC measurement and Data-analysis: measurement of the cultivation supernatant via HPLC-UV/RI and gained data analysis.

The outlined procedure was also adopted for a rapid parallelization to speed up the implementation of the already established modification, which was intended as a foundation for further manipulation and combination with the shikimate pathway, ultimately yielding a compound derived from both pathway precursors. Based on the results from the previous section, which indicated no 3-HP production for episomally expressed MCRpCa, both without and with chromosomally integrated *acc1**** lone or the combination of chromosomally integrated *acc1****-*mcr*$_{Ca}$, a simultaneous stepwise integration, along with the full integration of all modifications listed in Table 1, was conducted in parallel. However, the utilization of linearized plasmids p0380 (*acs*$_{Se}^{L641P}$ and *ald6*) and p0382 (*pdc1*) for the integration of the target genes posed challenges, even after substituting the flanking homologous integration regions with newly amplified ones from the target strain to accommodate for any sequence deviations.

Eventually, the successful integration event was verified. However, resulting strains lacked evidence of 3-HP production, except for the fully modified strains harboring all modifications (step 1, Table 2). For two strains, ST022 and ST023, 3-HP production was detected (Figure 31). ST023 is the strain using the episomal reporter configuration, while ST022 carries the *mcr*$_{Ca}$ reporter gene genomically integrated.

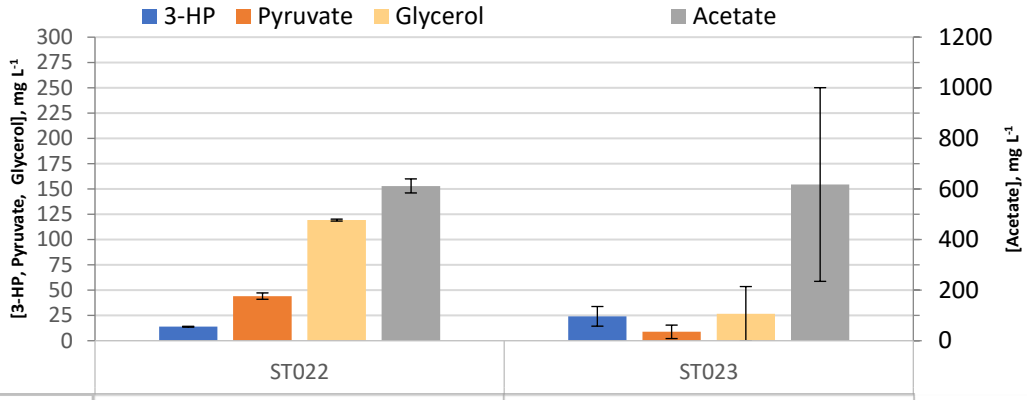

	ST022	ST023
mcr$_{Ca}$ plasmid	-	+
*ACC1****	-	+
*ACC1****-*mcr*$_{Ca}$	+	-
ACS$_{Se}$*-*ALD6*	+	+
PDC1	+	+

Figure 31: Results of 3-HP reporter production in strains ST022 and ST023 based on strain ST003. Additionally, the amount of upstream intermediates pyruvate, acetate, and glycerol were detected. Signals were detected with HPLC-UV at 210 nm for 3-HP (blue), pyruvate (orange), and acetate (grey) and with HPLC-RI for glycerol (yellow). Cultivation was conducted in YNB SC-medium utilizing the Biolector at 72 h, 1200 rpm, 30 °C, and 85 % humidity (Biolector, M2P labs GmbH, Germany).

By comparing the solely genomical by implemented modifications of ST022 with the episomal reporter configuration in ST023, it is evident that ST023 strains yield higher 3-HP titers (24.11±9.70 mg L^{-1}) with comparable acetate titer but significantly lower glycerol and pyruvate levels than ST022. ST022 could produce 13.83±0.44 mg L^{-1} 3-HP, which is approximately half of the 3-HP amount of ST023. This result presents a different scenario than the one depicted in the results of Kildegaard and coworkers, in which the episomal plasmid yielded the lowest yields. [76] However, results for the same configuration as presented here are not shown. Kildegaard and coworkers were able to produce 3-HP only from using episomal expression and single integration expression of *acc1***-mcr$_{Ca}$*, for which no 3-HP could be detected here.

One potential reason for the episomal approach lacking any success could be that the carboxylase (*acc1****) and the *mcr$_{Ca}$* were not expressed from the same source. This, however, was the case in the study (Kildegaard et al., 2016,) where both genes were either located on a plasmid or in the genome. The expression of genes from the genome compared to 2µ-plasmid-based is different. The plasmid-based approach results in a wide range of expression performance, differing up to 2 orders of magnitude compared to the much narrower, albeit lower, expression pattern of genome-based expressions. [67] This difference could partly explain the disparities in the results, especially considering that Suyama and coworkers could increase 3-HP production by preventing MCR protein degradation in *Schizosaccharomyces pombe*. [209] An extreme expression spike of a plasmid-based enzyme could potentially trigger a stress response during yeast growth, inducing a similar degradation of high amounts of a single enzyme. This may also affect the expression fluctuations reported for plasmid expressions [67] and might explain the notably higher deviations in the results for ST023 using the plasmid compared to ST022.

However, the genome-integrated versions and the integration of the other modifications only yielded 3-HP when every modification was integrated, unlike what is presented in the literature, where much higher titers could be achieved. This could be explained by the cultivation conditions and probably by the possibility of 3-HP being degraded and trapped inside the cells due to the low pKa, as discussed in Chapter 2.2.4. The steady substrate and energy supply in the form of glucose seems to have led to a steady and higher 3-HP production, as is evident in the results presented in the literature. [76,110,194,206] This high 3-HP production could have covered a low 3-HP degradation process hiding in the background, as indicated by the results of Liu et al. and others. By deleting *uga1,* an increase of 3-HP was achieved. However, this gain was only around 5 %, still representing a degradation ability for such high titers, yielding differences of nearly 500 mg L^{-1} over the course of the whole cultivation (10.77 g L^{-1} to 11.25 g L^{-1}). Low 3-HP overall yields could have a significant impact, especially when glucose slowly depletes, cutting substrate and energy

supply, possibly even before the reported 96 h cultivation duration. [203] Considering the possible 3-HP trapping inside the cells, a cell-pellet disruption experiment (Chapter 4.8.1) revealed that the 3-HP released from the cells always stays below the extracellular 3-HP concentration (Figure 32).

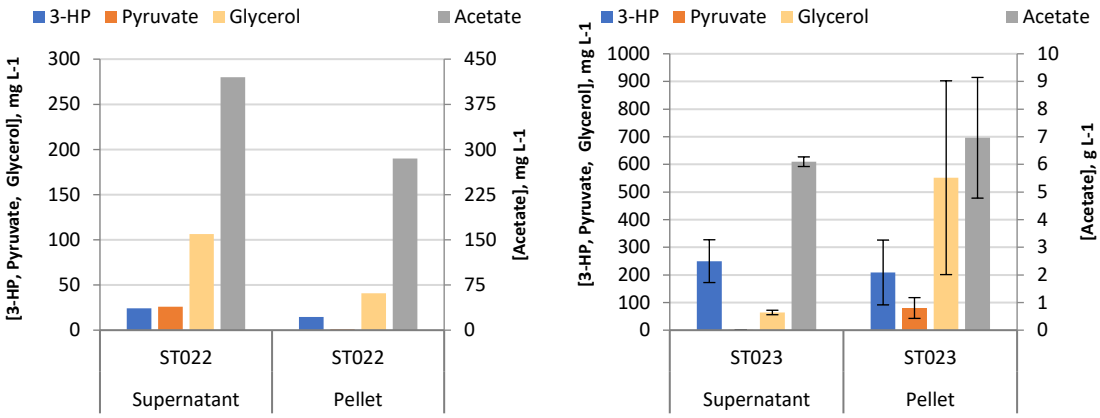

Figure 32: Compound titers of ST022 (left) and ST023 (right) measured in the supernatant and the corresponding cell pellet (cytosol). Left: Single sample cultivation of ST022 in YNB SC-medium. Right: ST023 cultivation in YPD medium, n=3. Signals were detected with HPLC-UV at 210 nm for 3-HP (blue), pyruvate (orange), and acetate (grey) and with HPLC-RI for glycerol (yellow).

The ratio of intracellular 3-HP to extracellular 3-HP ranges from 0.6 to 0.8 (pellet: (ST022) 14.76 mg L^{-1} / (ST023) 208.78±117.38 mg L^{-1}, supernatant: (ST022) 24.12 mg L^{-1} / (ST023) 249.66±77.40 mg L^{-1}). The results shown in Figure 32 indicate that 3-HP, although deprotonated and contributing to intracellular acidification, is actively exported to the extracellular medium. This export must continuously occur because of the high extracellular 3-HP yields reported (two-digit gram scale) in the literature and would reduce the pH of the medium to a level where significant amounts of undissociated 3-HP would diffuse back into the cell, where it accumulates upon deprotonation again. [76,194,205,206,208] The findings of Liu and colleagues support this since the overexpression of an endogenous monocarboxylate permease increased 3-HP yields and tolerance of *S. cerevisiae*. [206] Furthermore, the fact that ST023 is cultivated in a more nutritious medium yielding significantly higher 3-HP concentration (YPD medium, Figure 32), underscores the high energy need for the 3-HP production, as likewise demonstrated in the literature. [76,195]

Nevertheless, the present work proceeded with the generated strains, ST022 and ST023. The following planned modification involved the overexpression of ADH2p and TPI1p. However, during the curse of this work and to accelerate the implementation process, together with new insights from the literature, the initial ADH2p overexpression strategy was changed. The overexpression of ADH2p would likely not significantly impact ethanol conversion due to the presence of several other alcohol dehydrogenase (ADH) genes, despite ADH2p being a

major oxidizer of ethanol. [210] Therefore, considering the literature on this topic and the high affinity of the ADH enzyme to acetaldehyde (mentioned in Chapter 1.4.1), the general production of ethanol should be reduced primarily by deleting one of the major ADHs. It is stated, that *adh1* is under normal conditions constitutively active and one of the major ethanol producers and is 3 times slower in alcohol conversion. [210] A previous study already demonstrated the positive impact of deleting one of the major ADHs (adh1 and adh4) in the cytosol for n-butanol. [134] Combining this with the 3-HP titer-increasing overexpression of Tpi1p ([127], Chapter 1.4.1), the gene for *tpi1* was integrated into the genome, while deleting *adh1*, which accelerates the process by coupling these steps. Another beneficial effect found in the literature was the potential positive impact on shikimate derived products, hence ADH1p is also involved in the degradation associated with the Ehrlich pathway. [211] To implement this, an integration plasmid (pI-dADH1::TPI1, Table 7) with homologous *adh1* flanking sequences and the *S. cerevisiae tpi1* gene was constructed using PCR and Gibson assembly (Chapter 4.6.3.1 and Chapter 4.6.7.1). A *tef1-tdh1* promotor terminator combination was selected, as this was reported to increase the expression of *ptef1*-controlled genes (Chapter 2.2.2). [67] The strains ST022 and ST023 were used for the transformation (Chapter 4.7.4) with the linearized pI-dADH1::TPI1 (Figure 33). This was also attempted with the ST020 and ST021 strains. However, no 3-HP could be detected during the cultivation of the few growing cells.

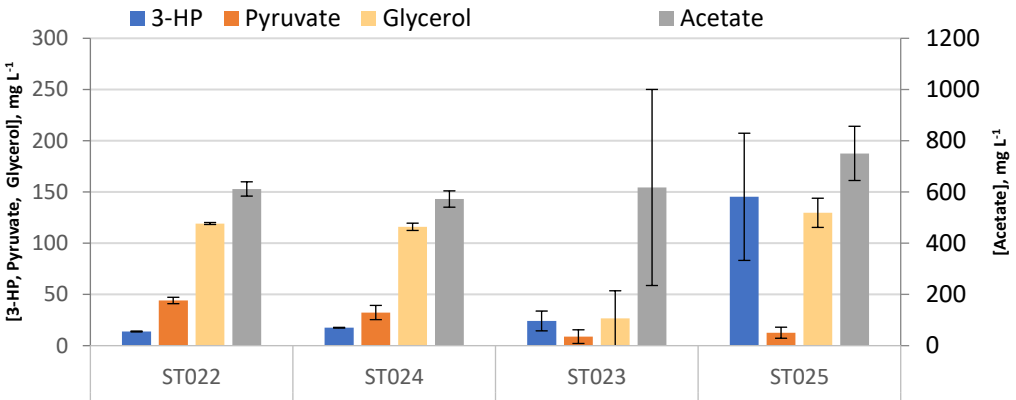

	ST022	ST024	ST023	ST025
mcr_{Ca} plasmid	-	-	+	+
*ACC1****	-	-	+	+
*ACC1***-*mcr_{Ca}	+	+	-	-
ACS_{Se}*-ALD6*	+	+	+	+
PDC1	+	+	+	+
ADH1::TPI1	-	+	-	+

Figure 33: 3-HP reporter production in strains ST022 and ST023 compared to their *adh1::tpi1* carrying versions ST024 and ST025 (all based on strain ST003). The amount of upstream intermediates, pyruvate, acetate, and glycerol, was detected. Signals were detected with HPLC-UV at 210 nm for 3-HP, pyruvate, and acetate and with HPLC-RI for glycerol. Cultivations were conducted in YNB SC-medium utilizing the Biolector at 72 h, 1200 rpm, 30 °C, and 85 % humidity (Biolector, M2P labs GmbH, Germany).

The studies involving TPI1p overexpression and *adh1* deletion from the literature, state an up to 120 % increase in 3-HP titers for the use of TPI1p and an up to 4-fold 3-HP titer increase for *Δadh1* (among other used deletions). [127,134] The results from Figure 33 for the strains ST022 and ST024 (only genome-based integration) do not show comparable results. The yield increased around 30 % (13.83±0.44 mg L^{-1} and 17.55±0.31 mg L^{-1}), when deleting *adh1* and overexpressing TPI1p. In contrast, the 3-HP titer improvement ranges up to 6-fold from strain ST023 (plasmid mcr_{Ca}) compared to ST025 (plasmid mcr_{Ca} + *Δadh1::tpi1*) (24.11±9.70 mg L^{-1} and 145.29±62.08 mg L^{-1}), albeit with a wide deviation range. Even the lowest-yielding sample exhibited a 2-fold increase, nearly reaching the reported improvement, by the mentioned studies. Considering the results from ST024 (genomic mcr_{Ca} + *Δadh1::tpi1*) and the lowest results from ST025 (plasmid mcr_{Ca} + *Δadh1::tpi1*), the failure to reach comparable literature-reported results may be attributed to the fact that these studies directly measured malonyl-CoA. In contrast, in the presented experiments, malonyl-CoA needed to be converted in an energy-demanding reaction. Additionally, only *adh1* was deleted, whereas in the corresponding study, additional genes involved in ethanol and glycerol production were deleted as well, potentially contributing to the strain's (ST024 and ST025) lower performance. The intended reduction in glycerol production could not be observed, as glycerol levels remained the same or were even higher, indicating elevated TPI1p activity not solely selectively directs flux in the malonyl-CoA generating direction. When considering the average and highest results from ST025, the 3-HP titer improvement exceeded what was reported in the literature.

However, these results, which showed similar or better performance (6-fold increase) than the literature (Figure 33) were generated with the strains using the episomal reporter system, which in the literature resulted in lower 3-HP levels and is subject to high fluctuations in 3-HP yield, as previously mentioned and discussed. Furthermore, obtaining results from strains employing the episomal reporter system was challenging and required numerous cultivation attempts, resulting in only a few positive outcomes. Another reason for these high deviations could be attributed to the detection method itself. The produced 3-HP concentrations were challenging to identify because of the used method is only reliable in detecting 3-HP when using the UV (210 nm) chromatogram. For the RI detector, which shows higher signal intensities for 3-HP, the signals for glycerol and 3-HP overlap at the exact same retention time (Rt) (Supplements 1.2iv). This overlay resulted in problems in the initial use of this method. Notably, the reliability of the measurement seems to work better for higher 3-HP concentrations because the signal is not very strong overall, consistently staying below 10 mAU signal intensity even with concentrations of over 300 mg L^{-1} 3-HP standard. Therefore, measurements of higher 3-HP concentrations work better. However, another problem arises: a Rt shift of 0.02 to 0.04 min between the samples of the calibration curve of

the same run of up to 0.1-0.2 min between the different runs (0.149 min in Supplements 1.2iv). This combination made the detection of 3-HP a challenging task.

Although the modification standardly was verified via colony- (Chapter 4.6.3.5), PCR (Chapter 4.6.3.1), as well as sequencing attempts (Chapter 4.6.8), some uncertainties and suspicions arose regarding the detection method and validity of 3-HP production. Therefore, the generated strains were tested for 3-HP production using nuclear magnetic resonance spectroscopy (NMR, Chapter 4.10.2) to check whether the actual molecule could be detected.

2.2.6 3-HP detection via nuclear magnetic resonance (NMR)

As evident from the results discussed in preceding chapters, doubts about the reliability of the chosen HPLC method and the substantial fluctuations in 3-HP results, particularly for strains employing the plasmid-based reporter approach, emerged. Consequently, qualitative evidence for the presence of 3-HP in the cultivations from the generated strains was necessary. Employing a combination of lyophilization and extraction (Chapter 4.9.2) along with various NMR solvents, ^{1}H and ^{13}C NMR spectra of 3-HP were measured and analyzed (Chapter 4.10.2). Initial measurements were performed using reduced (Chapter 4.9.1) and pure 3-HP standard samples to compare the 3-HP NMR spectra. Subsequent steps involved performing extraction experiments on 3-HP spiked medium samples compared to basis strain cultivation (ST003, no 3-HP) using an adapted and modified protocol from the literature. [212] Figure 34 summarizes the relevant ^{1}H NMR results from the initial experiments, providing general information about 3-HP and confirming the validity of the extraction method. Results from the literature and simulations with ChemDraw (chemical drawing program by PerkinElmer) indicated two distinct triplets at around 3.8-3.5 ppm for H_2(C-O)- and 2.4-2.3 ppm for H_2(C-COO) for the ^{1}H NMR spectrum, as well as signals at 35-38 ppm for C(H_2-COOH), 57-66 ppm for C(H_2-OH), and 173-177 ppm for C(OOH) in the ^{13}C NMR spectrum. [212,213]

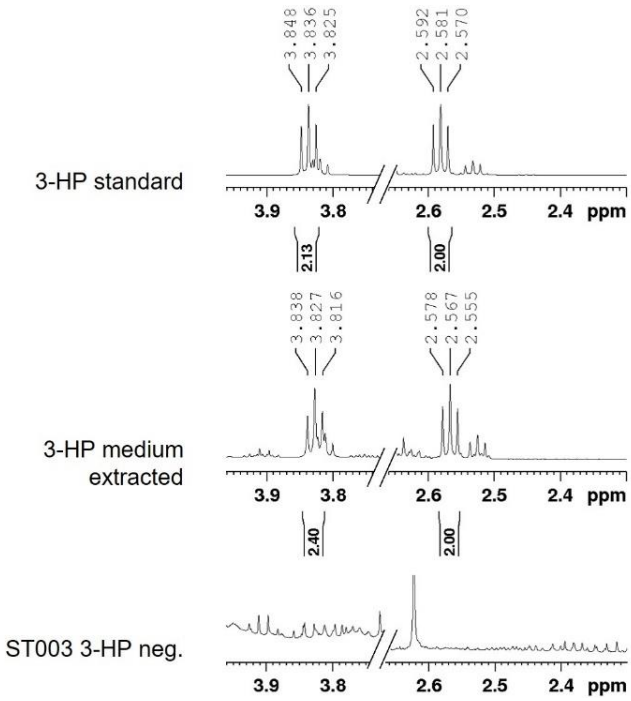

Figure 34: ^{1}H NMR of 3-HP to verify the extraction method and compound detection. Samples from the top: 3-HP standard dissolved in $CDCl_3$, 3-HP medium extracted: medium spiked with 3-HP and extracted, ST003 3-HP neg.: basic strain cultivated and extracted as negative sample. ^{1}H NMR 500 MHz, 298 K, $CDCl_3$ as solvent.

As evident, 3-HP exhibits two distinct triplets at 3.83 ppm and 2.57 ppm, with the integration area of the H_2(C-O)- triplet slightly higher than the other. Both triplets display a slight roofing effect, indicating proton coupling of adjacent protons (3 or fewer bonds apart), as present in 3-HP. The 3-HP standard and the 3-HP extracted from the medium showed a detectable 3-HP signal, in contrast to the negative sample (ST003 3-HP neg.). Subsequently, the cultivation and extraction processes were repeated with the previously introduced producing strains ST020-24. However, ST025 could not be analyzed, given that the cultures grew unreliable, considering the high fluctuations observed in the production results in conjunction with the respective preceding high number of cultivation attempts. Figure 35 presents the 3-HP detection results from ST020-24 compared to an extracted standard sample. The ppm values displayed below deviate from the previously illustrated results because the samples were measured with deuterated-methanol instead of $CDCl_3$ as before. The complete NMR spectra (^{1}H and ^{13}C) can be found in the Supplements (Chapter 1.2v).

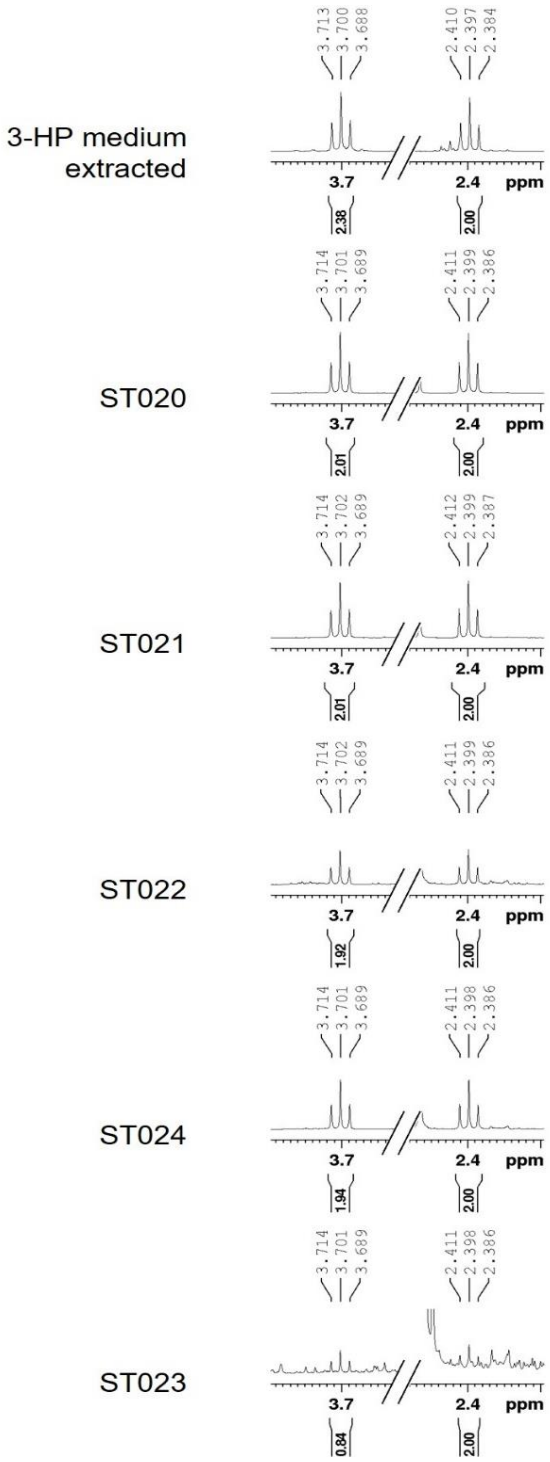

Figure 35: 3-HP ^{1}H NMR spectra from medium and ST020-24 shaking flask cultivations (YNB SC-medium, 30 °C, 250 rpm, 72 h). Samples from the top: 3-HP medium extracted: medium spiked with 3-HP and extracted, ST020-24: shaking flasks cultivated producing strains extracted for 3-HP. ^{1}H NMR 500 MHz, 298 K, CD_4 as solvent.

As evident from Figure 35, all samples produced 3-HP, as indicated by matching ppm values (deviating only 0.002 ppm) and integrations. However, consistent with suspicions regarding plasmid-based reporter strains, the ST023 sample shows only a very faint signal with matching ppm, but not for the integrations (0.84 vs. 2.00). This discrepancy could be attributed to the triplet at 2.39 ppm, which is overlapping with other small signals, increasing the integration area compared to that of the 3.7 ppm triplet. Unfortunately, no signal could be

detected in the ^{13}C NMR spectrum (Supplements 1.2v). These measurements confirm the suspicions regarding the reliability of the HPLC method for small 3-HP amounts and the production attempted from a plasmid-based system. However, this is only a qualitative approach showing that all strains generated here produce 3-HP, probably including the ST023, as of the results of Figure 35, albeit in minimal amounts. This necessitates further measurements involving the cultivation of ST023 to be certain, especially given the high variations in 3-HP yields, if any results can be generated at all, considering the numerous cultivations needed to obtain the shown results for ST023.

On the other hand, the remaining strains (ST020-22, ST024) worked well, and malonyl-CoA levels could be successfully increased based on 3-HP yields. This should also be true for ST023 because, even when the 3-HP production is an issue, acetate levels were always on an equal or even higher level, like for ST022 (Figure 32 and Figure 33). This indicates comparable pathway modification impacts, even when not directed to 3-HP production; the final goal was increased malonyl-CoA provision. Therefore, employing 3-HP as a reporter compound, relying on its conversion through $MCRp_{Ca}$ without modulation of energy supply, was unsuitable for this context's intended malonyl-CoA level enhancement approach.

Summarizing the results thus far, all undertaken modifications have proven successful in malonyl-CoA level elevation. However, the selected verification method, for the sake of convenience and potential time-saving, was not reliable. The reporter system is very energy-demanding (NADPH, Figure 26), only working effectively and reliably with a constant energy supply, which means bioreactor or fed-batch cultivation and specifically tailored energy supply, introduced through additional modifications as reported in the literature. [76,194,206] Additional cultivations in a bioreactor with generated strains could underscore that. However, further energy supply and necessary changes were not aimed for the goal of higher malonyl-CoA provision. This also means a direct detection system (malonyl-CoA biosensor, [126,127,192]), as intended in Chapter 2.2.2 would have been better for the intended purpose. Furthermore, other potential problems arising from 3-HP would not play any role, like possible degradation or intracellular acidification. [202,203,206,208,209] Unfortunately, the results presented in this Chapter 2.2 were only intended as a first step and to create a basis for this work, implementing a malonyl-CoA-producing strain; hence, there was none.

Nevertheless, such a high malonyl-CoA-producing strain could be successfully generated, even with a modification combination of *Δadh1::tpi1* not reported so far. Further, combining the upstream modification with a TY1 multicopy integration with a fed-batch cultivation would result in a strain efficiently producing 3-HP or malonyl-CoA-derived products on a gram scale. As this multicopy integration approach was already shown in comparable work. [76,104,206] The TY1 multicopy integration was a topic that was also worked on because

the TY1 integration has already been proven to be better compared to TY4 regarding final strain growth (personal communication with Dr. Fabian Thomas). Unfortunately, this could not be tested in course of the present thesis. Regarding the planned modification presented in Table 1, all but two could be implemented. The ADH2 overexpression was substituted with the *Δadh1::tpi1* approach. The *gpd1* deletion, however, could not be tested, which could have had a beneficial effect on glycerol level reduction, as TPI1p overexpression did not result in the envisioned reduction. However, the deletion was reported to impair yeast growth. Therefore, a promoter exchange and transcription downregulation would also be advantageous if further explored. [134] Further steps regarding whole RNA isolations and genomic DNA preparations were undertaken and completed. However, the intended transcriptome sequencing and analysis as well as genomic DNA sequencing using Nanopore DNA sequencing, could not be done in the end. This would have further verified the modification work, providing additional information regarding transcription patterns, potential off-target integrations, and TY copy number determination.

Nevertheless, with the data presented here, the successful modification of the malonyl-CoA pathway could be illustrated, albeit not all planned modifications could be integrated. Further cultivations with constant glucose and energy supply could lead to interesting results. Using the strains presented in this chapter, the work proceeded with the combination of the shikimate pathway and malonyl-CoA modifications in a single *S. cerevisiae* strain.

2.3 Part 3 – Engineering the shikimate pathway

The significance of molecules such as phenylalanine and tyrosine in the biosynthesis of numerous NPs is just as important as that of malonyl-CoA. Am illustrative example is resveratrol, which is synthesized from phenylalanine and three malonyl-CoA units, combining precursors originating from glycolysis and the shikimate pathway (Chapter 1.1.2). [31]. Another instance of the importance of shikimate pathway-derived precursors is cryptophycin, discussed in Chapter 2.1, and synthesized by a hybrid system involving PKS and NRPS. This synthase system employs amino acids, specifically tyrosine and malonyl-CoA as substrates for the chain extension reaction, with a phenylalanine derivative likely serving as the starter molecule (Figure 12, Chapter 2.1). [174] Other interesting compounds with similar precursor requirements, belonging to a class of substances frequently discussed in public debates and potentially benefiting from this precursor combination, but not yet explored, could include aromatic phytocannabinoids biosynthesized in a suitable yeast chassis strain. These compounds share the need for the mentioned three malonyl-CoA units and an aromatic starter unit. [26,174,214]

As detailed in Chapter 1.5, phenylalanine and tyrosine are synthesized through the shikimate pathway, where the synthesis pathway diverges from prephenate to form either phenylalanine or tyrosine.

2.3.1 Planned modifications to the shikimate pathway

In alignment with the methodology employed for malonyl-CoA increment, an extensive literature review was conducted to formulate a strategy to augment shikimate-based precursors, specifically phenylalanine and tyrosine. Essential insights, highlighted in Chapter 1.5 were considered, such as the feedback inhibition of ARO3p and ARO4p by phenylalanine and tyrosine, along with the exclusive inhibition of ARO7p by tyrosine. [142] However, it was noted that these inhibitions could be mitigated through gene mutations involving the substitution of specific amino acids at designated sites ($ARO3p^{K222L}$, $ARO4p^{K229L}$, $ARO7p^{G141S}$). [163,164,215] Additionally, it was observed that the five reaction steps catalyzed by ARO1p presented a bottleneck in the conversion of shikimate to shikimate-3-phosphate, a challenge successfully addressed by the heterologous expression of AroLp from *E. coli*. [151]

Considering these findings and a thorough literature review, the modifications described by Rodriguez et al., 2015 were identified as yielding the best results for shikimate-derived products at that time. [151] The planned procedure and its corresponding steps are outlined in Table 4 below and visualized in Figure 36. This approach involved the deletion of *aro10* and *pdc5*, coupled with the genomic implementation of $ARO4p^{K229L}$, $ARO7p^{G141S}$, and $AroLp_{Ec,}$ to facilitate rapid implementation of these modifications to increase AAA precursors.

Table 4: Overview of the planned modifications to increase phenylalanine and tyrosine levels.

Step	Modification	Enzyme	Gene	Source
1	Overexpression	DHAP Synthase	$ARO4^{K229L}$	Rodriguez et al., 2015 [151]
		Chorismate mutase	$ARO7^{G141S}$	
	Deletion	Phenylpyruvate decarboxylase	ARO10	
2	Heterologous Overexpression	Shikimate Kinase II	AROL (*E. coli*)	
	Deletion	Pyruvate decarboxylase	PDC5	

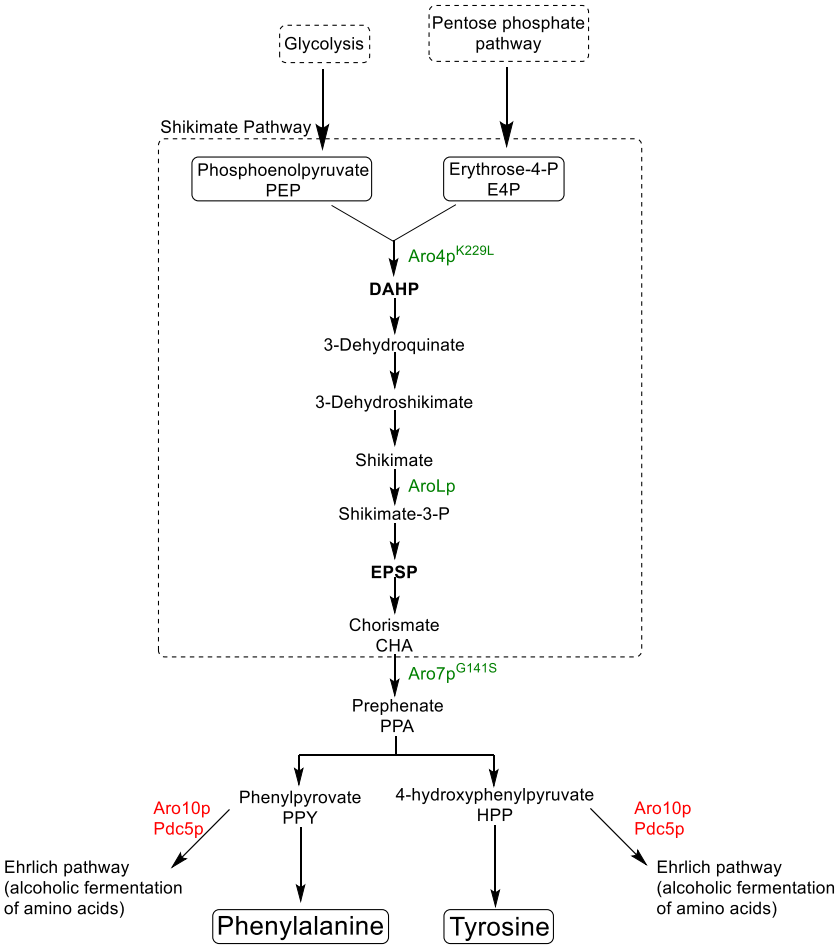

Figure 36: Schematic representation of the shikimate pathway in *S. cerevisiae* and the respective modifications reportd in Rodriguez et al., 2015. [151] Highlighted in green are the enzymes for overexpression and in red are the genes for deletion. DHAP: 3-deoxy-D-arabino-heptulosonic acid 7-phosphate, EPSP: 5-enolpyruvylshikimate-3-phosphate, Aro4: 3-deoxy-D-arabino-heptulosonate-7-phosphate (DAHP) synthase, Aro7: chorismate mutase, Aro10: phenylpyruvate decarboxylase, Pdc5: pyruvate decarboxylase.

The strategy mentioned above was selected considering the EasyClone kit, as highlighted and acquired in Chapter 2.2.3. This kit, generously provided by Irina Borodina from DTU, includes plasmids containing the necessary genes for modifying the shikimate pathway and a read-out system. A fast and uncomplicated implementation of a p-coumaric acid (p-CA) read-out method was possible. Only one additional enzyme, the tyrosine ammonia-lyase (TALp), responsible for deaminating tyrosine and directly converting it to p-CA (Figure 37), was required for this purpose. Furthermore, an HPLC method, already utilized in our laboratory, was customized to meet the measurement needs for p-CA (Chapter 4.10.1.1). [216]

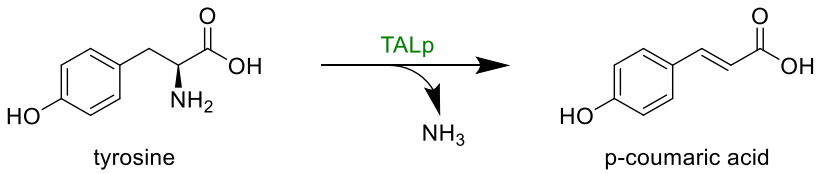

Figure 37: The reaction catalyzed by TALp involves the introduction of a double bond to tyrosine through deamination, resulting in the formation of p-CA.

2.3.1.1 PCRGate – Adaption, expansion, and implementation

A PCR-based cloning method was implemented to facilitate plasmid construction and cloning for the modification of the shikimate pathway and enhance molecular cloning capabilities within the research group, drawing inspiration from the principles of Golden Gate assembly and Green Gate cloning. [70,217] The Golden Gate assembly technique employs two enzymes for the *in vitro* restriction and ligation reaction, taking advantage of type IIS restriction enzymes with their ability to cut DNA at a defined distance from the recognition sequence. [218] This allows for the specific overlap of target DNA fragments. The critical aspect for the success of the reaction involves designing oligonucleotides so that the recognition site of the restriction endonuclease is excised, eliminating its presence in the newly T4 ligase-ligated product (Figure 38). Adapting and expanding the overhangs used to connect fixed modules, as demonstrated by Lampropoulos et al. in 2013, a template for designing oligonucleotides accommodating up to 9 DNA insert fragments was developed (Table S47 in Supplements). [217] Additionally, a destination vector (Table 7) with a distinct and differing antibiotic selection marker from the donor plasmid was prepared to facilitate rapid cloning and transformation, eliminating the need for an overnight (ON) *DpnI* reaction (Chapter 4.6.4.1). This new PCR-based PCRGate cloning technique allows for rapid cloning with ready-to-use plasmids, including sequencing, within a few days (Chapter 4.6.7.2). This was necessary due to the varying quality and efficacy of the in-house Gibson assembly mix, which too often posed challenges in cloning many fragments.

The process can be summarized in four steps: the primer design using the template (Table S47), the actual PCR, the restriction digestion with *Esp3I,* and ligation in one reaction, eventually followed by the transformation of *E. coli*. This process eliminates the need for *DpnI* digestion because of the antibiotic switch of the donor and target plasmid as well as the purification step after the PCR.

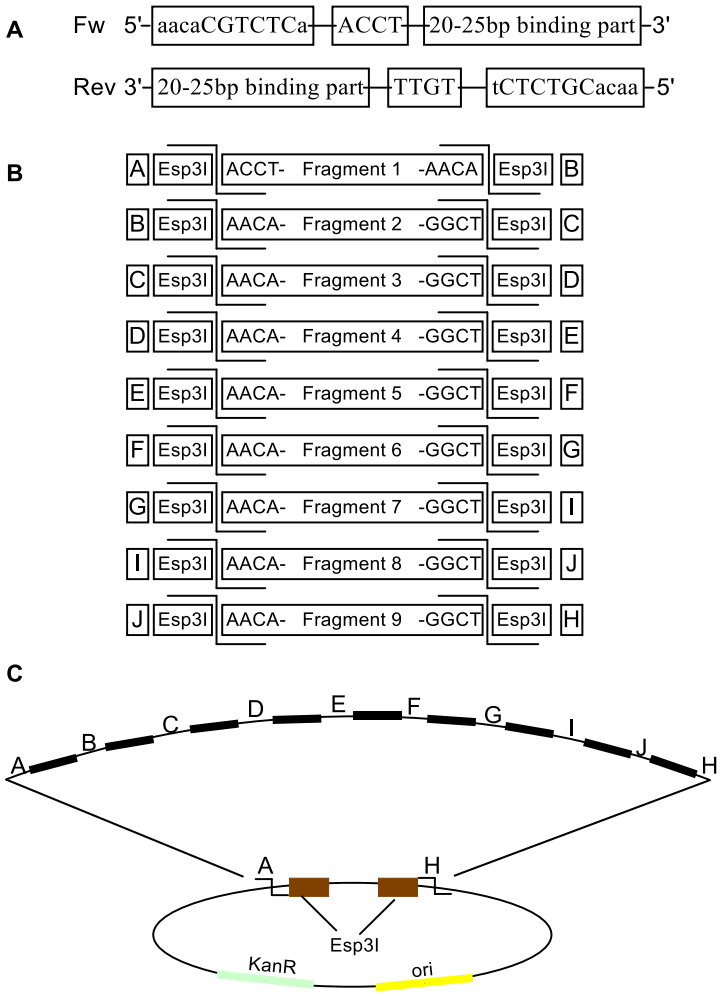

Figure 38: Graphic depicting the used PCRGate design. A) Oligonucleotide layout with the Esp3I recognition site, the 4 bp overlap and the complementary binding part of the oligonucleotide. B) The sequential assembly of the modules is achieved by 4 overlapping nucleotides of the 5'-end with the preceding modules' 3'-end. C) Scheme of the assembly process of the used PCRGate.

An example for the oligonucleotide design templates can be found in the Supplements and used for rapid cloning, speeding up the process to a grade where the desired plasmid can already be used within a few days (validation via sequencing included and completed). This method represents an inexpensive, versatile, and easy-to-use cloning method, especially when the Gibson assembly lacks the promised reliability. In conclusion, no extra equipment or other expensive material is needed compared to the prepared Gibson assembly (mix comprised of many ingredients).

2.3.2 Plasmid-based p-CA production as reporter compound

The necessary genes for the shikimate pathway modifications, as detailed in Table 4 and Figure 37, were provided by Irina Borodina from DTU on the plasmids p02747, pCfB9114, and p0872 (Table 7). [151] However, a brief standard nucleotide BLAST comparison unveiled that the provided TAL was not the TAL from *Flavobacterium johnsoniae* ($TALp_{Fj}$), as utilized in Rodriguez et al., 2015. Instead, the TALp from *Herpetosiphon aurantiacus* ($TALp_{Ha}$) was

included with the plasmids (Supplements 1.2vi). [151] Nevertheless, the obtained TALp$_{Ha}$ was also characterized alongside TALp$_{Fj}$ by Jendresen and colleagues, demonstrating comparable performance when expressed from the yeast genome compared to each other. The same study noted a significantly higher p-CA production yield when expressed from a 2µ-plasmid in relation to the genome-implemented versions. Unfortunately, this was only demonstrated for TALp$_{Fj}$, while TALp$_{Ha}$ was not studied similarly. [219]

Therefore, for the p-CA read-out system, a high-copy 2µ episomal plasmid expression approach was selected. The received TALp$_{Ha}$ was subcloned in the high copy number 2µ episomal plasmid pEpi-haTal-Ura3-2µ (Table 7). This mirrors the approach used for the malonyl-CoA detection, as a plasmid-based approach was opted to generate a reversible read-out system to monitor the progress of the shikimate pathway modifications without the need to finally remove the read-out mechanism from the genome.

To assess the anticipated yields of p-CA and whether there is a disparity in p-CA production in the two strains, previously generated (Chapter 2.1), the TALp$_{Ha}$ was then introduced via transformation into the producing strains of *S. cerevisiae* CEN.PK2-1C ST003 and ST004 (Table S43). Following the transformation of the yeast strains with the newly generated episomal plasmid (pEpi-haTal-Ura3-2µ), the colonies were cultured and compared against the wild-type cells without plasmids for each strain and in two media (YNB SC-mdeium and YPD medium, Figure 39). The tyrosine ammonia-lyase TAL converts the tyrosine to p-CA through deamination.

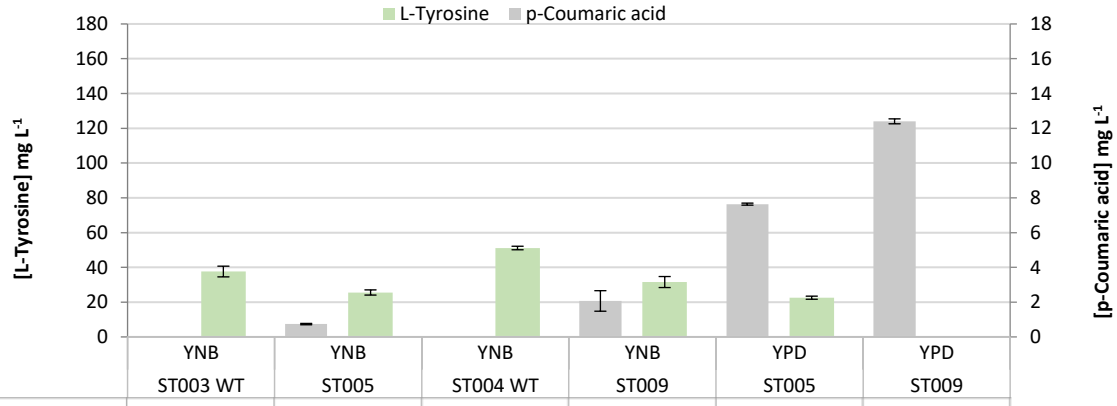

	YNB ST003 WT	YNB ST005	YNB ST004 WT	YNB ST009	YPD ST005	YPD ST009
tal$_{Ha}$ plasmid	-	+	-	+	+	+
ARO10::ARO4/7	-	-	-	-	-	-
PDC5::aroL$_{Ec}$	-	-	-	-	-	-

Figure 39: Effects the TALp$_{Ha}$ episomal plasmid-based overexpression has on tyrosine levels and p-CA in the WT strains ST003 and ST004 cultivated in YNB SC-medium and YPB medium. Green columns indicate the measured tyrosine concentration and grey columns the p-coumaric acid concentration. Signals were detected by HPLC-UV at 280 nm for tyrosine and 310 nm for p-CA. Cultivation was conducted in YNB SC-medium and YPD medium utilizing the Biolector, 72 h, 1200 rpm, 30 °C, 85 % humidity (Biolector, M2P labs GmbH, Germany).

Overexpressing $TALp_{Ha}$ in two nearly identical strains, distinguished only by one factor, led to significantly different p-CA concentrations. As anticipated, samples containing the wildtype yeast exhibited no detectable p-CA production (Figure 39). However, for cells harboring $TALp_{Ha}$, ST009 (ST004 + $TALp_{Ha}$) demonstrated over twice the p-CA concentration (2.07±0.59 mg L^{-1}) compared to ST005 (ST003 + $TALp_{Ha}$) cells (0.74±0.04 mg L^{-1}). When comparing p-CA production in YPD medium for both strains, better growth and production abilities were evident, as expected. Cultivating strain ST005 (ST003 + $TALp_{Ha}$) in YPD yielded 10 times the amount of p-CA than the same cultivation in YNB SC medium (7.64±0.058 mg L^{-1}). Similarly, for ST009 (ST004 + $TALp_{Ha}$), a 6-fold increase (12.4±0.14 mg L^{-1}) was achieved simply by changing the medium. These results highlight a notable discrepancy, with a more than 100-fold to 20-fold difference from the results reported by Rodriguez et al. in 2015 (>240 mg L^{-1}). In their study, the average producers using only tyrosine ammonia lyase already yielded 0.24±0.03 g L-1 despite utilizing a CEN.PK strain (CEN.PK102-5B). [151] A more recent Nature study obtained only 12.9 mg L^{-1} when using only plasmid-based $TALp_{Fj}$ (shake-flask, Feedbeads, 96 h), which is in line with the p-CA yields obtained in YPD medium (Figure **39**) and is only a little less than double the amount of ST005. [153]

As mentioned earlier, genomic $TALp_{Ha}$ performs as good as genomic $TALp_{Fj}$. [219] Comparing the results of Figure 39 with the 12.9 mg L^{-1} (Liu et al., 2019 [153]), these results indicate a similar performance of $TALp_{Ha}$ when expressed from a 2µ-plasmid, as this results were not reported so far. [219] Moreover, other studies only achieved similarly small titer of p-CA when using an episomal plasmid approach. Employing a *tal* from *Rhodobacter capsulatus* concentrations of 3.85 mg L^{-1} (batch, shaking flask, 120 days) and 1.7 mg L^{-1} (batch, shaking flasks, 72 h), respectively, only were attained in two other comparable studies. [152,156] The TAL used in these studies, was also characterised in the previously mentioned study (Jendresen et al., 2015, [219]), and produced only 50 % to 10 % p-CA compared to the $TALp_{Ha}$ or $TALp_{Fj}$, respectively. These differences (percentages) roughly match to the results presented (Figure 39 with $TALp_{Ha}$, 12.9 mg L^{-1} with $TALp_{Fj}$ [153]). The p-CA production from Figure 39, therefore, is realistic when compared to the amounts reported with similar approaches. However, taking Rodriguez and coworkers results as reference the results obtained here and in the comparable mentioned literature theoretically should reach around 20 to 100 mg L^{-1}. Interestingly, the production rates (12.9 mg L^{-1}[153], 3.85 mg L^{-1} [156], 1.7 mg L^{-1} [152]), do not align with the yields described by Rodriguez and coworkers (>240 mg L^{-1}, fed-batch medium, 72 h, 96 deep well plate). [151] In summary, all mentioned studies, including the results shown here, using comparable approaches yielded significantly lower p-CA concentration, with promotors of comparable strength (*pgk1* and *tef1* [67]) and similar strain backgrounds, partly with the same cultivation approach (fed-batch medium and

Feedbeads) or even better (shake flask vs. 96 deep well) and longer conditions (120/96 h vs. 72 h). [152,153,156,219]

The observed differences can likely be attributed to several factors: $TALp_{Ha}$ has a broader substrate specificity than $TALp_{Fj}$ and is only slightly less efficient in substrate conversion, producing just one-quarter and one-fifth of p-CA in *E. coli* and *L. lactis*, respectively. Moreover, plasmid-based expression with a 2µ origin of replication exhibited significant variability in copy number, leading to fluorescence fluctuations by up to two orders of magnitude. [67,219] However, these observations solely should not result in such significant differences in p-CA yield between Rodriguez et al. 2015 compared to the above-mentioned yields. The biggest impact most likely is the use of fed-batch medium cultivation, and given the fact that the medium switch from defined minimal to complete medium increased p-CA titers by up to 10-fold (Figure 39) shows that the used medium has the potential to increase compound production significantly. However, it is questionable whether the influence of cultivation can explain the aforementioned differences of 20 to 100-fold and more.

Despite these observed differences, it appears that even minor and unrelated factors can significantly impact compound biosynthesis. This impact can also be seen here for the ST004 strain, genotypically harboring a Mig1p binding site deletion (*Δmig1-bs*) that seems to affect the p-CA production by a factor of 2 to 4 (Figure 39). Both strains are otherwise identical in all aspects; the only difference is this deletion in the Mig1p binding site in the g*al4* promotor region, which further decouples glucose repression effects despite being unrelated to the modified pathway. [184]

In summary, it was successfully demonstrated that p-CA could be produced from a plasmid-based expression system, with yields that align with literature values. The exception is that there seems to be a discrepancy in reported p-CA yields from the reference work compared to the obtained results and those stated from comparable literature, indicating towards additional factors impacting p-CA production, with the cultivation conditions seemingly contributing the most. Furthermore, the unrelated deletion of *Δmig1-bs* in ST004 seems to positively affect p-CA yields. To further increase p-CA titer and tyrosine precursor levels, it was proceeded with the introduction of the planned modifications (Table 4).

2.3.3 Effects of *ΔPdc5::AroL* and *ΔAro10::Aro4/7* in ST003

The genes for $aroL_{Ec}$, $aro4^{K299L}$, and $aro7^{G141S}$ were subcloned in new integrative plasmids (Table 7). The new design ensures that implementing the genes for overexpression would simultaneously knockout the genes for decarboxylases *aro10* and *pdc5*. These two genes play crucial roles in fusel alcohol formation through decarboxylation of the α-keto acid variants of the transaminated (aromatic) amino acid in the Ehrlich pathway following the

tyrosine and phenylalanine biosynthesis. [220–223] This approach was intended to speed up the implementation process, to rapidly proceed with the combination of the pathway modifications and beyond. The following Figure 40 shows the results of the implemented modifications into the ST003 based strains.

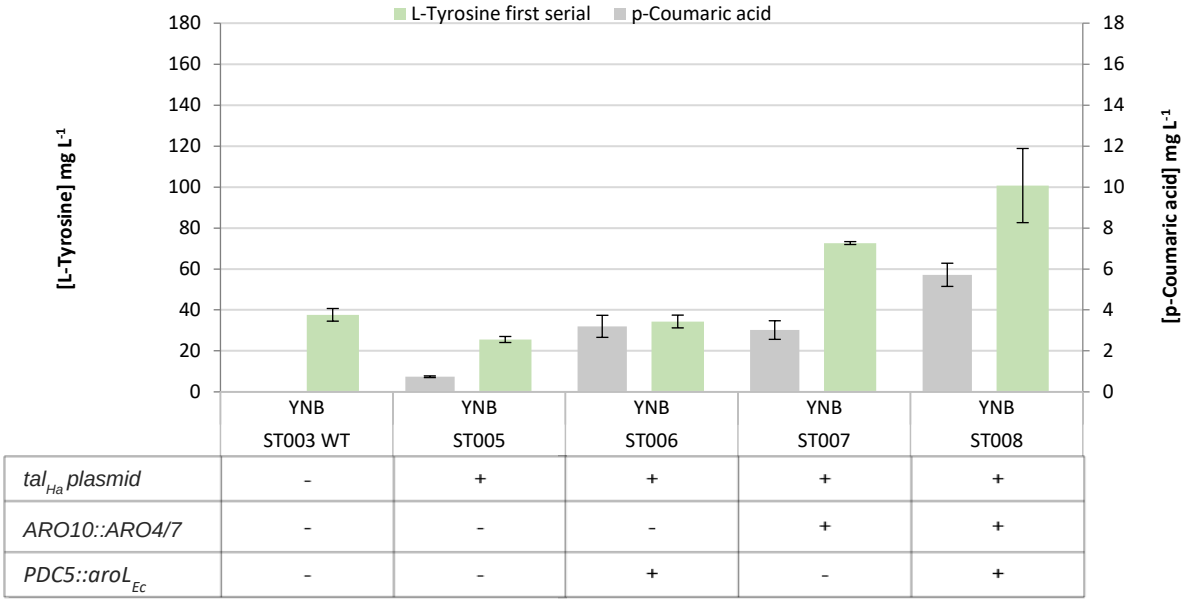

Figure 40: Production of p-CA in *S. cerevisiae* using ST003 as base strain, showing each modification and its effect. Green columns indicate the measured tyrosine concentration and grey columns that of the p-coumaric acid. Signals were detected with HPLC-UV at 280 nm for tyrosine and 310 nm for p-CA. Cultivation was conducted in YNB SC-medium utilizing the Biolector at 72 h, 1200 rpm, 30 °C, and 85 % humidity (Biolector, M2P labs GmbH, Germany).

The sequential incorporation of shikimate pathway modifications into strain ST003 increased the flux toward tyrosine and phenylalanine, leading to elevated intracellular levels, as indicated by higher p-CA signals. The signals reveal that p-CA concentrations for strains ST006 and ST007 are nearly identical, exceeding 3 mg L^{-1}. However, for the ST006 variant, the signal is slightly higher (+0.18 mg L^{-1}). The best cell line of each variant yielded nearly 4 mg L^{-1} in both cases (not shown), with the ST006 variant producing 0.1 mg L^{-1} more p-CA than the ST007 variant. Upon combining all modifications (*ΔPdc5::AroL* and *ΔAro10::Aro4/7,* ST008), the p-CA concentration nearly doubles (5.71±0.57 mg L^{-1}) compared to either ST006 or ST007 alone. Moreover, the best clone achieved more than double the concentration, with 6.67 mg L^{-1} of p-CA. This demonstrates a nearly perfect linear process with each modification and the combined modifications in p-CA production. The same trend can be observed when the tyrosine concentration is measured. This indicates that the conversion catalyzed by $TALp_{Ha}$ cannot keep up with the tyrosine production rates induced through the new modification. This observation aligns with the observations of Liu et al., 2019. TAL can act as a bottleneck; therefore, a PAL branch was implemented to generate p-CA from phenylalanine. [153] In addition to the YNB SC-medium, YPD medium is a standard, more nutritious medium for yeast cultivation. Cultivation in YPD medium was therefore tested in the following Figure 41.

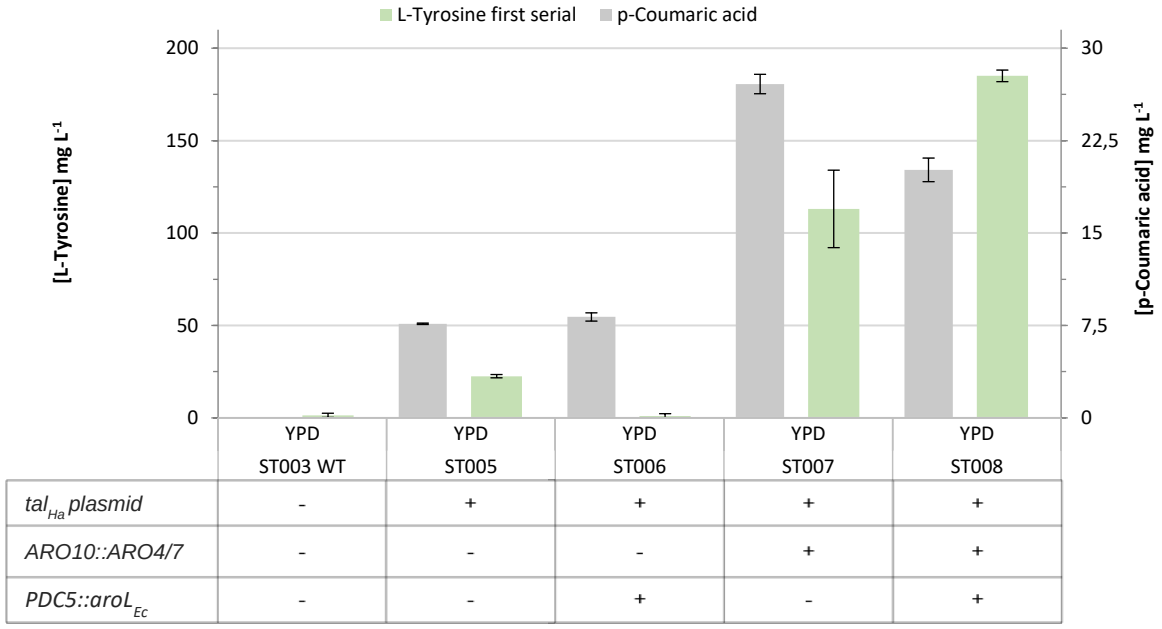

Figure 41: Effects on p-CA production in YPD medium on the modified ST005-8 strains based on ST003. Green columns indicate the measured tyrosine concentration and grey columns that of the p-coumaric acid. Signals were detected with HPLC-UV at 280 nm for tyrosine and 310 nm for p-CA. Cultivation was conducted in a YPD medium utilizing the Biolector at 72 h, 1200 rpm, 30 °C, and 85 % humidity (Biolector, M2P labs GmbH, Germany).

Comparing the results on p-CA production in YNB SC medium and YPD medium for each strain (ST005-8) reveals, as expected, better growth and production abilities in YPD (Figure 40 and Figure 41). Cultivating strain ST005 in YPD gave 10 times the amount of p-CA than the same cultivation in YNB SC-medium (0.74±0.04 mg L vs. 7.64±0.058 mg L^{-1}), even surpassing the full modified ST008 in YNB SC-medium (5.71±0.57 mg L^{-1}). In comparison, strain ST006 shows only a 2.5-fold increase (8.19±0.33 mg L^{-1}), whereas ST007 displays a 9-fold increase (27.09±0.79 mg L^{-1}) in p-CA yield when compared to their YNB SC medium equivalents. Surprisingly, using the fully modified strain ST008 cultivated with YPD did not increase the p-CA concentration (20.13±0.96 mg L^{-1}) compared to ST007.

These results, and the maximum 10-fold increase in p-CA concentration, are consistent with the findings in Chapter 2.3.2. Although ST008 yielded relatively low concentrations, this could be attributed to the 2µ plasmid variability mentioned before or to the previously reported phenylalanine feedback inhibition of the prephenate dehydrogenase *tyr1* reported. This inhibition could be alleviated by introducing a heterologous TYR1p or reducing the phenylalanine pool by implementing a phenylalanine ammonia-lyase (PAL) branch. [67,153,209]

However, when considering the 5.71 mg L^{-1} yielded in YNB SC-medium and applying the factors of 6 to 10 by which the other strains (ST005, ST007) increased upon media change, ST008 should theoretically produce up to 57 mg L^{-1}. Even when only combining the yields of

ST006 and ST007, a theoretical p-CA production concentration of around 35 mg L^{-1} could be expected.

These results are 30 to 50 times lower than the p-CA production in Rodriguez et al., with a strain modified similarly. Considering the difference in cultivation conditions, applying the feed-in-time or fed-batch medium with the generated strains presented here, would likely generate p-CA titers in the same range. Besides the used media, the differences could additionally be attributed to the different locations of the implemented genes. Rodriguez et al., 2015 employed previously characterized integration sites specifically selected for genome modification and overexpression. [62,63] Comparing the result with strains having similar modifications (*aro4+aro7*) from the literature, Moa and colleagues obtained nearly the same p-CA amount (6.4 mg L^{-1}) as ST008 in YNB SC-medium (5.71 mg L^{-1}), lacking only the *aro10* and *pdc5* deletions but instead used the *eno2* and *tal1* genes to direct flux towards E4P. [152] On the other hand, Suástegui and coworkers showed that the overexpression of *tal1* to increase E4P supply, actually decreased target compound production, which could explain the low titers Mao and colleagues reported. [152,166] ST008 cultivated in minimal medium reached nearly the same amount, as stated by Mao. Cultivating ST008 in YPD reaches more than 3 times the amount, underscoring that the elimination of the precursor loss to the Ehrlich pathway has a bigger impact on p-CA yield than the E4P supply. This is further supported by Li as well as Liu and coworkers, achieving nearly 6 to 10-fold higher titers (compared to Mao et al., 2017) with the same modifications (without *tal1*) used here (49.821 mg L^{-1} Li et al., 2020, 35 mg L^{-1} Liu et al. 2019). [153,156]

Nevertheless, the relatively low p-CA yields reported here, together with the results from similar studies with comparable and even longer cultivation conditions (35 mg L^{-1} at 96 h, YNB SC-medium, feed beads and 49 mg L^{-1} at 120 h, YNB SC-medium, shaking flasks), show a significant discrepancy when comparing the results from Rodriguez et al., 2015. [153,156] Liu and coworkers (same group and supervision) mentioned this discrepancy in their studies, coming to the same conclusion and attributing it to the suspected difference in cultivation conditions. For their summarizing study on p-CA producing modification published in Nature, they reproduced the same modification in the same manner as reported in Rodriguez et al., 2015, with the same, but longer (96 h) cultivation conditions applied here (batch, 2 % glucose), stating to yield only 22.3 mg L^{-1} p-CA. [153] This is perfectly in line with what was reported above using a shorter cultivation time (72 h), even exceeding the 22.3 mg L^{-1}, with the single *ΔAro10::Aro4/7* integration, showing the suitability and comparability to the established literature for the adapted and altered engineering approach. This approach was also implemented in the second production strain ST004 used and generated in our working group, as the plasmid-based test of Chapter 2.3.2 yielded even better p-CA production results with this strain.

2.3.4 Effects of *ΔPdc5::AroL* and *ΔAro10::Aro4/7* in *Δmig1-bs* ST004

The parent strain ST004, in all aspects identical to ST003 except the *Δmig1-bs* deletion in *gal4*, underwent the same modification procedure in consecutive order, mirroring the approach taken with ST003 in the previous chapter. However, it is immediately apparent that the measured concentrations of p-CA are significantly higher than their corresponding variants when ST003 was used as the parent strain. This can be seen in Figure 42 compared to Figure **40**.

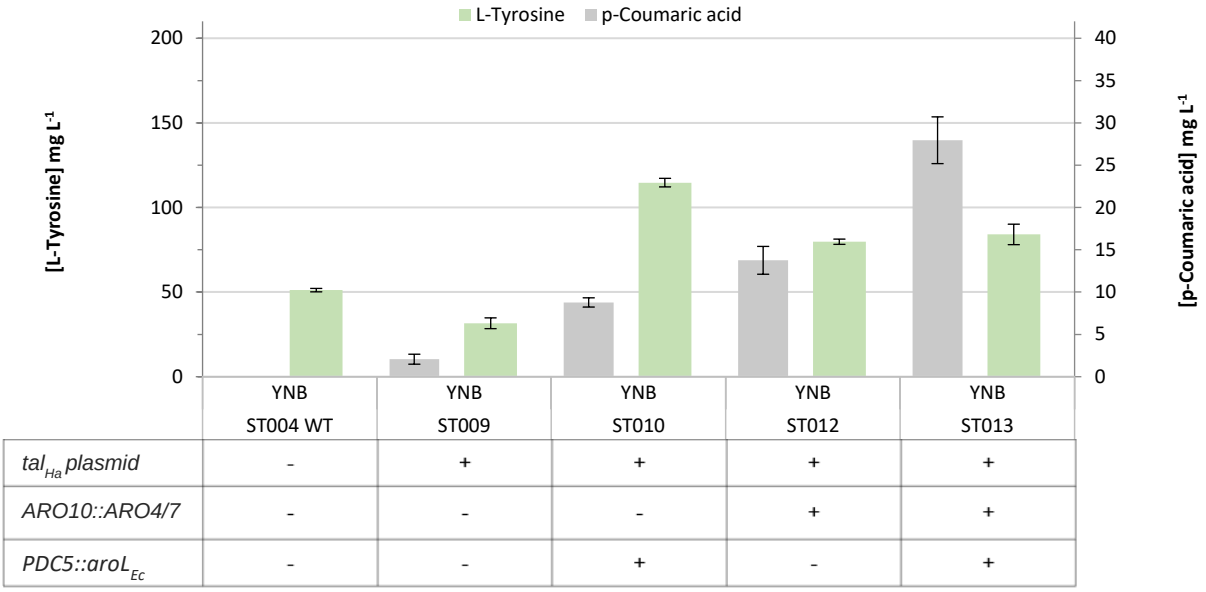

Figure 42: Production of *p*-coumaric acid in *S. cerevisiae* using ST004 as parent strain, showing each modification and its effect in YNB SC-medium. Green columns indicate the measured tyrosine concentration and grey columns that of the p-coumaric acid. Signals were detected with HPLC-UV at 280 nm for tyrosine and 310 nm for p-CA. Cultivation was done in YNB SC-medium, 72 h, 1200 rpm, 30 °C, 85 % humidity (Biolector, M2P labs GmbH, Germany).

Upon examining the p-CA concentrations in each strain, a gradual, step-by-step increase is observed with each modification step (Figure 42), albeit not as pronounced as when ST003 was the parent strain (Figure 40). Unlike ST006 and ST007, showing nearly the same p-CA concentration, the strains ST010 and ST012 yielded p-CA concentration, on average, 2.7 to 4.5 times higher than their counterparts above (Figure 40), with ST012 surpassing ST010 by more than one-third (8.71±3.2 mg L^{-1} p-CA for ST010 and 13.75±1.64 mg L^{-1} p-CA for ST012).

Combining *ΔPdc5::AroL* and *ΔAro10::Aro4/7* in ST013, unlike in ST008, not only doubles the p-CA concentration but, on average, nearly triples it (27.95±2.76 mg L^{-1}) compared to the single modification of ST010. The best cultivation sample measured even gave 4 to 6 times the amount of p-CA (55.12 mg L^{-1}). This batch approach in minimal medium nearly matches the results of Li and Liu and coworkers with their extended and improved cultivation conditions discussed in the previous Chapter 2.3.3, and even exceeds the stated

22.3 mg L^{-1} at 96 h cultivation with the same reproduced modifications by Liu et al., 2019. [153] When using feed beads, they could double that amount ([153] in supplements, ~45 mg L^{-1}), meaning that applying the same conditions here, the strain would likely exceed theirs, reaching probably 55-60 mg L^{-1} or even more, given the fact that the best single producers already exceeded that amounts in a batch approach (55.12 mg L^{-1}). This means at least a 25 % improvement compared to the results reported in the literature. Mirroring the medium change from YNB SC-medium to YPD medium as reported before, Figure 42 shows this approach for ST009-13.

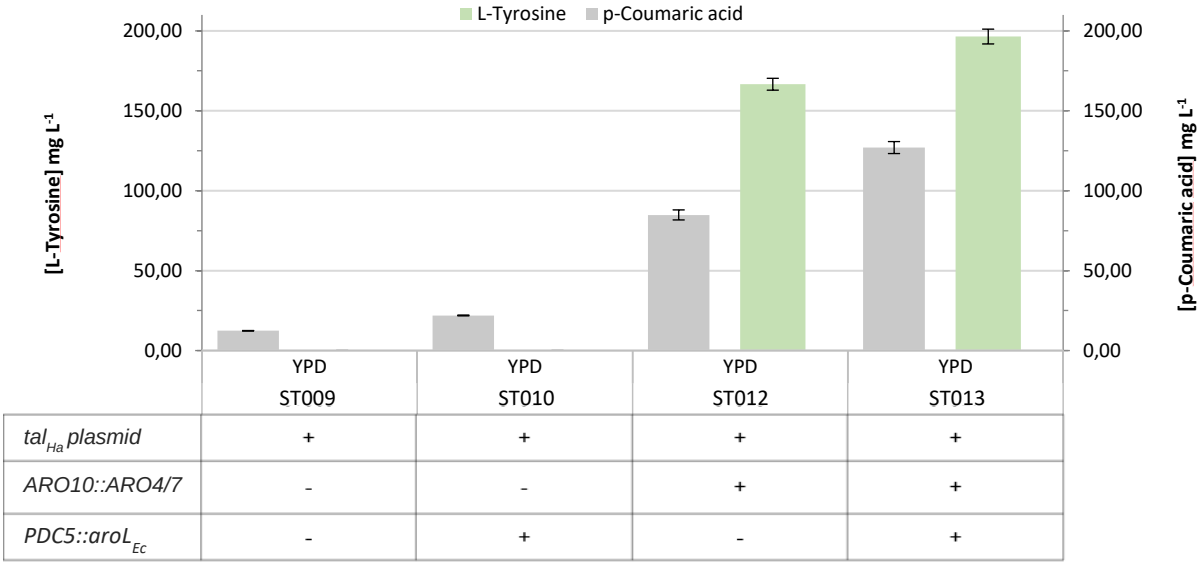

Figure 43: Production of *p*-coumaric acid in *S. cerevisiae* using ST004 as parent strain, showing each modification and its effect in YPD medium. Green columns indicate the measured tyrosine concentration and grey columns indicate that of the p-coumaric acid. Signals were detected with HPLC-UV at 280 nm for tyrosine and 310 nm for p-CA. Cultivation was conducted in YPD medium, 72 h, 1200 rpm, 30 °C, and 85 % humidity (Biolector, M2P labs GmbH, Germany).

As observed previously and in the prior chapter during the plasmid-based p-CA production test, the shift from YNB SC-medium to YPD increased p-CA titers. When comparing ST003-based strains (ST005-8) with its p-CA production, ST004-based strains (ST009-13) presents a similar but distinct pattern. Initiating with notably superior production capabilities in minimal medium, as described earlier, ST009 to ST012, like the ST005 to ST008 samples, exhibits an upward trend in p-CA production in YPD with each modification, although the progression is more linear. Cultivating ST009 in YPD medium yielded one-third more p-CA (12.4±0.14 mg L-1) than under the same conditions as ST005 (ST003 based, 7.64±0.058 mg L^{-1}). Strains ST010 and ST012 show increasing p-CA concentrations with each step, culminating in ST013, which combines both modifications, reaching an average of 127.01±3.74 mg L^{-1} p-CA. This represents a 6-fold increase compared to ST010 and one-third more than the ST012 strain. Switching cultivation conditions from YNB SC-medium to YPD medium with ST004-based strains significantly increases the p-CA production of 2- to 6-fold between the different media with the same strains. Nonetheless, this improvement is not as

substantial as for the ST003-based strains, where a 6-fold increase was the minimum. However, the overall yield is significantly higher when comparing strains with the same modifications. For instance, ST012, compared to ST007, shows 3 times higher p-CA product concentration.

These results were obtained under non-improved batch cultivation conditions without additional feeding or modified media. [151,153,155,224] As discussed earlier (Chapter 2.3.3), the presented results are realistic and comparable with similar approaches from the literature compared with ST003-based and modified strains, considering comparable cultivation conditions. [152,153,156] However, with the ST004-based modified strains, the p-CA titers reached up to 130.60 mg L^{-1} in the best cultivation sample (ST013), exceeding the comparable results from the previous chapter by at least 2-fold (theoretical ST008 yield of 55 mg L^{-1}) up to 3.7-fold (theoretical ST008 additive yield (~35 mg L^{-1}) and Liu et al., 2019 with 35 mg L^{-1}). [153] As stated by members of the same working group, the results of Rodriguez et al., 2015 could not be achieved by applying batch cultivation conditions with elongated cultivation time. [153] However, when ST013 was compared to those results, it exceeded them by 25 % with shorter cultivation conditions (results above). Applying the same cultivation conditions to ST013, p-CA titers of 1.9 g L^{-1} and higher could be reached, as described by Rodriguez and coworkers. Even applying the doubling rule of thumb deduced from the supplemented results by Liu and coworkers to ST013 cultivated in YPD medium using Feedbeads with 96 h cultivation time would likely already yield 260- mg L^{-1} only if doubled. However, the different media additionally increased the yield to 4.7-fold, potentially reaching 1.2 g L^{-1}. These theoretical considerations reveal that the strains generated here are on the same level or even better, with the same (*aroL*$_{Ec}$, *aro4*^{K299L}, and *aro7*^{G141S} and Δ*aro10* and *Δpdc5*), however, slightly different modifications (integration into *aro10* and *pdc5* unlike X3 targeted integration) identified from the existing literature. Further cultivation would prove this and maybe even surpass the calculations and results from the reference study.

Exploring further enhancements for these strains could involve the additional incorporation of the phenylalanine ammonia-lyase (PAL) branch. In a direct comparison, Liu and colleagues demonstrated the superiority of the PAL branch (producing p-CA via phenylalanine) by employing a phenylalanine ammonia lyase (*pal2*$_{At}$), cinnamic acid hydroxylase (*c4h*$_{At}$), and a cytochrome P450 reductase (*atr2*$_{at}$) from *Arabidopsis thaliana*, along with a cytochrome B5 (*CYB5*) from *S. cerevisiae.* This PAL branch exhibited significantly higher efficiency (337.6 mg L^{-1}) compared to the TAL branch (12.9 mg L^{-1}) used here. [153] This outcome seems counterintuitive since tyrosine concentrations are often reported to be higher than phenylalanine. [225,226] This branch, which involves two additional steps to form p-CA via cinnamic acid, appears to be more complex than the simple conversion of tyrosine to p-CA in one step. In this context, the involvement of the two additional enzymes appears crucial

for achieving high and efficient p-CA production from this particular branch. Implementing the PAL branch in the ST013 strain has the potential to yield p-CA titers exceeding 600 mg L^{-1}, as reported by Liu and colleagues. [153]

A comparison of ST013 with the final strain of Li and colleagues, featuring modified fermentation conditions yielding 11.342 mg L^{-1} of caffeic acid at a maximum p-CA concentration of below 90 mg L^{-1}, suggests that ST013 could surpass these results under the same conditions. [156] Despite representing the highest reported p-CA concentration to date (12.9 g L^{-1}) in a heavily modified strain [153], almost testing everything potentially impacting p-CA production, further improvements could be explored. In addition to the reported modifications, deleting phenylacrylic acid decarboxylase (pad1) and ferulic acid decarboxylase (fdc1) might enhance p-CA concentration. These decarboxylases convert p-CA to 4-vinylphenol in *S. cerevisiae* and have not been reported in the context of p-CA production on the scale mentioned. [156,224,227] Considering additional modifications to the cultivation conditions is also crucial, as higher p-CA production rates were reported at pH 6 compared to pH 4.5 (13.65 and 9.45 mg L^{-1} h^{-1} at pH 6 and 4.5, respectively). [224] If the objective is to further increase the p-CA production or just the tyrosine and phenylalanine levels the work of Liu and colleagues can be utilized as template, either to pick the modification that seems suited or to identify new targets or potential directions to further explore an improve production capabilities, achieving comparable or even higher results. A step in this direction could be the use of strain ST004, which appears to be suitable and for the production of compounds derived from the shikimate pathway, and additionally also research into the reasons for this could be interesting.

In general, the conversion of tyrosine to p-CA works better in ST004 than in ST003. This difference is evident even with the plasmid-based variants, where p-CA concentration in ST005 is less than half of that in ST009, and the difference gets even more substantial with further modifications. Considering this concentration difference between ST004 and ST003, the *mig1* binding site deletion in *gal4* and the resulting increased transcription and translation of *gal2* (galactose permease), *gal5* (phosphoglucomutase), g*al7* (galactose-1-phosphate uridyl transferase), *gal10* (UDP-glucose-4-epimerase), somehow affects p-CA production in yeast. Normally, with ST004 lacking *gal80* and the *mig1* binding sites, the *gal* genes are activated when galactose enters the cell (constitutive active GAL2p), inducing *gal*-promotors, even when glucose is present. Nevertheless, this is not expected to impact other metabolic pathways or contribute additional energy to glycolysis by providing glucose-6-phosphate from galactose conversion, as the *gal1* deletion renders galactose inaccessible for conversion. The *mig1* deletion primarily serves to further decouple *gal4* transcription initiation of the *gal* genes, leading to constitutively active *gal* promoters in CEN.PK2-1C yeast strains. [228] However, the Mig1 protein affects not only the galactose gene expression but also influences several

hundred other genes and factors, including TEF1, PGK1, ARO9, and TAT1 (amino acid transporter for tyrosine). [229,230] While the Mig1 deletion decouples *gal4* transcription initiation of the *gal* genes, positively affecting p-CA production in ST004-derived strains, the precise impact of the deregulated Gal-network or the slightly more available Mig1p remains to be fully understood. It is essential to acknowledge that the complexities of cellular metabolism and genetic interactions make it challenging to predict outcomes precisely. Whether due to the interconnected nature of cellular processes and pathways, unforeseen impacts on feedback regulation, or the initiation of stress responses inducing metabolic changes to cope with the altered conditions, detailed experimental analyses and further investigations would be required to unravel the underlying mechanisms conclusively.

As described and reported in Chapter 2.3 and following the identified integration approach of the desired modifications (Figure 36) to increase the flux through the shikimate pathway, enhancing tyrosine and phenylalanine as potential NP precursors was successful. Achieving p-CA titers comparable to or surpassing those reported in the literature was achieved using simple unmodified batch cultivations. Extrapolating the reported results of the achieved strains to the cultivation approach stated in the literature, possibly optimizing the pH, could generate p-CA titers in the vicinity or even higher than those reported in Rodriguez et al., 2015 which served as the template for the work in this chapter. Therefore, additional cultivation with automated feeding using tools like the Robolector and Biolector (M2P labs GmbH, Germany) or a Bioreactor would be needed. With such approaches, titers exceeding 1 g L^{-1} can easily be possible.

2.4 Part 4 – Combining malonyl-CoA and shikimate pathway modifications

The synthesis of pharmacologically and biotechnologically interesting compounds often requires not only precursor molecules derived from aromatic amino acids such as phenylalanine or tyrosine but also involves the use of acetyl-CoA or malonyl-CoA, particularly in the context of PKS-NRPS hybrid megasynthases. This was exemplified by case of cryptophycin in Chapter 2.1 or indicated by the potentially beneficial effect when working with aromatic phytocannabinoids. [49,174,214] Another commonly cited example is resveratrol, which utilizes three malonyl-CoA molecules and one tyrosine derivative, p-CA-CoA. [31,35,153,231] Numerous publications have explored the elevation of these precursors, describing products derived from the shikimate pathway and malonyl-CoA pathway. [76,93,101,106,109,110,134,151–153,155,156,224]

The previous chapter demonstrated the successful introduction of reported modifications, leading to the development of new yeast strains capable of providing heightened levels of tyrosine, phenylalanine, and malonyl-CoA, as reported in earlier results. [76,151] The

integration of these two pathways within a single yeast strain was envisioned to establish a robust platform for heterologous compound production based on these precursors, aligning with the overall objective of this research. This potential had already been showcased in existing literature. [31,153]

Chapter 2.2.1 and 2.3.1 laid out the planned and implemented modifications, initially designated as mere reproduction work, serving only as the foundation to the combined production capabilities of both pathways, allowing for the combinatorial synthesis of compounds such as resveratrol or cryptophycin. Figure 44 summarizes the aimed combination of modifications to be implemented in the newly realized production strains based on *S. cerevisiae* CEN.PK2-1C in our research group.

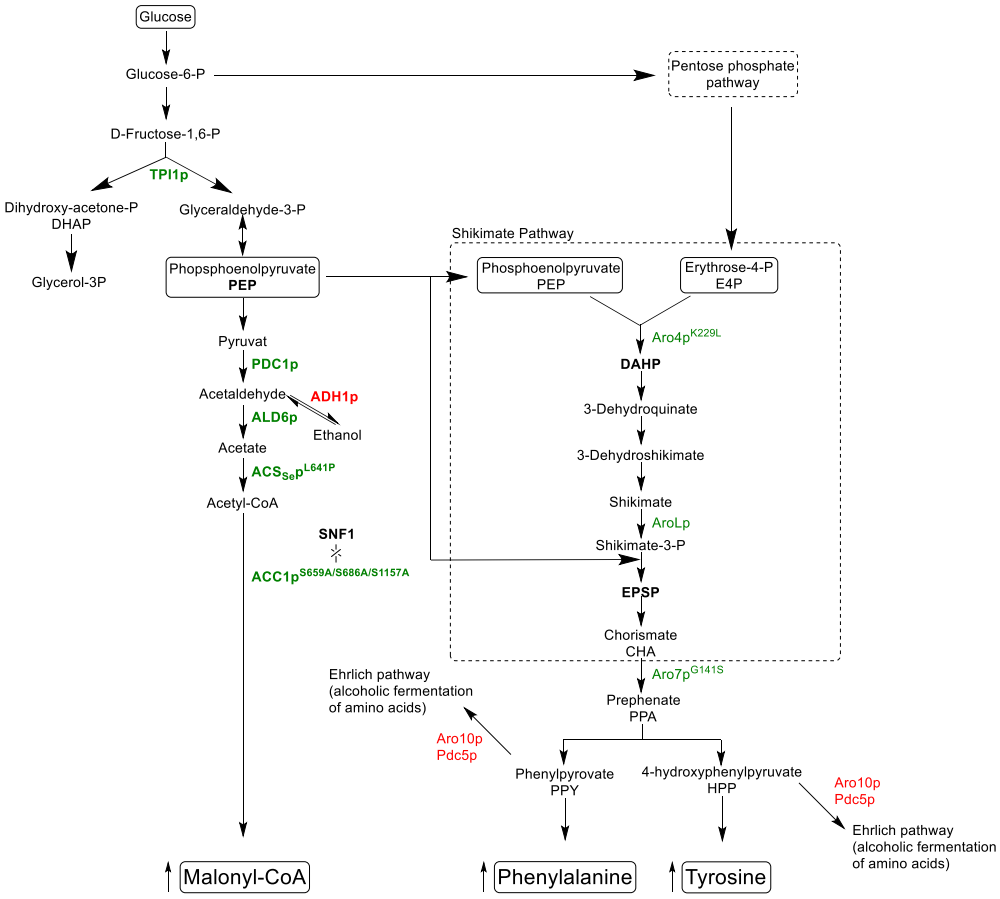

Figure 44: Summery of the modifications implemented in yeast as production strain illustrated in Chapter 2.2, elevating malonyl-CoA levels and Chapter 2.3, improving phenylalanine and tyrosine provision. Overexpressed enzymes are shown in green, and deletions are highlighted in red. Glucose-6-P: glucose-6-phosphate.

Based on the strains and modifications implemented from the malonyl-CoA section (Chapter 2.2) the modifications for the shikimate pathway presented in Chapter 2.3 were subsequently introduced, with the goal of at generating a strain that incorporates modifications for both pathways.

2.4.1 Combining shikimate and malonyl-CoA pathway in a single strain

The yeast strain serving as the basis for implementing the shikimate pathway was ST023, as introduced in Chapter 2.2. This strain selection was motivated by the ease of removing the mcr_{Ca} plasmid, along with the exhibited yields and the highly parallelized engineering approach for both pathways. However, time constraints and challenges in further investigations limited the exploration of alternative strains. Nevertheless, experiments and modification approaches were conducted, including implementing the same modifications into ST025 and the malonyl-CoA pathway modifications into the high p-CA producing strain ST013. Unfortunately, by the end of this study, positive results for these efforts were not achieved.

In contrast, the successive implementation of *Δaro10::aro4-aro7* and *Δpdc5::aroL*$_{Ec}$ into the ST024 strain was successfully carried out, as depicted in Figure 45.

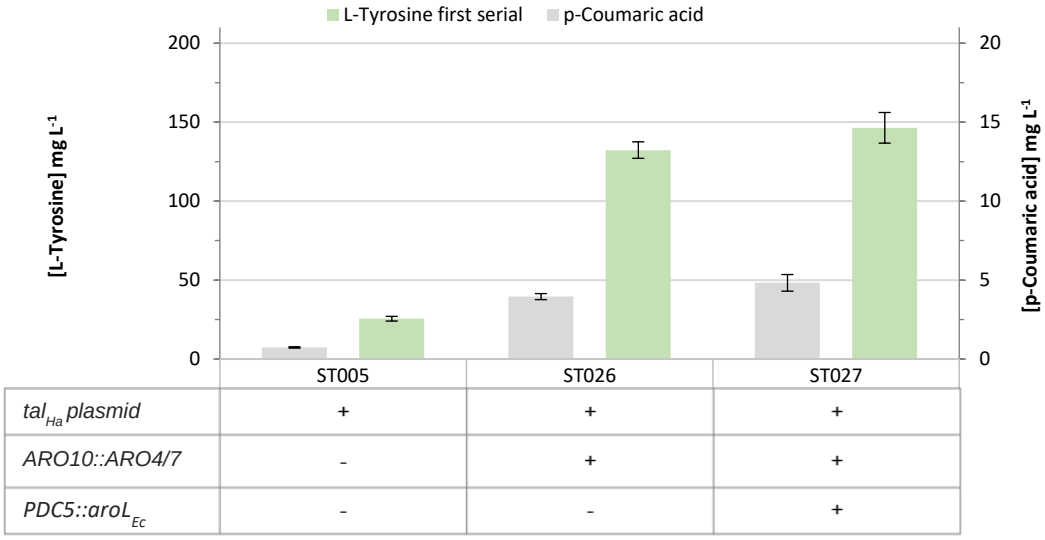

Figure 45: Effects of the sequential strain modification on p-CA and tyrosine production in ST026 and ST027 based on strain ST024. Green columns indicate the measured tyrosine concentration and grey columns that of the p-coumaric acid. Signals were detected with HPLC-UV at 280 nm for tyrosine and 310 nm for p-CA. Cultivation was conducted in YNB SC-medium utilizing the Biolector at 72 h, 1200 rpm, 30 °C, and 85 % humidity (Biolector, M2P labs GmbH, Germany).

Following the integration of all modifications into ST027, the strain produced nearly 5 mg L^{-1} of p-CA, with the best-producing single cultivation of almost 6 mg L^{-1}. These results align with those reported for strain ST008, including the significant increase in p-CA production and tyrosine levels upon *Δaro10::aro4-aro7* implementation compared to the wildtype or plasmid-containing strains. Figure 45 also includes ST005 as a plasmid-only reference, given the measurement challenges preventing the use of ST024 in the same configuration. These measurements could not be repeated. Therefore, the results for ST005 were used, hence its similarities to ST024 (same basis strain, ST003). The p-CA titer increased in the same manner as reported before for ST005 compared to ST006 (0.74±0.04 mg L^{-1} compared to 3.20±0.54 mg L^{-1} (ST006)). However, the improvement is slightly higher in ST026 than in

ST006 (+20 %). This is also supported when comparing the tyrosine levels of ST003 (no $TALp_{Ha}$) with ST024 (no $TALp_{Ha}$) and ST024 with ST028 (no $TALp_{Ha}$ + *Δaro10::aro4-aro7*). ST024 generally shows a higher tyrosine level than the wildtype ST003 strain and the improvement in tyrosine titer from ST024 to ST028 is more than 2.6-fold (Supplements 1.2vii). This alone further emphasizes the positive impact of malonyl-CoA modifications on tyrosine production and the *Δaro10::aro4-aro7* significantly increases p-CA level and the original target, tyrosine.

However, ST027 exhibited a more modest increase in p-CA and tyrosine levels (only +20 to 10 %), falling short of the improvements observed in ST008, representing a nearly 2-fold (p-CA) and plus 30 % (tyrosine) increase in ST008 (Figure 40). Comparing tyrosine levels of ST027 and ST029 (no $TALp_{Ha}$ + *Δpdc5::aroL*$_{Ec}$) supports the marginal 10 % improvement upon *Δpdc5::aroL*$_{Ec}$ introduction in ST027 (Figure 45 and Supplements 1.2vii). This raises questions about the effectiveness of the *Δpdc5::aroL*$_{Ec}$, suggesting that the modification may not function optimally in strains with elevated malonyl-CoA levels, or it might not have been successfully implemented. Consequently, these results would originate from variations occurring during cultivation. Hence, the genomic implementation could not yet be verified in the end. Nonetheless, an improvement, albeit small, can be concluded based on the combined and verified results reported in both Chapter 2.3 and the results in this section.

A notable observation, comparing the same cultivation conditions, is the apparent synergistic effect of malonyl-CoA modifications on p-CA and tyrosine production. This synergy is evident in the comparison between ST026 (3.96±0.19 mg L^{-1}) and ST007 (3.20±0.54 mg L^{-1}) for p-CA, and particularly pronounced on tyrosine levels, between ST027 (146.44±9.69 mg L^{-1}) and ST008 (100.72±18.10 mg L^{-1}, Figure 40). A similar pattern is observed when comparing the tyrosine levels of wildtype ST003 with fully malonyl-CoA modified strain ST024 (based on ST003), showing an 8-fold increase despite the relatively low initial tyrosine concentrations, as described above (Supplements 1.2vii).

This observed effect, coupled with the insights from previous chapters, underscores the success of the double pathway enhancement in ST027. The potential metabolic pull effect, possibly facilitated by increased malonyl-CoA production, directs the flux through glycolysis. This probably leads to improved provision of PEP from glycolysis and E4P from the pentose phosphate pathway. Similar approaches employing enforced downstream pull effects were reported for ergosterol and mevalonate in *S. cerevisiae*. [137,232]

As discussed in the previous chapter (Chapter 2.3), the lower yields of p-CA compared to literature results are likely attributed to differences in cultivation conditions. Notably, Liu and coworkers reported similarly low p-CA yield when reproducing the same modifications employed by Rodriguez and coworkers. [153] This trend becomes evident when comparing similar engineering efforts from other studies, where batch cultivations only achieved

approximately 20 mg L^{-1} titers. [152,154,156] Underscoring this discrepancy with attention-seeking reports of exceptionally high p-CA titers in the reference literature. [151] Furthermore, the limited to negligible improvements observed in transitioning from single modified strains to the fully engineered ones (ST007 to ST008 in YPD medium (Figure 41) and ST026 to ST027 (Figure 45)) could be attributed to a bottleneck in TYR1p, as discussed earlier. Addressing this inhibition of TYR1p by phenylalanine can further enhance p-CA production and subsequently increase flux towards tyrosine and phenylalanine. This enhancement was demonstrated by introducing the PAL-branch, using feedback-resistant TYR1p (*Medicago truncatula*) or a bi-functional phenylalanine/tyrosine ammonia lyase (PAL/TAL). [31,153]

Combining both pathways in a single production strain, as intended here, was previously illustrated to be highly promising for resveratrol production, even reaching the highest titers reported so far (1155.0±14.3 mg L^{-1}, batch cultivation). Remarkably, this was achieved with fewer modifications to enhance malonyl-CoA titers compared to the present work, involving only *acc1* and *acs*. Consequently, it was concluded that malonyl-CoA is likely not the limiting factor, suggesting that excessively high levels may not be crucial for heterologous compound production using malonyl-CoA and amino acids. [31] Therefore, the focus on engineering the flux through the shikimate pathway becomes more critical for heterologous compound production in yeast. This observation is anticipated to be applicable to the biosynthesis of compounds such as cryptophycin, using similar amounts of malonyl-CoA units as resveratrol; however, it involves tyrosine and, presumably, phenylalanine derivatives (Figure 12). [174] Shifting the metabolic engineering efforts from malonyl-CoA to the additional utilization of phenylalanine, achieved through a bifunctional ammonia lyase or a dedicated phenylalanine ammonia lyase (PAL), holds the potential to further increase the flux through the shikimate and AAA pathway (see above). This strategic shift would also be advantageous for cryptophycin biosynthesis, where cinnamic acid, a product of such ammonia lyases, is presumed to initiate the PKS-NRPS biosynthesis. [174]

These insights, however, overlook the challenges reported with the reported results and approach in Chapter 2.2. It was demonstrated in that section that the applied engineering efforts could increase malonyl-CoA levels detected through 3-HP. This implies that malonyl-CoA is provided at higher levels, as reported in Meng et al., 2023 with a single integrated *acc1.* However, in this work, the use of the triple mutated *acc1****, along with the upstream modifications, proved not to be the bottleneck in, for instance, resveratrol biosynthesis. Combining the above-reported strains (ST026 or ST027) with the feedback-alleviating approach for TYR1p will likely yield resveratrol titers in the same range (around 1 g L^{-1}) as reported in previous work. [31] Taking that further, the best p-CA-producing strain (ST013) could further be engineered for malonyl-CoA provision, as it was already started but could not provide positive results at the end of this work. For instance, with the introduction of the

multicopy TY4, or even better with TY1 (favorable growth behavior) *acc1* integration and the potential incorporation of a bi-functional PAL/TALp, this potentially achieves comparable amounts of resveratrol or analogous compounds. This prospect is particularly interesting since the resveratrol titer was the highest reported so far, only using single integrations with moderate malonyl-CoA provision modification, unlike the approach reported here.

In summary of the considerations presented here, the engineering efforts undertaken here align with comparable approaches documented in the literature. Consequently, the results and observations stated in existing studies can be theoretically transferred to the results obtained in this work. It is plausible that, with further simple cultivation experiments and a few more modifications, potentially incorporating a stilbene synthase for resveratrol production, similar, if not improved, results reported in the literature could be attained. Especially when the cultivation condition would be adjusted to mirror those employed in previous studies, including the extended cultivation times of 96 to 120 h, in contrast to the 72 h utilized in this work. [31,152–154] Further investigations are required.

In conclusion, summarizing the outcomes of this work: the initial project involving the implementation of the PPTase sfp_{Bs} via CRISPR/Cas9 was successfully carried out, including assessments of gene transcription and enzyme functionality, conferring ACP/PCP activation ability for PKS, NRPS, and similarly working synthases for respective compound biosynthesis approaches in yeast.

The implementation and continuation of the engineering strategy to elevate cytosolic malonyl-CoA levels, derived from the reference literature by Kildegaard and coworkers, proved successful. This is evident for the strains ST020, ST021, ST022 and ST023. This success likely extends to strains ST024 and ST025, despite the limitations of the plasmid-based approach and the metrological constraints. This is supported by consistent positive results in other strains employing the same modifications and indications in the NMR results. Further testing using an alternative reporter system should prove that.

The same approach, when applied to the shikimate engineering effort based on the work by Rodriguez and coworkers, yielded success, as demonstrated in strains ST008 and ST013. Yields were comparable, realistic, and potentially surpassing results reported in similar work from other studies. However, the reference work for this effort appears to be excessively attention-grabbing, as confirmed by other work of the same group. A similar situation is observed for the malonyl-CoA engineering reported by Kildegaard et al., 2016 (also part of the same research group), with both excluding important aspects of their work, which had to be provided through the results of other studies.

The combination of both pathways in a single strain worked as well. However, further work verifying the genome implementation would be needed. Since the malonyl-CoA provision

is not crucial for combinatorial compound biosynthesis using precursors from both pathways, further emphasis must be placed on the shikimate and AAA biosynthesis pathways.

Overall, most of the efforts thus far have been successful, although the implementation took an extended time to be implemented from scratch. Therefore, it leaves insufficient room to generate new and sufficient results that could contribute scientific knowledge, at least within the scope of this work.

Chapter III Conclusion and future perspectives

3.1 *S. cerevisiae* as a production chassis for PKS/NRPS based NPs

The demand for NPs is steadily increasing in our society, particularly given growing concerns about global warming, the recent energy crisis linked to fossil fuels, and the emergence of antibiotic-resistant microorganisms. In light of these issues, biotechnological approaches utilizing renewable feedstock emerge as a promising alternative for generating natural products. [50,169,170] Aromatic compounds, a diverse class of chemicals with various applications such as biofuels [233], pharmaceuticals [234], aromatic agents [235], and food additives (e.g., tryptophan, tyrosine, and phenylalanine [236,237]), stand to benefit from a biotechnological approach. [47,72,113] Specifically, aromatic amino acids like tyrosine, phenylalanine, and tryptophan, which serve as precursors for nutraceuticals and drugs, present challenges due to their complex nature and the inefficiencies in extracting them from plants. By shifting production to microbial cell factories, genetically engineered, for the enhanced production of aromatic compounds, aromatic amino acids, and other derivatives using the shikimate pathway, significant progress has been achieved, demonstrating high yields and proving to be exceptionally promising and feasible .[72,151]

Many studies in this field utilize *S. cerevisiae* as a host to produce secondary metabolites. Several factors drive this choice. Firstly, the biosynthesis of these metabolites often involves P450 enzymes, which are challenging to express at high levels. *S. cerevisiae*, being a eukaryote, is a preferred option for the heterologous expression of eukaryotic P450s. [162] Secondly, yeast, particularly baker's yeast, stands out as an ideal candidate for the production of biological molecules. Baker's yeast is widely employed in both industry and academia, as its status of being safe (GRAS, generally regarded as safe), capacity for high-density fermentation, and genetic controllability, as well as easy genomic manipulability contribute to its increasing appeal for biotechnological and pharmaceutical applications. These factors made yeast a go-to candidate for producing valuable compounds and proteins not naturally occurring in yeast, with many examples exhibited in previous chapters. [6,55,60,127] The success of such applications and production of heterologous compounds often aligned with the development of numerous new techniques over the years. [62–65,69–71] With these, yeast has undergone substantial engineering to produce a diverse range of secondary metabolites through various pathways. [72–76,151,161] To capitalize on the accumulated knowledge in yeast engineering, combining these efforts and creating a yeast platform strain that supplies precursor molecules in sufficient levels represents the next step in maximizing the utility of yeast cell factories. Recent demonstrations of this potential include PKS and NRPS, as well as their hybrid systems. [36] Aromatic small molecules, particularly as precursors in type I multi-domain megasynthases such as NRPS and PKS-NRPS hybrid systems, hold a significant interest in biotechnology for generating pharmaceutically active

NPs like cryptophycin, vancomycin, and phytocannabinoids, among others. [31,33,156,170,174,214,238,239]

All these factors collectively position *S. cerevisiae* as an optimal chassis for NP production, introducing genetic information to assemble them based on the already present high titers of precursor molecules needed for *in vivo* production. With the successful incorporation of a PPtase (sfp_{Bs}) the first step in the generation of such a promising chassis strain was achieved by establishing the functional PPtase with its activating role in bioactive compound biosynthesis of PKS and NRPS, generating the basis strains ST003 and ST004. These strains were used to further introduce malonyl-CoA and shikimate pathway modifications.

3.2 Engineering yeast for elevated malonyl-CoA precursor provision

The high potential of yeast, as finally paraphrased in the previous and preceding chapters, is based on the mentioned compounds (e. g. resveratrol, cryptophycin, phytocannabinoids), relying on precursors derived from two prominent pathways. These precursors, represented mainly by tyrosine, phenylalanine, and malonyl-CoA, derived from the shikimate and malonyl-CoA pathway, have previously been demonstrated to be crucial for heterologous compound production. Recent examples of produced compounds, either derived solely from one pathway or both pathways combined, yielded product titers in the scale of grams per liter. [31,76,151,153]

For the generation of such a chassis strain, the most promising modifications were selected for both pathways separately and with the first attempts to combine them in one platform strain. The introduction of the pathway modification with the combined utilization of both pathways was initially intended to be the first step in further modifying this strain to attain similar and even higher titers than reported in the literature. [76,151] Emphasising on rapid strain generation through attaining the genes already used in successful reports ($acc1^{S659A,S686A,S1157A}$, *ald6, pdc1,* $acs_{Se}{}^{L641P}$, *tpi1* and $aro4^{K229L}$, $aro7^{G141S}$, $aroL_{Ec}$) and the corresponding reporter systems (3-HP and p-CA) to minimize the work needed to modify both pathways individually and combined. Target strains were modified and elevated levels of the targeted precursors could be reported, as concluded from reported compound titers.

For malonyl-CoA, the decision for 3-HP as a reporter system, along with the method used to evaluate the progress of the modifications through determining 3-HP concentrations, has proven to be challenging and not the best choice, given the targeted compound was malonyl-CoA and not 3-HP. One reason for that probably lies in the energy-demanding two-step conversion of malonyl-CoA to 3-HP, consuming two NADPH molecules for one 3-HP molecule, placing an additional energy burden on the metabolic network of the engineered

yeast. [195] This limitation hindering 3-HP production was also addressed and confirmed in the study of Qin and colleagues. [109] Such limitations could potentially be reduced by overexpressing ALD6, increasing the flux through glycolysis, and increasing NADPH production with increased ALD6 activity, hence its preference for NADPH and its role in cytosolic NADPH production. [240] This potentially leads to an increased flux through the glycolysis to cope with the high NADPH demand of 3-HP production. Additionally it could partly explain the discrepancy in the yield reported here with that reported in the literature, where the increased NADPH provision increased 3-HP production. [76] However, the relatively high 3-HP titers before engineering NADPH supply with plasmid-based and single genomic integrated modifications could not be reached here. Only the multicopy integration yielded reliable and relatively high yields; however, it was not in the vicinity of the reported results. The plasmid-based production problems may be attributed to the high expression and copy number fluctuation, respectively, and potentially a stress-induced increased enzyme degradation response, as previously reported and discussed earlier. [67,209] Additional to that, the recently discovered degradation ability of yeast for 3-HP intermediates (*uga1*), as well as the observed decreasing 3-HP titer upon glucose depletion, could play a negative role in failed 3-HP detection in the first modification attempts, discussed in the previous Chapter 2.2.4. [202,203,206] Another more likely explanation could be the fact that the plasmids were lost during cultivation, which was the case for a recent study using dissected $MCRp_{Ca}$ variants, splitting the enzyme into two enzymes, each catalyzing one reaction step. The split expression experiments revealed a plasmid loss of the malonate semialdehyde catalyzing subunit, probably attributed to the toxicity of the malonate semialdehyde intermediate produced. Using this dissected variant also significantly increased 3-HP production, additionally suggesting that single enzyme $MCRp_{Ca}$ is also a limiting factor for 3-HP production. [241] These points, coupled with measurement-associated problems, especially because of low intensities and RT shifts, rendered the 3-HP detection challenging for the low concentrations generated in this work.

Nonetheless, the 3-HP production closely associated with the malonyl-CoA level could successfully be increased in the generated strains ST020 to ST024. Although the evidence for 3-HP in ST023 is not as strong as for the other, the success in the other strains with the same modifications, coupled with the results from ST023, indicated successful intracellular malonyl-CoA level improvement. The mixed results for the plasmid-based 3-HP production are most likely attributed to a potential plasmid loss during cultivations, which could also explain the high variability in the results. However, when comparing the results with the reference literature, it becomes evident that the generated 3-HP titers do not match the titers reported in these studies. [76,153,194,241] The underlying reasons for that are most likely the cultivation conditions. Hence, switching from minimal medium to YPD medium increased 3-HP yields.

The cultivation conditions employed in the literature are predominantly characterized by fed-batch and bioreactor cultivations. [76,151–153,194,219] These conditions ensure constant substrate and energy supply for cell growth and compound production, which would render the problem of the potential NADPH depletion by $MCRp_{Ca}$ for 3-HP production, the potential low-level 3-HP degradation, and the reported 3-HP degradation upon glucose depletion neglectable, yielding substantially higher 3-HP titers. This, however, introduces the potential and reported problem of the 3-HP induced intracellular acidification, which with the associated stress of the necessary active export of 3-HP into the surrounding cell medium. These are factors that need to be considered when encountering probable problems associated with those factors. Nevertheless, this discrepancy in the reported product titers was also reported and admitted in a different study, failing to achieve previously reported product titers of the same research group, which is the same as the reference work of Kildegaard et al., 2016. [151,153] This underscores the importance of the cultivation conditions. However, it also implies that important information probably was not included in these publications. Moreover, it highlights the energy-demanding reporter system, which probably only works reliably with constant substrate and energy supply, as provided by the used conditions in the literature.

Unfortunately, the implementation of the selected genes was only intended to be a first step, creating a basis to work with and introduce more modifications. This was achieved with the introduction of the *Δadh1::tpi1* modification, successfully further increasing the 3-HP titer, and thus far was not reported in this configuration. However, the challenges posed by the measurement method and initial failures to generate 3-HP were highly time-consuming, the remaining time in the end was limited, and further and more thorough work, be it further cultivations or modifications, could not be conducted. It underscores the fact that the reporter system, used out of alleged simplicity, was not suitable to increase the malonyl-CoA level solely. Using 3-HP as a reporter and the associated challenges with $MCRp_{Ca}$-based 3-HP production brought more problems than saved time. As discussed previously, the initially envisioned biosensor approach would likely have been a better option for this. Nonetheless, the TY1 multicopy integration and the other upstream modifications of Table 1, including those not implemented, could further increase malonyl-CoA titers, as discussed earlier. Apart from the introduced modifications and those described in the introduction, another potential, and recent approach could be beneficial. Zhang and coworker employed the mitochondrion for 3-HP production, albeit that the engineered NADPH supply had the biggest impact on 3-HP improvements. Additional expression of mitochondrial *hfa1* as well as finetuned induced expression of mutated *acc1*** inside the mitochondria, could further increase 3-HP yield, in some cases up to 2,65-fold. [110] Making the mitochondria a potential and promising target for further engineering approaches.

Despite the extensive work undertaken on malonyl-CoA-derived products in the literature as well as the initial focus of this work on 3-HP derived from malonyl-CoA, it was stated that malonyl-CoA provision is not a limiting factor in the generation of heterologously produced compounds necessitating precursors from both, shikimate and malonyl-CoA pathways. [31] So, the successfully introduced modifications increasing malonyl-CoA are most likely sufficient for subsequent combinatorial compound production.

3.3 Shikimate pathway engineering and combined pathway modifications

The other successful task undertaken in this thesis was engineering a shikimate pathway-modified strain providing elevated phenylalanine and tyrosine levels. The selected modification method (*ΔPdc5::AroL* and *ΔAro10::Aro4/7*) and p-CA reporting system were analogue to the malonyl-CoA modifications. However, it has been proven to be as fast and unproblematic as intended, unlike for malonyl-CoA as reported previously. As reported in Part 3 of this work (Chapter 2.3), the modifications of the shikimate pathway could successfully be implemented and work well, which is consistent with prior literature findings. [151] Nevertheless, similar to the observed yield discrepancies for 3-HP, this study also encountered analogous variations compared to the literature. However, upon comparison with the existing strains ST008 and, notably, ST013, they displayed outcomes that align with and possibly surpass those reported in the literature, as previously discussed in Chapter 2.3.4. [152,153,156] When analyzing comparable reports from the literature, it became clear that the most probable reason for the relatively low yields originates in the batch cultivation approach. This observation was supported by reproduction attempts in the literature, which failed to reproduce these results. Instead, the reproduced yields were acknowledged to be comparable under identical conditions, highlighting the selected cultivation conditions as a critical factor affecting reported high yields. [153] Using the insights from this report, together with the observed improvements from switching to a more wholesome medium, fed-batch or bioreactor cultivations with extended cultivation periods are likely to yield results comparable to those demonstrated in the literature with the simultaneous integration and knock-out approach used in this work. However, the verification of this hypothesis requires further experimentation. In particular, when focusing on the production of p-CA, modifying the cultivation conditions to a pH of 6 has been reported to yield higher p-CA concentrations, potentially further improving target compound yields. [224] The choice of p-CA as the reported compound, in contrast to the 3-HP reporter compound, is highly suitable for monitoring the engineering approach. On one hand, it is reliably detectable using the modified method employed. [216] On the other hand, it serves as a common precursor for various subsequent compounds, including resveratrol, caffeic acid, naringenin, and kaempferol. [31,116,117,156] Although the primary target was the elevation of tyrosine and phenylalanine levels, which is closely related to the p-

CA yields, p-CA seems to be an important downstream factor increasing the flux through the shikimate pathway. Therefore, to further increase p-CA and its preceding precursor, the introduction of a feedback-resistant TYR1p could alleviate the phenylalanine-inhibited TYR1p from yeast, as recently identified. [153] Alternatively, a PAL branch could circumvent this bottleneck, demonstrating superior p-CA-producing capabilities compared to direct tyrosine conversion, albeit requiring the expression of four additional enzymes, as discussed earlier. As reported, introducing a bi-functional PAL/TAL could simplify this approach, yielding cinnamic acid next to p-CA in the process. [31] This approach potentially broadens the spectrum of subsequent heterologous compounds, including cryptophycin mentioned in Part 1 (Chapter 2.1), with its potential starter molecule, cinnamic acid. [174] Furthermore, a recent study postulated and confirmed that aromatic phytocannabinoid biosynthesis in plants involves cinnamic acid as an initiator for the biosynthesis before its reduction and activation, using isotope-labelled phenylalanine in their feeding experiments. [214] Through enzyme engineering, this pathway could potentially include p-CA as a precursor. Further considering cannabinoids as potential targets for subsequent compound biosynthesis, employing the identified stilbene synthase-type PKS from *Radula marginata* has the potential to produce dihydrostilbene acid or its direct precursor. This compound serves as an intermediate in the biosynthesis of perrottetinene, a substance that closely resembles the chemical structure of tetrahydrocannabinol. [242–244]

These compounds, however, also require the utilization of malonyl-CoA units. Combining both pathways is highly promising, having already yielded products with titers in the gram range. [31,153] With Part 4 (Chapter 2.4) of this thesis, the first steps of the initial aim, to combine both pathway modifications in one working strain, were successfully taken. The strain ST023, modified for malonyl-CoA and because of the removable plasmid, was successfully modified for elevated p-CA production. Both pathways seem to have a synergistic effect, demonstrated by the slightly better production titers of mainly tyrosine but also p-CA compared to their non-malonyl-CoA modified counterparts. Further experiments are necessary to verify this success thoroughly. However, the results obtained for the analogous non-malonyl-CoA-modified strains can be transferred and extrapolated to the results of the strain only harboring the shikimate pathway modifications, especially as the cultivation conditions play a significant role in compound yields derived from both pathways. Furthermore, expanding the malonyl-CoA modification to ST013 would likely be even more favorable, hence its superior p-CA titer yields compared to ST003-based strains. However, the underlying reasons remain undetermined and require further thorough investigations. Nevertheless, even a simple multicopy integration, preferably TY1-based, let alone the whole upstream modifications utilized in this work, likely would yield a yeast production platform on the same level reported in the literature for the best studies so far. This is supported by the fact that malonyl-CoA is

not the limiting factor in compound biosynthesis using precursors from both pathways, as discussed and reported earlier. [31] Additionally, by introducing the *Δadh1::tpi1* modification, which had a beneficial effect on malonyl-CoA provision, the synergistic effect, mentioned before, could potentially be further improved, as overexpressing ADH1p was reported to increase flux through the Ehrlich pathway, meaning deleting adh1 would further prevent degradation through this pathway. [211]

In conclusion, although an exciting topic, metabolic engineering poses challenges, and the strategies selected and employed in this context have demonstrated some serious disadvantages, particularly in the case of 3-HP. Nevertheless, the selected modifications identified from literature results have been successfully implemented for both pathways, with some additional developments (*tpi1*) and the eventual combination in one production strain (ST027). Further experiments and cultivations are necessary and likely to yield similar titers as reported in the literature.

Chapter IV Material and Methods

4.1 Devices

The following table shows the devices used during this work.

Table 5: Overview of the devices used in this work.

Description	Product	Manufacturer
Centrifuge	Centrifuge 5415 D + Rotor F45-24-11	Eppendorf
	Centrifuge 5415 R + Rotor F45-24-11	Eppendorf
	Centrifuge 5424	Eppendorf
	4K15c	Sigma
	Centrifuge 5810 R	Eppendorf
	MyFuge™	Benchmark scientific
	Mini centrifuge ROTILABO®	Carl ROTH
Thermomixer	Thermomixer comfort	Eppendorf
Photometer	UV Spectrophotometer UV-1800	Shimadzu
	NanoDrop™ one	Thermo Fisher Scientific
Mixer	Vortex-Genie 2	Scientific Industries
	REAX 2000	Heidolph
	LAB VORTEX with mixing head	Heathrow Scientific
Pipette	Research Pro, multi-channel, 8-channel, 5-100 µl	Eppendorf
	Research Pro, multi-channel, 8-channel, 50-1200 µl	Eppendorf
	Research Plus, 2-20 µl, 20-200 µl, 100-1000 µl	Eppendorf
Shaker	Orbitron, 2.5 cm displacement	Infors
Incubator	HT Multitron Standard, 5 cm displacement	Infors
	WTB Binder KB-53 Incubator	Binder
Safety cabinet	Herasafe KS	Thermo Scientific
Microplate reader	FLUOstar Omega multidetection microplate reader	BMG Labtech
H_2O filtration System	GenPure UV-TOC x-CAD Plus Benchtop	TKA Thermo Scientific
PCR-Thermocycler	Mastercycler® nexus GX2 flexlid	Eppendorf
	Veriti™ Thermal Cycler, 96-Well	Applied Biosystems
	FlexCycler2 PCR Thermal Cycler	Analytik jena

Description	Product	Manufacturer
Gel documentation	AlphaImager™ Gel Imaging System	Alpha Innotech
	UVsolo + UVIdoc	Biometra/UVITEC Cambrige
Gel electrophoresis	Electrophoresis Power Supply EV243	Consort
	Power Supply Model 200/2.0	Biorad
DNA concentration determination	NanoDrop™ One microvolume-UV/VIS-spectrophotometer	Thermo Scientific
Rotary evaporator	Vacuum Pump V-700	Büchi
	Vacuum Controller V-850	Büchi
	Rotavapor R-210	Büchi
	Distillation Chiller B-741	Büchi
Drying/Evaporation	Alpha 1-4 LSC	Christ
	Chemistry Hybrid Pump RC6	Vacuubrand
	Concentrator plus	eppendorf
	RS4	Vacuubrand
HPLC	1260 Infinity II Binary Pump	Agilent
	1260 Infinity II Multisampler	Agilent
	1260 Infinity II Multicolumn Thermostat	Agilent
	1260 Infinity II Diode Array Detector HS	Agilent
	1260 Infinity High Performance Degasser	Agilent
	1200 Infinity High Performance Degasser	Agilent
	1260 Infinity Binary Pump	Agilent
	1260 Infinity Multisampler	Agilent
	1260 infinity Refractive Index Detector	Agilent
	1260 infinity 210 nm wavelength detector	Agilent

4.2 Microorganisms, Plasmids and Oligonucleotides

4.2.1 Microorganisms

All microorganisms used in this work can be found in Table 6. The *E. coli* strain DH5α was used for all cloning and plasmid amplification work and the *S. cerevisiae* strain CEN.PK2-1C in its two variations were used for all pathway modification experiments.

Table 6: Basis strains used in this work.

Strain	Genotype	Source
***E. coli* DH5α**	F– Φ80lacZΔM15 Δ(lacZYA-argF) U169 recA1 endA1 hsdR17 (rK–, mK+) phoA supE44 λ– thi-1 gyrA96 relA1 (Infos von DH5α™ von Life Technologies)	TU Dortmund Technische Biochemie
***S. cerevisiae* CEN.PK2-1C Δpep4 Δgal1 Δgal80**	MATa; gal1::loxP; pep4::loxP; gal80::loxP ura3-52; trp1-289; leu2-3,112; his3Δ 1; MAL2-8C; SUC2	TU Dortmund Technische Biochemie
***S. cerevisiae* CEN.PK2-1C Δpep4 Δgal1 Δgal80 Δmig1**	MATa; gal1::loxP; pep4::loxP; gal80::loxP; Dmig1; ura3-52; trp1-289; leu2-3,112; his3Δ 1; MAL2-8C; SUC2	TU Dortmund Technische Biochemie

4.2.2 Vectors and Plasmids

Table 7 lists all base vectors and plasmids used in this work with their properties. The corresponding maps can be found in the Supplements 1.1.

T**able 7: Vectors and Plasmid used in this work.**

Vector	Size [bp]	Features	Source
pDionysos-GlcRepfree	6.883	pGal1, tCyc1, pUC ori, Leu2d, Amp^R, ura3, 2 µ ori, f1 ori	TU Dortmund
pDionysos-GlcRepfree-Sfp-B.Sub.	7.408	pgal1, tcyc1, pUC ori, Leu2d, Amp^R, ura3, 2 µ ori, f1 ori, pGal1, BsSfp, tCyc1	This work
p426_Cas9_gRNA-ARS720a	11.117	Amp^R, 2 µ ori, pUC ori, plac, lacI, pT3, ptyrosine, cut720a, gRNA scaffold, snr52T, SpCas9, Factor Xa site, tcyc1, pT7, f1 ori, ura3,	Apel et al., 2017 [68]
pCutX-Lys5 knockout plasmid	11.117	Amp^R, 2 µ ori, pUC ori, plac, lacI, pT3, ptyrosine, cutLys5, gRNA scaffold, snr52T, SpCas9, Factor Xa site, tcyc1, pT7, f1 ori, ura3,	This work
p0343	17.851	Amp^R, X2UP, tAdh1, $scAcc1^{S659A, S1157A}$, pTef1, pPgk1, CaMcr, tCyc1, loxP-KlUra3-LoxP, X2Dw, pUC ori	DTU

Vector	Size [bp]	Features	Source
p0343*	17.851	Amp^R, X2UP, tAdh1, scAcc1^{S686A,S659A,S1157A}, pTef1, pPgk1, CaMcr, tCyc1, loxP-KlUra3-LoxP, X2Dw, pUC ori	This work
p0343*-acc1***	13.000	Amp^R, X2UP, tAdh1, scAcc1^{S686A,S659A,S1157A}, pTef1, loxP-KlUra3-LoxP, X2Dw, pUC ori	This work
p0380	11.909	Amp^R, X3UP, tAdh1, seAcs^{L641P}, pTef1, pPgk1, ScAld6, tCyc1, loxP-KlLeu2-LoxP, X3Dw, pUC ori	DTU
p0382	7.991	Amp^R, X4UP, tAdh1, scPdc1, pTef1, tCyc1, loxP-His5-LoxP, X4Dw, pUC ori	DTU
p02747	8.517	Amp^R, X3UP, tAdh1, pPgk1, EcAroL, tCyc1, loxP-KlLeu2-LoxP, X3Dw, pUC ori	DTU
pCfB9114	7.725	Amp^R, XII1UP, tAdh1, ScAro4^{K229L}, pTef1, pPgk1, ScAro7^{G141S}, tCyc1, XII1Dw, pUC ori	DTU
p0376	17.308	AmpR, TY4 5', tAdh1, scAcc1^{S659A,S1157A}, pTef1, pPgk1, CaMcr, tCyc1, loxP-KlUra3-degradation tag-LoxP, TY4 3', pUC ori	DTU
p0376*	17.308	AmpR, TY4 5', tAdh1, scAcc1$^{S686A,S659A, S1157A}$, pTef1, pPgk1, CaMcr, tCyc1, loxP-KlUra3-degradation tag-LoxP, TY4 3', pUC ori	This work
p0474	17.122	Amp^R, TY4 5', tAdh1, scAcc1^{S659A,S1157A}, pTef1, pPgk1, CaMcr, tCyc1, KlUra3-degradation tag, TY4 3', pUC ori	DTU
p0474*	17.122	Amp^R, TY4 5', tAdh1, scAcc1$^{S686A,S659A, S1157A}$, pTef1, pPgk1, CaMcr, tCyc1, KlUra3-degradation tag, TY4 3', pUC ori	This work
pDesti-H-A-Esp3I-Kan-ColE1	1809	Kan^R, ColE1 ori, Overlap segment A, Overlap segment H,	This work

Vector	Size [bp]	Features	Source
p0872	8160	Amp^R, XI-5 Dw, loxP-SpHis5-LoxP, tCyc1, pTef1, $TALp_{Ha}$, tAdh1, XI-5 Up	DTU
pI-dADH1::TPI1	6033	Amp^R, pUC ori, ADH1-HR Up, pTef1, TPI1p, tTdh1, loxP-NAT-LoxP, ADH1-HR Dw,	This work
pEpi-haTal-Ura3-2µ	6740	Kan^R, ColE1 ori, tAdh1, $TALp_{Ha}$, pTef1, ura3, 2 µ ori,	This work
pI-deltaPDC5-EcAroL	7489	Amp^R, Pdc5 Up, tAdh1, pPgk1, $AroL_{Ec}$, tCyc1, loxP-Kl.Leu2-LoxP, Pdc5 Dw, pUC ori	This work
pI-deltaARO10-Aro4,Aro7	8265	Amp^R, Aro10 Up, tAdh1, $Aro4^{K229L}$, pTef1, pPgk1, $Aro7^{G141S}$, tCyc1, loxP-SpHis5-LoxP, Aro10 Dw, pUC ori	This work
pCaMCR-TRP1	10743	Amp^R, pTef1, pPgk1, CaMcr, tCyc1, TRP1, 2µ ori, pUC ori	This work

4.2.3 Oligonucleotides

All used oligonucleotides were designed with the help of the Clone Manager 9/10 software.

The designed oligonucleotides were ordered from Sigma-Aldrich®, which were delivered deprotected and desalted in lyophilised condition. The most important criterium for stable melting points T_m of the oligonucleotides is the desalination state.

To use the oligonucleotides for cloning and sequencing, the recommended amount of filtered (0.2 µm pore size) ultrapure H2O was added to a concentration of 100 µmol/L. This was diluted with a ratio of 1:10 before the use in PCR reactions or sequencing.

Table 8: Oligonucleotides used for the cloning experiments. Vector specific sequences are shown in small letters. Complementary sequences for the hybridisation to the insert are depicted in capital letters. Added nucleobases for the introduction of mutations, stop codons or frameshifts are written in bold letters, cutting sites for restrictions enzymes are underlined. T_m: melting temperature of the complementary part of the oligonucleotide, T_A: melting point of the completely hybridised oligonucleotide.

Name	Length [bp]	Sequence (5'→3')	T_m [°C]	T_A [°C]
OSY-fw-pDio-Gib	33	atcatgtaattagttatgtcacgcttacattca	65	
OSY-rv-pDio-Gib	31	ggtttttctccttgacgttaaagtatagag	65	
OSY-fw-Sfp-pDio-Oh	59	actttaacgtcaaggagaaaaaacc**AAAAAA**ATGAAGATTTACGGAATTTATATGGACC	73	

Name	Length [bp]	Sequence (5'→3')	T_m [°C]	T_A [°C]
OSY-rv-Sfp-pDio-Oh	49	agcgtgacataactaattacatgatTTATAAAAGCTCTTCGTACGAGAC	72	
OSY-fw-Seq.-Sfp-pDio	20	taaagattcgaagcgatgat	56	
OSY-rv-Seq.-Sfp-pDio	20	ataatgttacatgcgtacac	55	
OSY-F-up720a	25	caccacccaggaattgagtttctat	66	
OSY-R-up720a-Ov-pG	60	cccgctcggcggcttctaatccgtTGTAAACTCAATTATACAAATAAACGAACAATCAAC	64	
OSY-F-pG-s-tC-cass	38	ttgtataattgagtttacaACGGATTAGAAGCCGCCGA	69	
OSY-R-pG-s-tC-cass	46	gtttgctttttgtcactctcttgGCAAATTAAAGCCTTCGAGCGTC	67	
OSY-F-dw720a-ov-tC	61	tgggacgctcgaaggctttaatttgcCAAGAGAGTGACAAAAAGCAAACTTATAAATAGT	65	
OSY-R-dw720a	26	ccgtttaattccaagagaaggagaag	65	
Oligo-for-HR-Up	90	TGTTCAAATCTATGCAGCCAGCTGCTGCAGTTGTTTGGCTGCTCTATAGTA**TAAA**GCTTAAATTTTCAAGAGCTGAAATTTGACAAGGGC		81
Oligo-for-HR-Dw	90	GCCCTTGTCAAATTTCAGCTCTTGAAAATTTAAGC**TTTA**TACTATAGAGCAGCCAAACAACTGCAGCAGCTGGCTGCATAGATTTGAACA		81
pCutX-Rv-gRNA-exchange	23	aaagtcccattcgccacccgaag	72	
OSY_pCutX-Lys5-gRNA-exchange-Fw	68	CTTCGGGTGGCGAATGGGACTTT**TTTGGCTGCTCTATAGTAAC**gttttagagctagaaatagcaagtt	60	
0006_OSY-pCutX-up-gRNA-seq.-Fw	19	ggtttaaggcgcaagactg	64	
0007_OSY-pCutX-dw-gRNA-seq.-Rv	18	cccgatgtatgggtttgg	63	
Sfp-RNA-PCR-Fw (Up716)	20	acaaggacgagcagacagac	67	
Sfp-RNA-PCR-Rv (Dw863)	20	tccggaagctcaatggatac	64	
ATi rev ACS1 cDNA PCR	19	cagtatagcccttgcgaac	66	
0074_LGW_ACS1_f_oü	18	atgtcgccctctgccgta	69	
OSY-111-ACC1-Mut-(S686A)-Fw	47	CAAGATTA**G**CCGTTGACTCtatgactactttgttggaagttgaaaac	63	
OSY-112-ACC1-Mut-(S686A)-Rv	45	GAGTCAACGG**C**TAATCTTGtagcagcaacttcttctttccaatag	66	
113_OSY-ACC1-Seq.-Primer2-Fw	19	gccatcgggtggtactttg	66	
OSY-MCR-remov-2nd-Fw	42	CATGCGATAAGCGATATGCGATatcgcgtcagctgaagcttc	68	
OSY-MCR-remov-2nd-Rv	37	ATATCGCATATCGCTTatcgcatgcacacaccatagc	68	

Name	Length [bp]	Sequence (5'→3')	T_m [°C]	T_A [°C]
OSY-MCR-remov-2nd-Fw (p0474)	48	CATGCGATAAGCGATATGCGATATcgcgtgatcccaatacaacagatc	68	
1R-pTEF1-Ov(ADH2) (Sequencing primer MCR removal)	50	CTATTCAATCATTGCGCttatttcaaagtcttcaacaatttttctttatc	61	
0057_AXP-R704-TY4(b) (Sequencing primer MCR removal)	20	aaggcgatgcattgggtcag	64	
0248_OSY_Plasmid-bBone-Amp-Fw-Univ_Up	22	ctcagcgcggccgcaaatttaa	71	
0249_OSY_Plasmid-bBone-Amp-Rv-Univ_Up	21	cagcgcggccgcatttaaatc	70	
OSY-MCR-pPGK1-Fw	48	tggggatttaaatgcggccgcgctgcgatGGAAGTACCTTCAAAGAAT	62	
0171 TB	18	cttcgagcgtcccaaaac	64	
OSY 1-tTRP1-Fw	58	gggaagctccaccccggttgataatcaTGTATATTTTCCTGTACAATCAATCAAAAAG	62	
OSY 4-pTRP-Rv	45	TATTTAAATTTGCGGCCGCGCTGAGtgaattagtcgcgctgggag	67	
OSY-2µ ori-Fw-(Ov-0171)	51	GAAGGTTTTGGGACGCTCGAAGAGCttatcgatgataagctgtcaaagatg	62	
OSY-2µ ori-Rv-(OvTRP)	46	gattatcaaccggggtggagcttccCATTGCGAATACCGCTTCCAC	67	
OSY-ADH1-HR-Up-fw	46	AACACGTCTCAACCTtagccctagacttgatagccatcatcatatc	67	
OSY-ADH1-HR-Up-rv	36	AACACGTCTCTTGTTtccaacttaccgtgggattcg	68	
OSY-pTEF-st-fw	37	AACACGTCTCAAACaccttgccaacagggagttcttc	68	
OSY-pTEF1-ed-rv	56	AACACGTCTCTAGCctttgtaattaaaacttagattagattgctatgctttctttc	65	
OSY-TPI1-st-fw	44	AACACGTCTCAGGCTAAaaaaatggctagaactttctttgtcgg	65	
OSY-TPI1-ed-rv	51	AACACGTCTCTCTGActtagtttctagagttgatgatatcaacaaattctg	65	
OSY-tTDH1-st-fw	58	AACACGTCTCATCAGtaaagcaatcttgatgaggataatgattttttttgaatatac	65	
OSY-tTDH1-ed-rv	43	AACACGTCTCTGCaggcccgttcagggtaatatattttaaccg	67	
OSY-NATloxP-st-fw	84	AACACGTCTCACTGccttaatataacttcgtataatgtatgctatacgaagttatcggcagtatagcgaccagcattcacatac	67	
OSY-NATloxP-ed-rv	80	AACACGTCTCTTAGTcctaataacttcgtatagcatacattatacgaagttatctggtagtcggtctcctacagtttagc	66	

Name	Length [bp]	Sequence (5'→3')	T_m [°C]	T_A [°C]
OSY-ADH1-HR-Dw-st-fw	37	AACACGTCTCAACTActgtaggtcaggttgctttctc	65	
OSY-ADH1-HR-Dw-ed-rv	34	AACACGTCTCTCCTAatggaatttgggcggaggg	68	
OSY-Fw-AmpR-pUCori	23	cttaagactggccgtcgttttac	66	
OSY-Rv-AmpR-pUCori-TalOv	47	TCTCAGGTATAGCATGAGGTCGCTCctcgcgataatgttcagaattg	61	
0112_AXP_s_Zeo20	20	gagcgacctcatgctatacc	65	
OSY-pURA-Rv-Ov-2µOri	26	cttatcatcgataaGAGCTCGTTTTATTTAGGTTCTATCG	62	
OSY-2µori-Rv-Ov-AmpR-ori	46	TTGTAAAACGACGGCCAGTCTTAAGgggcttttctgattatcaacc	61	
OSY-2µori-Fw-Ov-pURA3	50	gatatcagatccactagtggcctatgCTTATCGATGATAAGCTGTCAAAG	61	
PDC5-Fw-No Ext. Prom. 5'	20	caagactgaacccgaatccc	66	
PDC5-Rv-Ext. Prom. 3' (Ov insert)	80	caggtatagcatgaggtcgctcatcgcacgcattccatgcgagctcgctgaggacttaatCGCGACCTTTGGATATGGAG	66	
PDC5-Fw-Ext. Term. 5' (Ov insert)	82	agttattaggtaggtgatatcagatccactagtggcctatgcacccaattcgccctatagCAATTGACTGCCGCTACTAACG	66	
PDC5-Rv-No Ext. Term. 3'	20	ggcatgttggcctctgtttc	67	
OSY-Fw-AmpR-pUC ori-PDC5ov	76	attaagaaacagaggccaacatgccgcgcggccgcaagcccaggggggcccgagCTTAAGACTGGCCGTCGTTTTAC	66	
OSY-Rv-AmpR-pUC ori	54	gggattcgggttcagtcttggcgcggccGCATCTCGCGATAATGTTCAGAATTG	61	
0112_AXP_s_Zeo20	20	gagcgacctcatgctatacc	65	
0343_OSY_Rv-Primer Insert (Ov Down) 3'	23	gccactagtggatctgatatcac	64	
ARO10-Fw-No Ext. Prom. 5'	27	gtttgttaagaataatttggcgaaccc	64	
ARO10-Rv-Ext. Prom. 3' (Ov insert)	81	gtaggtcaggttgctttctcaggtatagcatgaggtcgctctcatcgcacgcattccatgGAAAGTGAGCTGCCGCTGTAG	69	
ARO10-Fw-Ext. Term. 5' (Ov insert)	80	gctatacgaagttattaggtgatatcagatccactagtggcctatgcacccaattcgcccGGCTTTCGGCTCACCACTTG	69	
ARO10-Rv-No Ext. Term. 3'	23	cttggcaaaccttcgacgttgac	69	
Rv-Primer Insert (Ov Down) 3'	23	gccactagtggatctgatatcac	64	
OSY-Fw-AmpR-pUC ori-ARO10ov	76	aggtcaacgtcgaaggtttgccaaggcgcggccgcaagcccaggggggcccgagCTTAAGACTGGCCGTCGTTTTAC	66	

Name	Length [bp]	Sequence (5'→3')	T_m [°C]	T_A [°C]
OSY-Rv-AmpR-pUC ori-ARO10ov	61	gggttcgccaaattattcttaacaaaggcgcggccgcatCTCGCGATAATGTTCAGAATTG	61	

4.3 Media and Additives

All media used were prepared according to the following recipes and then sterilized at 12 °C for 20 min (Autoclave: Table 5). The ingredients listed in the following table are sufficient to prepare 1 L medium with ultrapure H_2O (TKA Thermo Scientific GenPure UV-TOC x-CAD Plus Benchtop). For solid media, 2 % (w/v) agar-agar was added prior to autoclaving. The components marked with the symbol * were not autoclaved and were sterile filtered (0.2 µm pore size) before addition to the autoclaved media. Separately autoclaved solutions were marked with the symbol **. For selective cultivation of microorganisms, the corresponding antibiotics (Table 11) were added.

4.3.1 Media for *E. coli*

The following table shows all ingredients used for the media for *E. coli* cultivation.

Table 9: Media for *E. coli* cultivation.

Denotation	Components		Comments
LB-Medium	10 g L^{-1}	tryptone	pH 7.4
	5 g L^{-1}	yeast extract	
	10 g L^{-1}	NaCl	
SOB-Medium	20 g L^{-1}	tryptone	pH 7.4
	5 g L^{-1}	yeast extract	
	10 g L^{-1}	NaCl	
	10 g L^{-1}	KCl	
	10 g L^{-1}	$MgCl_2$ x 6 H_2O	
	10 g L^{-1}	$MgSO_4$ x 7 H_2O	
SOC-Medium		SOB-Medium	pH 7
	+ 20 mM	Glucose	

4.3.2 Media for *S. cerevisiae* cultivation

The following table details the ingredients employed in the media designed for cultivating *S. cerevisiae*. The SD-Drop-out medium comprises amino acids crucial for yeast cell growth, excluding essential amino acids required to exert the necessary selection pressure. This medium was either manually prepared following the Merck-prescribed

composition or utilized as a ready-made synthetic yeast dropout medium, adjusted for autotrophy. [245] Following the sterilization of the yeast nitrogen bases (YNB) solution, the required filtered SD-Drop-out mixture (0.2 µm pore size) was introduced, along with the appropriate quantity of sterile sugar. The remaining volume was supplemented with sterile ultrapure H_2O (TKA Thermo Scientific GenPure UV-TOC x-CAD Plus Benchtop), reaching a total volume of 500 mL or 1 L.

Table 10: Media for *S. cerevisiae* cultivation.

Denotation	Components		Comments
YPD-Medium	10 g L^{-1}	Yeast extract	Autoclaved separately
	20 g L^{-1}	Peptone	
	40 ml L^{-1}	50 % Glucose	Added before each cultivation
YNB-Medium*	6.7 g L^{-1}	Yeast nitrogen base	
	1.39-1.92 g L^{-1}	SD-Drop-out medium	
	40 ml L^{-1}	50 % Glucose	Added before each cultivation

4.4 Antibiotics and instable Media additives

For the selective cultivation of the microorganisms, a specific selection pressure was used that corresponds to the resistance genes encoded on the plasmids and vectors with which the microorganisms were transformed. As the antibiotics used are unstable at RT, they are stored at -20 °C and added immediately before cultivation.

Table 11: Used antibiotics in this work.

Media additives	Stock solution	Solvent	Final concentration	Source
Ampicillin	100 mg ml^{-1}	Ultrapure H_2O	100µg mL^{-1}	Roth
Kanamycin	50 mg ml^{-1}	Ultrapure H_2O	50µg mL^{-1}	Roth
Hygromycin B Gold	100 mg mL^{-1}	HEPES buffer	100µg mL^{-1}	Invitrogen
Zeocin	100 mg mL^{-1}	HEPES buffer	100µg mL^{-1}	Invitrogen
Nourseothricin	100 mg mL^{-1}	Ultrapure H_2O filtered (0.2 µm pore size)	100µg mL^{-1}	Jena Bioscience
G418 (Geneticin)	100 mg mL^{-1}	HEPES buffer	100µg mL^{-1}	Invitrogen

4.5 Solutions, Buffer and commercial Enzymes and Kits

4.5.1 Buffer and Solutions

All components of the buffers and solutions used are listed in this chapter. Unless otherwise stated, all components refer to a volume of 1 L. Ultra-pure H_2O (TKA Thermo Scientific GenPure UV-TOC x-CAD Plus Benchtop) was used for all solutions and buffers.

Table 12: Solutions and buffers for SDS gel electrophoresis.

Description	Components		Comments
5 x Running buffer	250 mM	Tris	
	1.92 M	Glycine	
	0,5 % (w/v)	SDS	
Coomassie staining solution	2 mM	Coomassie brilliant blue G250	
	55 %	Methanol	
	9.2 % (v/v)	Acetic acid	
APS 10 %	10 %	APS	Total volume 10 ml, Aliquots, Stored at -20 °C

Table 13: Buffer and solutions for agarose gel electrophoresis.

Description	Components		Comments
50 x TAE-Buffer	2 M	Tris	pH 8.2
	1 M	Acetic acid	
	50 mM	EDTA	
1 % Agarose gel	1 %	Agarose (w/v)	Heated in microwave
	In TAE 1 x		
	1:1000	20 mg mL^{-1} Ethidium bromide	

Table 14: Buffer for *E. coli* plasmid isolation. Solution I-IV were prepared for a final volume of 50 ml ultrapure H_2O.

Description	Components		Comments
Solution I*	25 mM	Tris (pH 8.0)	ph 8.4, stored at 4 °C
	10 mM	EDTA (pH 8.0)	
	50 mM	Glucose	
	0.1 mg mL^{-1}	RNase	
Solution II*	0.2 M	NaOH	
	34.7 mM	SDS	
Solution III*	3 M	Sodium acetate	pH 5.5
Solution IV*	5 M	LiCl	

Table 15: Additional buffer for plasmid isolation from *S. cerevisiae* using the NucleoSpin Plasmid (NoLid) kit (Macherey-Nagel, Table 22)

Description	Components		Comments
Wash buffer	10 mM	EDTA	pH 8.0
Sorbitol buffer	1.2 mM	sorbitol	
	10 mM	$CaCl_2$	
	0.1 mM	Tris/HCl (pH 7.5)	
	35 mM	B-mercaptoethanol	

Table 16: Buffer and solutions for yeast colony PCR.

Description	Components		Comments
Lysis buffer	20 mM	Tris	pH 8.0, stored on bench
	25 mM	NaCl	
	2.5 mM	EDTA	
	0.05 % (w/v)	SDS	
Wash buffer	10 mM	Tris	pH 8.0, stored on bench
	0.1 % (w/v)	Tween-20	

Table 17: Buffer and solutions for Gibson assembly. All components for the 5 x ISO buffer are given for a total volume of 6 ml and for the 3.2 x Gibson cloning master mix are given for a total volume of 0.5 ml.

Description	Components		Amount	Comments
5 x ISO Buffer	1 M	Tris-HCl pH 7.5	3 ml	Stored at -20 °C in 320 µl aliquots
	2 M	$MgCl_2$	150 µl	
	100 mM	dNTPs (dGTP, dCTP, dATP, dTTP)	240 µl	
	1 M	DTT	300 µl	
		PEG-8000	1.5 g	
	100 mM	NAD	300 µl	
	filtered (0.2 µm pore size) ultrapure H_2O		to 6 ml	
3.2 x Gibson cloning master mix		5 x ISO buffer	320 µl	Aliquote in 5 µl aliquots and store at -20 °C, do not add water
	10 U/µl	T5 exonuclease	0.64 µl	
	2 U/µl	High Fidelity DNA polymerase	20 µl	
	40 U/µl	Thermostable Taq ligase	160 µl	

Table 18: Buffers for the preparation of chemical ultra-competent *E. coli* cells. PIPES was prepared in 100 ml ultrapure H_2O.

Description	Components		Comments
Inoue buffer	55 mM	$MnCl_2$ x 4 H_2O	Always prepare fresh buffer before use
	15 mM	$CaCl_2$ x 2 H_2O	
	250 mM	KCl	
	10 mM	PIPES (0.5 M, pH 6.7)	
PIPES	0.5 M	piperazine-N,N′-bis(2-ethanesulfonic acid)	pH 6.7, aliquots of 10 ml stored at -20 °C
	pH adjustment	KOH (0.5 M)	

Table 19: Buffers and solutions for the preparation of chemical ultra-competent *S. cerevisiae* cells and their transformation. PEG 3350 and single-stranded carrier DNA (ssDNA) were prepared in 100 ml. Frozen competent cell solution was prepared in 10 ml.

Description	Components		Comments
PEG 3350	50 % (w/v)	PEG 3350	
Li acetate	1 M	Li acetate	
TE buffer	10 mM	Tris	pH 8.0
	1.3 mM	EDTA	
ssDNA (2.0 mg mL^{-1})	200 mg	Salmon sperm DNA	Aliquot 1 ml, store at -20 °C
	Sterile TE buffer		
FCC solution	5 % (v/v)	Glycerol	Filtered (0.2 µm pore size)
	10 %(v/v)	DMSO	

Table 20: Buffer and solutions for HPLC.

Description	Components	
Buffer A		Ultrapure H_2O
	0.05 %	Formic acid (v/v)
Buffer B		Methanol
	0.05 %	Formic acid (v/v)
Sugar-HPLC mobile phase		Ultrapure H_2O
	0.05 %	H_2SO_4 (v/v)

4.5.2 Commercial Enzymes, Solutions and Kits

Table 21: Overview of the used enzymes for cloning, PCR, and other uses in this work. NEB: New England Biolabs.

Enzyme	Source	Uses
Q5 High-Fidelity 2X Master Mix	NEB	PCR for the amplification of specific target DNA
Red *Taq* DNA Polymerase 1.1 x Master Mix	VWR	PCR for the amplification of specific target DNA in colony PCRs
T5 exonuclease	NEB	Used in 3.2 x Gibson cloning master mix for Gibson assembly reactions
Phusion® High-Fidelity DNA polymerase	NEB	
Thermostable *Taq* DNA ligase	NEB	

Enzyme	Source	Uses
T4 DNA Ligase	NEB	Used in GoldenGate assembly
*Esp3*I	NEB	
LunaScript® RT SuperMix	NEB	Used for reverse transcription
*Not*I	NEB	Used for linearisation of integrative plasmid
*Dpn*I	NEB	Methylated DNA restriction

Table 22: Overview over the commercial substances, solutions, and kits.

Description	Product	Source
DNA-Ladder	GeneRuler™ 1kb Plus DNA Ladder	Thermo Scientific
Loading Dye	6 x TriTrack DNA Loading Dye	Thermo Scientific
Filter paper	Whatman® filter paper no.1	Merck
Mini kit for plasmid DNA purification	NucleoSpin® Plasmid (NoLid)	Macherey-Nagel
Mini kit for gel extraction and PCR clean up	NucleoSpin® Gel and PCR Clean-up	Macherey-Nagel
Mini kit for DNA extraction, clean up, and concentration	NucleoSpin® DNA Yeast	Macherey-Nagel
Mini kit for RNA extraction, clean up, and concentration	NucleoSpin® RNA Plus kit	Macherey-Nagel
Ligase buffer	T4 DNA ligase buffer (10 x)	NEB
Kit for reverse transcription	LunaScript® RT SuperMix Kit	NEB

4.6 Molecular biological methods

4.6.1 DNA analysis with Agarose gel electrophoresis

To separate and analyse DNA fragments generated by PCR (Chapter 4.6.3) or restriction digestion (Chapter 4.6.4), 0.8-1.5 % (w/v) agarose gels were used. The composition of the utilized buffers can be found in Table 13. The gel was prepared with 1 x TAE buffer, 1:1000 ethidium bromide (for DNA visualisation under UV-light after intercalating into dsDNA), and heated in the microwave till everything was dissolved and poured into the electrophoresis

chamber. After the gel polymerised, it was placed in the running chamber filled with 1 x TAE buffer till the gel was completely covered with buffer. The DNA samples were mixed with 6 x DNA loading dye, whereas 1-50 µl DNA samples were used and mix 1:6 with the 6 x DNA loading dye. If this is not possible the mixing ratio was 1:1 with very small DNA sample amounts (1 µl). For preparative gels with subsequent DNA purification (chapter 4.6.5.1) the whole DNA sample was used. Each electrophoresis approach was performed with 2-5 µl of DNA-Ladder (GeneRuler™ 1 kb DNA Ladder Plus, Thermo Scientific, Figure 46) for size comparison. DNA sample separation was done at 100-140 V for 30-45 min.

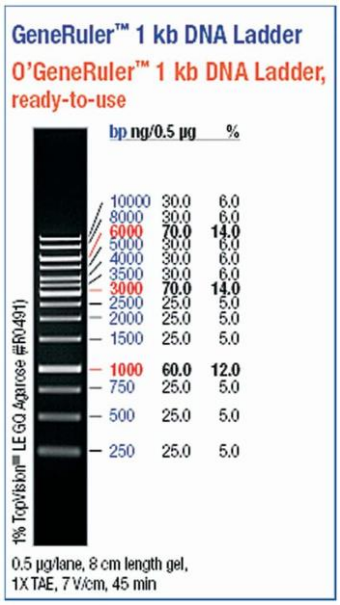

Figure 46. Used DNA-Ladder (GeneRuler™ 1 kb DNA Ladder Plus, Thermo Scientific) for DNA size comparison.

For DNA fragment detection, with the help of ethidium bromide, the gel was analysed and documented with UV light in the AlphaImager™ Gel Imaging System.

4.6.2 Amplification of plasmid-DNA with *E. coli*

With the help of the microorganism *E. coli* DH5α (Table 6) and its inherent DNA replication machinery upon its cell growth and division live cycle, plasmid DNA was amplified. The cells were cultivated in LB-Medium (Table 9) mixed with the corresponding antibiotics (Table 11) for the vector specific selection pressure. The transformed cells (Chapter 4.7.2) were incubated at 37 °C, 200 rpm overnight in sterile 13 ml tubes (tube 13 ml, 100 x 16 mm, PP, Sarstedt) with 2 ml medium or sterile 100 ml Erlenmeyer flasks (no baffles) with approx. 10 ml medium.

4.6.3 Polymerase chain reaction (PCR)

The amplification via polymerase chain reaction (PCR) of the desired genes and DNA fragments was done from DNA fragments, isolated plasmid DNA or from lysed cells. For each PCR the polymerase, the annealing temperature and additive as well as the protocol was adjusted. For multiple PCRs with the same protocol and to ensure reproducibility, master-mixes were prepared and then divided into the small 200 µl PCR reactions (Biozym).

4.6.3.1 Amplification of target Genes

The amplification of specific DNA sequences was achieved with PCR, which consists of a repetitive three step protocol (denaturation, hybridisation/annealing, elongation), with two flanking oligonucleotides, a DNA polymerase, single nucleotides and a DNA template. [246] For cloning experiments, a DNA polymerase with high precision and accuracy is needed to amplify the anticipated DNA target, therefore the Q5 High-Fidelity 2X Master Mix (New England Biolabs (NEB)) was used. For the PCR reactions different thermocycler (Mastercycler® nexus GX2 flexlid, Eppendorf, Veriti™ Thermal Cycler, 96-Well, Applied Biosystems) and different reaction volumes were used. The volume was depending on the amount of DNA fragment that was needed. Test reactions had volumes of around 12.5 µl and preparative reactions used 25 µl and 50 µl.

Table 23: General overview of PCR reactions and their composition.

Components	Amount [Test]	Amount [Preparative]	
DNA-Template (10-50 ng)	1-4 µl	1-5 µl	1-5 µl
Oligonucleotide fw (10 µm)	0.75 µl	1.25 µl	2.5 µl
Oligonucleotide rev (10 µm)	0.75 µl	1.25 µl	2.5 µl
Nuclease free H_2O	3.75-0.75 µl	9-5 µl	19-15 µl
Q5 High-Fidelity 2X Master Mix	6.25 µl	12.5 µl	25 µl
Sum Σ	12.5 µl	25 µl	50 µl

For the generation of the desired DNA fragments, DNA templates from diverse plasmids (Table 7), DNA fragments and genomic DNA (*E. coli* and *S. cerevisiae*, Table 6) were used. The right annealing temperature for each priming oligonucleotide combination was calculated using the Tm Calculator from NEB. [247]

Table 24: General Summery of the PCR programs used for the amplification of target DNA fragments with Q5 High-Fidelity 2X Master Mix (NEB). The annealing temperature was adjusted for each PCR reaction according to the T_m of the oligonucleotides used. The number of cycles was also adjusted to optimize the DNA fragment yields. denat.: denaturation, anneal.: annealing/hybridisation, elong.: elongation.

Temperature	98 °C	98 °C	50-70 °C	72 °C	72 °C	4 °C
Time	30 sec	10 sec	20 sec	30 sec/kb	2 min- 10 min	∞
Step	denat.	denat.	anneal.	elong.	elong.	end
Cycles	1	30-55			1	1

To visualise and analyse the success of the PCR reaction 1 µl of the reaction mix was mixed with 1 µl of the 6 x TriTrack DNA Loading Dye (Table 22) and a gel electrophoresis (Chapter 4.6.1) was done.

4.6.3.2 Reverse transcription of isolated RNA

The reverse transcription is basically a PCR with RNA as template converting it back to DNA, which is call complementary DNA (cDNA). With the help of a reverse transcriptase and short oligonucleotides complementary to the 3' end of the RNA the cDNA is synthesized. This cDNA in turn can then be used as a template for subsequent PCRs (Chapter 4.6.3.1) analysing the genes of interest (Chapter 4.6.1).

For the reverse transcription the LunaScript® RT SuperMix Kit from NEB was used. Its single-tube supermix contains hexamer and oligo-dT primers, dNTPs, MurinRNase inhibitor and the Luna® reverse transcriptase (+/-RT). For each reverse transcription reaction two reaction tube were prepared. One tube, for the positive reaction, containing the reaction mix with +RT and the other, the negative reaction, contains no -RT. This procedure is done to check whether the samples still contain genomic DNA (fragments would be present in the -RT samples after subsequent PCR). In the following tables the reaction mix composition with a total volume of 20 µl and the reverse transcription reaction program can be found.

Table 25: Composition of reverse transcription reaction with +/-RT (positive reaction, +RT).

Components	**Amount**
LunaScript RT SuperMix (5X)	4 µl
RNA sample (up to 1 µg)	max 16 µl
Nuclease free H_2O	Fill up to total volume (X µl)
Sum Σ	20 µl

Table 26: Composition of reverse transcription reaction without +/-RT (negative control, -RT).

Components	Amount
No-RT Control Mix (5X)	4 µl
RNA sample (up to 1 µg)	max 16 µl
Nuclease free H_2O	Fill up to total volume (X µl)
Sum Σ	20 µl

For the revere transcription reactions different thermocycler (Mastercycler® nexus GX2 flexlid, Eppendorf, Veriti™ Thermal Cycler, 96-Well, Applied Biosystems) were used.

Table 27: Reverse transcription reaction program used for the conversion of RNA to cDNA fragments with LunaScript +/-RT SuperMix (5X) (NEB). denat.: denaturation, anneal.: annealing/hybridisation, elong.: elongation.

Temperature	25 °C	55 °C	95 °C	10 °C
Time	2 min	10 min	1 min	∞
Step	anneal.	elong.	denat.	end
Cycles	1			

After the reverse transcription was performed a subsequent PCR (Chapter 4.6.3.1) for target genes or mRNA and a gel electrophoresis (Chapter 4.6.1) were performed.

4.6.3.3 Site-directed deletion, insertion, and mutagenesis via PCR

To introduce or delete one or more base pairs and alter the amino acid sequence of the desired enzyme or add e.g. a Kozak sequence in front of the genes for *S. cerevisiae* [248], PCRs were performed according to Liu and Naismith [249]. The oligonucleotides for the mutagenesis were designed so that the mutation is located in the middle of the 25 nucleotide (nt) overlapping parts (T_m~55 °C) of the 5’ end of the priming oligonucleotide. The non-overlapping 3’ end of the priming oligonucleotides was designed with a melting point 5-10 °C higher than the melting point of the overlapping 5’ end (Figure 47).

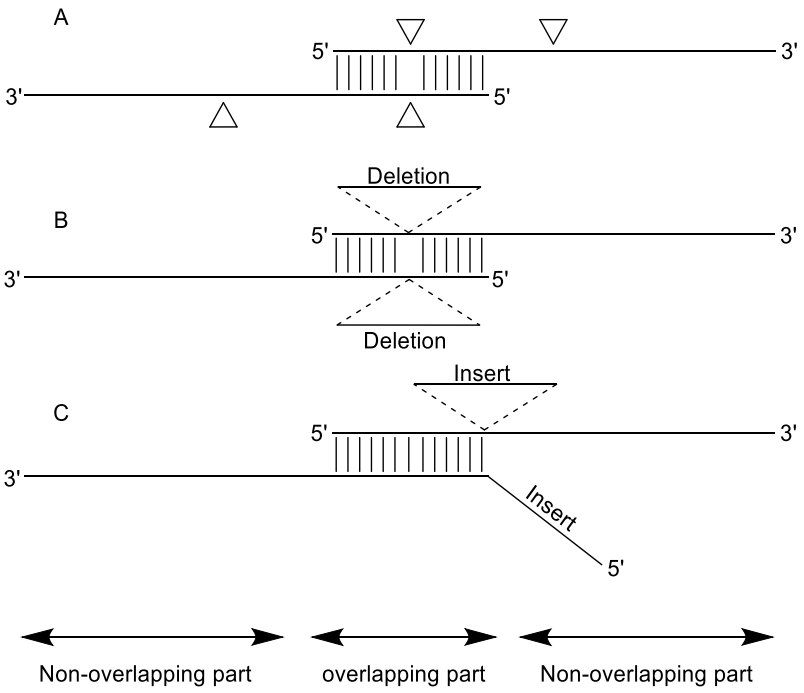

Figure 47: Schematic overview of the oligonucleotide design for (A) single/multiple base pair alteration, (B) deletion, and (C) insert of DNA fragments. The figure was adapted from Liu und Naismith 2008. [249]

Oligonucleotides for deletion and insertion were designed similarly to the mutagenesis oligonucleotides but missing a part for the deletion or inserting a part for insertion, like shown in Figure 47. The PCR protocol was then performed like described in Table 24, with the difference that the annealing temperature ~5 °C lower than that for the non-complementary part of the oligonucleotides and only 12-18 cycles. For multiple site mutation, insertions or deletions, after the 12-18 initial cycles an additional step with 1-12 cycles and ~5 °C lower than the complementary part of the oligonucleotides was performed.

After the PCR was done 5 µl of the PCR reaction was analysed via gel electrophoresis (Chapter 4.6.1) and the rest of the reaction was digested with *Dpn*I (digesting methylated template DNA), at 37 °C and 1h or ON. 1-5 µl of the digestion reaction was used to transform competent *E. coli* cells (Chapter 4.7.1 and Chapter 4.7.2), cultivating and harvesting them, with subsequent purification of plasmid DNA (Chapter 4.6.5).

4.6.3.4 Colony PCR for the verification of *E. coli* colonies

The colony PCR of *E. coli* works the same way a normal PCR (Chapter 4.6.3.1) works, however the template is not free, already pure DNA but the whole *E. coli* cell. Moreover, another polymerase enzyme is used, namely the Red Taq DNA Polymerase1.1 x Master Mix (VWR, cheaper with lower accuracy). To speed up the working process the Q5 High-Fidelity 2X Master Mix (NEB) can also be used to directly generate usable DNA fragments from the

plasmids of the transformed cells. The following Table 28 shows the reaction components for the Red Taq DNA Polymerase1.1 x Master Mix (VWR) in normal and colony PCR approaches.

Table 28: General overview of the reaction components for the Red Taq DNA Polymerase 1.1 x Master Mix (VWR) in normal and colony PCR.

Components	Amount [Colony PCR]	Amount [Test]	
DNA-Template (10-50 ng) or 1 colony (agar plate)	1 colony	1 µl	1-5 µl
Oligonucleotide fw (10 µm)	0.5 µl	0.5 µl	1 µl
Oligonucleotide rev (10 µm)	0.5 µl	0.5 µl	1 µl
Nuclease free H_2O	-	-	0-4 µl
Red Taq 1.1 x Master Mix	10 µl	10 µl	45 µl
Sum Σ	11 µl	12 µl	50 µl

After the performed PCR reaction (program in Table 29) PCR results were analysed with gel electrophoresis (Chapter 4.6.1) using the whole PCR reaction mix in 1 % agarose gel.

Table 29: General Summery of the PCR programs used for the amplification of target DNA fragments with Red Taq DNA Polymerase 1.1 x Master Mix (VWR). The annealing temperature was adjusted for each PCR reaction according to the T_m of the oligonucleotides used. The number of cycles was also adjusted to optimize the DNA fragments yields. denat.: denaturation, anneal.: annealing/hybridisation, elong.: elongation.

Temperature	95 °C	95 °C	50-70 °C	72 °C	72 °C	4 °C
Time	2 min	30 sec	30 sec	1 min/kb	5 min-10 min	∞
Step	denat.	denat.	anneal.	elong.	elong.	end
Cycles	1	35			1	1

4.6.3.5 Colony PCR for the verification of *S. cerevisiae* Colonies

The colony PCR protocol for *S. cerevisiae* cells is based on the principle that DNA can be entrapped and retained by Whatman® filter paper no.1. The protocol is adapted from Zou et al. 2017 describing a novel method of nucleic acid purification from plant, animals and microbes. [250] The Whatman® filter paper no.1 (Table 22) was cut in small pieces of about 2 to 4 mm and stored in a 1.5- or 2-ml reaction tube.

The PCR reaction tubes (200 µl reaction tubes, Biozym) were filled with 35 µl of the lysis buffer (Table 16) and the cells of one colony was resuspended in each of the reaction tubes till the liquid was milky. One piece of Whatman® filter paper no.1 was added to the cell suspension, shortly mixed by stirring and incubated for 1 min. The liquid was removed and

30 µl of the washing buffer (Table 16) was added, the suspension was incubated for 30 sec to 1 min. After stirring carefully, the remaining liquid was removed and the PCR mix like in Chapter 4.6.3.4 Table 28 was added and the PCR was performed like in Table 24 and Table **29** depending on the master mix that was used (Table 21).

4.6.4 Restriction digestions of DNA

The restriction digestion of DNA is based on the principle that restriction endonucleases are able to cut the DNA double strand either randomly or at a specific site. [251,252] These enzymes can be classified into four types whereas the type II restriction endonucleases became the most commonly used type in microbial biology. [252] The DNA can be cut within or outside a specific, mostly palindromic recognition site generating “sticky” ends, where one of the single DNA strands is longer than the other, or “blunt” ends, where both single strands of the DNA are equally cut. [253] Methods like the general restriction and ligation cloning or the Golden Gate assembly are harnessing the abilities of restriction endonucleases. [70]

All restriction enzymes used in this work are listed in Table 21.

4.6.4.1 Removing methylated DNA using *Dpn*I

PCR generated fragments (Chapter 4.6.3), which will be further used in cloning experiments were treated with *Dpn*I. In Each PCR reaction mix that was not purified via gel electrophoresis (Chapter 4.6.1), 1 µl *Dpn*I was used to digest all methylated template DNA that could interfere in final transformation experiments (Chapter 4.7.2). After the *Dpn*I-PCR reaction mix is incubated at 37 °C ON the mix was purified using the NucleoSpin® Gel and PCR Clean-up Kit (Macherey-Nagel, Chapter 4.6.5.1) and either directly transformed, nick repair in *E. coli* with complete plasmid PCR, or used in Gibson and adapted PCRGate assembly (Chapter 4.6.7.2).

4.6.4.2 Restriction digestion for linearisation or cloning

To implement exogenous DNA into the *S. cerevisiae* genome a relatively high amount (µg) of linear DNA with homologous flanking regions is needed. For that purpose, the integrative plasmids (Table 7) were generated (Chapter 4.6.7), harbouring the required pathway modification genes, selection marker, and homologous flanking regions. These, easy to amplify plasmids needed to be linearised. The linearization was done with the restriction endonuclease *Not*I as previously described. [194] Another approach was the restriction digestion for the adapted PCRGate assembly (Chapter 4.6.7.2) preparing the DNA fragments for assembly. For these reactions a volume of 25 µl or 50 µl according to Table 30 was used.

The reaction mix was incubated at 37 °C, 200 rpm ON and afterwards the reaction was stopped at 65 °C for 10 min. After using the linearized DNA for the transformation of *S. cerevisiae* (Chapter 4.7.4) the rest of the reaction was stored at -20 °C.

Table 30: Overview of the restriction digestion reaction mix used to linearize the integrative plasmids (Table 7) or prepare DNA fragments for the assembly reaction (Chapter 4.6.7.2). The reaction buffer was selected based on the recommendation from NEB "NEBuffer Activity/Performance Chart with Restriction Enzymes" for each restriction enzyme (Table 21).

Components	Amount [25 µl approach]	Amount [50 µl approach]
Plasmid DNA [10-100 µg]	10-21.5 µl	20-44 µl
10 x NEBuffer 3.1/2.1/1.1 or CutSmart	2.5 µl	5 µl
Restriction enzyme	1 µl	1 µl
Filtered (0.2 µm pore size) ultrapure H2O	fill up to total volume	
Sum Σ	25 µl	50 µl

4.6.5 DNA Purification Methods

4.6.5.1 DNA Purification with commercial Kits

All kits used for DNA purification were purchased from Macherey-Nagel (Düren, Germany) and can be found in Table 22.

i. NucleoSpin® Plasmid (NoLid) DNA purification

For the plasmid isolation from *E. coli* and *S. cerevisiae* the NucleoSpin® Plasmid (NoLid) DNA purification (Table 22) was used. The isolation and purification of the desired plasmid DNA was done according to the protocol (MN user manual Plasmid DNA purification, 09/2022, Rev. 13) provided by Macherey-Nagel, skipping the optional washing step with the AW buffer, and drying the silica membrane at 60 °C in the thermomixer (Eppendorf). A total of 5 ml cultivation Volume was used when cultivated in sterile 13 ml tubes (tube 13 ml, 100 x 16 mm, PP, Sarstedt) and around 2 ml when cultivated in sterile 100 ml Erlenmeyer flasks (Chapter 4.6.2). An overview of the protocol is shown in Table 31.

Table 31: Overview over the handling steps of the NucleoSpin® Plasmid (NoLid) DNA purification protocol used to isolate and purify plasmid DNA from *E. coli*.

Step		Procedure
1	Cultivate and harvest bacterial cells	2 ml reaction tube, 11000 xg, 30 sec
2	Cell lysis	Add: 250 µl Buffer A1 250 µl Buffer A2 Incubate: 5 min, RT Add: 300 µl Buffer A3
3	Clarification of the lysate	11000 xg, 5-10 min
4	Bind DNA	Transfer supernatant onto no lid silica membrane tube in collection tube, 11000 xg, 1 min
5	Wash silica membrane	Discard flow through, add: 600 µl Buffer A4, onto silica membrane, 11000 xg, 1 min
6	Dry silica membrane	Discard flow through, 11000 xg, 2 min
7	Elute DNA	Discard collection tube, place silica column in new 1.5 ml reaction tube, Dry: 1 min, 60 °C in thermomixer (Table 5) Add: 30-50 µl filtered (0.2 µm pore size) ultrapure H2O, Incubate: 1 min, RT 11000 xg, 1 min

To isolate plasmid DNA from *S. cerevisiae* an additional wash buffer and sorbitol buffer (Table 15) as well as lyticase, for cell wall digestion was needed. Table 32 shows an overview of the steps for the plasmid isolation from yeast.

Table 32: Overview over the handling steps of the supplementary plasmid DNA isolation protocol for S. cerevisiae. Additional information of the NucleoSpin® Plasmid (NoLid) DNA purification protocol used to isolate and purify plasmid DNA from *E. coli*.

Step		Procedure
1	Harvest yeast cells	Use 3 ml yeast ON culture (OD_{600} <10), 2 ml reaction tube, 5000 xg, 10 min
2	Wash cells	Discard supernatant, add: 1 ml wash buffer, resuspend, 5000 xg, 10 min
3	Resuspend pellet	Resuspend cells in 600 µl sorbitol buffer
4	Digest cell wall	Add: 200 U lyticase Incubate: 30 min, 30 °C
5	Isolate spheroplasts	2000 xg, 10 min
6	Isolate plasmids	Continue with step 2 of the NucleoSpin® Plasmid (NoLId) DNA purification protocol (Table 31)

After eluting the plasmid DNA, the DNA concentration was determined with the NanoDrop™ One microvolume-UV/VIS-spectrophotometer (Thermo Scientific, Table 5, Chapter 4.6.6).

ii. NucleoSpin® Gel and PCR Clean-up

With the NucleoSpin® Gel and PCR Clean-up kit, DNA fragments generated via PCR (Chapter 4.6.3) were purified. Purification was done either from agarose gel cut outs of conducted gel electrophoresis (Chapter 4.6.1) or directly from PCR reaction samples (Chapter 4.6.3) using the provided protocol (MN user manual, PCR clean-up and gel extraction, 04/2022, rev. 07). In Table 33 an overview over the handling steps of the protocol is shown.

Table 33: Overview over the handling steps of the NucleoSpin® Gel and PCR Clean-up protocol.

Step		Procedure [PCR Clean up]	Procedure [Gel extraction]
1	PCR Clean up Gel extraction	200 µl NTI buffer/ 100 µl PCR volume,	200 µl NTI buffer/ 100 mg gel Disolving Gel: 50 °C, 5-10 min, 500 rpm (thermomixer, Table **5**)
2	Bind DNA	Transfer solution into silica column, 11000 xg, 30 sec	
3	Wash silica membrane	Discard flow through 2 washing steps: add 700 µl NT3 buffer, 11000 xg, 30 sec	
4	Dry silica membrane	Discard flow through, 11000 xg, 1 min	

Step		Procedure [PCR Clean up]	Procedure [Gel extraction]
5	Elute DNA	Dry 1 min, 60 °C (thermomixer, Table 5), Add: 15-30 µl filtered (0.2 µm pore size) ultrapure H2O, incubate 1 min, RT 11000 xg, 1 min	

After eluting the DNA, the concentration was determined with the NanoDrop™ One microvolume-UV/VIS-spectrophotometer (Thermo Scientific, Table 5, Chapter 4.6.6).

iii. NucleoSpin® DNA Yeast

For the isolation of genomic DNA from yeast cells generated via transformation (Chapter 4.7.4) the NucleoSpin® DNA Yeast kit (MN user manual, Genomic DNA from yeast, 7/2022, rev. 02) was used. For that the cultivated yeast cells (Chapter 4.7.5), cultivated in 13 ml tubes (tube 13 ml, 100 x 16 mm, PP, Sarstedt) or 100 ml sterile Erlenmeyer flasks, were pelleted and the pellet was used for genomic DNA isolation according to the protocol in Table **34**.

Table 34: Overview over the handling steps of the NucleoSpin® DNA yeast protocol.

Step		Procedure
1	Prepare sample	< 100 mg yeast pellet +100 µl BE
2	Lyse sample	Transfer sample in NucleoSpin® Bead Tube Type C, Add: 40 µL buffer MG and 10 µL liquid Proteinase K Agitate bead tubes 15–20 min 11.000 x g, 30 sec
3	Adjust binding conditions	Add: 600 µl buffer MG Vortex for 3 sec 11000 xg, 30 sec
4	Bind DNA	Load the supernatant onto the NucleoSpin DNA yeast column 11000 xg, 30 sec
5	Wash silica membrane	1. Step: 500 µl buffer BW → 11000 xg, 30 sec 2. Step: 500 µl buffer B5 → 11000 xg, 30 sec
6	Dry silica membrane	11000 xg, 30 sec
7	Elute DNA	Add: 100 µl buffer BE Incubate for 1 min at RT 11000 xg, 30 sec

After the elution step the DNA was used for PCR (Chapter 4.6.3).

iv. NucleoSpin® RNA Plus

For the isolation of RNA from generated yeast cells the NucleoSpin® RNA Plus kit (MN user manual, RNA isolation, 04/2023, rev. 06) was used. For that the cultivated yeast cells (Chapter 4.7.5), cultivated in 13 ml tubes (tube 13 ml, 100 x 16 mm, PP, Sarstedt) or 100 ml sterile Erlenmeyer flasks, were pelleted and the pellet was used for RNA isolation according to the protocol in Table 35.

Table 35: Overview over the handling steps of the NucleoSpin® RNA Plus protocol with an addition of a DNase incubation step.

Step		Procedure
1	Homogenize sample	< 100 mg yeast pellet +350 µl Buffer LBP
+	lyse sample	Transfer sample in NucleoSpin® Bead Tube Type C Agitate bead tubes 15–20 min 11.000 x g, 30 sec
2	Remove gDNA	Transfer supernatant to a new reaction tube and add 1 µl DNase incubate 10 min at 37 °C incubate 10 min at 75 °C
3	filtrate lysates	Load the supernatant onto the NucleoSpin® gDNA Removal Column 11000 xg, 30 sec
3	Adjust RNA binding conditions	Add: 100 µl buffer BS and mix
4	Bind DNA	Transfer the whole lysate to the NucleoSpin® RNA Plus Column 11000 xg, 30 sec
5	Wash silica membrane	1. Step: 200 µl buffer WB1 → 11000 xg, 15 sec 2. Step: 600 µl buffer WB2 → 11000 xg, 15 sec
6	Dry silica membrane	Add 250 µl buffer WB2 → 11000 xg, 2 min
7	Elute DNA	Add: 2x 30 µl RNase free H_2O Incubate for 1 min at RT 11000 xg, 1 min

After eluting the RNA, concentration was determined with the NanoDrop™ One microvolume-UV/VIS-spectrophotometer (Thermo Scientific, Table 5, Chapter 4.6.6). The

samples were subsequently used for reverse transcription (Chapter 4.6.3.2) and the PCR utilizing the generated cDNA (Chapter 4.6.3.1).

4.6.5.2 Alkalic lysis of *E. coli* cells for high yields of plasmid DNA

For the alkalic lysis of the transformed cells, 2 ml of the ON cultures (Chapter 4.6.2) were pelleted for 1 min, full speed at RT (Centrifuge 5418 D /5424, Eppendorf). The supernatant was discarded, and the pellet was resuspended in 50 µl of solution I. The cells were lysed by adding 100 µl solution II and were carefully inverted 6-8 times. After approx. 1 min 75 µl of solution III and 225 µl of solution IV were added and everything was mixed by inverting 6-8 times. After centrifugating for 20 min, full speed at RT the supernatant was separated into a new 1.5 ml tube for further ethanol and isopropanol precipitation (Chapter 4.6.5.3). All solutions used for this protocol (solution I-IV) can be found in Table 14. Alternative to the conventional alkalic lysis, cells were lysed, and the plasmid DNA was purified with the help of kits from Macherey-Nagel (Chapter 4.6.5.1).

4.6.5.3 Ethanol and Isopropanol precipitation

To purify and precipitate DNA, typically ethanol is used. [254] Nevertheless, also isopropanol can be used for the precipitation. For that purpose, the supernatant of the alkaline plasmid isolation (Chapter 4.6.2) was mixed with 2.5 times the volume of absolute ethanol (-20 °C) or with one volume equivalent of isopropanol (-20 °C, inverting 5-6 times). After that the sample mix was centrifugated for 20 min, full speed at 4 °C (Centrifuge 5415 R, Eppendorf), the supernatant was discarded, and the pellet was washed with 70 % ethanol. The sample was centrifugated again (20 min, full speed, 4 °C) and the supernatant was carefully discarded. The 1.5 ml reaction tube containing the DNA pellet was placed in the thermomixer (thermomixer comfort, 1.5 ml, Eppendorf) and dried at 42 °C for a few minutes. When no ethanol was left over the pellet was dissolved in 50 µl filtered (0.2 µm pore size) ultrapure H_2O. If the pellet became too dry it will not dissolve easy.

In the end the concentration and purity of the dissolved DNA was determined with the NanoDrop™ One microvolume-UV/VIS-spectrophotometer (Thermo Scientific, Table 5, Chapter 4.6.6).

4.6.6 DNA quantification

The quantification of the purified DNA samples (Chapter 4.6.5) obtained by plasmid isolation (Chapter 4.6.2) and PCR (Chapter 4.6.3) was performed on a NanoDrop™ One microvolume-UV/VIS-spectrophotometer (Thermo Scientific). The DNA is measured at its

absorption maximum of 260 nm with a purity indicator given through the ratio of the absorption at 260 nm divided by the absorption at 280 nm (A_{260}/A_{280}). A ration of A_{260}/A_{280} of 1.7-1.9 indicates no contamination.

The device was calibrated with 2 µl of the solution the DNA was dissolved in, as reference, usually ultrapure H_2O, or elution buffer, delivered with the NucleoSpin Plasmid (NoLid) kit (MN, Table 22). After that the 2 µl of the DNA solution was measured. After each measurement the surface of the optical path was cleaned with ultrapure H_2O and dried.

4.6.7 Strategies for new Vector Cloning

Traditionally, restriction digestion and ligation have been the go-to methods for cloning new plasmids. However, as our understanding has advanced, several novel and modified cloning techniques have emerged, proving to be more efficient and often yielding greater success.

4.6.7.1 Gibson assembly

One of the most common cloning methods used in the research group was the Gibson isothermal assembly, which allows for connecting several DNA-fragments, mostly generated through PCR (Chapter 4.6.3.1) in one-step isothermal *in vitro* reaction. [71] The methods take advantage of the hybridisation abilities of complementary DNA sequences and the different properties of the three enzymes critical for the reaction, the 5'-T5 exonuclease (T5 exo), Phusion® polymerase (Phusion pol.), and the T4 DNA *Taq* Ligase (*Taq* lig, Table 21). By designing the oligonucleotides with overlapping complementary sequences, when amplifying the targeted DNA fragments, these fragments can be connected via the overlapping regions like shown in Figure 48. When the fragments are added to the Gibson reaction mix the 5'-T5 exonuclease degradants the ssDNA strand of the fragments from the 5' end, which leads to the hybridisation of the complementary sequence regions. The remaining gaps are than filled through the Phusion® polymerase with the free dNTPs and the strands are covalently connected with the help of the *Taq* DNA ligase, eventually.

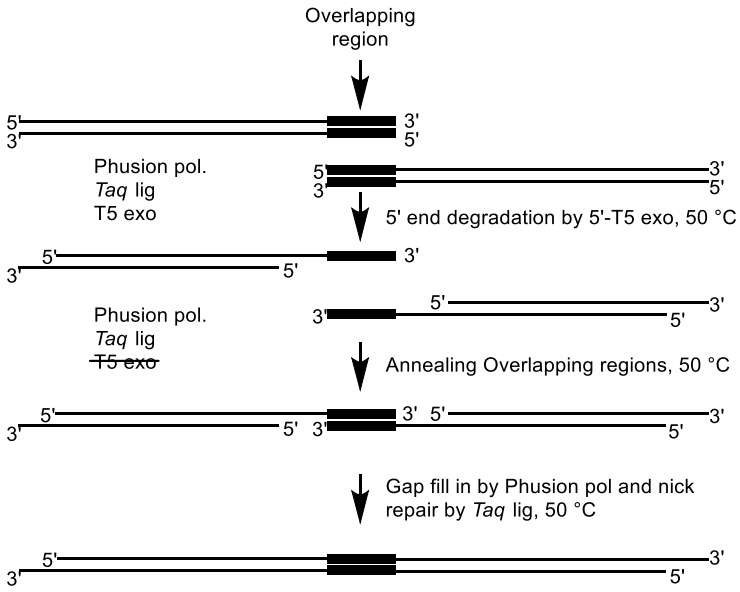

Figure 48: Working principle of the one-step isothermal Gibson assembly reaction. Two DNA fragments are covalently connected through sharing the overlapping regions in one-step isothermal reaction. Figure was adapted from Gibson et al. 2009. [71]

After designing the oligonucleotides (Chapter 4.2.3) and generating all DNA fragments (Chapter 4.6.3) for the Gibson assembly reaction, 100 ng of vector backbone DNA was used with the appropriately calculated DNA insert fragments [255] and added to the 3.2 x Gibson cloning master mix (Table 17). The reaction was performed for 60 min at 50 °C in a thermomixer (thermomixer comfort, 1.5 ml, Eppendorf) and after that directly used for transforming *E. coli* cells (Chapter 4.7.2). The screening for correct colonies was done by colony PCR (Chapter 4.6.3.4), analysed via gel electrophoresis (Chapter 4.6.1) and finally validated through sequencing (Chapter 4.6.8). The following table shows the Gibson assembly reaction mix composition.

Table 36: Pipetting scheme for the Gibson assembly reaction. The amount of DNA used for each fragment is calculated with the NEBioCalculator using 100 ng of vector backbone as starting point and its bp size. [255]

Components	**Amount**
Vector backbone DNA [100 ng]	X µl
Insert DNA fragment 1 [x ng, 1:1-5:1 ration]	X µl
Insert DNA fragment 2 [x ng, 1:1-5:1 ration]	X µl
Insert DNA fragment x [x ng, 1:1-5:1 ration]	X µl
3.2 x Gibson cloning master mix	5 µl (1 aliqout)
Ultrapure H_2O (filtered 0.2 µm pore size)	fill up to 11 µl
Sum Σ	11 µl

4.6.7.2 PCRGate Cloning

To expand the molecular cloning capabilities in the working group, for assembling multiple DNA fragments a PCR based cloning method was adapted from the principles of the Golden Gate assembly and Green Gate cloning. [70,217] The Golden Gate assembly uses two enzymes to assemble multiple DNA fragments in an *in vitro* restriction and ligation reaction. Thereby exploiting the properties of the type IIS restriction enzymes, by cutting the DNA in a defined distance to the recognition sequence, so the cutting site can be specially designed for target overlapping of specific DNA fragments. [218] The key aspect for the successful reaction is designing the oligonucleotides so that the recognition site of the restriction endonuclease is cut out and therefore does not appear in the T4 ligase ligated product (Figure 38). By adapting and expanding the overhangs used to connect the fixed modules in Lampropoulos et al. 2013 an oligonucleotide designing template for up to 9 insert DNA fragments was designed (Table S47 in Supplements 1.2). [217] Also, a destination vector with a deviating antibiotic selection marker for rapid cloning and transformation without the need for an ON *Dpn*I reaction (Chapter 4.6.4.1) was prepared (Table 7).

With the oligonucleotide design table (example in Table S47) the oligonucleotides for fragment generation can be design according to the number of insert to be assembled. After every fragment is generated via simple PCR (Chapter 4.6.3.1), 100 ng of the biggest DNA fragment (mostly the vector backbone) is used for the calculation (NEBiocalculator, [255]) of the amounts for each insert DNA fragment and destination vector (purified (Chapter 4.6.5.1ii) or directly after the PCR reaction). For the restriction *Esp3*I, and for the ligation the T4 ligase was added (Table 21). All ingredients for the reaction mix are shown in Table 37.

Table 37: Pipetting scheme for the PCRGate assembly reaction. The amount DNA used for each fragment is calculated with the NEBioCalculator using 100 ng of biggest DNA fragment as starting point and its bp size. [255]

Components	**Amount**
Destination vector [100 ng, if biggest DNA fragment]	X µl
Insert DNA fragment 1 [x ng, 1:1 ration]	X µl
Insert DNA fragment 2 [x ng, 1:1 ration]	X µl
Insert DNA fragment x [x ng, 1:1 ration]	X µl
T4 DNA ligase buffer (10 x)	2 µl
Esp3I	2 µl
T4 DNA Ligase	0.5 µl
Ultrapure H_2O (filtered 0.2 µm pore size)	fill up to 20 µl
Sum Σ	20 µl

The restriction and ligation reaction was performed in a PCR-thermocycler (Table 5) and 200 µl reaction tubes (Biozym) according to the protocol in Table 38. After that 1 µl of the reaction was used for *E. coli* transformation (Chapter 4.7.2). The results were validated by colony PCR (Chapter 4.6.3.4) and sequencing (Chapter 4.6.8).

Table 38: Program for the PCRGate assembly method used in this work.

Temperature	37 °C	37 °C	16 °C	65 °C	4 °C
Time	15 min	2 min	5 min	5 min	∞
Step	restriction	restriction	ligation	inactivation	end
Cycles	1	30-50		1	1

4.6.8 DNA Sequencing

Cloning and assembling (Chapter 4.6.7) new plasmids always represents the risk of errors during the cloning processes as well as the DNA fragment generation via PCR (Chapter 4.6.3). Despite using a very accurate polymerase (Q5 High-Fidelity 2X Master Mix, NEB), the possibility of point mutations, which could render a protein inactive remains. Even missing parts in the assembly process, doubling or other error can occur. To rule out any mistakes the plasmids and the genes were sequenced using an extern sequencing provider, Mircosynth Seqlab GmbH. Each sequencing sample contained a total volume of 12 µl consisting of 3 µl sequencing oligonucleotides (10 µm), filtered (0.2 µm pore size) ultrapure H_2O, and the purified DNA sample (Chapter 4.6.5) in 1.5 ml reaction tube. The following Table **39** shows the sequencing sample composition recommended by Mircosynth Seqlab for a successful sequencing reaction.

Table 39: Recommended requirements by Mircosynth Seqlab.

Template	**Concentration**	**Volumes**
Plasmid	40-100 ng/µl	Premixed: 12 µl DNA template solution + 3 µl 10 µM sequencing oligonucleotides
PCR product	General rule: 1.5 ng/µl per 100 bp	
PCR 1000-2000 bp	30 ng/µl	
PCR 500-1000 bp	15 ng/µl	
PCR 250-500 bp	7.5 ng/µl	
PCR 100-250 bp	4 ng/µl	

4.7 Microbiological methods

4.7.1 Protocol for chemical ultra-competent *E. coli* cells

The protocol used in the working group for ultra-competent DH5α *E. coli* cells is derived and adapted from the literature. [256]

For ultra-competent DH5α *E. coli* cells 10 ml LB-medium (Table 9) was inoculated with a single colony of DH5α *E. coli* cells with or without antibiotics at 37 °C, 200 rpm over the day. After approx. 7-8 hours a main culture of 100 ml LB-medium in an Erlenmeyer flask with baffles was inoculated to an OD_{600nm} of 0.5 and incubated ON at 20 °C, 200 rpm. After the OD_{600nm} reached 0.55 the flasks were transferred to an ice water bath for 10 min. The cells were harvested in 50 ml screw cap tubes (tubes 50 ml, 114 x 28 mm, PP, Sarstedt) at 2500 xg for 10 min, 4 °C. The supernatant was discarded, and the residual medium was removed by placing the screw cap tubes upside down on a paper towel for 2 min. The cell pellet in each screw cap tube then was gently resuspended in 16 ml of ice-cold Inoue buffer (Table 18) and centrifugated again at 2500 xg for 10 min, 4 °C. The supernatant was removed like described before and the pellets were again gently resuspended in 4 ml ice-cold Inoue buffer each, before adding 0.3 ml DMSO. The bacterial suspension was mixed by swirling and stored on ice for 10 min. The suspension was quickly aliquoted into sterile 1.5 ml reaction tubes (Eppendorf) by dispensing 100 µl. The tubes were immediately frozen in a liquid nitrogen bath and the tubes were stored at -80 °C.

4.7.2 Heat-shock transformation of *E. coli*

E. coli cells can become competent for the uptake of external DNA in different ways. One way is to use a chemical method with the help of an excess of Ca^{2+} ions. The most efficient way to transform *E. coli* cells with exogenous DNA is to transform the cells in their exponential growth phase. To increase the readiness to take up DNA a heat shock is used during the transformation protocol. [257]

To amplify plasmid DNA after cloning experiments (Chapter 4.6.7) or simply to yield high amounts of plasmid DNA for e. g. yeast transformation (Chapter 4.7.4), the plasmid needs to enter the cells. First the ultra-competent *E. coli* cells (Chapter 4.7.1) were thawed on ice and 1-5 µl of DNA (plasmid, ~10 ng) was added to the cell suspension and mixed via stirring. The mix was incubated for 10 min on ice. After that the cells were heated at 42 °C (heat-shock) for 1 min in a thermomixer (thermomixer comfort, 1.5 ml, Eppendorf) and subsequently incubated on ice for 2 min. Now 450 µl of SOC medium (Table 9) were added and the transformation approach was incubated for 30 min at 37 °C, 300 rpm (thermomixer comfort, 1.5 ml,

Eppendorf). When using ampicillin as a selection marker (Table 11) the SOC medium and the 30 min incubation step can be skipped, but for all other antibiotics it is necessary. Finally, the transformation mix is plated on LB agar plates containing the plasmid specific antibiotic and incubated ON at 37 °C. On the next day the single colonies were used for colony PCR (Chapter 4.6.3.4) and cultivation in liquid media (Chapter 4.6.2 and Chapter 4.7.5).

4.7.3 Protocol for chemical competent *S. cerevisiae* cells

The protocol for chemical competent *S. cerevisiae* cells used in this work was modified according to Gietz und Schiestl 2007. [258] For competent yeast cells a preculture of 10 ml selective medium (Table 10, Table 9) in 100 mL Erlenmeyer flasks (with baffles) was incubated ON at 30 °C, 200 rpm (Orbitron, 2.5 cm displacement). The main culture of 50 mL YPD-medium (Table 10) in 500 mL Erlenmeyer flasks (with baffles) was inoculated to an OD_{600} of 0.1 to 0.2 and incubated at 30 °C, 200 rpm to an OD_{600} between 0.5 to 0.6. When the desired OD_{600} was reached the cell culture was transferred to sterile 50 ml screw cap tubes (tubes 50 ml, 114 x 28 mm, PP, Sarstedt) and harvested via centrifugation (2000 xg, 5 min, RT). The remaining cell pellet was washed by careful resuspending with 25 mL sterile ultrapure H_2O (0.2 µm pore size) and centrifugated again under previous conditions. After removing the supernatant, the pellet was resuspended in 0.5 mL sterile ultrapure H_2O (0.2 µm pore size) and transferred to a sterile 1.5 mL reaction tube (Eppendorf) for centrifugation (2000 xg, 5 min, RT). The resulting pellet finally was resuspended in sterile filtered frozen competent cell (FCC) solution (Table 19) and split into 50 µl aliquots in sterile 1.5 mL reaction tubes (Eppendorf). The aliquots were stored in a Styrofoam box with lid and frozen at -80 °C till further use.

The prepared competent cell aliquots were tawed for subsequent transformation experiments (Chapter 4.7.4).

4.7.4 Transformation of *S. cerevisiae*

Before using alkali cations and polyethylene-glycol (PEG), the transformation of *S. cerevisiae* was very laborious.[259] Despite being not the most effective transformation method the 1983 established alkali cation and PEG method is one of the most common method used for transforming yeast. [259,260] After using single stranded carrier DNA in the alkali cation and PEG method the efficacy increased dramatically. [259] Together with the protocol of Gietz und Schiestl, 2007 for yeast transformation, reducing the procedure time, a modified version of the transformation protocol is used. [258]

For the transformation protocol, to integrate exogenous DNA into the yeast genome or introduce plasmid DNA into the yeast cell, a transformation mix was prepared according to

Table 40. The ssDNA had to be freshly denaturized for each transformation experiment by incubating the tubes with ssDNA at 95 °C for 5 min (thermomixer comfort, 1.5 ml, Eppendorf), following 2 min on ice. The DNA for the transformation was also prepared in a DNA mix shown in Table 41.

Table 40: Components for the transformation mix used in the yeast cell transformation protocol. Amounts given were for one transformation attempt.

Component	Amount
PEG 3350 (50 % (w/v))	260 µl
Li acetate 1 M	36 µl
Freshly denaturated ssDNA (2 mg ml^{-1})	50 ml
Sum Σ	346 µl

Table 41: DNA mix composition for yeast cell transformation.

Component	Amount
DNA (500 ng plasmid, 1-5 µg for genome integration)	x µl
Filtered ultrapure H_2O (0.2 µm pore size)	Fill to final volume
Sum Σ	14 µl

Chemical competent yeast cells (Chapter 4.7.3) were defrosted for 0.5-1 min at 37 °C and pelleted at 13000 xg for 2 min. The supernatant was discarded, and the pellet was resuspended in 14 µl of the DNA mix before the transformation mix was added and mixed via pipette and vortex before the heat-shock. The heat-shock was performed in the thermomixer (thermomixer comfort, 1.5 ml, Eppendorf) at 42 °C for 40 min. After that the cells were centrifugated for 30 sec at 13000 xg and the supernatant was discarded. The resulting pellet was resuspended in 1 ml YPD medium and incubated for an additional 4 hour at 30 °C. Transformations using only URA3 selection markers can be plated directly onto YPD agar plates and do not require a 4-hour incubation step. The plated cells were then incubated at 30 °C for several days, till colonies are visible and big enough to be used for yeast colony PCR (Chapter 4.6.3.5) or for the inoculation in liquid cultures for genome isolation (Chapter 4.6.5.1iii), cultivation and storage (Chapter 4.7.5), or the cultivation in Biolector experiments (Chapter 4.7.5.1).

4.7.5 Cultivation and Storage of *E. coli* and *S. cerevisiae*

The media used in this section are shown in Table 9 (*E. coli*) and Table 10 (*S. cerevisiae*). The antibiotics for selection and their appropriate concentration can be found in Table 11. The cultivations were done in a 1:10 ration of medium to flask volume (Erlenmeyer

flasks) or in sterile 13 ml tubes (tube 13 ml, 100 x 16 mm, PP, Sarstedt) for 2 ml plasmid isolation and purification experiments (Chapter 4.6.2 and Chapter 4.6.5). The incubation was done with an agitation of 200 rpm at 30 °C (*E. coli*) or 37 °C (*S. cerevisiae*) ON.

4.7.5.1 Biolector cultivation and HPLC sample preparation

For rapid screening and highly parallelised cultivation of the modified and selected yeast cells, the Biolector system from M2P labs GmbH was used. With this system 48 different cultivations approaches can be done in parallel. For that a 48 well FlowerPlate was used, with and without transparent bottoms. The transparent bottoms enable live tracking of the growth progress of each cultivation. For every well 1000 µl cultivation medium of Table 10 was used depending on the respective selection marker used for the modifications. Each well was inoculated with one yeast colony and cultivated for 72 h at 1200 rpm agitation and 30 °C with 80 % humidity. Upon completion of the 72 h cultivation the cells were transferred to 1.5 ml reaction tubes (Eppendorf) and harvested via centrifugation (30 min, full speed, Centrifuge 5418 D /5424, 5415 R, Eppendorf). The supernatant was transferred to fresh 1.5 ml reaction tube and 500 µl of that were filtered (0.2 µm poresize) and mix 1:1 with sterile ultrapure H_2O (TKA Thermo Scientific GenPure UV-TOC x-CAD Plus Benchtop) in a HPLC vial. The samples were either directly measured via HPLC (Chapter 4.10.1) or stored at -20 °C till analysis.

For a better comparability already selected producing strains were pre-cultivated ON (Chapter 4.7.5) and used for the inoculation of each well at an OD_{600} of 0.5. These cultivations were done in triplets.

4.8 Protein biochemical methods

4.8.1 *S. cerevisiae* cell disruption

To disrupt the resilient yeast cell, a protocol was employed, combining the established disruption protocol for yeast cells used in the research group with the Nucleospin® DNA Yeast kit (Chapter 4.6.5.1iii). Following yeast cell cultivation and harvest (Chapter 4.7.5) the pellet was washed with ultrapure H_2O (TKA Thermo Scientific GenPure UV-TOC x-CAD Plus Benchtop). For the disruption, 0.5 ml or 1 ml reaction tubes were used. The cell pellet was transferred to these tubes and filled to the top with glass beads (Roth, Glass beads 0.75 - 1.0 mm). Ultrapure H_2O (TKA Thermo Scientific GenPure UV-TOC x-CAD Plus Benchtop) was added until all the air was removed, and the tubes were sealed. After agitating the cells for 15 min at 4 °C full speed (LAB VORTEX with mixing head, Heathrow Scientific), the suspension was transferred to new 1.5 ml reaction tubes (Eppendorf) and centrifugated (5 min,

full speed, Centrifuge 5418 D /5424, Eppendorf). The resulting supernatant was transferred to a HPLC vial for measurement (Chapter 4.10.1.2).

4.9 Methods for Extracting and Concentrating

4.9.1 Speedvac DNA evaporation

To reduce volume from DNA or compound solutions, the Concentrator plus (Eppendorf) was employed. This centrifuge-style device utilizes vacuum, rotation, and heat to eliminate excess volume from samples. The 1.5 ml reaction tubes (Eppendorf) were positioned in the concentrator, and the solvent-specific program was selected and applied to reduce the sample volume.

4.9.2 Isolation and Extraction of 3-Hydroxypropionic acid

To extract 3-HP from the medium of the cultivated strains, the yeast cells were cultivated and harvested (Chapter 4.7.5) to obtain the resulting supernatant. For larger volume cultivations (50 ml or more), the supernatant medium volume was initially reduced. This involved transferring the supernatant to a round-bottom flask, freezing it to -196 °C using liquid N_2, and removing water from the supernatant via overnight lyophilization (Lyophille alpha 1-4 LSC, Martin Christ Gefriertrocknungsanlagen GmbH). The resulting residues were dissolved in 10-25 ml ultrapure H_2O (TKA Thermo Scientific GenPure UV-TOC x-CAD Plus Benchtop), depending on the cultivation volume, and then extracted.

The extraction protocol was adapted and modified based on a literature protocol. [212] The reduced supernatant volume was adjusted to a pH of 1-2 with HCl to protonate the 3-HP molecules for better extraction results. The extraction was performed three times using three times the volume of ethyl acetate based on the supernatant volume. The resulting ethyl acetate volume was dried with dry $MgSO_4$. This $MgSO_4$ was added until no more clumps formed. Subsequently, the ethyl acetate was filtered and evaporated (Buchi 23022A020 Rotary Evaporator, Diagonal Condenser, Professional Controller, 115V, BÜCHI Labortechnik GmbH) until no solvent remained. The residues were dissolved either in $CDCl_3$ or D-methanol for NMR measurements (Chapter 4.10.2).

4.10 Analytical Methods

4.10.1 High-performance liquid chromatography (HPLC)

The HPLC (high-performance liquid chromatography) in this work was performed on a 1260 Infinity II LC System (Agilent Santa Clara, USA) for shikimate derived products. For malonyl-CoA derived product a 1260/1200 Infinity LC System with a 1260 Infinity binary pump, refractive index (RI) detector, 210 nm wavelength detector and multicolumn thermostat in combination with a 1200 Infinity autosampler and vacuum degassing unit (Agilent Santa Clara, USA) was used. All peak areas of interest were integrated with OpenLab CDS (Agilent, Santa Clara, USA) and quantification was performed using a standard curve.

4.10.1.1 *p*-Coumaric acid and Tyrosine analysis

The method used for the quantification of tyrosine and p-CA was adapted from Steinmann et al. 2022. [216] Sample separation was achieved on a reversed-phase (RP) EC 100/2 Nucleoshell RP18 column (100 × 2 mm), with a particle size of 2.7 µm (MN). All samples were analysed using a gradient method with two solvents: 0.05 % formic acid in degassed ultrapure H_2O (A) (c) and 0.05 % formic acid in degassed methanol (B). With a flow rate of 0.3 ml/min, the following gradient was used: 0-2 min 98 % A, 2-4 min 98-75 % A, 4-15 min 75-70 % A, 15-18 min 70-10 % A, 18-20 min 10 % A, 10-98 % 20-21 min A and 21-26 min 98 % A. The injection volume was 5 µl and column temperature was set to 30 °C. p-CA was detected at 310 nm and tyrosine at 280 nm. Retention time for p-CA was 9.05 min and for tyrosine 1.25 min.

4.10.1.2 3-Hydroxypropionic acid analysis

The method used for the 3-HP analysis and quantification was a standard isocratic sugar analysis method in our laboratory. All samples were measured with an isocratic protocol of 0.05 mM H_2SO_4 in ultrapure H_2O (TKA Thermo Scientific GenPure UV-TOC x-CAD Plus Benchtop), 15 min degassed and a flowrate of 0.5 ml min^{-1} on a Metab-AAC HPLC-column (BF-series, 300 x 7.8 mm), with a particle size of 10 µm (ISERA GmbH, Düren, Germany). The column temperature was set to 40 °C and 3-HP was detected at 210 nm at a retention time of 16.4 min to 16.6 min depending on the samples in the measurement run. Because of this retention time discrepancy for each measurement a series of 3-HP standards was measured every time. A series of 12 dilutions was prepared starting from the highest concentration of 10 g/L going down as far as 4.88 mg/L. The 3-HP standard was purchased from Sigma Aldrich as 30 % solution in water. The standard series samples were prepared using 50 % of the

medium the cells were cultivated in with 50 % H_2O (TKA Thermo Scientific GenPure UV-TOC x-CAD Plus Benchtop), to ensure the same conditions as for the 3-HP culture samples.

4.10.2 3-HP analysis with nuclear magnetic resonance (NMR)

To confirm actual 3-HP production in the generated production strains, the nuclear magnetic resonance (NMR) method was employed. The extracted and concentrated cultivation samples were dissolved in 0.5 to 1.0 ml $CDCl_3$ and D-methanol, respectively. These solutions were then transferred to NMR tubes for NMR measurements. The measurement was performed outside of the research group. The measurement spanned several hours measuring signal intensity in the ^{1}H and ^{13}C NMR spectrum. The measurements were carried out at 298 K with a frequency of 500 Hz for ^{1}H and 125 Hz for ^{13}C. The resulting spectra were analysed using the Bruker TopSpin® NMR software.

Abbreviations

+/-RT	with/without reverse transcriptase
µm	micometer
µmol	micromol
^{13}C	carbon-13 isotope
^{1}H	hydrogen-1 isotop, Protium
2-OG	2-oxoglutarate
3-HP	3-hydroxypropionic acid
5-FOA	5-fluoroorotic acid
AAA	aromatic amino acids
A-ALDp	acetylating acetaldehyde dehydrogenase
acc1	acetyl-CoA carboxylase
ACLp	citrate lyase
ACP	acyl carry domains
acs1	acetyl-CoA synthase
acs_{Se}^{L641P}	acetyl-CoA synthase from *Salmonella enterica*
ADH	alcohol dehydrogenase
adh1	alcohol dehydrogenase
ADP	adenosine diphosphate
AGAP	any-gene-any-plasmid
ald2	aldehyde dehydrogenase again
ald6	aldehyde dehydrogenase
anneal.	annealing/hybridisation
APS	Ammonium persulfate
aro10	2-oxo-acid (phenylpyruvate) decarboxylase
ARO2	bifunctional chorismate synthase

ARO4p	DAHP synthase
ARO7p	chorismate mutase
aro8/9	aromatic aminotransferase,
aroA$_{Ec}$	EPSP synthase from *E. coli*
aroB$_{Ec}$	dehydroquinate synthase from *E. coli*
aroL$_{Ec}$	shikimate kinase from *E. coli*
AroLp$_{Ec}$	shikimate kinase from *E. coli*
AT	acyltransferase
ATP	adenosine triphosphate
Bacillus subtilis	*B. subtilis*
BC	before christ
BMBF	Bundesministerium für Bildung und Förderung
bp	base pair
C domain	condensation
C. aurantiacus	*Chloroflexus aurantiacus*
Cas9	(CRISPR)–associated protein 9
$CDCl_3$	Deuterated chloroform
CHA	chorismate
cit1/2/3	citrate synthase
CO_2	carbon dioxid
CoA	coenzyme A
CRISPR/Cas9	clustered regularly interspaced short palindromic repeats
crRNA	CRISPR RNA
dATP	Deoxyadenosine triphosphate
dCTP	Deoxycytidine triphosphate
denat.	Denaturation
dGTP	Deoxyguanosine triphosphate

DH	dehydratase
DHAP	dihydroxyacetone phosphate
DHAP	dihydroxyacetone phosphate
DHCHC	5-dihydrocyclohex-1-ene-carboxylic acid
DHQ	3-dehydroquinic acid
DHS	3-dehydroshikimate
DMAPP	dimethylallyl diphosphate
DNA	deoxyribonucleic acid
dNTP	Deoxynucleotide Triphosphate
dsDNA	double stranded DNA
DTT	Dithiothreitol
dTTP	Thymidine triphosphate
DTU	Technical University of Denmark
DXP	2-C-methyl-d-erythritol-4-phosphate pathway
E domain	epimerases
E. coli	*Escherichia coli*
e. g.	exempli gratia
E4P	D-erythrose-4-phophate
E4P	erythrose-4-phosphate
EDTA	Ethylenediaminetetraacetic acid
elong.	elongation
eno1-2	phosphopyruvate hydratase
EPSP	5-enolpyr- uvylshikimate-3-phosphate
ER	enol reductase
EPSP	3-enolpyruvyl-shikimate 5-phosphate
F. johnsoniae	*Flavobacterium johnsoniae*
F6P	fructose-6phosphate

FA	fatty alcohols
FAEE	fatty acid ethyl ester
fas3	acetyl-CoA carboxylase
FCC	frozen competent cell
FFA	free fatty acids
FPP	farnesyl diphosphate
G3P	glyceraldehyde 3-phosphate
G3P	glyceraldehyde-3-phosphate
G3P	glyceraldehydes-3-phosphate
G6P	glucose-6-phosphate
G6P	glucose-6-phosphate
GABA	gamma-aminobutyrate
GFP	Green fluorescence protein
GGPP	geranylgeranyl diphosphate
Gln	glutamine
Glu	glutamate
gnd1	phosphogluconate dehydrogenase
gpd1	glycerol-3-Phosphate Dehydrogenase
gpd1	Glycerol-3-phosphate dehydrogenase
GRAS	generally regarded as safe
GYC	glyoxylate cycle
h	hour
H. aurantiacus	*Herpetosiphon aurantiacus*
H^+	hydrogen proton
H_2O	water
HPLC	high-performance liquid chromatography
Hz	Hertz

IC_{50}	Half-maximal inhibitory concentration
InGP	indole-3-glycerol phosphate synthase
IPP	isopentenyl diphosphate
K	Kelvin
kb	kilobase
KR domain	the β–keto reductase
KR	β–keto reductase
KS	ketosynthase
L	liter
L. lactis	*Lactococcus lactis*
L. mesenteroides	*Leuconostoc mesenteroides*
LAT1	dihydrolipoamide acetyltransferase
LB-medium	lysogeny broth medium
LPD1	dihydrolipoamide dehydrogenase
M	Mol
mcr_{Ca}	malonyl-CoA reductase from *Chloroflexus aurantiacus*
MEP	non-mevalonate pathway
mg	milligram
Min	minute
mls1	malate synthase
mM	millimol
mmol	millimole
MN	Macherey-Nagel (Düren, Germany)
MT domain	methyltransferases
MVA	mevalonate pathway
NAD	nicotinamide adenine dinucleotide

NADH	reduced nicotinamide adenine dinucleotide
NAT	Nourseothricin Acetyltransferase
NEB	New England Biolabs
Nm	nanometer
NMR	nuclear magnetic resonance
NP	natural products
NRPS	non-ribosomal peptide synthase
nt	Nucleotide
OD_{600}	optical desity at 600 nm
ON	over night
PAL	phenylalanine ammonia-lyase
PAM	protospacer adjacent motif
p-CA	para-coumaric acid
PCP	peptide carry domains
PCR	polymerase chain reaction
PDA1 and PDB1	pyruvate dehydrogenase
pdc1	pyruvate decarboxylase
pdc1	pyruvate decarboxylase
pdc5	2-oxo-acid (pyruvate) decarboxylases
pdh	pyruvate dehydrogenase complex
PDX1	pyruvate dehydrogenase complex component X
PEG	polyethylene-glycol
PEG-8000	Polyethylene glycol
PEP	phosphoenolpyruvate
pgi1	phosphoglucose isomerase
pgk1	phosphoglycerate kinase
pha2	prephenate dehydratase

P_i	phosphate
PIPES	piperazine-N,N′-bis(2-ethanesulfonic acid
pKa	acid dissociation constant
PKS	polyketide synthase
ppm	parts per million
PPP	pentose phosphate pathway
PPtase	phosphopantetheinyl transferase
PRA	phosphoribosyl anthranilate
Pyr	pyruvate
Pyr	pyruvate
R5P	ribose-5-phosphate
RI	refractive index
RL5P	ribulose-5phosphate
RNA	Ribonucleic acid
RP	reversed-phase
rpm	revolutions per minute
Rt	retention time
RT	room temperature
S. entérica	*Salmonella enterica*
S. cerevisiae	*Saccharomyces cerevisiae*
S7P	sedoheptulose-7-phosphate
SC-medium	synthetic complete medium
SD-Medium	Synthetic drop-out Medium
SDS	Sodium dodecyl sulfate
Sec	seconds
$SFPp_{Bs}$	PPTases from *B. subtilis*
sgRNA	single-guide RNA

SOB-medium	super optimal broth medium
SOC-medium	super optimal broth medium with glucose
ssDNA	Single-stranded carrier DNA
T_a	melting point of the completely hybridised oligonucleotide
TAE	tris base, acetic acid and EDTA
tal1	transaldolase
$TALp_{Fj}$	tyrosine ammonia lyase from *F. johnsoniae*
$TALp_{Ha}$	Tyrosin-Ammoniak-Lyase from *H. aurantiacus*
TAT1	amino acid transporter for tyrosine
TCA	tricarboxylic acid cycle
tCPS1	terminator of CarboxyPeptidase yscS
tdh1-3	glyceraldehyde-3-phosphate dehydrogenase
tHis5	terminator of ATP phosphoribosyltransferase
tkl1	transketolase
T_m	melting temperature of the complementary part of the oligonucleotide
tpi1	triose-phosphate-isomerase
trp1	phosphoribosyl anthranilate (PRA) Isomerase,
trp2/3	anthranilate synthase complex
Trp3	indole-3-glycerol phosphate synthase (InGP) synthase
trp4	phosphoribosyltransferase
Trp5	tryptophan synthase
tyr1	prephenate dehydrogenase
uga1	gamma-aminobutyrate (GABA) transaminase
USER	Uracil specific excision reagent
UV	ultraviolett
UV/VIS	ultraviolet and visible

V	volume
v/v	volume per volume
vs.	versus
w/v	weight per volume
X5P	xylulose-5-phosphate
xfpk$_{Bb}$	phosphoketolase from *Bifidobacterium breve*
xPKp	ylulose-5-phosphate specific phosphoketolase from *L. mesenteroides*
Y. lipolytica	*Yarrow lipolytica*
ydiB$_{Ec}$	shikimate dehydrogenase from *E. coli*
YNB	yeast nitrogen base
YPD	yeast extract peptone dextrose
zwf1	glucose-6-phosphate dehydrogenase

List of Figures

List of Tables

Supplements

1.1 Vector maps and generated strains

Table S42: This table shows all vector maps of the plasmids used and described in this work. All maps were created with SnapGene® Viewer.

Vector name	Map
pDionysos-GlcRepfree	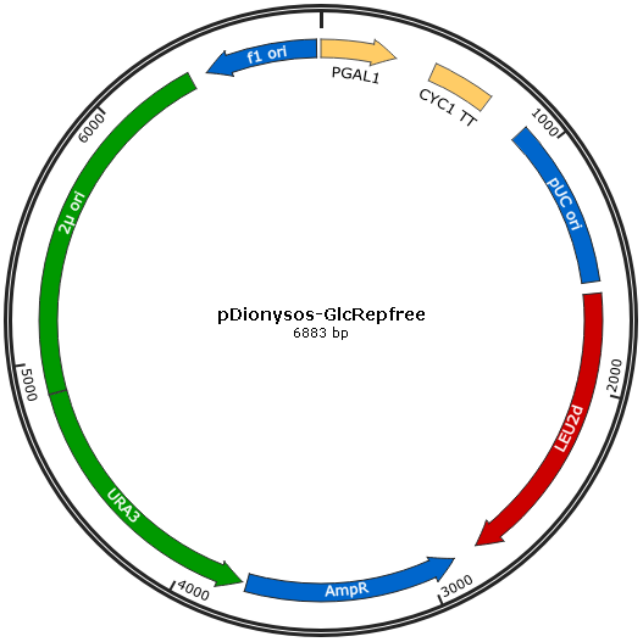
pDionysos-GlcRepfree-*sfp*-B.Sub.	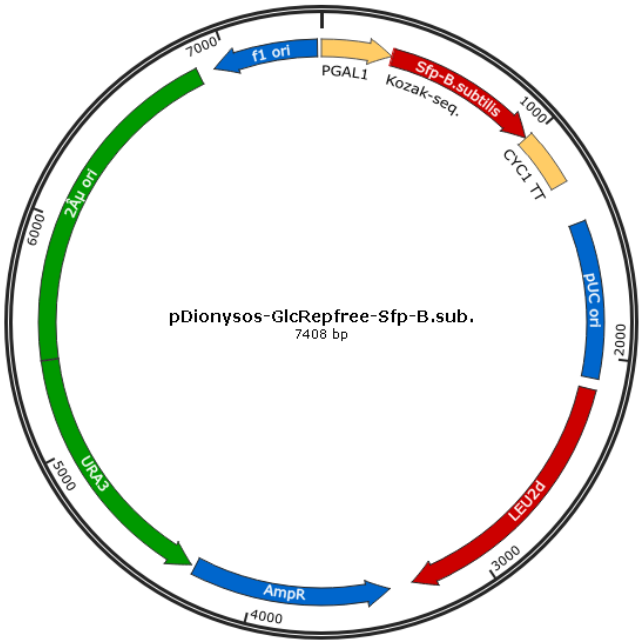

Vector name	Map
p426_Cas9_gRNA-ARS720a	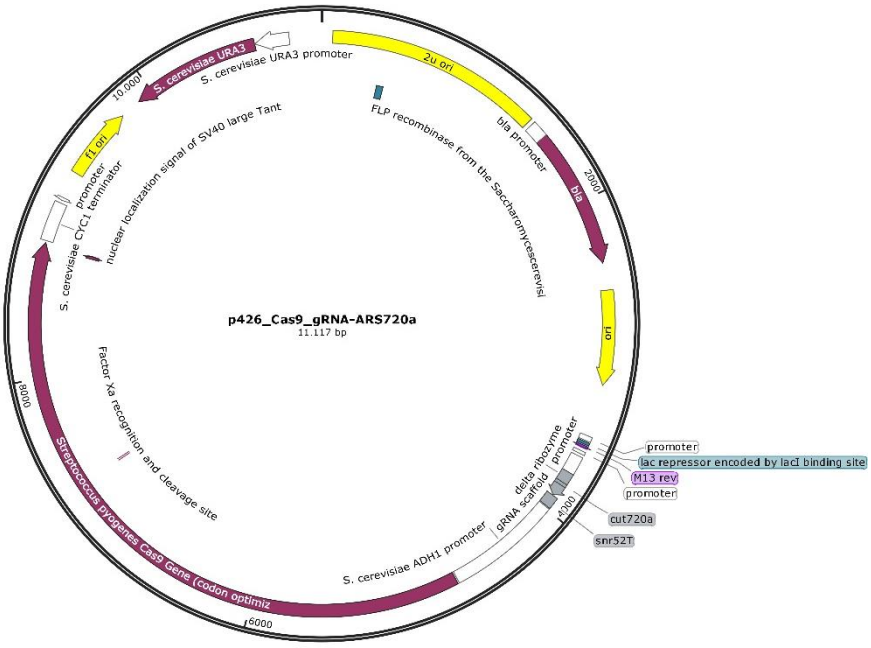
pCutX-Lys5-Knockout	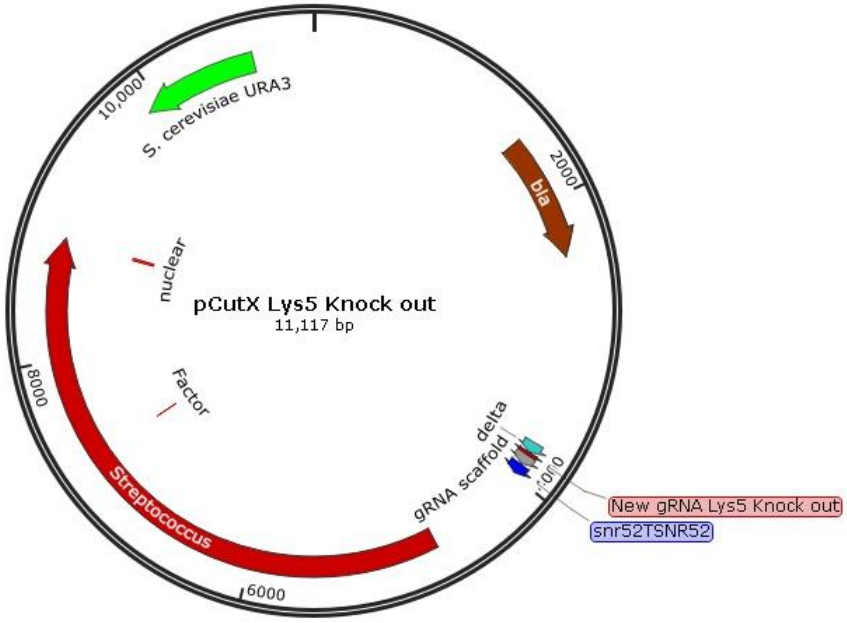

Vector name	Map
p0343/p0343*	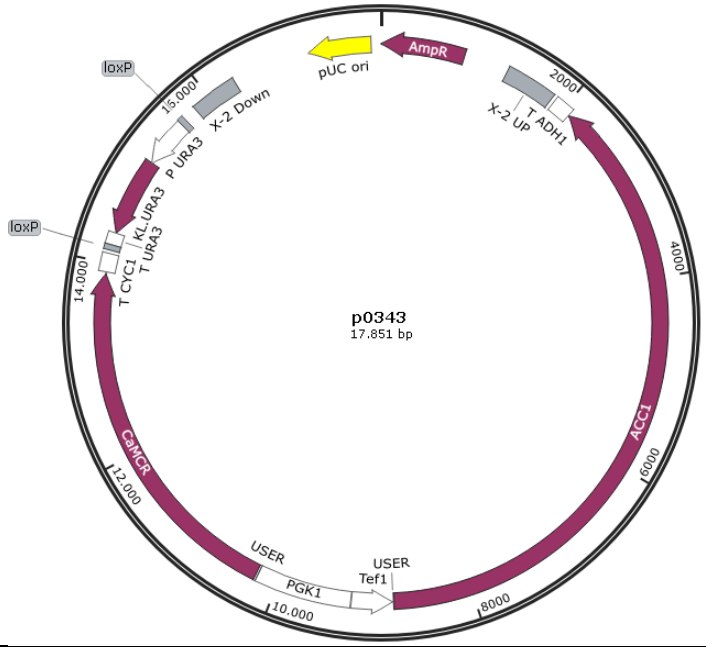
p0343*-acc1* **	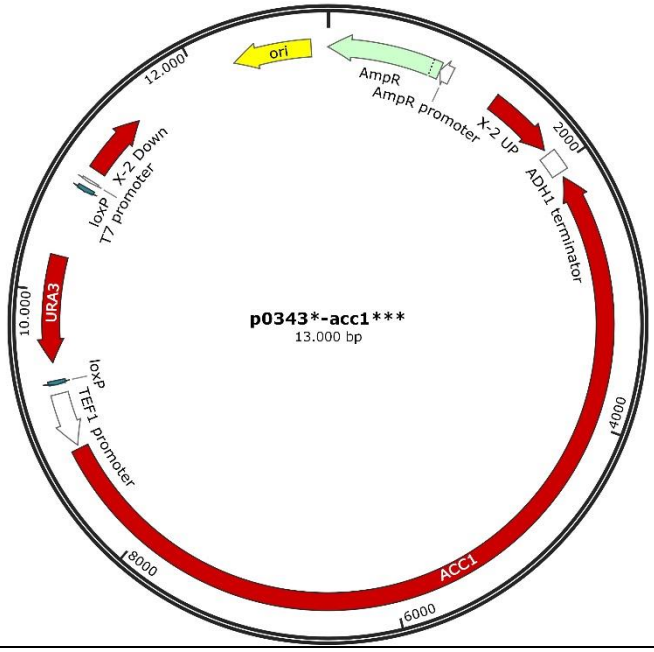

Vector name	Map
p0380	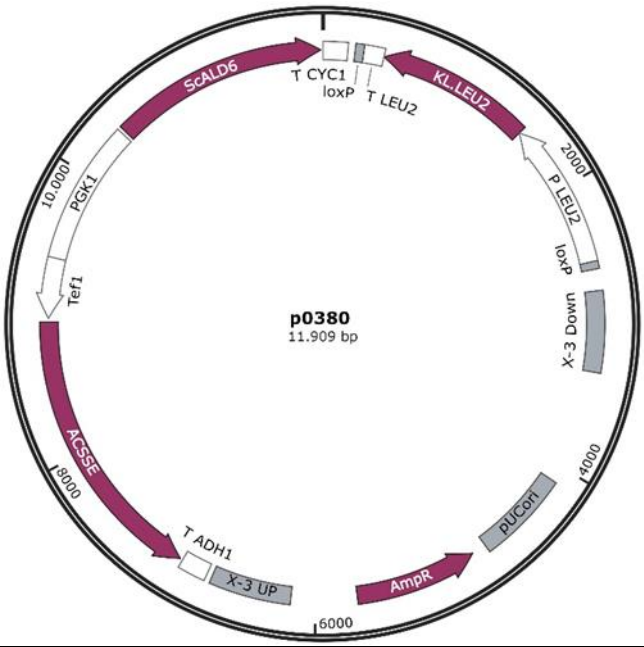
p0382	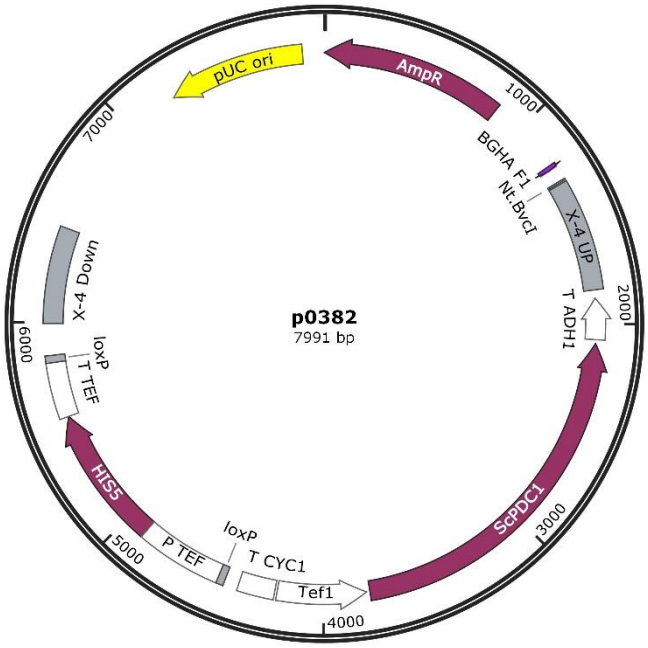

Vector name	Map
pCaMCR-TRP1	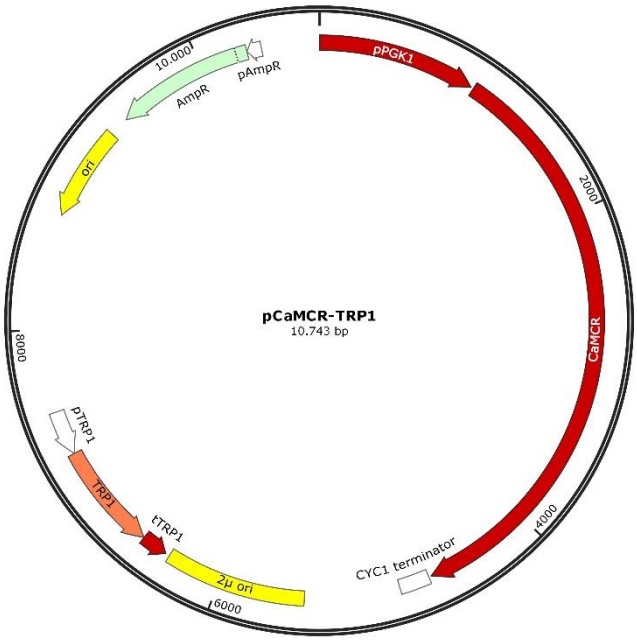
p02747	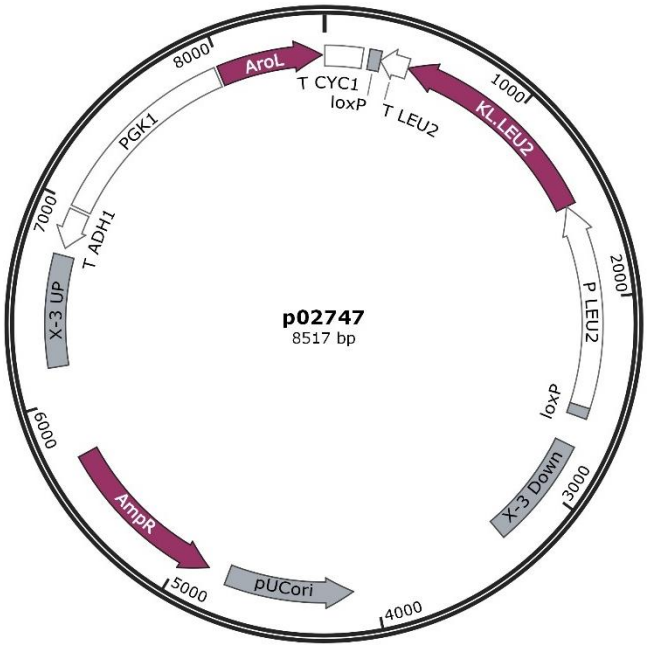

Vector name	Map
pCfB9114	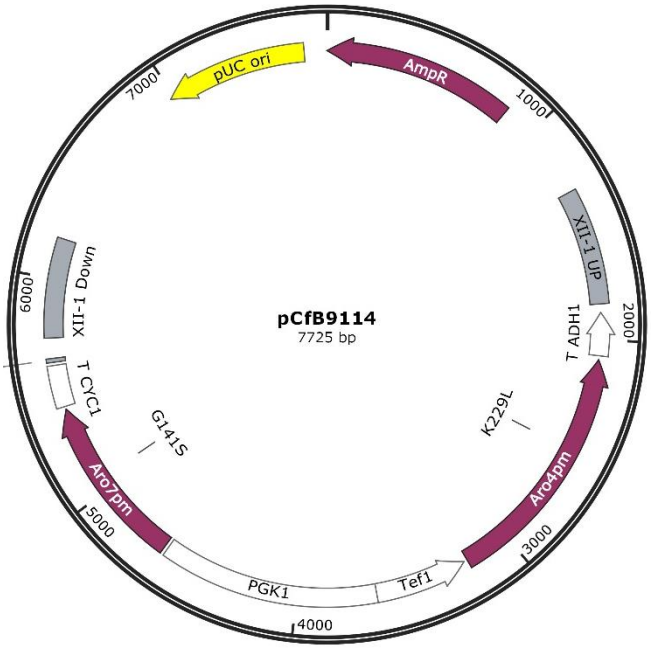
p0376/p0376*	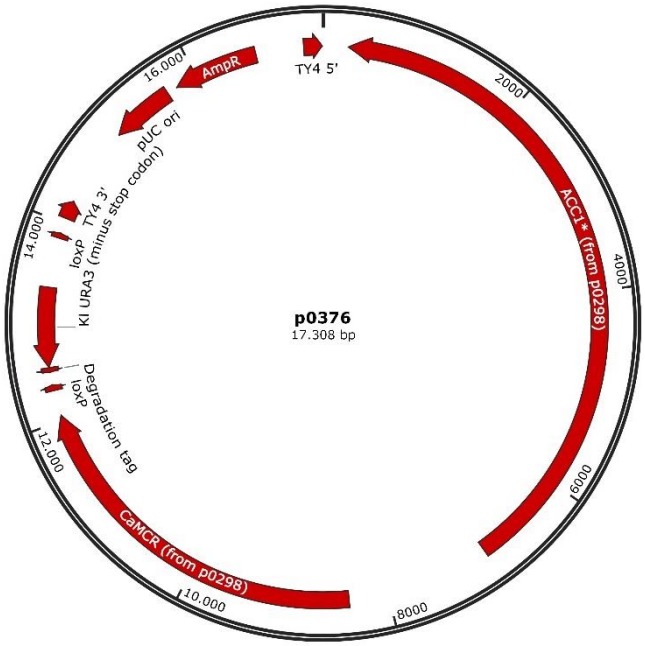

Vector name	Map
p0474/p0474*	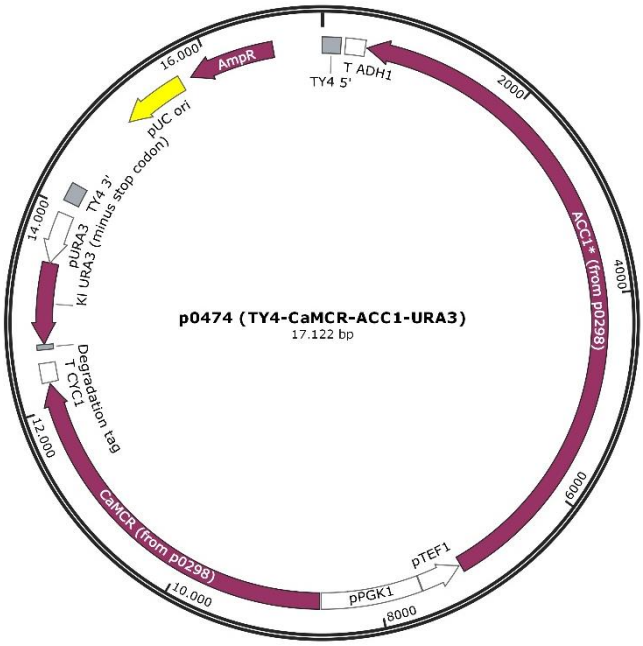
pDesti-H-A-Esp3I-Kan-ColE1	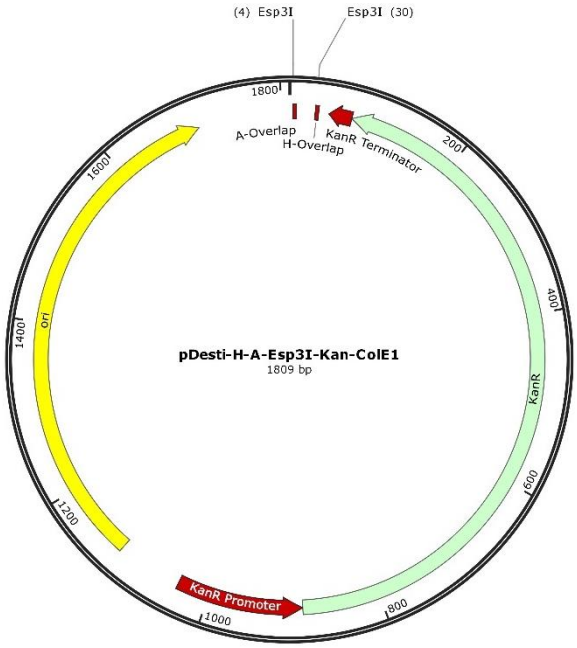

Vector name	Map
p0872	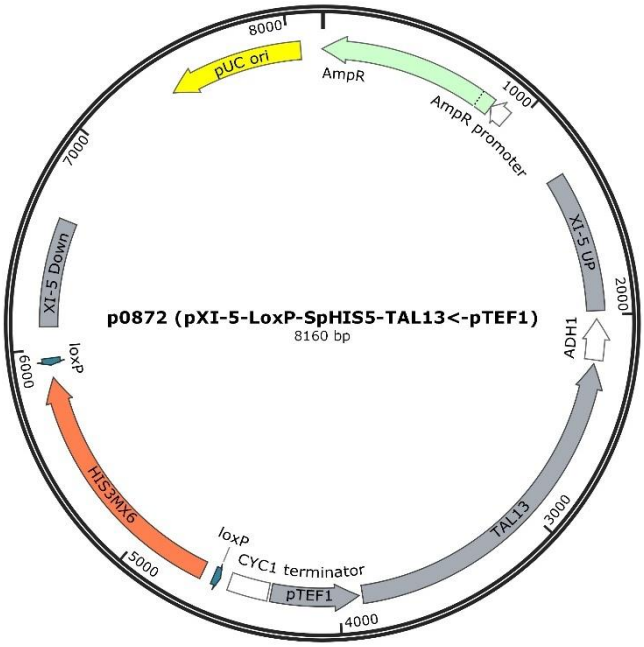
pEpi-haTal-Ura3-2µ	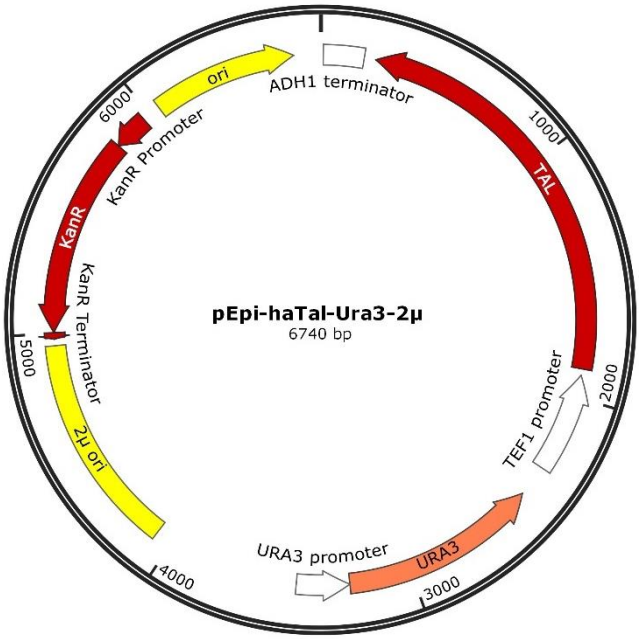

Vector name	Map
pI-deltaPDC5-EcAroL	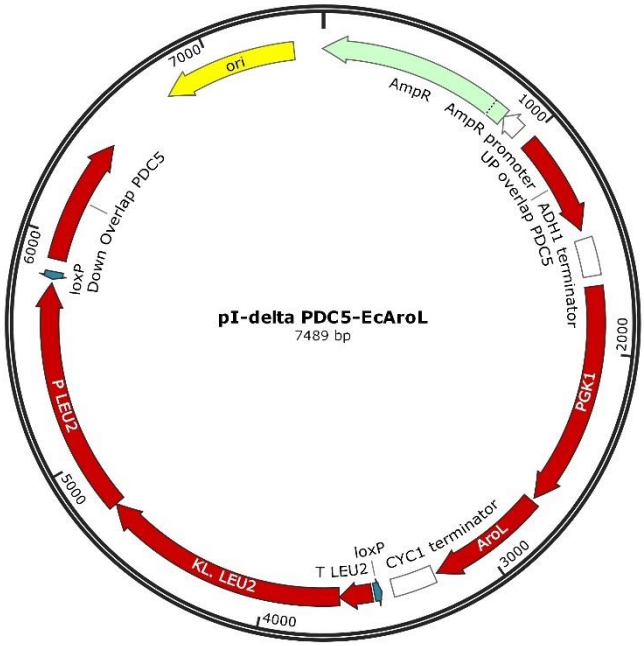
pI-deltaARO10-Aro4,Aro7	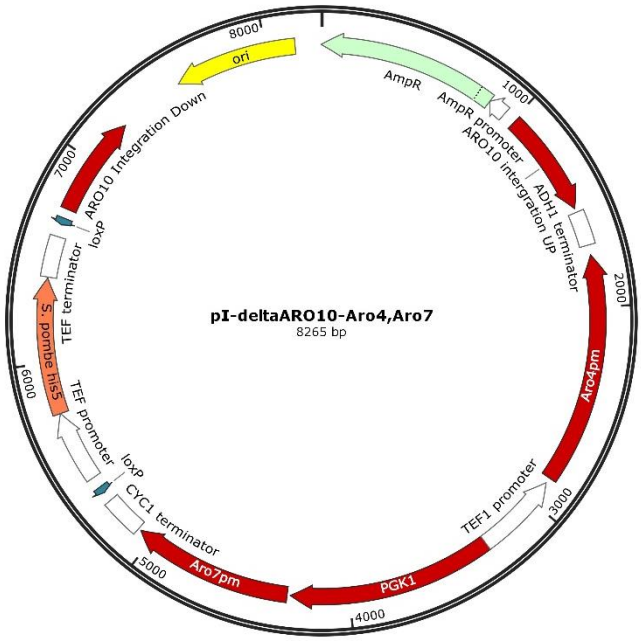

Vector name	Map
pI-dADH1::TPI1	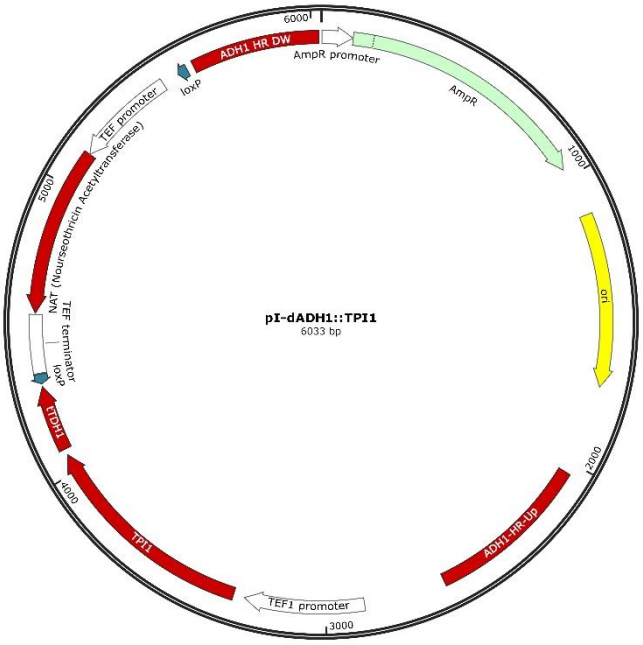

Table S43: List of the presented and generated strains during this work. The initial basis strains can be found in table 6.

Strain	Genotype
ST003	MATa; gal1::loxP; pep4::loxP; gal80::loxP ura3-52; trp1-289; leu2-3,112; his3Δ 1; MAL2-8C; SUC2; 720aΔ::P_{GAL1}-SFP_{Bs}-T_{CYC1}
ST004	MATa; gal1::loxP; pep4::loxP; gal80::loxP; Dmig1bs; ura3-52; trp1-289; leu2-3,112; his3Δ 1; MAL2-8C; SUC2; 720aΔ::P_{GAL1}-SFP_{Bs}-T_{CYC1}
ST005	ST003 + pEpi-haTal-Ura3-2µ
ST006	ST003 PDC5Δ::loxp-Kl.LEU2-loxp-P_{PGK1}-$AroL_{Ec}$-T_{CYC1}+ pEpi-haTal-Ura3-2µ
ST007	ST003 ARO10Δ::loxp-HIS5-loxp-T_{CYC1}-$Aro7^{G141S}$-P_{PGK1}-P_{TEF1}-$Aro4^{K229L}$-T_{ADH1} + pEpi-haTal-Ura3-2µ
ST008	ST003 ARO10Δ::loxp-HIS5-loxp-T_{CYC1}-$Aro7^{G141S}$-P_{PGK1}-P_{TEF1}-$Aro4^{K229L}$-T_{ADH1} + PDC5Δ:: loxp-Kl.LEU2-loxp-P_{PGK1}-$AroL_{Ec}$-T_{CYC1} + pEpi-haTal-Ura3-2µ
ST009	ST004 + pEpi-haTal-Ura3-2µ
ST010	ST004 PDC5Δ::loxp-Kl.LEU2-loxp-P_{PGK1}-$AroL_{Ec}$-T_{CYC1}+ pEpi-haTal-Ura3-2µ
ST012	ST004 ARO10Δ::loxp-HIS5-loxp-T_{CYC1}-$Aro7^{G141S}$-P_{PGK1}-P_{TEF1}-$Aro4^{K229L}$-T_{ADH1} + pEpi-haTal-Ura3-2µ

ST013	ST004 ARO10Δ::loxp-HIS5-loxp-T_{CYC1}-Aro7^{G141S}-P_{PGK1}-P_{TEF1}-Aro4^{K229L}-T_{ADH1} + PDC5Δ:: loxp-Kl.LEU2-loxp-P_{PGK1}-AroL$_{Ec}$-T_{CYC1} + pEpi-haTal-Ura3-2µ
ST018	ST003 + pCaMCR-TRP1
ST019	ST004 + pCaMCR-TRP1
ST020	ST003 TY4::URA3-T_{CYC1}-Mcr$_{Ca}$-P_{PGK1}-P_{TEF1}- Acc1$^{S659A, S686A, S1157A}$-T_{ADH1}
ST021	ST004 TY4::URA3-T_{CYC1}-Mcr$_{Ca}$-P_{PGK1}-P_{TEF1}- Acc1$^{S659A, S686A, S1157A}$-T_{ADH1}
ST022	ST003 X-2Δ::loxp-URA3-loxp- T_{CYC1}-Mcr$_{Ca}$-P_{PGK1}-P_{TEF1}- Acc1$^{S659A, S686A, S1157A}$-T_{ADH1} + X-3 Δ:: loxp-Kl.LEU2-loxp-T_{CYC1}- Acs$_{Se}^{L641P}$-P_{PGK1}-P_{TEF1}-ALD6-T_{CYC1} + X-4Δ::loxp-HIS5-loxp-T_{CYC1}-P_{TEF1}-PDC1-T_{ADH1}
ST023	ST003 X-2Δ::loxp-URA3-loxp-P_{TEF1}- Acc1$^{S659A, S686A, S1157A}$-T_{ADH1} + X-3 Δ:: loxp-Kl.LEU2-loxp-T_{CYC1}- Acs$_{Se}^{L641P}$-P_{PGK1}-P_{TEF1}-ALD6-T_{CYC1} + X-4Δ::loxp-HIS5-loxp-T_{CYC1}-P_{TEF1}-PDC1-T_{ADH1} + pCaMCR-TRP1
ST024	ST022 ADH1Δ::loxp-NAT-loxp-P_{TEF1}-TPI1-T_{TDH1}
ST025	ST023 ADH1Δ::loxp-NAT-loxp-P_{TEF1}-TPI1-T_{TDH1} + pCaMCR-TRP1
ST026	ST023 ARO10Δ::loxp-HIS5-loxp-T_{CYC1}-Aro7^{G141S}-P_{PGK1}-P_{TEF1}-Aro4^{K229L}-T_{ADH1} + pEpi-haTal-Ura3-2µ
ST027	ST023 ARO10Δ::loxp-HIS5-loxp-T_{CYC1}-Aro7^{G141S}-P_{PGK1}-P_{TEF1}-Aro4^{K229L}-T_{ADH1} + PDC5Δ:: loxp-Kl.LEU2-loxp-P_{PGK1}-AroL$_{Ec}$-T_{CYC1} + pEpi-haTal-Ura3-2µ
ST028	ST023 ARO10Δ::loxp-HIS5-loxp-T_{CYC1}-Aro7^{G141S}-P_{PGK1}-P_{TEF1}-Aro4^{K229L}-T_{ADH1}
ST029	ST023 ARO10Δ::loxp-HIS5-loxp-T_{CYC1}-Aro7^{G141S}-P_{PGK1}-P_{TEF1}-Aro4^{K229L}-T_{ADH1} + PDC5Δ:: loxp-Kl.LEU2-loxp-P_{PGK1}-AroL$_{Ec}$-T_{CYC1}

1.2 Supplements – Results and Discussion

i. Results of PPTase integration

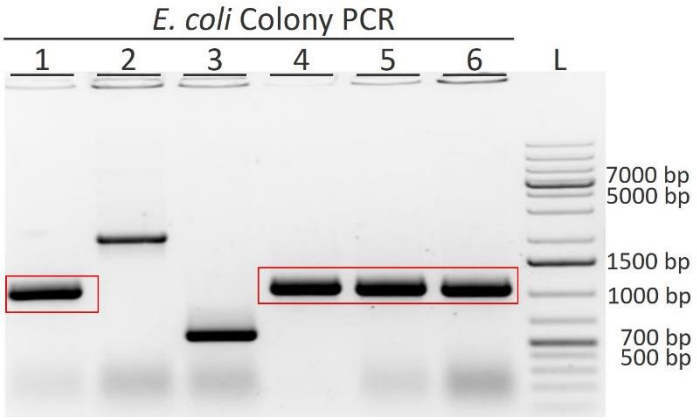

Figure S49: Picture of the *E. coli* colony PCR gel after the construction of the pDionysosGlcRepfree-*sfp* plasmid. Number from 1-6 indicate the picked colonies for testing. The red boxes highlight the positive fragments with the right size of 1060 bp. L: *GeneRuler™ 1 kb DNA Ladder Plus* from Thermo Scientific.

Figure S50: Agarose gel of yeast colony PCR with scheme of the PCR below. Red box highlights the positive colony (3238 bp) while all others are negative (2000 bp). Bold arrows on the scheme below indicate binding position of the used primers with the dashed arrows showing amplification direction. The roman numbers indicate the respective chromosome the cassette was implemented in. L: *GeneRuler™ 1 kb DNA Ladder Plus* from Thermo Scientific.

Figure S51: Yeast cells after 5-FOA selection on agar plates after 2 days of incubation at 30 °C. Left: YPD-agar plate no selection pressure, right: -URA-selection plate without uracil and no grown colonies indicating plasmid loss.

Figure S52: Results of the *sfp* integration cassette sequencing from the yeast genome. The sequences highlighted in green show matching sequence areas with the correct reference sequence. The red arrow indicates the starting point (atg) of the *sfp* sequence, while the stop highlights the ending (taa). Below the sequence a scheme shows the integration site with the integration cassette where the red box highlights the covered sequencing area.

ii. CRISPR-Cas9 mediated *lys5* knockout and sfp_{bs} PPTase functionality test

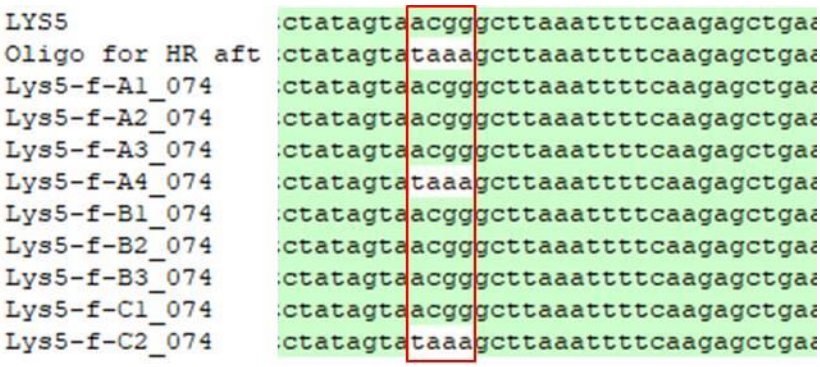

Figure S53: Sequencing result of the *lys5* knockout. The first sequence from the top represents the native l*ys5* sequence, below is the sequence as it should look after the knockout. Only colonies A4 and C2 (red box) carry the knocked out l*ys5* gene.

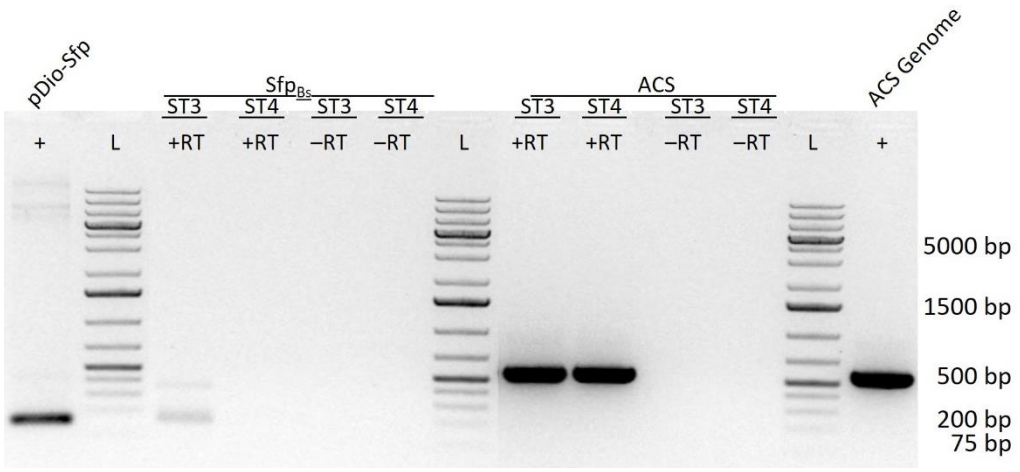

Figure S54: Agarose gel showing the *sfp$_{Bs}$* and *acs* PCR after RNA isolation without induction. The ST3/4 +RT samples show no or only a slightly visible fragment demonstrating no or only minor basal transcription of *sfp$_{Bs}$* under the control of the Gal1 promotor. The housekeeping gene *acs* was successfully amplified indicating the successful RNA isolation and reverse transcription. The negative controls are indicated in the empty lanes (-RT), while the positive controls are shown with the fragments generated from the pDionysos-*Sfp$_{Bs}$* plasmid (pDio-Sfp) and the *acs* sequence from the genome (ACS Genome). ST3/ST4: yeast strains harbouring the 720a::*sfp$_{Bs}$* modification (Table S43), +RT: RNA reverse transcription with reverse transcriptase, -RT: RNA reverse transcription without reverse transcriptase, L: GeneRuler™ 1 kb DNA Ladder Plus, Thermo Scientific.

iii. Mutation of *acc1* and the malonyl-CoA reductase (MCR) read-out system

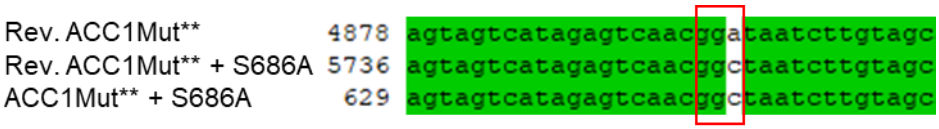

Figure S55: Representative sequencing result of the introduction of the third mutation into the acc1 gene. Shown is the exchange of the codon TCC for serine with GCC for alanine by simply changing a (t) to c (g) as highlighted with the red box.

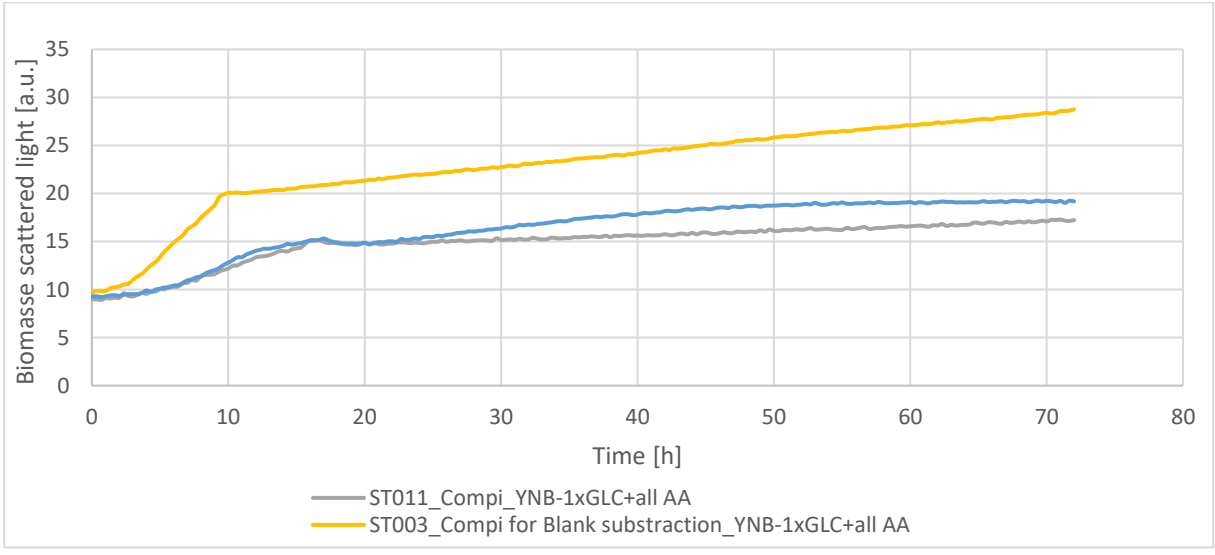

Figure S56: Growth behaviour based on biomass development of the strains ST003, ST020, ST021. Cultivation was conducted in YNB SC-medium utilizing the Biolector, 72 h, 1200 rpm, 30 °C, 85 % humidity (Biolector, M2P labs GmbH, Germany). a. u.: arbitrary unit.

Table S44: Effect of 3-HP on ST003 and ST004 growth. Both strains were cultivated in the absents and presents of 3-HP.

	OD600	OD660
ST003	16,48	16,38
ST003+3-HP	13,02	13
ST004	13,44	13,56
ST004+3-HP	12,06	12,34

Table S45: Example for the data attained from the 3-HP serial dilution. The data was also used for the comparison of the calibration curves prepared manually and attained from the program OpenLab CDS (Agilent, Santa Clara, USA) in Figure S57.

3-HP Serial Dilution	3-HP Signal UV 210 nm								UV	RI
	mg/L	Area_UV 210 nm	Area_RI	Calculated Conc. UV	Calculated Conc. RI	Diviation UV	Diviation RI	Formula:	y=0,38195x	y=290,22479x
3-HP 19 mg/L	19	5,51	5449,98	14,43	18,78	3,23	0,16		0,38195	290,22479
3-HP 39 mg/L	39	11,83	10725,43	30,97	36,96	5,68	1,45			
3-HP 78 mg/L	78	29,46	21958,85	77,13	75,66	0,61	1,65			
3-HP 156 mg/L	156	59,59	46187,71	156,02	159,14	0,01	2,22			
3-HP 312,5 mg/L	322	120,43	93393,82	315,30	321,80	4,38	0,21			
3-HP 625 mg/L	625	239,92	184739,05	628,15	636,54	2,22	8,16			
3-HP 1250 mg/L	1250	480,80	372683,74	1258,80	1284,12	6,23	24,13			
3-HP 2500 mg/L	2500	956,02	733539,35	2503,00	2527,49	2,12	19,44			
3-HP 5000 mg/L	5000	1933,09	1470917,52	5061,11	5068,20	43,21	48,23			
3-HP 10000 mg/L	10000	3807,06	2888818,74	9967,43	9953,73	23,03	32,72			

Table S46: Example for the data attained from acetate serial dilution. The data was also used for the comparison of the calibration curves prepared manually and attained from the program OpenLab CDS (Agilent, Santa Clara, USA) in Figure S58.

Serial Dilution	Acetate								UV	RI
	mg/L	Area_UV 210 nm	Area_RI	Calculated Conc. UV	Calculated Conc. RI	Diviation UV	Diviation RI	Formel:	y=0,35295x	y=156,77808x
Acetate 19 mg/L	19	6,13	3.048	17,36789914	19,4392609	1,154069589	0,310604359		0,35295	156,77808
Acetate 39 mg/L	39	14,39	6.379	40,7706474	40,6888514	1,252036784	1,194198278			
Acetate 78 mg/L	78	28	12.750	79,07635642	81,32724932	0,761098927	2,352720557			
Acetate 156 mg/L	156	58	25.440	164,9808755	162,2646482	6,350437952	4,429775239			
Acetate 312,5 mg/L	321,5	111	49.039	315,0587902	312,7939824	4,554623131	6,156084065			
Acetate 625 mg/L	625	222	97.681	628,7009491	623,0510668	2,616966236	1,378103859			
Acetate 1250 mg/L	1250	433	191.647	1225,952685	1222,410493	17,00401985	19,50872778			
Acetate 2500 mg/L	2500	862	381.111	2442,725599	2430,892316	40,49911767	48,86651194			
Acetate 5000 mg/L	5000	1.705	761.162	4831,279218	4855,02597	119,3036091	102,5121194			
Acetate 10000 mg/L	10000	3.565	1.582.392	10101,09081	10093,19402	71,48199448	65,89812566			

Compound:	3-HP-UV 210 nm
Signal:	VWD1A
Exp. RT:	16.550
Corr. Coeff.:	0.999981
Residual:	8.99021
RF RSD%:	
R²:	0.99996
Formula:	y = ax + b
a:	0.38195
b:	0.00000
c:	0.00000
d:	

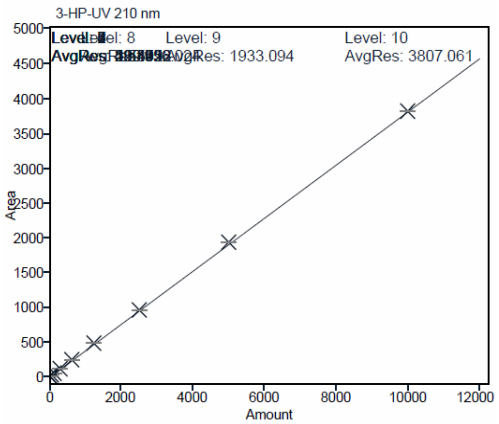

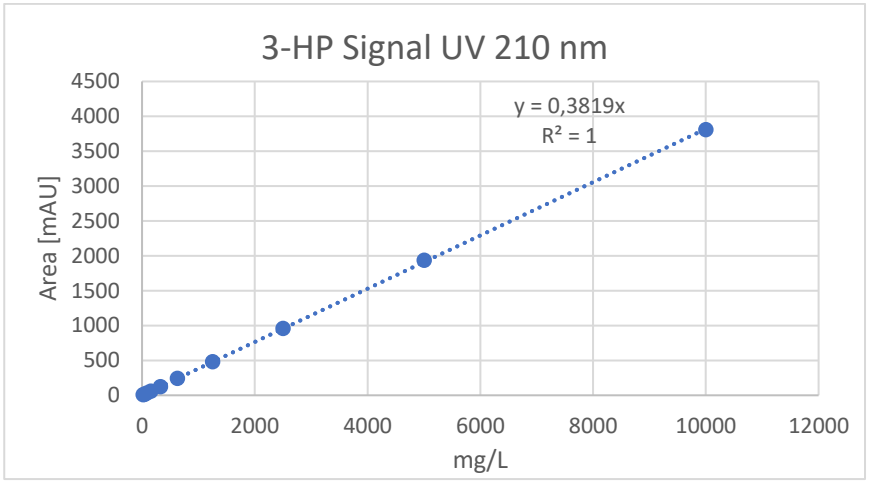

Compound:	3-HP-RI
Signal:	RID1A
Exp. RT:	16.750
Corr. Coeff.:	0.999966
Residual:	9152.87177
RF RSD%:	
R²:	0.99993
Formula:	y = ax + b
a:	290.22479
b:	0.00000
c:	0.00000
d:	

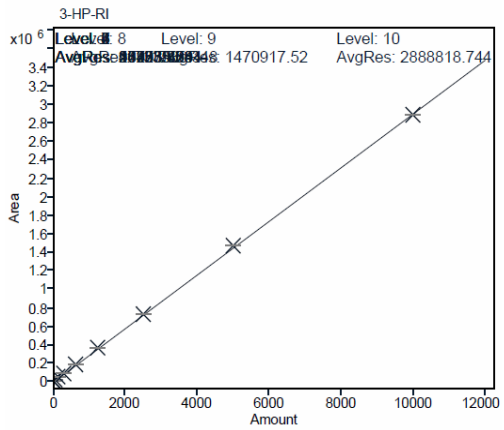

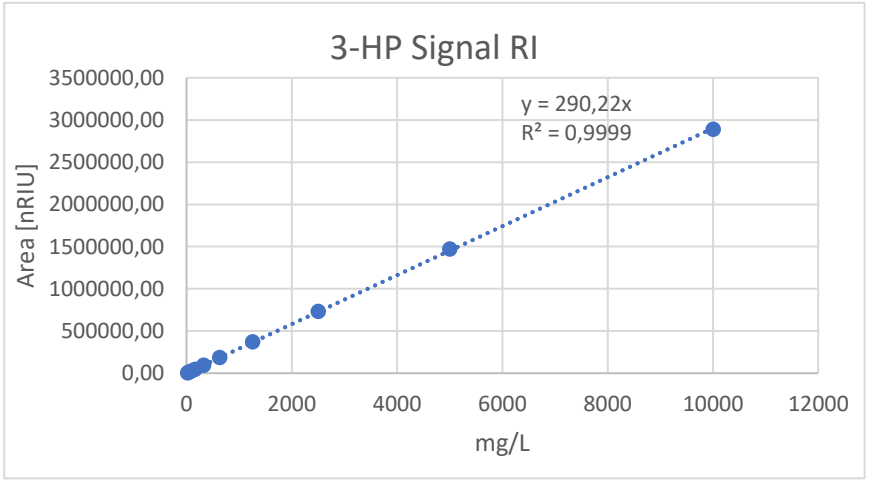

Figure S57: Obtained calibration curves from the 3-HP serial dilution and the data from Table S45. On the left side the calibration curves automatically generated from the OpenLab CDS (Agilent, Santa Clara, USA) and on the right side the calibration curve manually prepared. The upper diagrams show the calibration curves for the UV detected 3-HP and below the RI (refractive index) detector calibration curve. nRIU: nano Refractive Index Units, mAU: milli Absorbance Units.

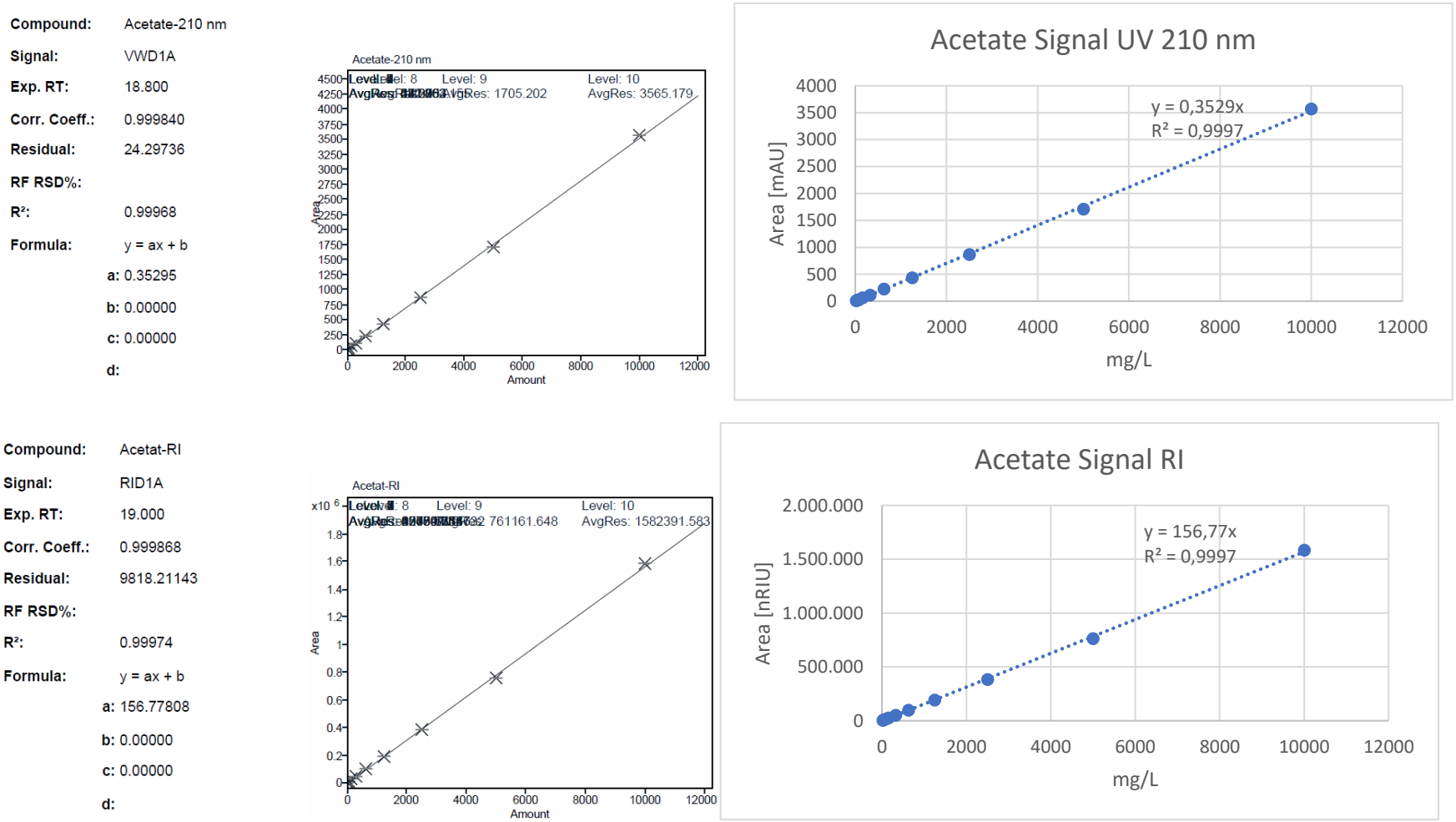

Figure S58: Obtained calibration curves from the acetate serial dilution and the data from Table S46. On the left side the calibration curves automatically generated from the OpenLab CDS (Agilent, Santa Clara, USA) and on the right side the calibration curve manually prepared. The upper diagrams show the calibration curves for the UV detected acetate and below the RI (refractive index) detector calibration curve. nRIU: nano Refractive Index Units, mAU: milli Absorbance Units.

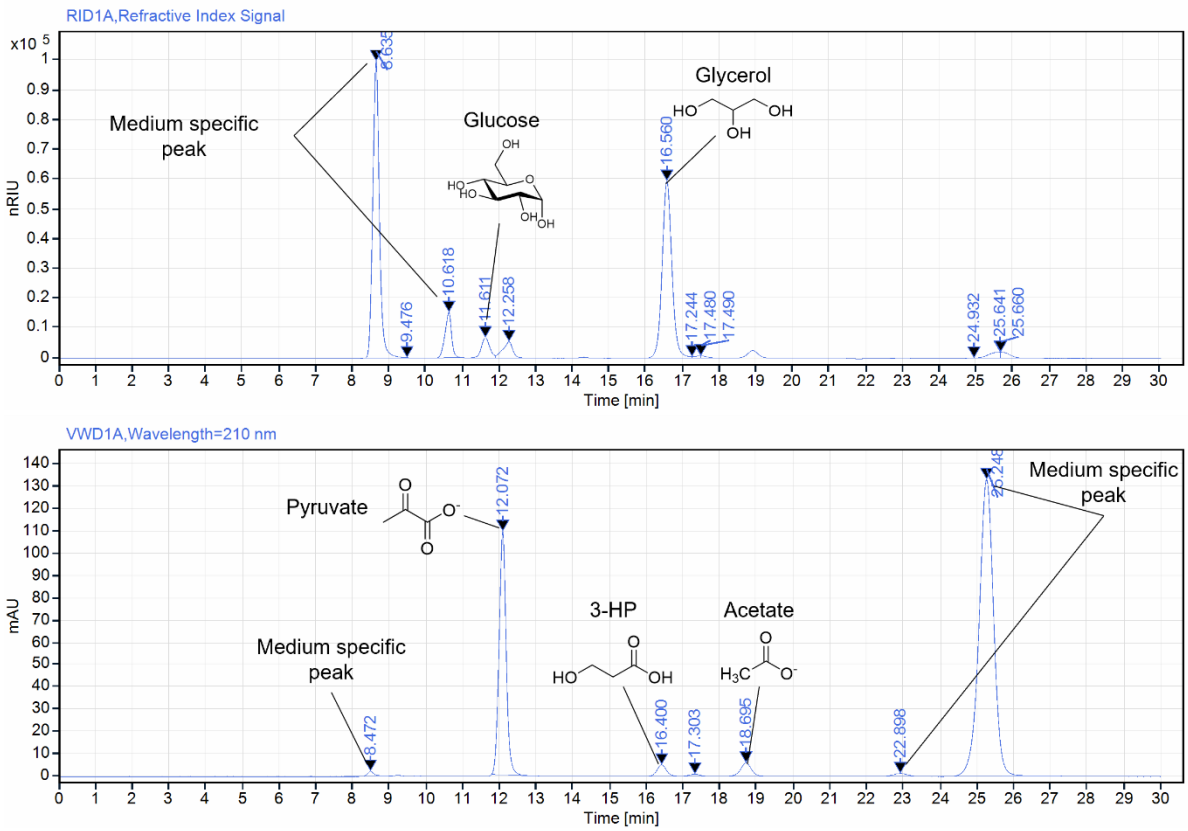

Figure S59: HPLC-UV/RI chromatogram (OpenLab CDS (Agilent, Santa Clara, USA)) for measured compound using the HPLC dedicated for carbohydrates, with the RI detector (above) and UV dector (210 nm, below). nRIU: nano Refractive Index Units, mAU: milli Absorbance Units.

iv. Yeast genome modification for malonyl-CoA level provision

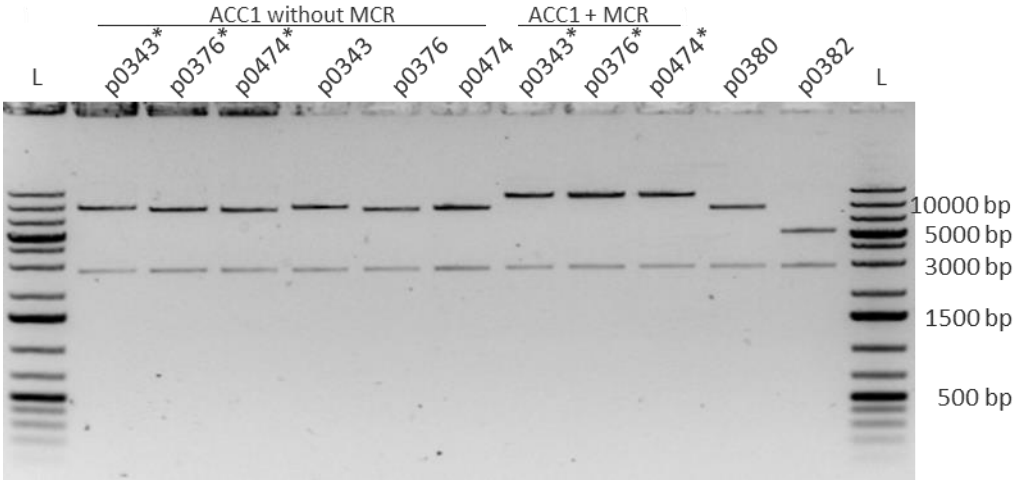

Figure S60: Results of the linearisation of the integration plasmids. The upper fragments represent the linear integration cassettes, while the lower fragments represent the rest of the plasmid. The * indicates plasmids holding the triple mutated *acc1*. The plasmids with *acc1* (p0343, p0376, p0474 with and without *) were linearised with and without the MCRp expression cassette, underlined right above each plasmid. The other plasmids (p0380 and p0382) are the plasmids containing acs_{se} and *ald6* (p0380) and *pdc1* (p0382). L: GeneRuler™ 1 kb DNA Ladder Plus, Thermo Scientific.

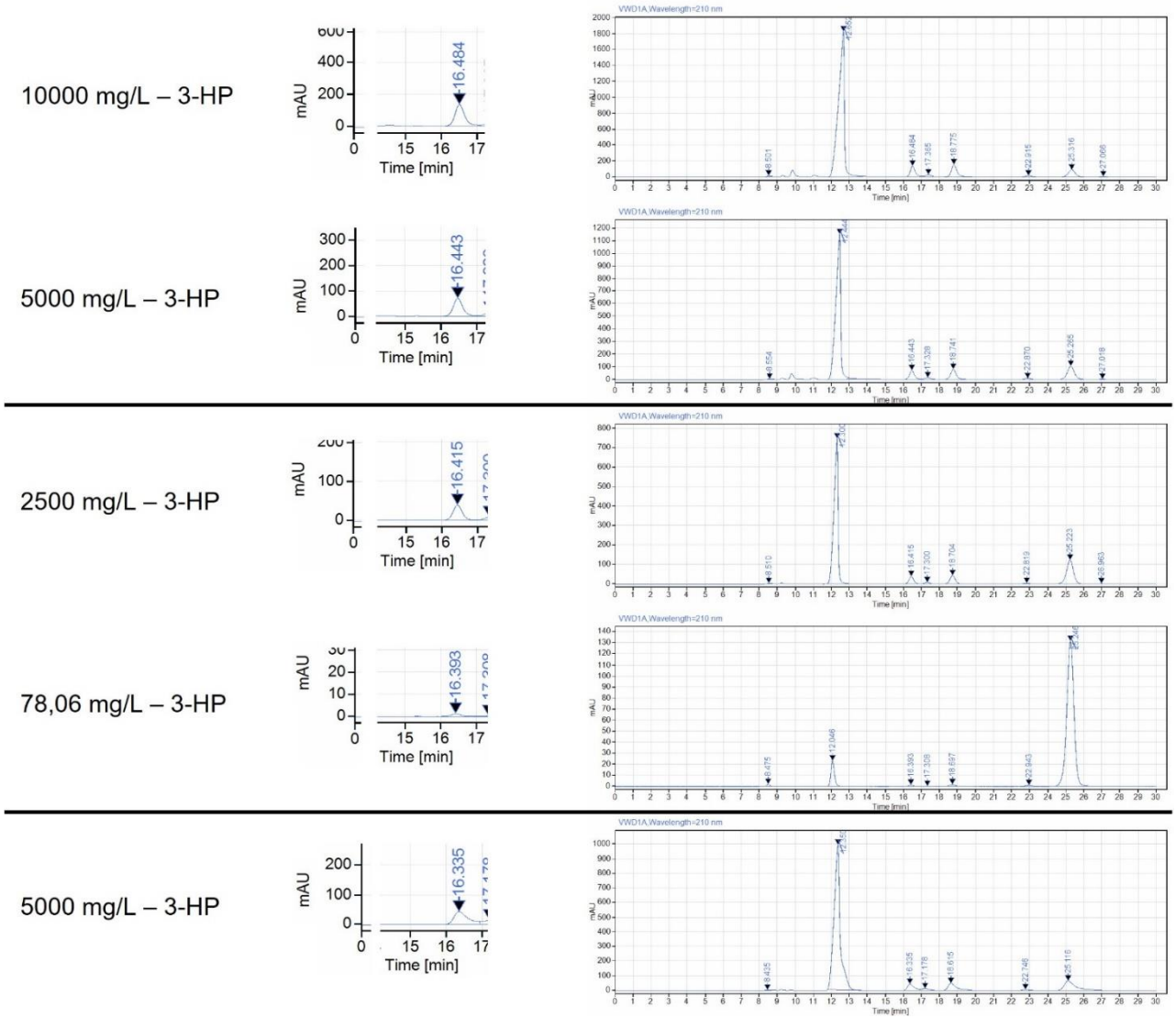

Figure S61: Comparison of 3-HP RT shift between samples of the same measurement run and between measurements. Different measurement runs are seperated with a bold line. Samples of the same measurement run are group together. The RT shift in samples of the same measurement run differ from 0,02 min to 0,04 min and when comparing RT of different measurement runs the RT differs up to 0,149 min. Displayed are, from left to right, the 3-HP concentration measured, the section with RT if interest and the whole UV 210 nm chromatogram of each sample. The data analysis was done with program OpenLab CDS (Agilent, Santa Clara, USA). mAU: milli Absorbance Units.

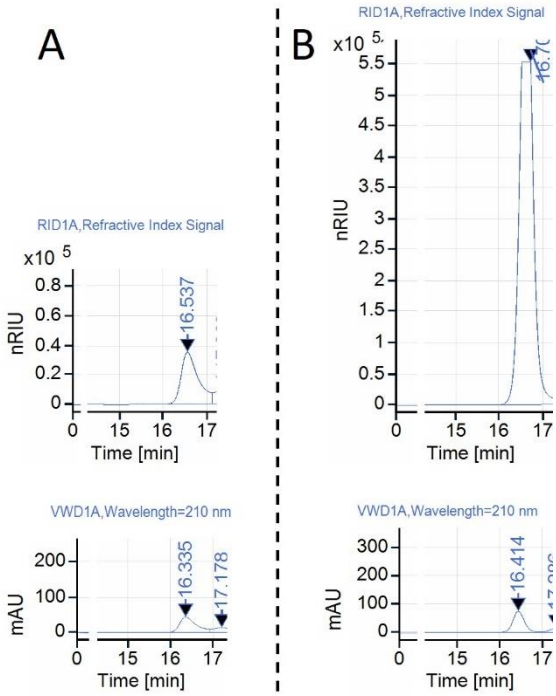

Figure S62: comparison of standard samples showing 5000 mg L^{-1} 3-HP samples without (A) and with (B) 5000 mg L^{-1} glycerol. A: 3-HP signal detected with the RI (above) and UV (210 nm, below) dector and no glycerol. B: 3-HP signal detected with the RI (above) and UV (210 nm, below) dector and 5000 mg L^{-1}glycerol added increasing the signal in the RI dector significantly but does not affect the UV signal. The data analysis was done with program OpenLab CDS (Agilent, Santa Clara, USA). nRIU: nano Refractive Index Units, mAU: milli Absorbance Units.

Table S47: Template for designing oligonucleotides for *Esp3I* PCRGate cloning (Chapter 4.6.7.2) adapted from GreenGate cloning. [217] This template table can be used to design the primer for the PCRGate cloning of up to 8 fragments, by simply pasting the in the specific sequence column. The respective cutting site ("Esp3I site and filling sequence" column) creating the overlap ("Overhang" column with the overlapping site labelled from A to H (bold letters)) and the *Esp3I* recognition site are simply added to the primer sequence. Each colour represents a fragment generated with the respective primer pair. The calculated temperature can also be filled in at the end. T_m: melting temperature of the complementary part of the oligonucleotide, T_A: melting point of the completely hybridised oligonucleotide.

Fragments	Primer Orientation			Esp3I site and filling sequence	Overhang		in frame addition	specific sequence		Tm	Ta
Fragment 1 (destination Vector)		(Kan-ColE1) Vector-ColE1-A	Rv				caaca	paste specific reverse primer complement sequence			
			5'	aacaCGTCTCt	aggt	**A**	gt	next to the ColE1 sequence	3'		
		Name					Caaca and gt can be added in front of forward primer sequences between the overhang and the primer sequence when used when reading frame is important.	paste specific primer sequence			
Fragement 2	Forward		**5'**	aacaCGTCTCa	acct	**A**			3'		
	Reverse		5'	aacaCGTCTCt	tgtt	**B**			3'		
Fragement 3	Forward		5'	aacaCGTCTCa	aaca	**B**			3'		
	Reverse		5'	aacaCGTCTCt	agcc	**C**			3'		
Fragement 4	Forward		5'	aacaCGTCTCa	ggct	**C**			3'		
	Reverse		5'	aacaCGTCTCt	ctga	**D**			3'		
Fragement 5	Forward		5'	aacaCGTCTCa	tcag	**D**			3'		
	Reverse		5'	aacaCGTCTCt	gcag	**E**			3'		
Fragement 6	Forwrad		5'	aacaCGTCTCa	ctgc	**E**			3'		
	Reverse		5'	aacaCGTCTCt	tagt	**F**			3'		
Fragement 7	Forward		5'	aacaCGTCTCa	acta	**F**			3'		
	Reverse		5'	aacaCGTCTCt	gcag	**G**			3'		
Fragement 8	Forward		5'	aacaCGTCTCa	tagt	**G**			3'		
	Reverse		5'	aacaCGTCTCt	ccta	**H**			3'		
Fragment 1 (destination Vector)		H-Kan-Vector (Kan-ColE1)	Fw					paste specific forward primer sequence			
			5'	aacaCGTCTCa	tagg	**H**		next to the Kan sequence	3'		

v. 3-HP detection via nuclear magnetic resonance (NMR)

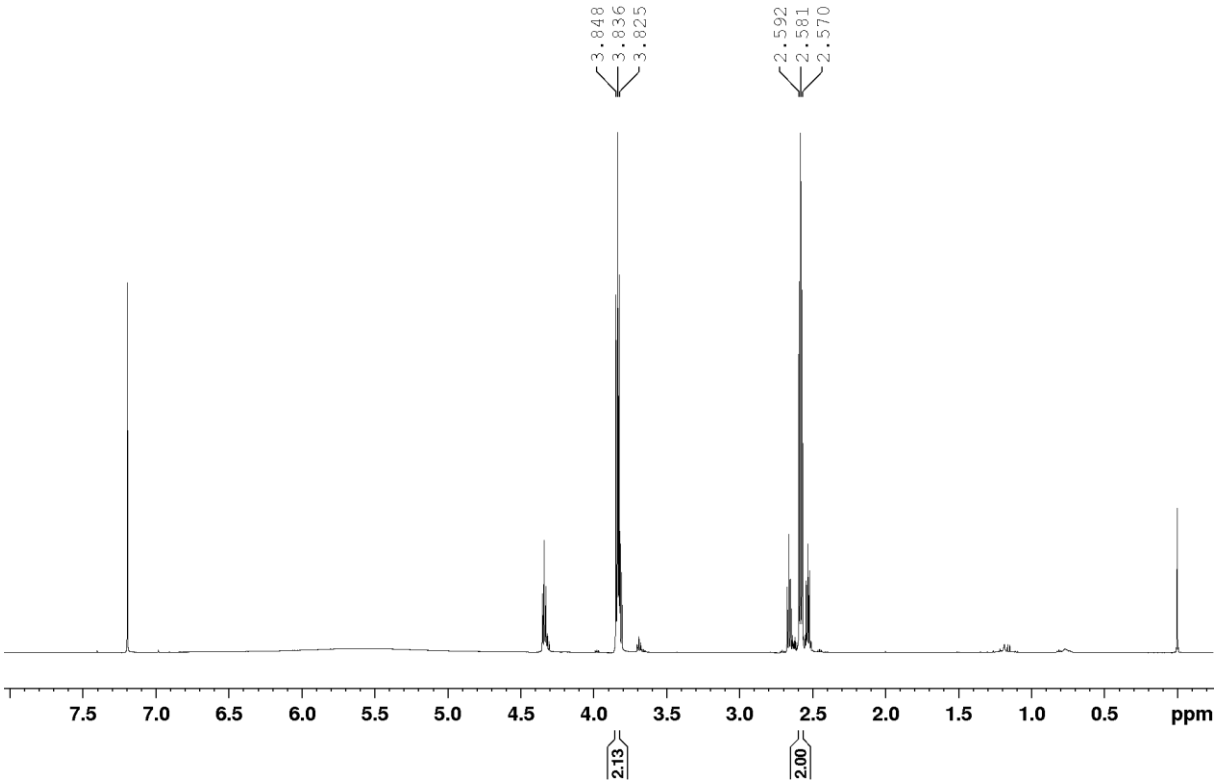

Figure S63: ^{1}H NMR spectrum (500 MHz, 298 K, $CDCl_3$) of 3-HP (standard sample) in $CDCl_3$.

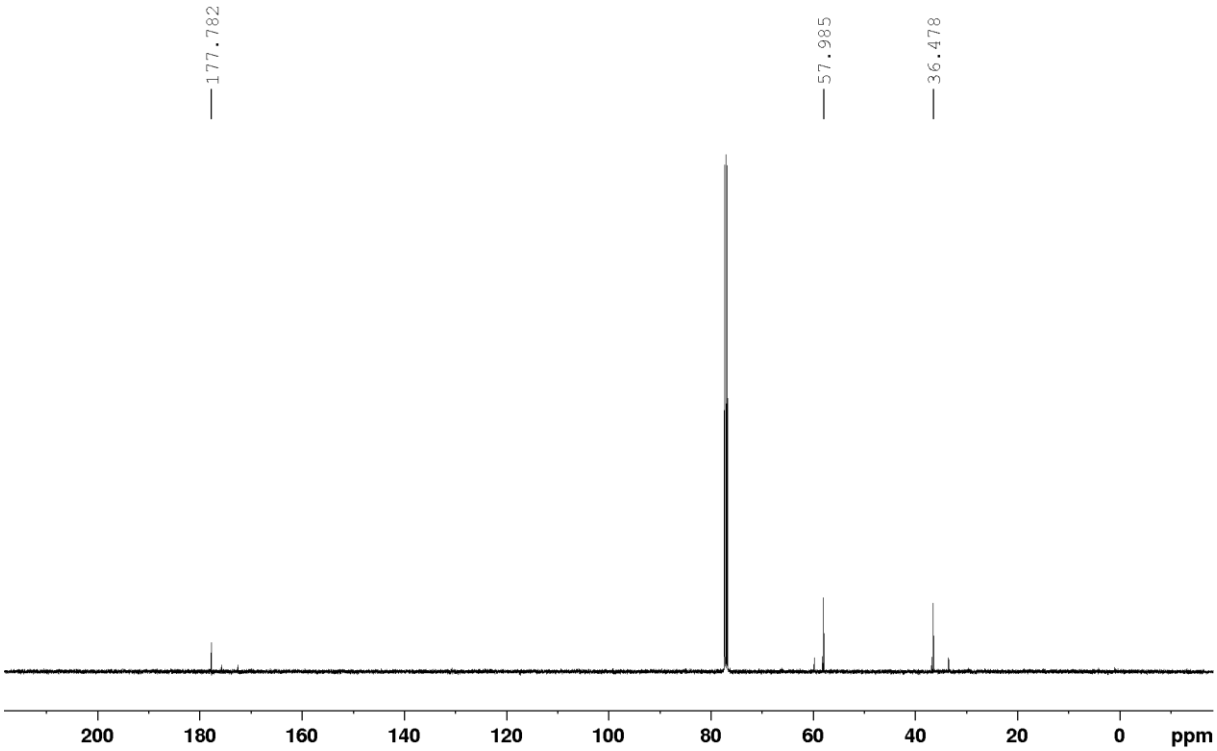

Figure S64: ^{13}C NMR spectrum (125 MHz, 298 K, $CDCl_3$) of 3-HP (standard samples) in $CDCl_3$.

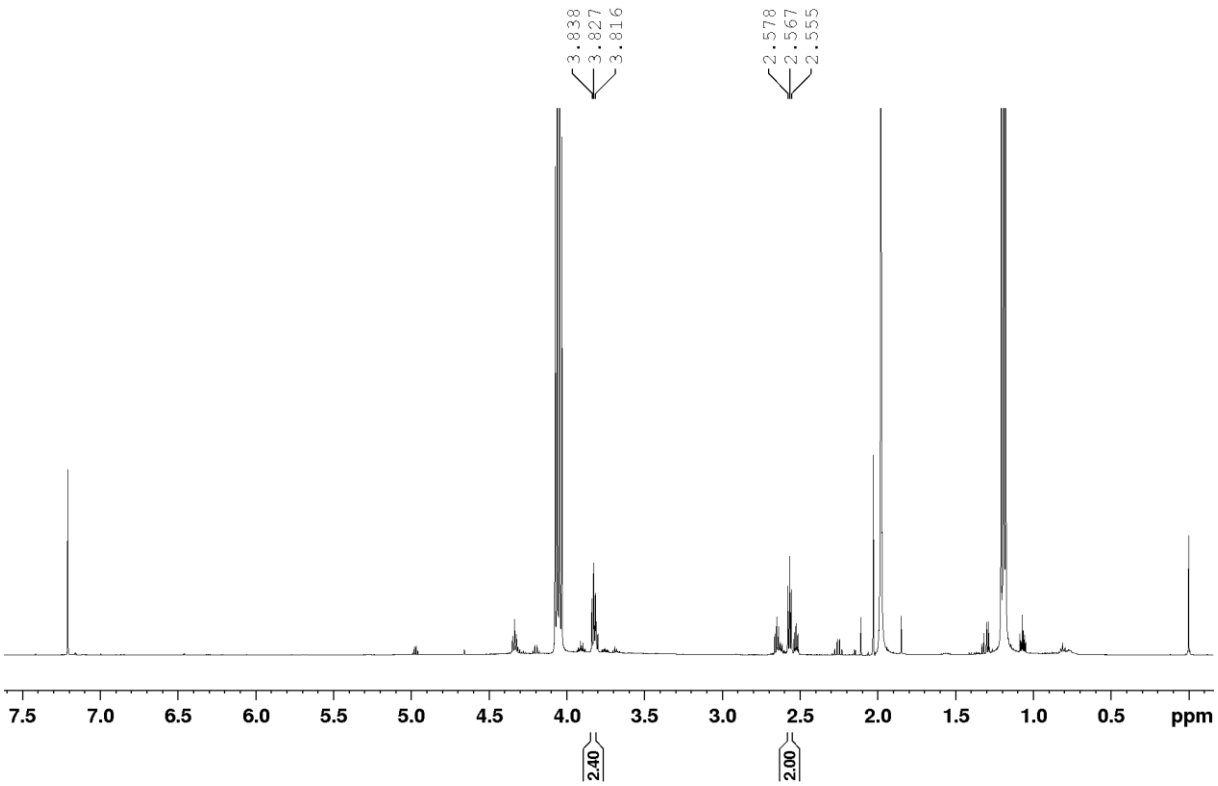

Figure S65: ^{1}H NMR spectrum (500 MHz, 298 K, $CDCl_3$) 3-HP 10 mg 3-HP extracted from YNB SC-Medium in $CDCl_3$.

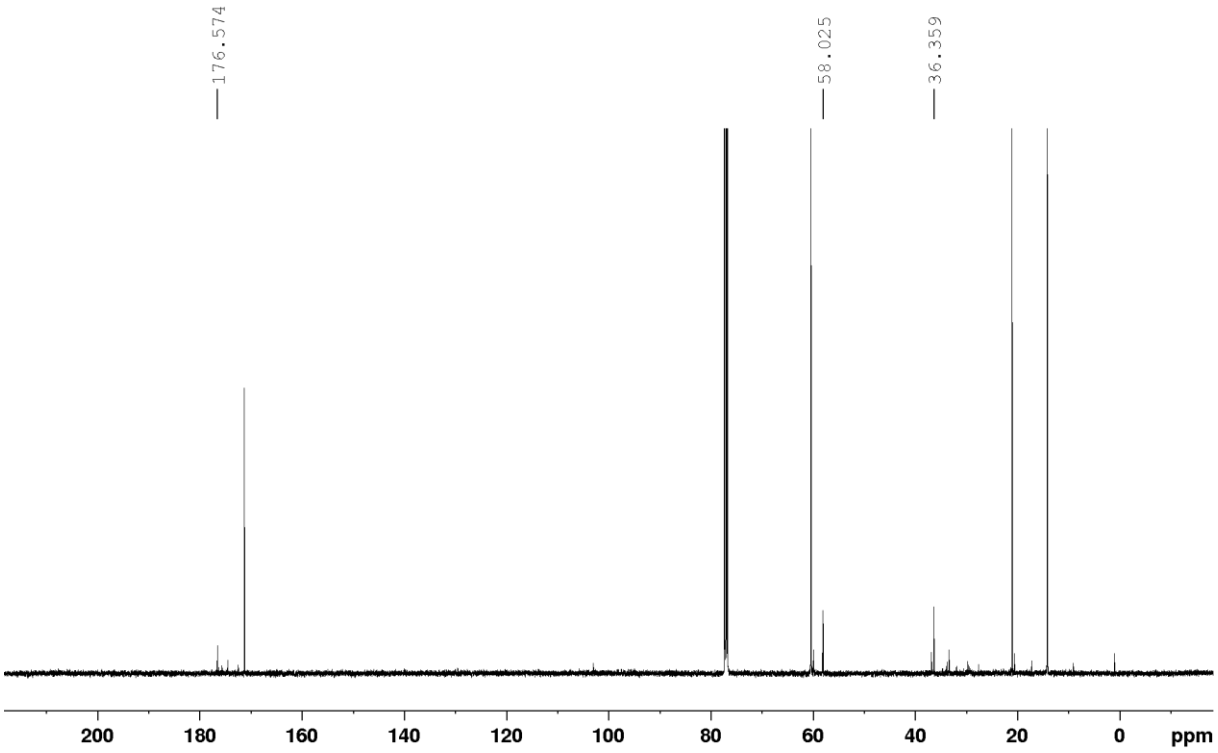

Figure S66: ^{13}C NMR spectrum (125 MHz, 298 K, $CDCl_3$) of 3-HP extracted from YNB SC-medium in $CDCl_3$.

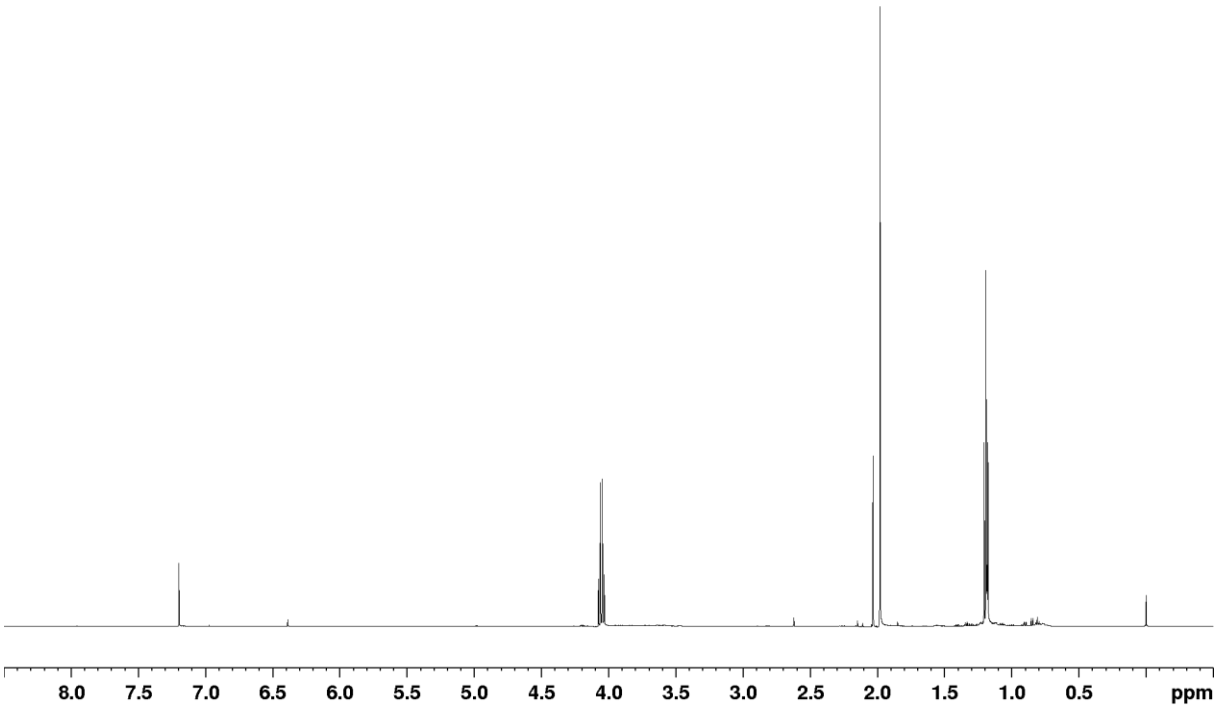

Figure S67: ^{1}H NMR spectrum (500 MHz, 298 K, $CDCl_3$) of 3-HP extracted from ST003 cultivations in $CDCl_3$.

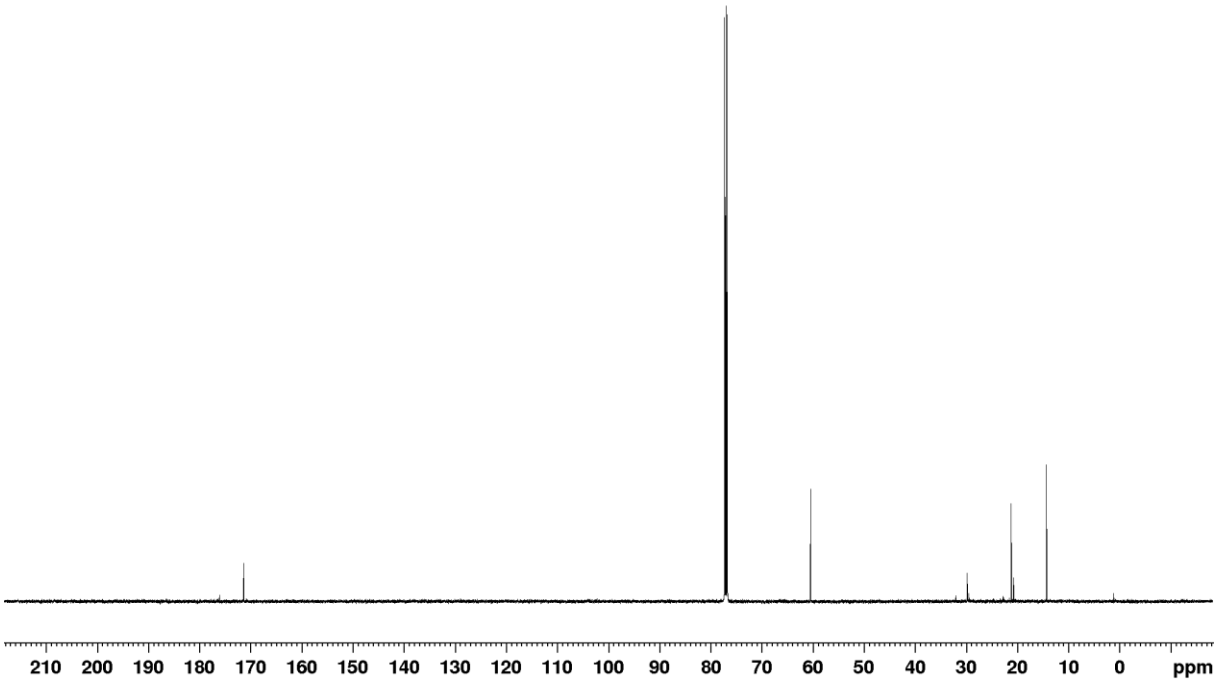

Figure S68: ^{13}C NMR spectrum (125 MHz, 298 K, $CDCl_3$) of 3-HP extracted from ST003 cultivations in $CDCl_3$.

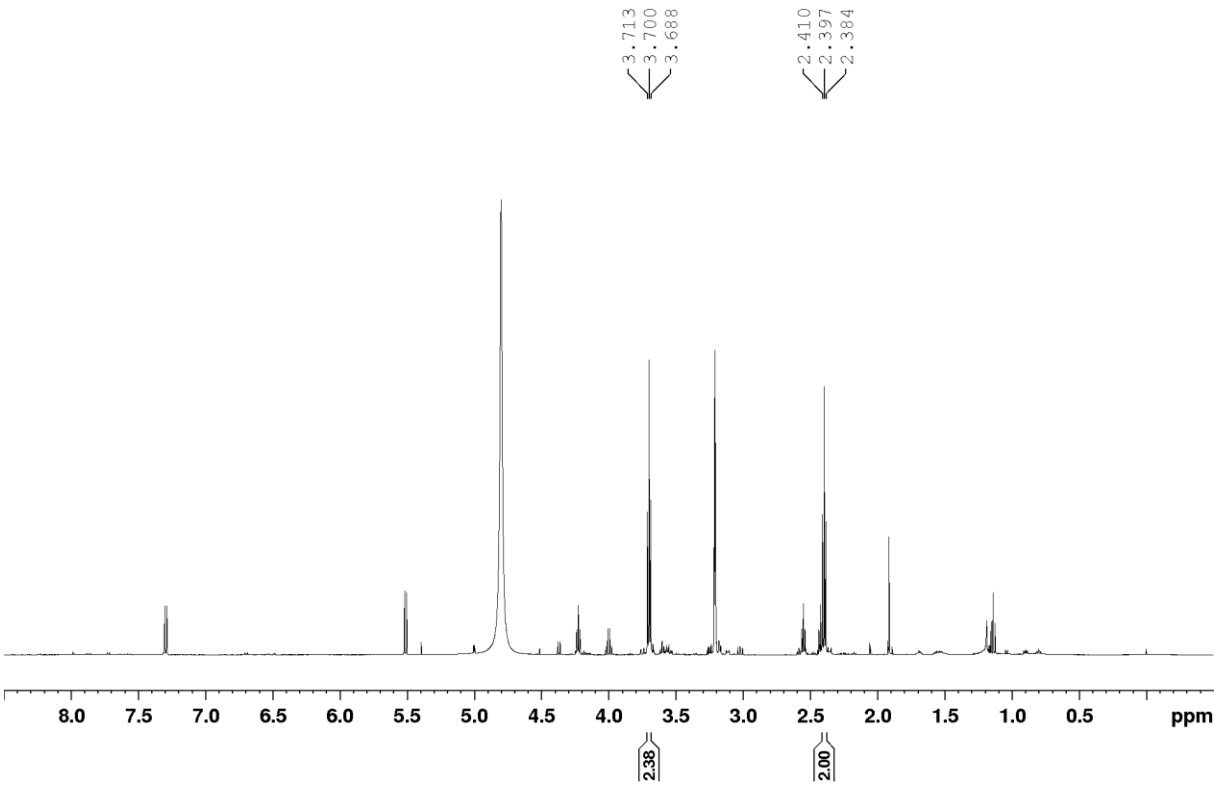

Figure S69: ^{1}H NMR spectrum (500 MHz, 298 K, MeOD) 3-HP extract from YNB SC-medium with MeOD as solvent.

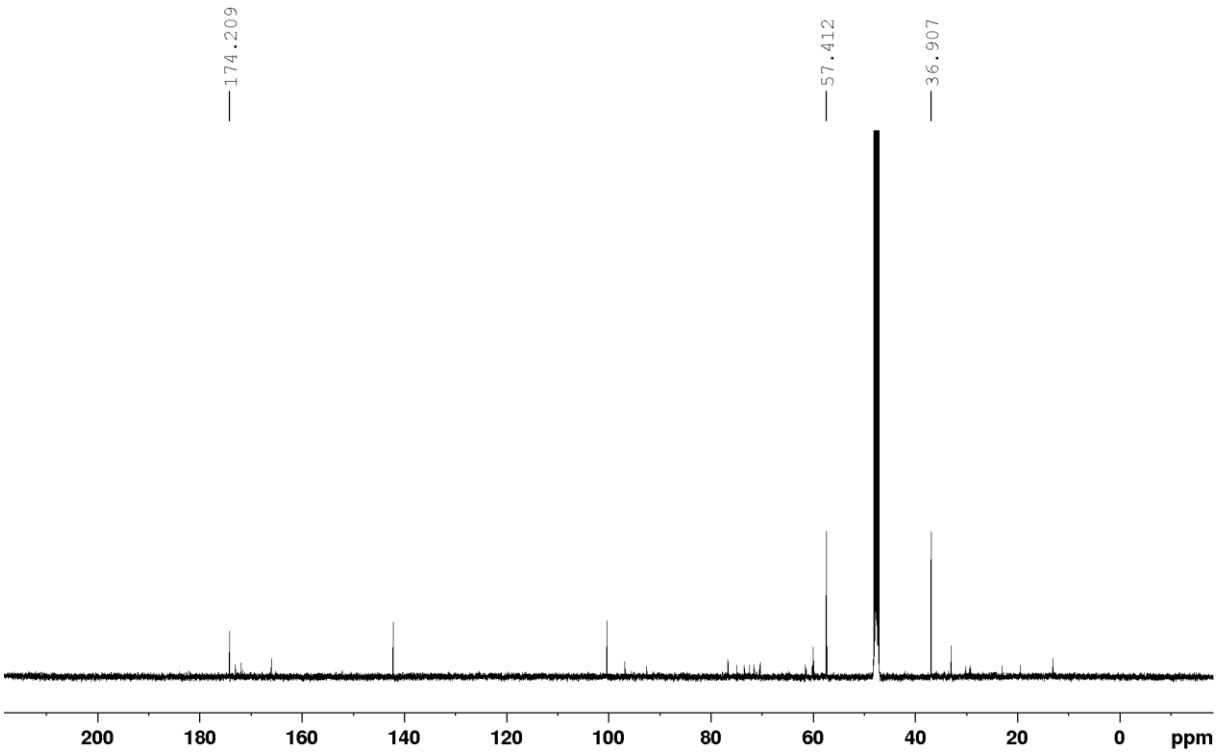

Figure S70: ^{13}C NMR spectrum (125 MHz, 298 K, MeOD) 3-HP extract from YNB SC-medium with MeOD as solvent.

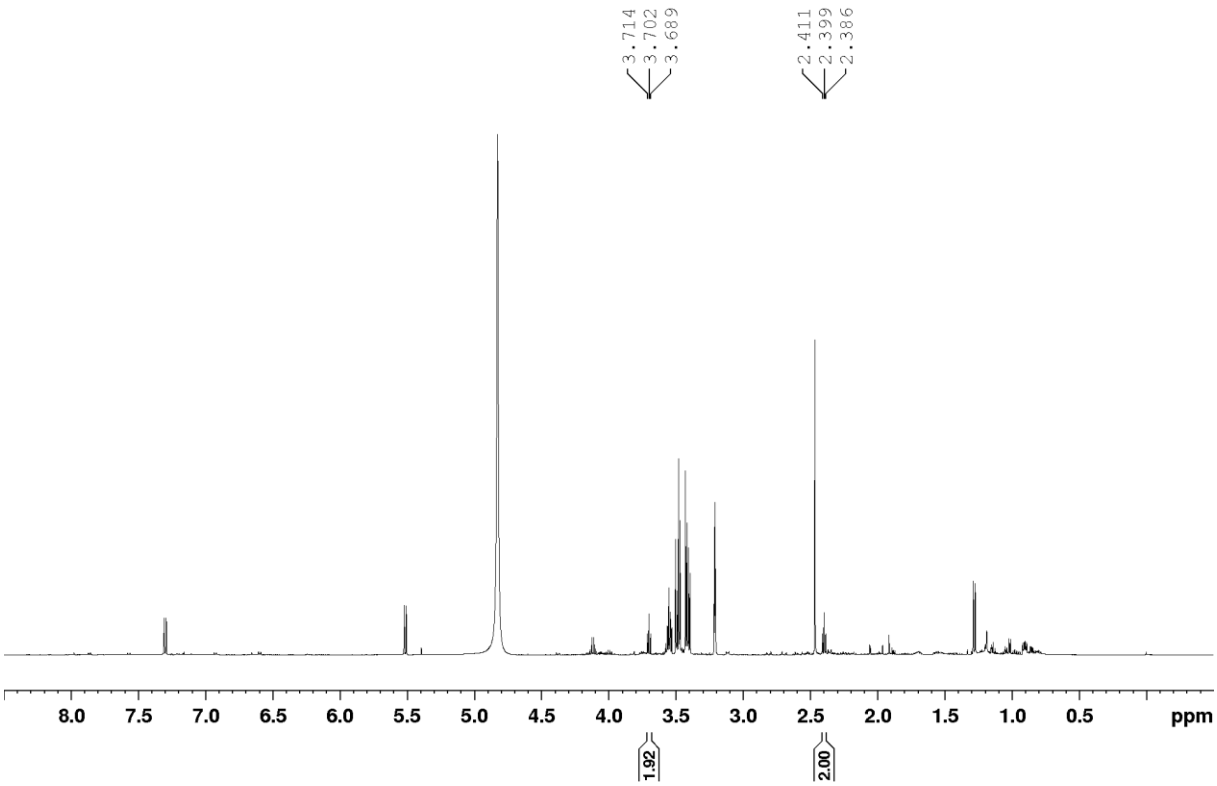

Figure S71: ^{1}H NMR spectrum (500 MHz, 298 K, MeOD) 3-HP extracted from ST022 cultivation.

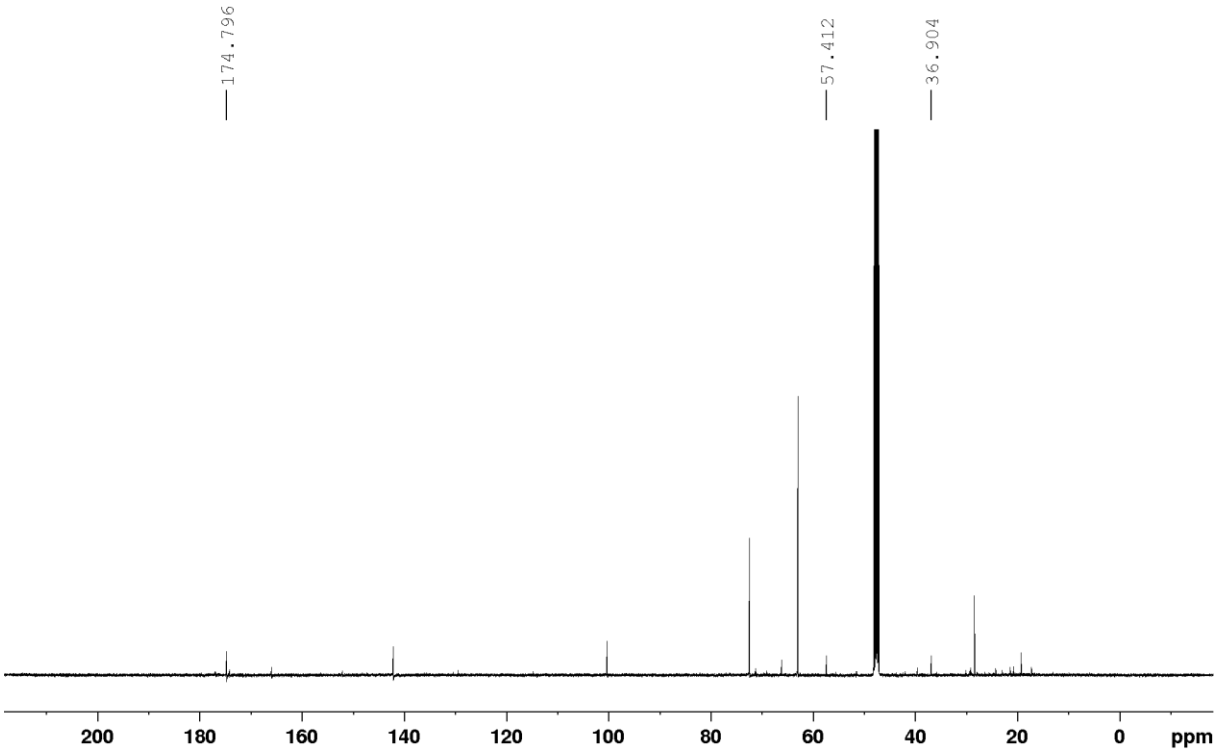

Figure S72: ^{13}C NMR spectrum (125 MHz, 298 K, MeOD) 3-HP extracted from ST022 cultivations.

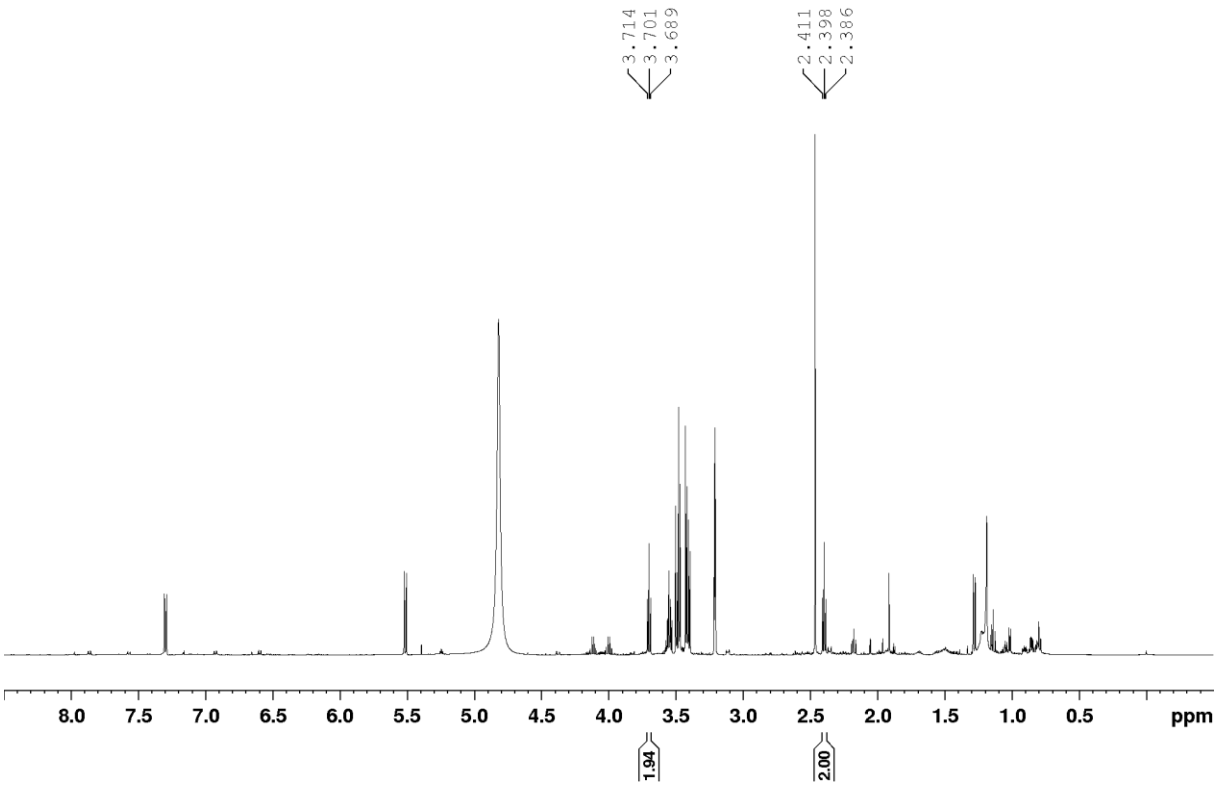

Figure S73: ^{1}H NMR spectrum (500 MHz, 298 K, MeOD) 3-HP extract from ST024 cultivations.

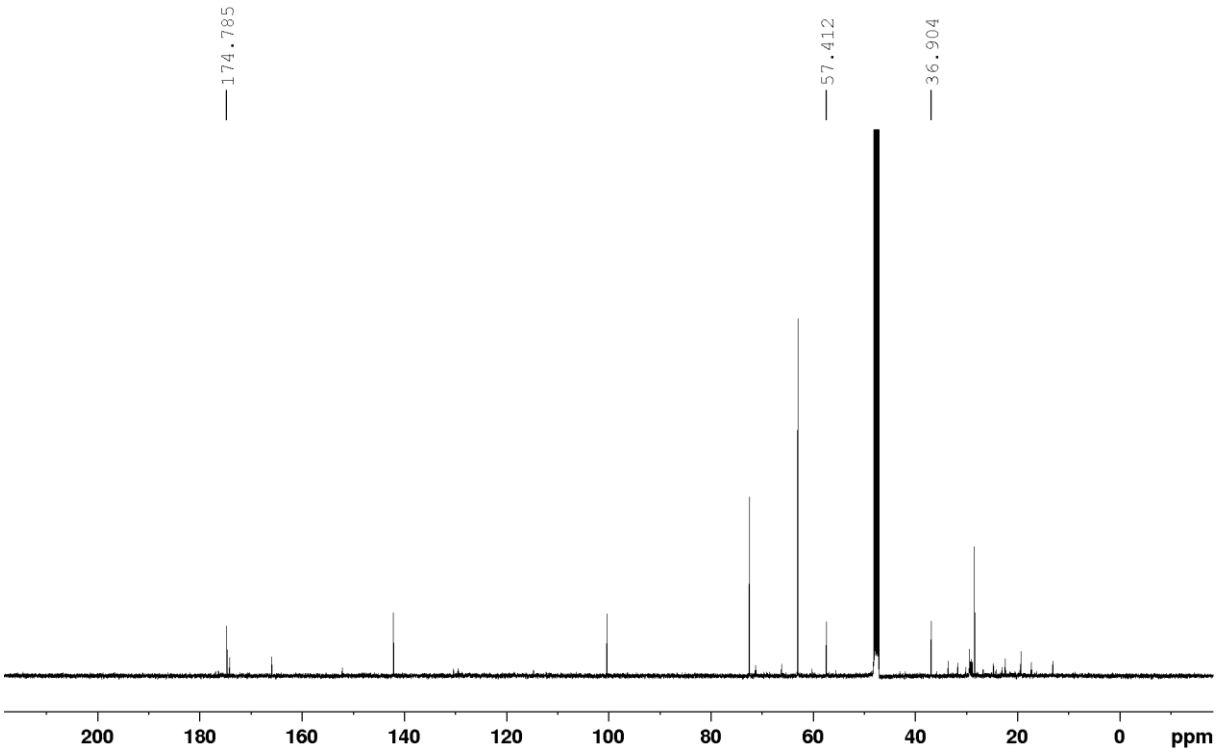

Figure S74: ^{13}C NMR spectrum (125 MHz, 298 K, MeOD) 3-HP extracted from ST024 cultivations.

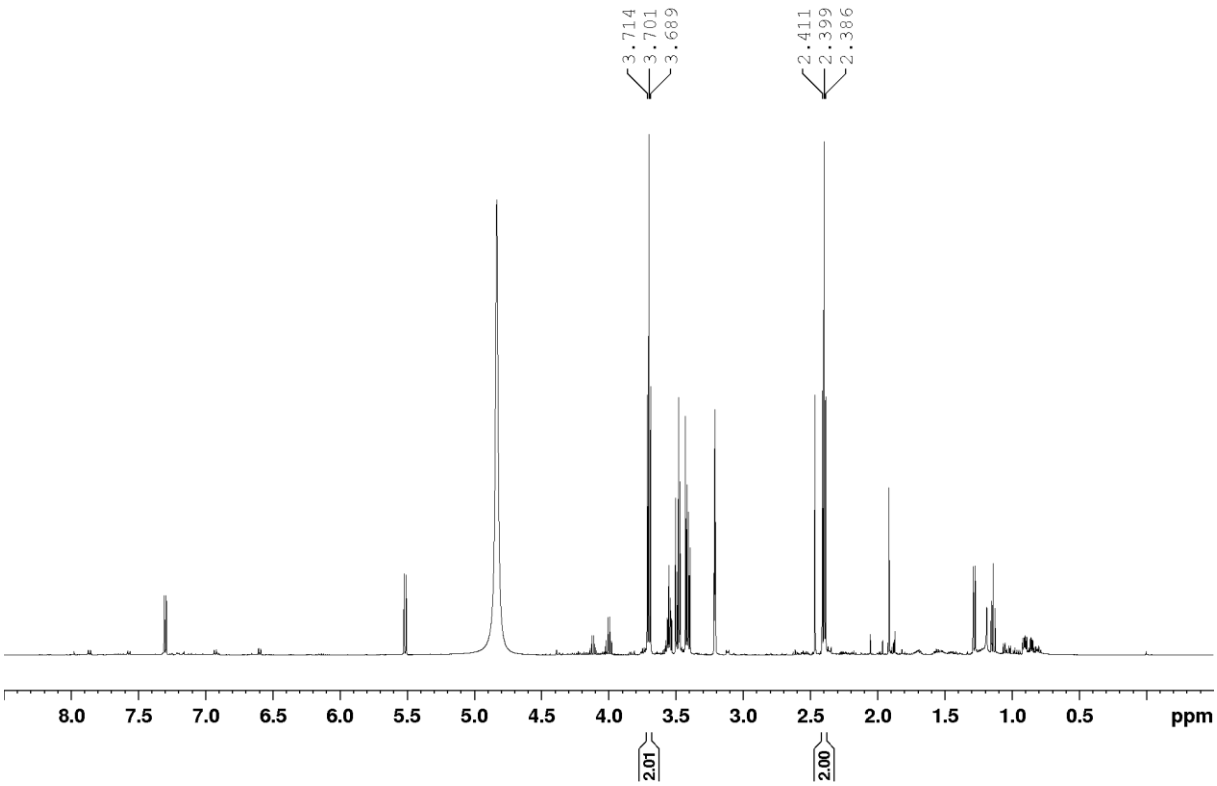

Figure S75: ^{1}H NMR spectrum (500 MHz, 298 K, MeOD) 3-HP extract from ST020 cultivations.

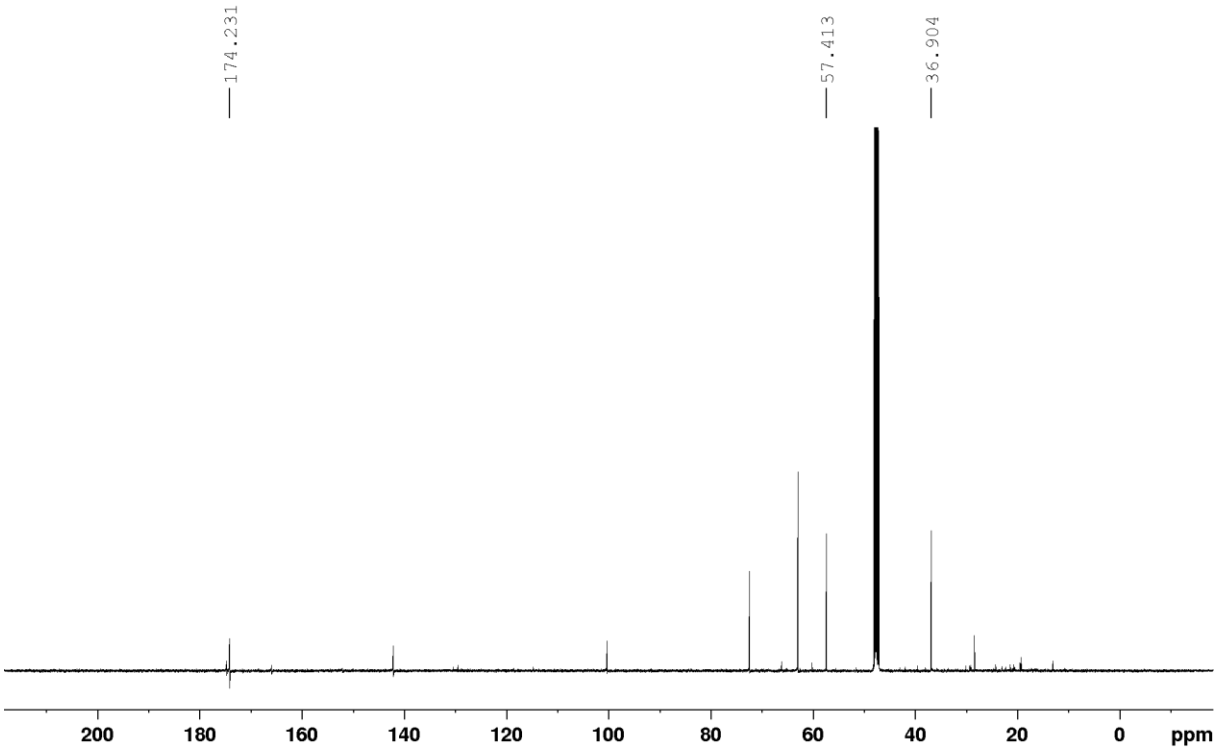

Figure S76: ^{13}C NMR spectrum (125 MHz, 298 K, MeOD) 3-HP extracted from ST020 cultivations.

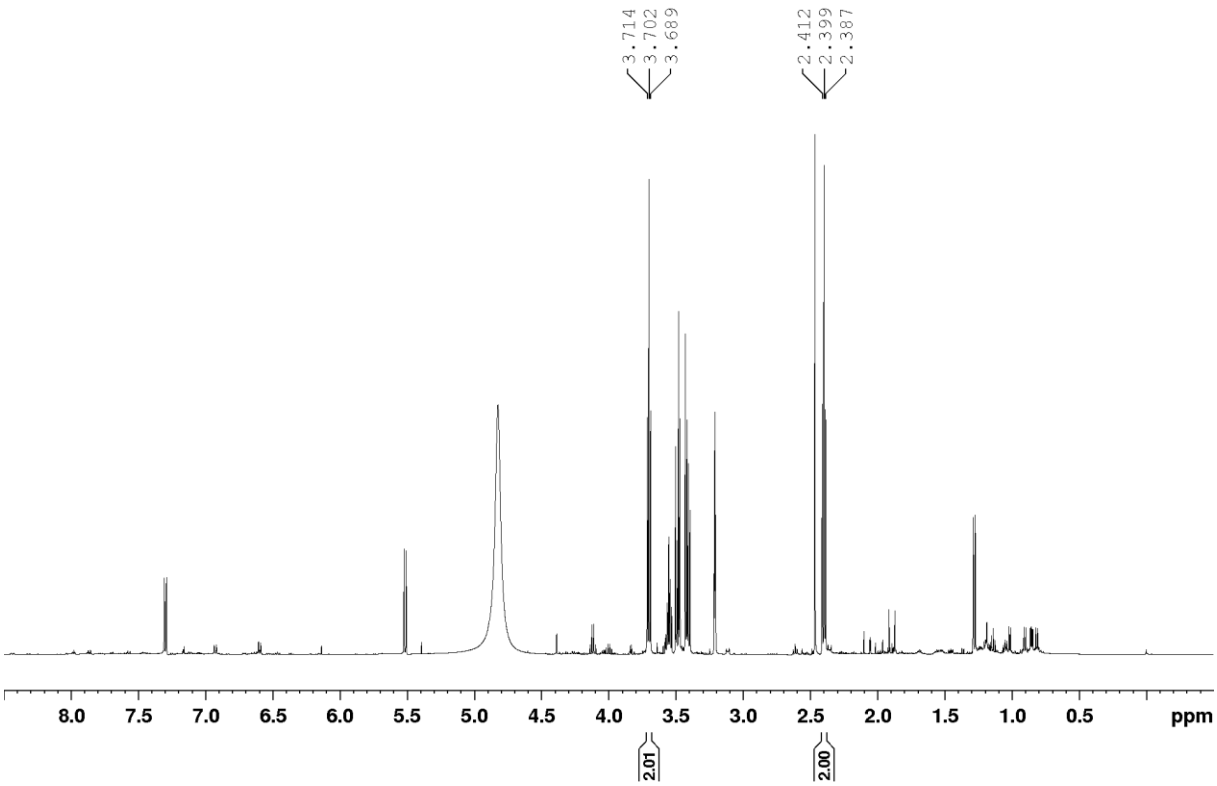

Figure S77: ^{1}H NMR spectrum (500 MHz, 298 K, MeOD) 3-HP extract from ST021 cultivations.

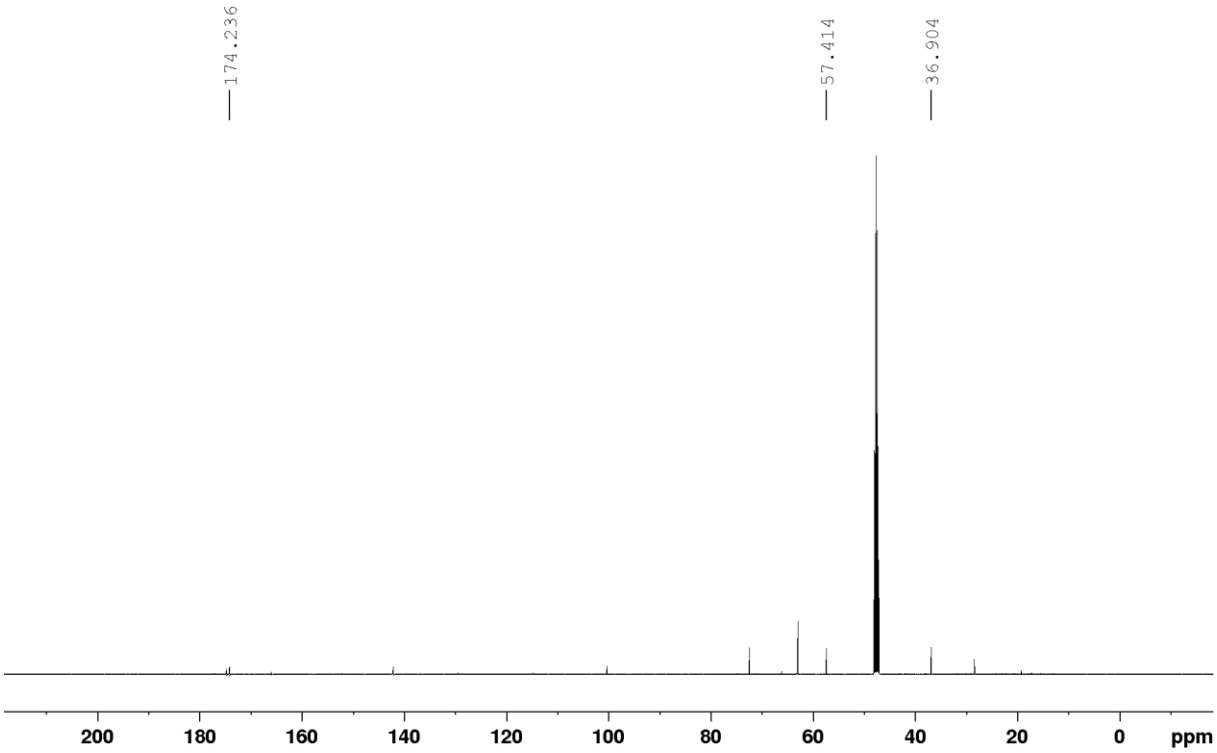

Figure S78: ^{13}C NMR spectrum (125 MHz, 298 K, MeOD) 3-HP extracted from ST021 cultivations.

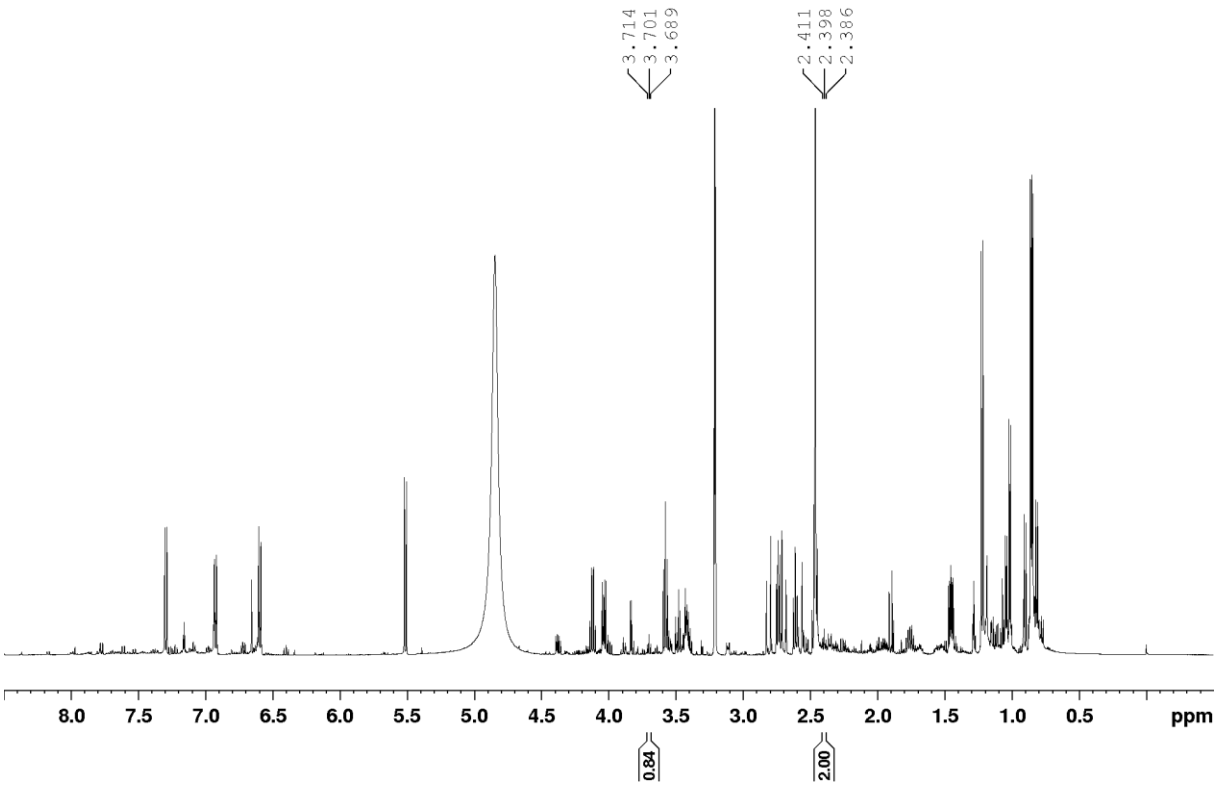

Figure S79: ^{1}H NMR spectrum (500 MHz, 298 K, MeOD) 3-HP extract from ST023 cultivations.

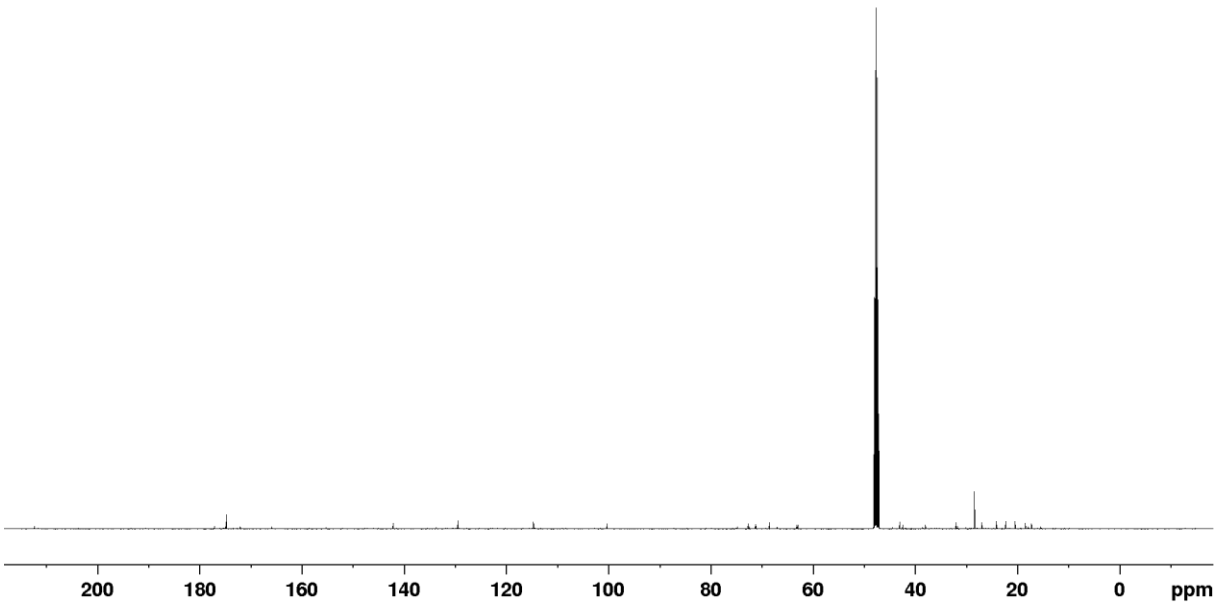

Figure S80: ^{13}C NMR spectrum (125 MHz, 298 K, MeOD) 3-HP extracted from ST023 cultivations.

vi. Plasmid-based *p*-coumaric acid production as reporter compound

Synthetic construct clone HaTAL1 histidine ammonia-lyase gene, complete cds

Sequence ID: KR095308.1 Length: 1659 Number of Matches: 1

Range 1: 1 to 1659 GenBank Graphics ▼ Next Match ▲

Score	Expect	Identities	Gaps	Strand
3064 bits(1659)	0.0	1659/1659(100%)	0/1659(0%)	Plus/Minus

Synthetic construct clone FjTAL tyrosine ammonia-lyase gene, complete cds

Sequence ID: KR095306.1 Length: 1521 Number of Matches: 1

Range 1: 556 to 601 GenBank Graphics ▼ Next Match ▲

Score	Expect	Identities	Gaps	Strand
63.9 bits(34)	1e-04	42/46(91%)	0/46(0%)	Plus/Minus

Figure S81: Standard nucleotide BLASTn sequence comparison of the received TALp sequence from DTU. Results indicate sequence consensus with the $TALp_{Ha}$ published by Jendresen et al., 2015. [219]

Table S48: Example for the data attained from tyrosine serial dilution. Data was analysed using the software OpenLab CDS (Agilent, Santa Clara, USA).

		Tyrosine 280,4 nm				
Sample name	Used conc.	Area UV	Calculated conc.	Standard diviation	Percentage Diviation	Formular
	[mg/L]	[mAU]	[mg/L]		[%]	y=mx+b
1,2 mg/L Tyr in YNB,H2O 1:1	1,2	131,88	0,49	0,50	59,34	m:
2,34 mg/L Tyr in YNB,H2O 1:1	2,34	138,86	1,70	0,46	27,65	5,779093347
4,68 mg/L Tyr in YNB,H2O 1:1	4,69	152,2	4,00	0,48	14,58	
9,375 mg/L Tyr in YNB,H2O 1:1	9,38	181,2	9,02	0,25	3,76	b:
18,75 mg/L Tyr in YNB,H2O 1:1	18,75	237,71	18,80	0,04	-0,27	129,0604256
37,5 mg/L Tyr in YNB,H2O 1:1	37,50	350,79	38,37	0,61	-2,31	
75 mg/L Tyr in YNB,H2O 1:1	75,00	574,02	76,99	1,41	-2,66	
150 mg/L Tyr in YNB,H2O 1:1	150,00	996,67	150,13	0,09	-0,09	
300 mg/L Tyr in YNB,H2O 1:1	300,00	1859,06	299,35	0,46	0,22	

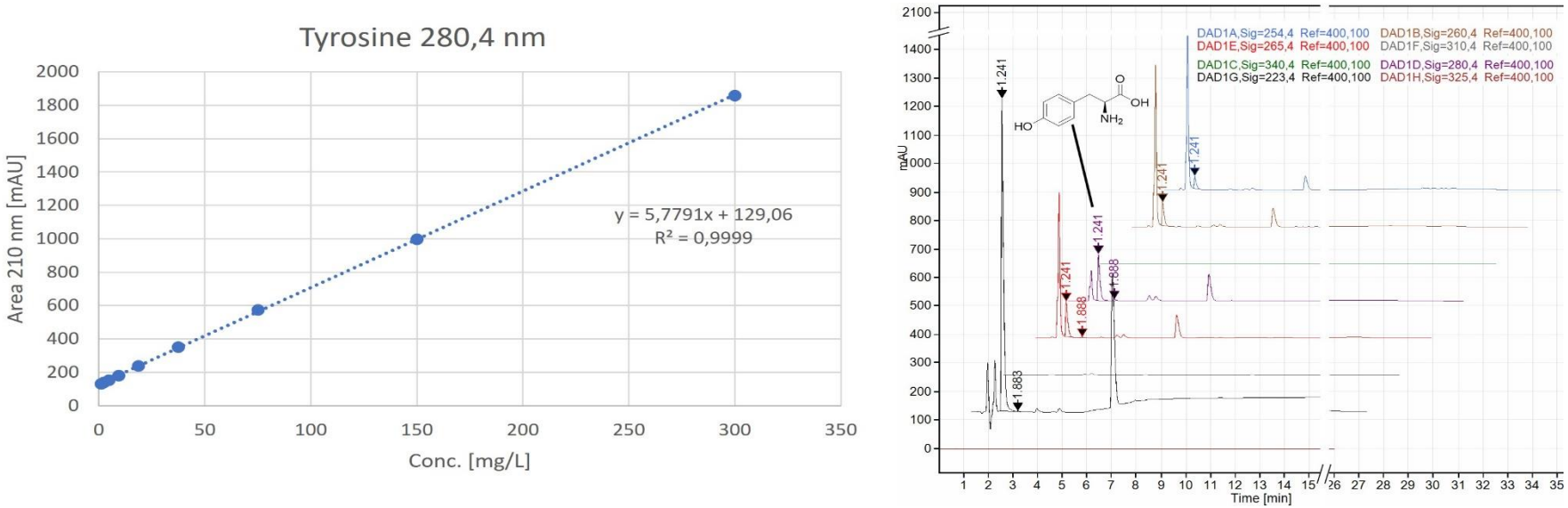

Figure S82: Example of a calibration curve attained using the data from Table S48 and an example of a tyrosine chromatogram generated with the software OpenLab CDS (Agilent, Santa Clara, USA).

Table S49: Example for the data attained from p-CA serial dilution. Data was analysed using the software OpenLab CDS (Agilent, Santa Clara, USA).

		Cumarsäure 310,4 nm				
Sample name	Used conc.	Area UV	Calculated conc.	Standard diviation	Percentage Diviation	Formular
	[mg/L]	[mAU]	[mg/L]		[%]	y=mx+b
1,5625 mg/L CA in YNB,H2O 1:1	1,5625	177,67	1,45	0,08	7,40	m:
3,125 mg/L CA in YNB,H2O 1:1	3,125	294,29	2,40	0,52	23,31	122,8004522
6,25 mg/L CA in YNB,H2O 1:1	6,25	679,48	5,53	0,51	11,47	
12,5 mg/L CA in YNB,H2O 1:1	12,5	1472,58	11,99	0,36	4,07	b:
25 mg/L CA in YNB,H2O 1:1	25	3068,69	24,99	0,01	0,04	
50 mg/L CA in YNB,H2O 1:1	50	6216,12	50,62	0,44	-1,24	
100 mg/L CA in YNB,H2O 1:1	100	12367,25	100,71	0,50	-0,71	
200 mg/L CA in YNB,H2O 1:1	200	24505,79	199,56	0,31	0,22	
400 mg/L CA in YNB,H2O 1:1	400	42275,33	344,26	39,41	13,93	
800 mg/L CA in YNB,H2O 1:1	800	61403,89	500,03	212,11	37,50	m:

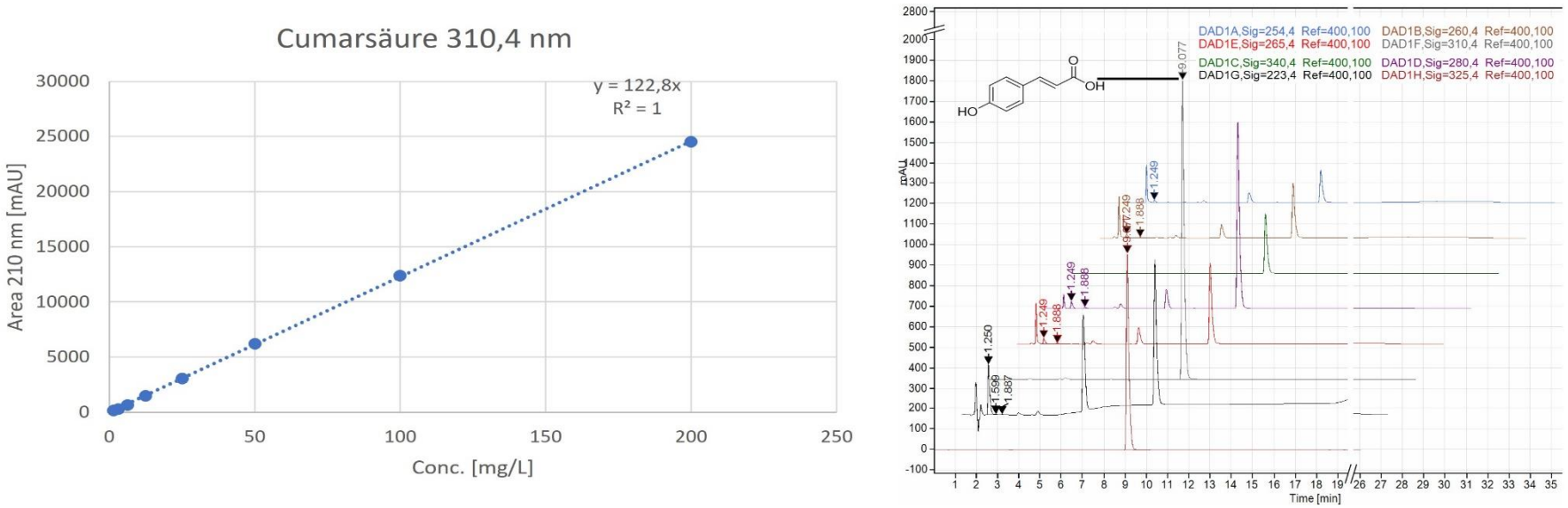

Figure S83: Example of a calibration curve attained using the data from Table S49 and an example of a p-CA chromatogram generated with the software OpenLab CDS (Agilent, Santa Clara, USA).

vii. Combining shikimate and malonyl-CoA pathway in a single strain

	ST003 WT	ST024	ST028	ST029
haTal1	-	-	-	-
ΔAro10::scAro4/7	-	-	+	+
ΔPdc5::ecAroL	-	-	-	+

Figure S84: Comparison of tyrosine level upon introduction of engineering modifications combining shikimate and malonyl-CoA pathway. Green columns indicate the measured tyrosine. Signals detected with HPLC-UV at 280 nm for tyrosine. Cultivation was conducted in YNB SC-medium utilizing the Biolector, 72 h, 1200 rpm, 30 °C, 85 % humidity (Biolector, M2P labs GmbH, Germany). ST003 WT: 37,62±3,09 mg L^{-1}; ST024: 49,44±4,85 mg L^{-1}; ST028: 131,11±0,29 mg L^{-1}; ST029: 53,85±1,11 mg L^{-1}.

Declaration of own work

Experiments, data analysis, data representation and writing of the present thesis were performed by myself exclusively.

Publications

None

Supervised Bachelor and Master thesis

Jonas Korb (2020), “Genomic integration of the genes ARO4K229L, ARO7G141S, and AroL in *Saccharomyces cerevisiae* to optimise the shikimate pathway”, Bachelorarbeit, Technische Universität Dortmund

Acknowledgements

First of all, I would like to thank my supervisor Professor Dr. Dr. h. c. Oliver Kayser (Chair of Technical Biochemistry, TU Dortmund, Germany) for the opportunity to work on this thesis and interesting topic.

I would like to thank Marco Aras, all the PhD students, the technicians, and assistance of the Biocenter, both current and former, for the great atmosphere and companion throughout the years. Special thanks to Kristine Hemmer, Bettina Höller, Jörg Fischer, Julian Dyrda, Chantale Zammarelli and Katharina Kuhr, for the support and organizing the daily business in and outside the lab.

In particular I would like to extend my gratitude to the other TB PhD students Julia, Leonie, Thanet, Alex, Fabian, Sophie, Christina, Saskia, and Nam for scientific input and the great time together.

Thank you very much for your excellent work to my student Jonas Korb.

Throughout our journey, special appreciation to Isa, for your enduring support and patience.

For their unwavering support in all situations in both good and bad times, their patience, which I can always count on, and without which I would not have made it, my deepest thanks to my family, my friends, and especially Hummel.

References

[1] Naeem, A.; Hu, P.; Yang, M.; Zhang, J.; Liu, Y.; Zhu, W.; Zheng, Q. Natural Products as Anticancer Agents: Current Status and Future Perspectives. *Molecules* **2022**, *27* (23), 8367. https://doi.org/10.3390/molecules27238367.

[2] Katz, L.; Baltz, R. H. Natural Product Discovery: Past, Present, and Future. *Journal of Industrial Microbiology and Biotechnology* **2016**, *43* (2–3), 155–176. https://doi.org/10.1007/s10295-015-1723-5.

[3] Ekiert, H. M.; Szopa, A. Biological Activities of Natural Products. *Molecules* **2020**, *25* (23), 5769. https://doi.org/10.3390/molecules25235769.

[4] Newman, D. J.; Cragg, G. M. Natural Products as Sources of New Drugs over the Nearly Four Decades from 01/1981 to 09/2019. *J Nat Prod* **2020**, *83* (3), 770–803. https://doi.org/10.1021/acs.jnatprod.9b01285.

[5] Fleming, A. On the Antibacterial Action of Cultures of a Penicillium, with Special Reference to Their Use in the Isolation of B. Influenzae. 1929. *Bull World Health Organ* **2001**, *79* (8), 780–790.

[6] Paddon, C. J.; Westfall, P. J.; Pitera, D. J.; Benjamin, K.; Fisher, K.; McPhee, D.; Leavell, M. D.; Tai, A.; Main, A.; Eng, D.; Polichuk, D. R.; Teoh, K. H.; Reed, D. W.; Treynor, T.; Lenihan, J.; Jiang, H.; Fleck, M.; Bajad, S.; Dang, G.; Dengrove, D.; Diola, D.; Dorin, G.; Ellens, K. W.; Fickes, S.; Galazzo, J.; Gaucher, S. P.; Geistlinger, T.; Henry, R.; Hepp, M.; Horning, T.; Iqbal, T.; Kizer, L.; Lieu, B.; Melis, D.; Moss, N.; Regentin, R.; Secrest, S.; Tsuruta, H.; Vazquez, R.; Westblade, L. F.; Xu, L.; Yu, M.; Zhang, Y.; Zhao, L.; Lievense, J.; Covello, P. S.; Keasling, J. D.; Reiling, K. K.; Renninger, N. S.; Newman, J. D. High-Level Semi-Synthetic Production of the Potent Antimalarial Artemisinin. *Nature* **2013**, *496* (7446), 528–532. https://doi.org/10.1038/nature12051.

[7] Williams, D. C.; Van Frank, R. M.; Muth, W. L.; Burnett, J. P. Cytoplasmic Inclusion Bodies in *Escherichia Coli* Producing Biosynthetic Human Insulin Proteins. *Science* **1982**, *215* (4533), 687–689. https://doi.org/10.1126/science.7036343.

[8] Horwitz, S. B. How to Make Taxol from Scratch. *Nature* **1994**, *367* (6464), 593–594. https://doi.org/10.1038/367593a0.

[9] Hiltpold, I.; Turlings, T. C. J. Manipulation of Chemically Mediated Interactions in Agricultural Soils to Enhance the Control of Crop Pests and to Improve Crop Yield. *J Chem Ecol* **2012**, *38* (6), 641–650. https://doi.org/10.1007/s10886-012-0131-9.

[10] Johann, S.; Mendes, B. G.; Missau, F. C.; Resende, M. A. D.; Pizzolatti, M. G. Antifungal Activity of Five Species of Polygala. *Braz. J. Microbiol.* **2011**, *42* (3), 1065–1075. https://doi.org/10.1590/S1517-83822011000300027.

[11] Huang, M.; Sanchez-Moreiras, A. M.; Abel, C.; Sohrabi, R.; Lee, S.; Gershenzon, J.; Tholl, D. The Major Volatile Organic Compound Emitted from Arabidopsis Thaliana Flowers, the Sesquiterpene (E)-β-Caryophyllene, Is a Defense against a Bacterial Pathogen. *New Phytologist* **2012**, *193* (4), 997–1008. https://doi.org/10.1111/j.1469-8137.2011.04001.x.

[12] Kappers, I. F.; Hoogerbrugge, H.; Bouwmeester, H. J.; Dicke, M. Variation in Herbivory-Induced Volatiles Among Cucumber (Cucumis Sativus L.) Varieties Has Consequences for the Attraction of Carnivorous Natural Enemies. *J Chem Ecol* **2011**, *37* (2), 150–160. https://doi.org/10.1007/s10886-011-9906-7.

[13] Atanasov, A. G.; Zotchev, S. B.; Dirsch, V. M.; Supuran, C. T. Natural Products in Drug Discovery: Advances and Opportunities. *Nat Rev Drug Discov* **2021**, *20* (3), 200–216. https://doi.org/10.1038/s41573-020-00114-z.

[14] Luo, Y.; Li, B.-Z.; Liu, D.; Zhang, L.; Chen, Y.; Jia, B.; Zeng, B.-X.; Zhao, H.; Yuan, Y.-J. Engineered Biosynthesis of Natural Products in Heterologous Hosts. *Chemical Society Reviews* **2015**, *44* (15), 5265–5290. https://doi.org/10.1039/C5CS00025D.

[15] Xie, X.; Kirby, J.; Keasling, J. D. Functional Characterization of Four Sesquiterpene Synthases from Ricinus Communis (Castor Bean). *Phytochemistry* **2012**, *78*, 20–28. https://doi.org/10.1016/j.phytochem.2012.02.022.

[16] Tholl, D. Terpene Synthases and the Regulation, Diversity and Biological Roles of Terpene Metabolism. *Current Opinion in Plant Biology* **2006**, *9* (3), 297–304. https://doi.org/10.1016/j.pbi.2006.03.014.

[17] Moss, G. P.; Smith, P. a. S.; Tavernier, D. Glossary of class names of organic compounds and reactivity intermediates based on structure (IUPAC Recommendations 1995). *Pure and Applied Chemistry* **1995**, *67* (8–9), 1307–1375. https://doi.org/10.1351/pac199567081307.

[18] Goldstein, J. L.; Brown, M. S. Regulation of the Mevalonate Pathway. *Nature* **1990**, *343* (6257), 425–430. https://doi.org/10.1038/343425a0.

[19] George, K.; Alonso-Gutierrez, J.; Keasling, J.; Lee, T. S. Isoprenoid Drugs, Biofuels, and Chemicals-Artemisinin, Farnesene, and Beyond (Vol 148, Pg 355, 2015). *Advances in Biochemical Engineering/Biotechnology* **2015**, *148*, 469–469. https://doi.org/10.1007/10_2015_310.

[20] Eisenreich, W.; Schwarz, M.; Cartayrade, A.; Arigoni, D.; Zenk, M. H.; Bacher, A. The Deoxyxylulose Phosphate Pathway of Terpenoid Biosynthesis in Plants and Microorganisms. *Chemistry & Biology* **1998**, *5* (9), R221–R233. https://doi.org/10.1016/S1074-5521(98)90002-3.

[21] Sangari, F.; Perez-Gil, J.; Carretero-Paulet, L.; García-Lobo, J.; Rodríguez-Concepción, M. A New Family of Enzymes Catalyzing the First Committed Step of the Methylerythritol 4-Phosphate (MEP) Pathway for Isoprenoid Biosynthesis in Bacteria. *Proceedings of the National Academy of Sciences of the United States of America* **2010**, *107*, 14081–14086. https://doi.org/10.1073/pnas.1001962107.

[22] Wani, M. C.; Taylor, H. L.; Wall, M. E.; Coggon, P.; McPhail, A. T. Plant Antitumor Agents. VI. Isolation and Structure of Taxol, a Novel Antileukemic and Antitumor Agent from Taxus Brevifolia. *J. Am. Chem. Soc.* **1971**, *93* (9), 2325–2327. https://doi.org/10.1021/ja00738a045.

[23] Ma, N.; Zhang, Z.; Liao, F.; Jiang, T.; Tu, Y. The Birth of Artemisinin. *Pharmacology & Therapeutics* **2020**, *216*, 107658. https://doi.org/10.1016/j.pharmthera.2020.107658.

[24] Markman, M. Managing Taxane Toxicities. *Support Care Cancer* **2003**, *11* (3), 144–147. https://doi.org/10.1007/s00520-002-0405-9.

[25] Croteau, R.; Ketchum, R. E. B.; Long, R. M.; Kaspera, R.; Wildung, M. R. Taxol Biosynthesis and Molecular Genetics. *Phytochem Rev* **2006**, *5* (1), 75–97. https://doi.org/10.1007/s11101-005-3748-2.

[26] Trantas, E.; Panopoulos, N.; Ververidis, F. Metabolic Engineering of the Complete Pathway Leading to Heterologous Biosynthesis of Various Flavonoids and Stilbenoids in Saccharomyces Cerevisiae. *Metabolic Engineering* **2009**, *11* (6), 355–366. https://doi.org/10.1016/j.ymben.2009.07.004.

[27] Li, H.; Gao, S.; Zhang, S.; Zeng, W.; Zhou, J. Effects of Metabolic Pathway Gene Copy Numbers on the Biosynthesis of (2S)-Naringenin in Saccharomyces Cerevisiae. *J Biotechnol* **2021**, *325*, 119–127. https://doi.org/10.1016/j.jbiotec.2020.11.009.

[28] Maeda, H.; Dudareva, N. The Shikimate Pathway and Aromatic Amino Acid Biosynthesis in Plants. *Annual Review of Plant Biology* **2012**, *63* (1), 73–105. https://doi.org/10.1146/annurev-arplant-042811-105439.

[29] Fester, K. Plant Alkaloids. In *eLS*; John Wiley & Sons, Ltd, Ed.; Wiley, 2010. https://doi.org/10.1002/9780470015902.a0001914.pub2.

[30] *Medicinal Plants: Chemistry, Pharmacology, and Therapeutic Applications*; Swamy, M. K., Patra, J. K., Rudramurthy, G. R., Eds.; CRC Press / Taylor & Francis Group: Boca Raton, FL, 2019.

[31] Meng, L.; Diao, M.; Wang, Q.; Peng, L.; Li, J.; Xie, N. Efficient Biosynthesis of Resveratrol via Combining Phenylalanine and Tyrosine Pathways in Saccharomyces Cerevisiae. *Microb Cell Fact* **2023**, *22* (1), 46. https://doi.org/10.1186/s12934-023-02055-9.

[32] Meng, Y.; Liu, X.; Zhang, L.; Zhao, G.-R. Modular Engineering of Saccharomyces Cerevisiae for De Novo Biosynthesis of Genistein. *Microorganisms* **2022**, *10* (7), 1402. https://doi.org/10.3390/microorganisms10071402.

[33] Zhang, L.-X.; Li, C.-X.; Kakar, M. U.; Khan, M. S.; Wu, P.-F.; Amir, R. M.; Dai, D.-F.; Naveed, M.; Li, Q.-Y.; Saeed, M.; Shen, J.-Q.; Rajput, S. A.; Li, J.-H. Resveratrol (RV): A Pharmacological Review and Call for Further Research. *Biomedicine & Pharmacotherapy* **2021**, *143*, 112164. https://doi.org/10.1016/j.biopha.2021.112164.

[34] Zaheer, K.; Humayoun Akhtar, M. An Updated Review of Dietary Isoflavones: Nutrition, Processing, Bioavailability and Impacts on Human Health. *Critical Reviews in Food Science and Nutrition* **2017**, *57* (6), 1280–1293. https://doi.org/10.1080/10408398.2014.989958.

[35] Li, M.; Kildegaard, K. R.; Chen, Y.; Rodriguez, A.; Borodina, I.; Nielsen, J. De Novo Production of Resveratrol from Glucose or Ethanol by Engineered Saccharomyces Cerevisiae. *Metab Eng* **2015**, *32*, 1–11. https://doi.org/10.1016/j.ymben.2015.08.007.

[36] Tippelt, A.; Nett, M. Saccharomyces Cerevisiae as Host for the Recombinant Production of Polyketides and Nonribosomal Peptides. *Microb Cell Fact* **2021**, *20* (1), 161. https://doi.org/10.1186/s12934-021-01650-y.

[37] Ray, L.; Moore, B. S. Recent Advances in the Biosynthesis of Unusual Polyketide Synthase Substrates. *Nat. Prod. Rep.* **2016**, *33* (2), 150–161. https://doi.org/10.1039/C5NP00112A.

[38] Yang, D.; Eun, H.; Prabowo, C. P. S. Metabolic Engineering and Synthetic Biology Approaches for the Heterologous Production of Aromatic Polyketides. *IJMS* **2023**, *24* (10), 8923. https://doi.org/10.3390/ijms24108923.

[39] Grininger, M. Enzymology of Assembly Line Synthesis by Modular Polyketide Synthases. *Nat Chem Biol* **2023**, *19* (4), 401–415. https://doi.org/10.1038/s41589-023-01277-7.

[40] Mulder, K. C. L.; Mulinari, F.; Franco, O. L.; Soares, M. S. F.; Magalhães, B. S.; Parachin, N. S. Lovastatin Production: From Molecular Basis to Industrial Process Optimization. *Biotechnology Advances* **2015**, *33* (6), 648–665. https://doi.org/10.1016/j.biotechadv.2015.04.001.

[41] Pickens, L. B.; Tang, Y. Decoding and Engineering Tetracycline Biosynthesis. *Metab Eng* **2009**, *11* (2), 69–75. https://doi.org/10.1016/j.ymben.2008.10.001.

[42] Wlodek, A.; Kendrew, S. G.; Coates, N. J.; Hold, A.; Pogwizd, J.; Rudder, S.; Sheehan, L. S.; Higginbotham, S. J.; Stanley-Smith, A. E.; Warneck, T.; Nur-E-Alam, M.; Radzom, M.; Martin, C. J.; Overvoorde, L.; Samborskyy, M.; Alt, S.; Heine, D.; Carter, G. T.; Graziani, E. I.; Koehn, F. E.; McDonald, L.; Alanine, A.; Rodríguez Sarmiento, R. M.; Chao, S. K.; Ratni, H.; Steward, L.; Norville, I. H.; Sarkar-Tyson, M.; Moss, S. J.; Leadlay, P. F.; Wilkinson, B.; Gregory, M. A. Diversity Oriented Biosynthesis via Accelerated Evolution of Modular Gene Clusters. *Nat Commun* **2017**, *8* (1), 1206. https://doi.org/10.1038/s41467-017-01344-3.

[43] Geng, H.; Liu, H.; Liu, J.; Wang, C.; Wen, J. Insights into the Metabolic Mechanism of Rapamycin Overproduction in the Shikimate-Resistant Streptomyces Hygroscopicus Strain UV-II Using Comparative Metabolomics. *World J Microbiol Biotechnol* **2017**, *33* (6), 101. https://doi.org/10.1007/s11274-017-2266-x.

[44] *KEGG PATHWAY: Tetracycline biosynthesis*. https://www.genome.jp/pathway/rn00253+R11516 (accessed 2023-09-18).

[45] Yoo, Y. J.; Hwang, J.; Shin, H.; Cui, H.; Lee, J.; Yoon, Y. J. Characterization of Negative Regulatory Genes for the Biosynthesis of Rapamycin in Streptomyces Rapamycinicus and Its Application for Improved Production. *J Ind Microbiol Biotechnol* **2015**, *42* (1), 125–135. https://doi.org/10.1007/s10295-014-1546-9.

[46] Khan, H.; Ullah, H.; Martorell, M.; Valdes, S. E.; Belwal, T.; Tejada, S.; Sureda, A.; Kamal, M. A. Flavonoids Nanoparticles in Cancer: Treatment, Prevention and Clinical Prospects. *Seminars in Cancer Biology* **2021**, *69*, 200–211. https://doi.org/10.1016/j.semcancer.2019.07.023.

[47] Azab, A.; Nassar, A.; Azab, A. N. Anti-Inflammatory Activity of Natural Products. *Molecules* **2016**, *21* (10), 1321. https://doi.org/10.3390/molecules21101321.

[48] Ben-Shabat, S.; Yarmolinsky, L.; Porat, D.; Dahan, A. Antiviral Effect of Phytochemicals from Medicinal Plants: Applications and Drug Delivery Strategies. *Drug Deliv Transl Res* **2020**, *10* (2), 354–367. https://doi.org/10.1007/s13346-019-00691-6.

[49] Staunton, J.; Weissman, K. J. Polyketide Biosynthesis: A Millennium Review. *Nat. Prod. Rep.* **2001**, *18* (4), 380–416. https://doi.org/10.1039/a909079g.

[50] Harvey, A. L.; Edrada-Ebel, R.; Quinn, R. J. The Re-Emergence of Natural Products for Drug Discovery in the Genomics Era. *Nat Rev Drug Discov* **2015**, *14* (2), 111–129. https://doi.org/10.1038/nrd4510.

[51] Kingston, D. G. I. Taxol: The Chemistry and Structure-Activity Relationships of a Novel Anticancer Agent. *Trends in Biotechnology* **1994**, *12* (6), 222–227. https://doi.org/10.1016/0167-7799(94)90120-1.

[52] Bailey, J. E. Toward a Science of Metabolic Engineering. *Science* **1991**, *252* (5013), 1668–1675. https://doi.org/10.1126/science.2047876.

[53] Nielsen, J. Metabolic Engineering. *Applied Microbiology and Biotechnology* **2001**, *55* (3), 263–283. https://doi.org/10.1007/s002530000511.

[54] Cohen, S. N.; Chang, A. C. Y.; Boyer, H. W.; Helling, R. B. Construction of Biologically Functional Bacterial Plasmids In Vitro. *Proceedings of the National Academy of Sciences* **1973**, *70* (11), 3240–3244. https://doi.org/10.1073/pnas.70.11.3240.

[55] Kjeldsen, T. Yeast Secretory Expression of Insulin Precursors. *Applied Microbiology and Biotechnology* **2000**, *54* (3), 277–286. https://doi.org/10.1007/s002530000402.

[56] Pickens, L. B.; Tang, Y.; Chooi, Y.-H. Metabolic Engineering for the Production of Natural Products. *Annu. Rev. Chem. Biomol. Eng.* **2011**, *2* (1), 211–236. https://doi.org/10.1146/annurev-chembioeng-061010-114209.

[57] Choi, K. R.; Jang, W. D.; Yang, D.; Cho, J. S.; Park, D.; Lee, S. Y. Systems Metabolic Engineering Strategies: Integrating Systems and Synthetic Biology with Metabolic Engineering. *Trends in Biotechnology* **2019**, *37* (8), 817–837. https://doi.org/10.1016/j.tibtech.2019.01.003.

[58] Hinnen, A.; Hicks, J. B.; Fink, G. R. Transformation of Yeast. *Proc Natl Acad Sci U S A* **1978**, *75* (4), 1929–1933. https://doi.org/10.1073/pnas.75.4.1929.

[59] Nielsen, J.; Jewett, M. C. Impact of Systems Biology on Metabolic Engineering of *Saccharomyces Cerevisiae*. *FEMS Yeast Research* **2008**, *8* (1), 122–131. https://doi.org/10.1111/j.1567-1364.2007.00302.x.

[60] Luo, X.; Reiter, M. A.; d'Espaux, L.; Wong, J.; Denby, C. M.; Lechner, A.; Zhang, Y.; Grzybowski, A. T.; Harth, S.; Lin, W.; Lee, H.; Yu, C.; Shin, J.; Deng, K.; Benites, V. T.; Wang, G.; Baidoo, E. E. K.; Chen, Y.; Dev, I.; Petzold, C. J.; Keasling, J. D. Complete Biosynthesis of Cannabinoids and Their Unnatural Analogues in Yeast. *Nature* **2019**, *567* (7746), 123–126. https://doi.org/10.1038/s41586-019-0978-9.

[61] Luo, X.; Reiter, M. A.; d'Espaux, L.; Wong, J.; Denby, C. M.; Lechner, A.; Zhang, Y.; Grzybowski, A. T.; Harth, S.; Lin, W.; Lee, H.; Yu, C.; Shin, J.; Deng, K.; Benites, V. T.; Wang, G.; Baidoo, E. E. K.; Chen, Y.; Dev, I.; Petzold, C. J.; Keasling, J. D. Author Correction: Complete Biosynthesis of Cannabinoids and Their Unnatural Analogues in Yeast. *Nature* **2020**, *580* (7802), E2–E2. https://doi.org/10.1038/s41586-020-2109-z.

[62] Mikkelsen, M. D.; Buron, L. D.; Salomonsen, B.; Olsen, C. E.; Hansen, B. G.; Mortensen, U. H.; Halkier, B. A. Microbial Production of Indolylglucosinolate through Engineering of a Multi-Gene Pathway in a Versatile Yeast Expression Platform. *Metabolic Engineering* **2012**, *14* (2), 104–111. https://doi.org/10.1016/j.ymben.2012.01.006.

[63] Jensen, N. B.; Strucko, T.; Kildegaard, K. R.; David, F.; Maury, J.; Mortensen, U. H.; Forster, J.; Nielsen, J.; Borodina, I. EasyClone: Method for Iterative Chromosomal Integration of Multiple Genes in Saccharomyces Cerevisiae. *FEMS Yeast Res* **2014**, *14* (2), 238–248. https://doi.org/10.1111/1567-1364.12118.

[64] Jinek, M.; Chylinski, K.; Fonfara, I.; Hauer, M.; Doudna, J. A.; Charpentier, E. A Programmable Dual RNA-Guided DNA Endonuclease in Adaptive Bacterial Immunity. *Science* **2012**, *337* (6096), 816–821. https://doi.org/10.1126/science.1225829.

[65] DiCarlo, J. E.; Norville, J. E.; Mali, P.; Rios, X.; Aach, J.; Church, G. M. Genome Engineering in Saccharomyces Cerevisiae Using CRISPR-Cas Systems. *Nucleic Acids Research* **2013**, *41* (7), 4336–4343. https://doi.org/10.1093/nar/gkt135.

[66] Jansen, G.; Wu, C.; Schade, B.; Thomas, D. Y.; Whiteway, M. Drag&Drop Cloning in Yeast. *Gene* **2005**, *344*, 43–51. https://doi.org/10.1016/j.gene.2004.10.016.

[67] Lee, M. E.; DeLoache, W. C.; Cervantes, B.; Dueber, J. E. A Highly Characterized Yeast Toolkit for Modular, Multipart Assembly. *ACS Synth. Biol.* **2015**, *4* (9), 975–986. https://doi.org/10.1021/sb500366v.

[68] Reider Apel, A.; d'Espaux, L.; Wehrs, M.; Sachs, D.; Li, R. A.; Tong, G. J.; Garber, M.; Nnadi, O.; Zhuang, W.; Hillson, N. J.; Keasling, J. D.; Mukhopadhyay, A. A Cas9-Based Toolkit to Program Gene Expression in *Saccharomyces Cerevisiae*. *Nucleic Acids Res* **2017**, *45* (1), 496–508. https://doi.org/10.1093/nar/gkw1023.

[69] Nour-Eldin, H. H.; Hansen, B. G.; Nørholm, M. H. H.; Jensen, J. K.; Halkier, B. A. Advancing Uracil-Excision Based Cloning towards an Ideal Technique for Cloning PCR Fragments. *Nucleic Acids Res* **2006**, *34* (18), e122. https://doi.org/10.1093/nar/gkl635.

[70] Engler, C.; Kandzia, R.; Marillonnet, S. A One Pot, One Step, Precision Cloning Method with High Throughput Capability. *PLoS One* **2008**, *3* (11), e3647. https://doi.org/10.1371/journal.pone.0003647.
[71] Gibson, D. G.; Young, L.; Chuang, R.-Y.; Venter, J. C.; Hutchison, C. A.; Smith, H. O. Enzymatic Assembly of DNA Molecules up to Several Hundred Kilobases. *Nat Methods* **2009**, *6* (5), 343–345. https://doi.org/10.1038/nmeth.1318.
[72] Averesch, N. J. H.; Krömer, J. O. Metabolic Engineering of the Shikimate Pathway for Production of Aromatics and Derived Compounds—Present and Future Strain Construction Strategies. *Front. Bioeng. Biotechnol.* **2018**, *6*, 32. https://doi.org/10.3389/fbioe.2018.00032.
[73] van Rossum, H. M.; Kozak, B. U.; Pronk, J. T.; van Maris, A. J. A. Engineering Cytosolic Acetyl-Coenzyme A Supply in Saccharomyces Cerevisiae: Pathway Stoichiometry, Free-Energy Conservation and Redox-Cofactor Balancing. *Metab Eng* **2016**, *36*, 99–115. https://doi.org/10.1016/j.ymben.2016.03.006.
[74] Lu, S.; Zhou, C.; Guo, X.; Du, Z.; Cheng, Y.; Wang, Z.; He, X. Enhancing Fluxes through the Mevalonate Pathway in Saccharomyces Cerevisiae by Engineering the HMGR and β-Alanine Metabolism. *Microb Biotechnol* **2022**, *15* (8), 2292–2306. https://doi.org/10.1111/1751-7915.14072.
[75] Fernandez-Moya, R.; Da Silva, N. A. Engineering Saccharomyces Cerevisiae for High-Level Synthesis of Fatty Acids and Derived Products. *FEMS Yeast Research* **2017**, *17* (7). https://doi.org/10.1093/femsyr/fox071.
[76] Kildegaard, K. R.; Jensen, N. B.; Schneider, K.; Czarnotta, E.; Özdemir, E.; Klein, T.; Maury, J.; Ebert, B. E.; Christensen, H. B.; Chen, Y.; Kim, I.-K.; Herrgård, M. J.; Blank, L. M.; Forster, J.; Nielsen, J.; Borodina, I. Engineering and Systems-Level Analysis of Saccharomyces Cerevisiae for Production of 3-Hydroxypropionic Acid via Malonyl-CoA Reductase-Dependent Pathway. *Microb Cell Fact* **2016**, *15*, 53. https://doi.org/10.1186/s12934-016-0451-5.
[77] Akram, M. Mini-Review on Glycolysis and Cancer. *J Canc Educ* **2013**, *28* (3), 454–457. https://doi.org/10.1007/s13187-013-0486-9.
[78] Chaudhry, R.; Varacallo, M. Biochemistry, Glycolysis. In *StatPearls*; StatPearls Publishing: Treasure Island (FL), 2023.
[79] Solis-Escalante, D.; Kuijpers, N. G. A.; Barrajon-Simancas, N.; Van Den Broek, M.; Pronk, J. T.; Daran, J.-M.; Daran-Lapujade, P. A Minimal Set of Glycolytic Genes Reveals Strong Redundancies in Saccharomyces Cerevisiae Central Metabolism. *Eukaryot Cell* **2015**, *14* (8), 804–816. https://doi.org/10.1128/EC.00064-15.
[80] Berger, L.; Slein, M. W.; Colowick, S. P.; Cori, C. F. ISOLATION OF HEXOKINASE FROM BAKER'S YEAST. *J Gen Physiol* **1946**, *29* (6), 379–391.
[81] *KEGG PATHWAY: Glycolysis / Gluconeogenesis - Saccharomyces cerevisiae (budding yeast)*. https://www.genome.jp/pathway/sce00010 (accessed 2023-09-25).
[82] Boonekamp, F. J.; Dashko, S.; Van Den Broek, M.; Gehrmann, T.; Daran, J.-M.; Daran-Lapujade, P. The Genetic Makeup and Expression of the Glycolytic and Fermentative Pathways Are Highly Conserved Within the Saccharomyces Genus. *Front. Genet.* **2018**, *9*, 504. https://doi.org/10.3389/fgene.2018.00504.
[83] Zgiby, S. M.; Thomson, G. J.; Qamar, S.; Berry, A. Exploring Substrate Binding and Discrimination in Fructose1,6-Bisphosphate and Tagatose 1,6-Bisphosphate Aldolases. *European Journal of Biochemistry* **2000**, *267* (6), 1858–1868. https://doi.org/10.1046/j.1432-1327.2000.01191.x.
[84] Rieder, S. V.; Rose, I. A. The Mechanism of the Triosephosphate Isomerase Reaction. *Journal of Biological Chemistry* **1959**, *234* (5), 1007–1010. https://doi.org/10.1016/S0021-9258(18)98120-2.
[85] Rose, Z. B. The Enzymology of 2, 3-Bisphosphoglycerate. In *Advances in Enzymology and Related Areas of Molecular Biology*; John Wiley & Sons, Ltd, 1980; pp 211–253. https://doi.org/10.1002/9780470122969.ch5.
[86] Axelrod, B.; Bandurski, R. S. PHOSPHOGLYCERYL KINASE IN HIGHER PLANTS. *Journal of Biological Chemistry* **1953**, *204* (2), 939–948. https://doi.org/10.1016/S0021-9258(18)66097-1.
[87] Romano, A. H.; Conway, T. Evolution of Carbohydrate Metabolic Pathways. *Research in Microbiology* **1996**, *147* (6–7), 448–455. https://doi.org/10.1016/0923-2508(96)83998-2.

[88] Westhead, E. W.; McLain, G. A Purification of Brewers' and Bakers' Yeast Enolase Yielding a Single Active Component. *Journal of Biological Chemistry* **1964**, *239* (8), 2464–2468. https://doi.org/10.1016/S0021-9258(18)93875-5.

[89] Granchi, C.; Bertini, S.; Macchia, M.; Minutolo, F. Inhibitors of Lactate Dehydrogenase Isoforms and Their Therapeutic Potentials. *CMC* **2010**, *17* (7), 672–697. https://doi.org/10.2174/092986710790416263.

[90] De Deken, R. H. The Crabtree Effect: A Regulatory System in Yeast. *Journal of General Microbiology* **1966**, *44* (2), 149–156. https://doi.org/10.1099/00221287-44-2-149.

[91] Bergman, A.; Hellgren, J.; Moritz, T.; Siewers, V.; Nielsen, J.; Chen, Y. Heterologous Phosphoketolase Expression Redirects Flux towards Acetate, Perturbs Sugar Phosphate Pools and Increases Respiratory Demand in Saccharomyces Cerevisiae. *Microb Cell Fact* **2019**, *18* (1), 25. https://doi.org/10.1186/s12934-019-1072-6.

[92] Krivoruchko, A.; Zhang, Y.; Siewers, V.; Chen, Y.; Nielsen, J. Microbial Acetyl-CoA Metabolism and Metabolic Engineering. *Metab Eng* **2015**, *28*, 28–42. https://doi.org/10.1016/j.ymben.2014.11.009.

[93] Li, X.; Guo, D.; Cheng, Y.; Zhu, F.; Deng, Z.; Liu, T. Overproduction of Fatty Acids in Engineered Saccharomyces Cerevisiae. *Biotechnol Bioeng* **2014**, *111* (9), 1841–1852. https://doi.org/10.1002/bit.25239.

[94] Pronk, J. T.; Yde Steensma, H.; Van Dijken, J. P. Pyruvate Metabolism inSaccharomyces Cerevisiae. *Yeast* **1996**, *12* (16), 1607–1633. https://doi.org/10.1002/(SICI)1097-0061(199612)12:16<1607::AID-YEA70>3.0.CO;2-4.

[95] Chen, Y.; Daviet, L.; Schalk, M.; Siewers, V.; Nielsen, J. Establishing a Platform Cell Factory through Engineering of Yeast Acetyl-CoA Metabolism. *Metab Eng* **2013**, *15*, 48–54. https://doi.org/10.1016/j.ymben.2012.11.002.

[96] Kim, K.-S. Saccharomyces Cerevisiae Contains Two Functional Citrate Synthase Genes. *MOL. CELL. BIOL.* **1986**, *6*.

[97] Suissa, M.; Suda, K.; Schatz, G. Isolation of the Nuclear Yeast Genes for Citrate Synthase and Fifteen Other Mitochondrial Proteins by a New Screening Method. *The EMBO Journal* **1984**, *3* (8), 1773–1781. https://doi.org/10.1002/j.1460-2075.1984.tb02045.x.

[98] Jia, Y.-K.; Bécam, A.-M.; Herbert, C. J. The CIT3 Gene of Saccharomyces Cerevisiae Encodes a Second Mitochondrial Isoform of Citrate Synthase. *Molecular Microbiology* **1997**, *24* (1), 53–59. https://doi.org/10.1046/j.1365-2958.1997.3011669.x.

[99] Al-Feel, W.; Chirala, S. S.; Wakil, S. J. Cloning of the Yeast FAS3 Gene and Primary Structure of Yeast Acetyl-CoA Carboxylase. *Proceedings of the National Academy of Sciences* **1992**, *89* (10), 4534–4538. https://doi.org/10.1073/pnas.89.10.4534.

[100] Witters, L. A.; Watts, T. D. Yeast Acetyl-CoA Carboxylase: In Vitro Phosphorylation by Mammalian and Yeast Protein Kinases. *Biochemical and Biophysical Research Communications* **1990**, *169* (2), 369–376. https://doi.org/10.1016/0006-291X(90)90341-J.

[101] Shi, S.; Chen, Y.; Siewers, V.; Nielsen, J. Improving Production of Malonyl Coenzyme A-Derived Metabolites by Abolishing Snf1-Dependent Regulation of Acc1. *mBio* **2014**, *5* (3), e01130-01114. https://doi.org/10.1128/mBio.01130-14.

[102] Chen, L.; Lee, J. J. L.; Zhang, J.; Chen, W. N. Comparative Proteomic Analysis of Engineered Saccharomyces Cerevisiae with Enhanced Free Fatty Acid Accumulation. *Appl Microbiol Biotechnol* **2016**, *100* (3), 1407–1420. https://doi.org/10.1007/s00253-015-7028-9.

[103] Hoja, U.; Marthol, S.; Hofmann, J.; Stegner, S.; Schulz, R.; Meier, S.; Greiner, E.; Schweizer, E. HFA1 Encoding an Organelle-Specific Acetyl-CoA Carboxylase Controls Mitochondrial Fatty Acid Synthesis in Saccharomyces Cerevisiae. *Journal of Biological Chemistry* **2004**, *279* (21), 21779–21786. https://doi.org/10.1074/jbc.M401071200.

[104] Liu, C.; Ding, Y.; Xian, M.; Liu, M.; Liu, H.; Ma, Q.; Zhao, G. Malonyl-CoA Pathway: A Promising Route for 3-Hydroxypropionate Biosynthesis. *Crit Rev Biotechnol* **2017**, *37* (7), 933–941. https://doi.org/10.1080/07388551.2016.1272093.

[105] Werpy, T.; Petersen, G. *Top Value Added Chemicals from Biomass: Volume I -- Results of Screening for Potential Candidates from Sugars and Synthesis Gas*; DOE/GO-102004-1992, 15008859; 2004; p DOE/GO-102004-1992, 15008859. https://doi.org/10.2172/15008859.

[106] Chen, X.; Yang, X.; Shen, Y.; Hou, J.; Bao, X. Increasing Malonyl-CoA Derived Product through Controlling the Transcription Regulators of Phospholipid Synthesis in *Saccharomyces Cerevisiae*. *ACS Synth. Biol.* **2017**, *6* (5), 905–912. https://doi.org/10.1021/acssynbio.6b00346.

[107] Maury, J.; Kannan, S.; Jensen, N. B.; Öberg, F. K.; Kildegaard, K. R.; Forster, J.; Nielsen, J.; Workman, C. T.; Borodina, I. Glucose-Dependent Promoters for Dynamic Regulation of Metabolic Pathways. *Front. Bioeng. Biotechnol.* **2018**, *6*, 63. https://doi.org/10.3389/fbioe.2018.00063.

[108] Hellgren, J.; Godina, A.; Nielsen, J.; Siewers, V. Promiscuous Phosphoketolase and Metabolic Rewiring Enables Novel Non-Oxidative Glycolysis in Yeast for High-Yield Production of Acetyl-CoA Derived Products. *Metab Eng* **2020**, *62*, 150–160. https://doi.org/10.1016/j.ymben.2020.09.003.

[109] Qin, N.; Li, L.; Ji, X.; Li, X.; Zhang, Y.; Larsson, C.; Chen, Y.; Nielsen, J.; Liu, Z. Rewiring Central Carbon Metabolism Ensures Increased Provision of Acetyl-CoA and NADPH Required for 3-OH-Propionic Acid Production. *ACS Synth Biol* **2020**, *9* (12), 3236–3244. https://doi.org/10.1021/acssynbio.0c00264.

[110] Zhang, Y.; Su, M.; Chen, Y.; Wang, Z.; Nielsen, J.; Liu, Z. Engineering Yeast Mitochondrial Metabolism for 3-Hydroxypropionate Production. *Biotechnol Biofuels Bioprod* **2023**, *16* (1), 64. https://doi.org/10.1186/s13068-023-02309-z.

[111] You, S. K.; Joo, Y.-C.; Kang, D. H.; Shin, S. K.; Hyeon, J. E.; Woo, H. M.; Um, Y.; Park, C.; Han, S. O. Enhancing Fatty Acid Production of Saccharomyces Cerevisiae as an Animal Feed Supplement. *J Agric Food Chem* **2017**, *65* (50), 11029–11035. https://doi.org/10.1021/acs.jafc.7b04485.

[112] Zhang, C.; Li, M.; Zhao, G.-R.; Lu, W. Harnessing Yeast Peroxisomes and Cytosol Acetyl-CoA for Sesquiterpene α-Humulene Production. *J Agric Food Chem* **2020**, *68* (5), 1382–1389. https://doi.org/10.1021/acs.jafc.9b07290.

[113] Runguphan, W.; Keasling, J. D. Metabolic Engineering of Saccharomyces Cerevisiae for Production of Fatty Acid-Derived Biofuels and Chemicals. *Metab Eng* **2014**, *21*, 103–113. https://doi.org/10.1016/j.ymben.2013.07.003.

[114] Feng, X.; Lian, J.; Zhao, H. Metabolic Engineering of Saccharomyces Cerevisiae to Improve 1-Hexadecanol Production. *Metab Eng* **2015**, *27*, 10–19. https://doi.org/10.1016/j.ymben.2014.10.001.

[115] de Jong, B. W.; Shi, S.; Siewers, V.; Nielsen, J. Improved Production of Fatty Acid Ethyl Esters in Saccharomyces Cerevisiae through Up-Regulation of the Ethanol Degradation Pathway and Expression of the Heterologous Phosphoketolase Pathway. *Microb Cell Fact* **2014**, *13* (1), 39. https://doi.org/10.1186/1475-2859-13-39.

[116] Lyu, X.; Ng, K. R.; Lee, J. L.; Mark, R.; Chen, W. N. Enhancement of Naringenin Biosynthesis from Tyrosine by Metabolic Engineering of Saccharomyces Cerevisiae. *J Agric Food Chem* **2017**, *65* (31), 6638–6646. https://doi.org/10.1021/acs.jafc.7b02507.

[117] Duan, L.; Ding, W.; Liu, X.; Cheng, X.; Cai, J.; Hua, E.; Jiang, H. Biosynthesis and Engineering of Kaempferol in Saccharomyces Cerevisiae. *Microb Cell Fact* **2017**, *16* (1), 165. https://doi.org/10.1186/s12934-017-0774-x.

[118] Yuan, S.-F.; Yi, X.; Johnston, T. G.; Alper, H. S. De Novo Resveratrol Production through Modular Engineering of an Escherichia Coli-Saccharomyces Cerevisiae Co-Culture. *Microb Cell Fact* **2020**, *19* (1), 143. https://doi.org/10.1186/s12934-020-01401-5.

[119] Suomalainen, H.; Keränen, A. J. A. The Effect of Biotin Deficiency on the Synthesis of Fatty Acids by Yeast. *Biochimica et Biophysica Acta* **1963**, *70*, 493–503. https://doi.org/10.1016/0006-3002(63)90788-1.

[120] Tehlivets, O.; Scheuringer, K.; Kohlwein, S. D. Fatty Acid Synthesis and Elongation in Yeast. *Biochimica et Biophysica Acta (BBA) - Molecular and Cell Biology of Lipids* **2007**, *1771* (3), 255–270. https://doi.org/10.1016/j.bbalip.2006.07.004.

[121] Woods, A.; Munday, M. R.; Scott, J.; Yang, X.; Carlson, M.; Carling, D. Yeast SNF1 Is Functionally Related to Mammalian AMP-Activated Protein Kinase and Regulates Acetyl-CoA Carboxylase in Vivo. *Journal of Biological Chemistry* **1994**, *269* (30), 19509–19515. https://doi.org/10.1016/S0021-9258(17)32198-1.

[122] Ficarro, S. B.; McCleland, M. L.; Stukenberg, P. T.; Burke, D. J.; Ross, M. M.; Shabanowitz, J.; Hunt, D. F.; White, F. M. Phosphoproteome Analysis by Mass Spectrometry and Its Application to Saccharomyces Cerevisiae. *Nat Biotechnol* **2002**, *20* (3), 301–305. https://doi.org/10.1038/nbt0302-301.

[123] Wang, J.; Xu, R.; Wang, R.; Haque, M. E.; Liu, A. Overexpression of ACC Gene from Oleaginous Yeast Lipomyces Starkeyi Enhanced the Lipid Accumulation in Saccharomyces Cerevisiae with Increased Levels of Glycerol 3-Phosphate Substrates. *Biosci Biotechnol Biochem* **2016**, *80* (6), 1214–1222. https://doi.org/10.1080/09168451.2015.1136883.

[124] Li, S.; Zhang, Q.; Wang, J.; Liu, Y.; Zhao, Y.; Deng, Y. Recent Progress in Metabolic Engineering of Saccharomyces Cerevisiae for the Production of Malonyl-CoA Derivatives. *Journal of Biotechnology* **2021**, *325*, 83–90. https://doi.org/10.1016/j.jbiotec.2020.11.014.

[125] de Jong, B. W.; Shi, S.; Valle-Rodríguez, J. O.; Siewers, V.; Nielsen, J. Metabolic Pathway Engineering for Fatty Acid Ethyl Ester Production in Saccharomyces Cerevisiae Using Stable Chromosomal Integration. *J Ind Microbiol Biotechnol* **2015**, *42* (3), 477–486. https://doi.org/10.1007/s10295-014-1540-2.

[126] Chen, X.; Yang, X.; Shen, Y.; Hou, J.; Bao, X. Screening Phosphorylation Site Mutations in Yeast Acetyl-CoA Carboxylase Using Malonyl-CoA Sensor to Improve Malonyl-CoA-Derived Product. *Front. Microbiol.* **2018**, *9*, 47. https://doi.org/10.3389/fmicb.2018.00047.

[127] Li, S.; Si, T.; Wang, M.; Zhao, H. Development of a Synthetic Malonyl-CoA Sensor in *Saccharomyces Cerevisiae* for Intracellular Metabolite Monitoring and Genetic Screening. *ACS Synth. Biol.* **2015**, *4* (12), 1308–1315. https://doi.org/10.1021/acssynbio.5b00069.

[128] Shiba, Y.; Paradise, E. M.; Kirby, J.; Ro, D.-K.; Keasling, J. D. Engineering of the Pyruvate Dehydrogenase Bypass in Saccharomyces Cerevisiae for High-Level Production of Isoprenoids. *Metab Eng* **2007**, *9* (2), 160–168. https://doi.org/10.1016/j.ymben.2006.10.005.

[129] Jessop-Fabre, M. M.; Jakočiūnas, T.; Stovicek, V.; Dai, Z.; Jensen, M. K.; Keasling, J. D.; Borodina, I. EasyClone-MarkerFree: A Vector Toolkit for Marker-Less Integration of Genes into Saccharomyces Cerevisiae via CRISPR-Cas9. *Biotechnol J* **2016**, *11* (8), 1110–1117. https://doi.org/10.1002/biot.201600147.

[130] Postma, E.; Verduyn, C.; Scheffers, W. A.; Van Dijken, J. P. Enzymic Analysis of the Crabtree Effect in Glucose-Limited Chemostat Cultures of Saccharomyces Cerevisiae. *Appl Environ Microbiol* **1989**, *55* (2), 468–477. https://doi.org/10.1128/aem.55.2.468-477.1989.

[131] Starai, V. J.; Gardner, J. G.; Escalante-Semerena, J. C. Residue Leu-641 of Acetyl-CoA Synthetase Is Critical for the Acetylation of Residue Lys-609 by the Protein Acetyltransferase Enzyme of Salmonella Enterica. *Journal of Biological Chemistry* **2005**, *280* (28), 26200–26205. https://doi.org/10.1074/jbc.M504863200.

[132] Shi, W.; Li, J.; Chen, Y.; Liu, X.; Chen, Y.; Guo, X.; Xiao, D. Metabolic Engineering of Saccharomyces Cerevisiae for Ethyl Acetate Biosynthesis. *ACS Synth Biol* **2021**, *10* (3), 495–504. https://doi.org/10.1021/acssynbio.0c00446.

[133] Kocharin, K.; Chen, Y.; Siewers, V.; Nielsen, J. Engineering of Acetyl-CoA Metabolism for the Improved Production of Polyhydroxybutyrate in Saccharomyces Cerevisiae. *AMB Express* **2012**, *2* (1), 52. https://doi.org/10.1186/2191-0855-2-52.

[134] Lian, J.; Si, T.; Nair, N. U.; Zhao, H. Design and Construction of Acetyl-CoA Overproducing Saccharomyces Cerevisiae Strains. *Metab Eng* **2014**, *24*, 139–149. https://doi.org/10.1016/j.ymben.2014.05.010.

[135] Ghosh, A.; Ando, D.; Gin, J.; Runguphan, W.; Denby, C.; Wang, G.; Baidoo, E. E. K.; Shymansky, C.; Keasling, J. D.; García Martín, H. 13C Metabolic Flux Analysis for Systematic Metabolic Engineering of S. Cerevisiae for Overproduction of Fatty Acids. *Front Bioeng Biotechnol* **2016**, *4*, 76. https://doi.org/10.3389/fbioe.2016.00076.

[136] Yu, T.; Zhou, Y. J.; Huang, M.; Liu, Q.; Pereira, R.; David, F.; Nielsen, J. Reprogramming Yeast Metabolism from Alcoholic Fermentation to Lipogenesis. *Cell* **2018**, *174* (6), 1549-1558.e14. https://doi.org/10.1016/j.cell.2018.07.013.

[137] Rodriguez, S.; Denby, C. M.; Van Vu, T.; Baidoo, E. E. K.; Wang, G.; Keasling, J. D. ATP Citrate Lyase Mediated Cytosolic Acetyl-CoA Biosynthesis Increases Mevalonate Production in Saccharomyces Cerevisiae. *Microb Cell Fact* **2016**, *15*, 48. https://doi.org/10.1186/s12934-016-0447-1.

[138] Kozak, B. U.; van Rossum, H. M.; Benjamin, K. R.; Wu, L.; Daran, J.-M. G.; Pronk, J. T.; van Maris, A. J. A. Replacement of the Saccharomyces Cerevisiae Acetyl-CoA Synthetases by Alternative Pathways for Cytosolic Acetyl-CoA Synthesis. *Metab Eng* **2014**, *21*, 46–59. https://doi.org/10.1016/j.ymben.2013.11.005.

[139] Kozak, B. U.; van Rossum, H. M.; Niemeijer, M. S.; van Dijk, M.; Benjamin, K.; Wu, L.; Daran, J.-M. G.; Pronk, J. T.; van Maris, A. J. A. Replacement of the Initial Steps of Ethanol Metabolism in Saccharomyces Cerevisiae by ATP-Independent Acetylating Acetaldehyde Dehydrogenase. *FEMS Yeast Res* **2016**, *16* (2), fow006. https://doi.org/10.1093/femsyr/fow006.

[140] Schadeweg, V.; Boles, E. Increasing N-Butanol Production with Saccharomyces Cerevisiae by Optimizing Acetyl-CoA Synthesis, NADH Levels and Trans-2-Enoyl-CoA Reductase Expression. *Biotechnol Biofuels* **2016**, *9* (1), 257. https://doi.org/10.1186/s13068-016-0673-0.

[141] Herrmann, K. M. The Shikimate Pathway: Early Steps in the Biosynthesis of Aromatic Compounds. *The Plant Cell* **1995**, *7* (7), 907–919. https://doi.org/10.2307/3870046.

[142] Braus, G. H. Aromatic Amino Acid Biosynthesis in the Yeast Saccharomyces Cerevisiae: A Model System for the Regulation of a Eukaryotic Biosynthetic Pathway. *Microbiological Reviews* **1991**, *55* (3), 349–370. https://doi.org/10.1128/mr.55.3.349-370.1991.

[143] Haslam, E. *The Shikimate Pathway: Biosynthesis of Natural Products Series*; Elsevier, 2014.

[144] Meuris, P. Feedback Inhibition of the DAHP Synthetases by tRNA in Saccharomyces Cerevisiae. *Molec. Gen. Genet.* **1973**, *121* (3), 207–218. https://doi.org/10.1007/BF00267048.

[145] Künzler, M.; Paravicini, G.; Egli, C. M.; Irniger, S.; Braus, G. H. Cloning, Primary Structure and Regulation of the ARO4 Gene, Encoding the Tyrosine-Inhibited 3-Deoxy-D-Arabino-Heptulosonate-7-Phosphate Synthase from Saccharomyces Cerevisiae. *Gene* **1992**, *113* (1), 67–74. https://doi.org/10.1016/0378-1119(92)90670-K.

[146] Duncan, K.; Edwards, R. M.; Coggins, J. R. The Pentafunctional Arom Enzyme of Saccharomyces Cerevisiae Is a Mosaic of Monofunctional Domains. *Biochemical Journal* **1987**, *246* (2), 375–386. https://doi.org/10.1042/bj2460375.

[147] Kradolfer, P.; Zeyer, J.; Miozzari, G.; Huetter, R. Dominant Regulatory Mutants in Chorismate Mutase of Saccharomyces Cerevisiae. *FEMS Microbiology Letters* **1977**, *2* (4), 211–216. https://doi.org/10.1111/j.1574-6968.1977.tb00942.x.

[148] Kradolfer, P.; Niederberger, P.; Hütter, R. Tryptophan Degradation in Saccharomyces Cerevisiae: Characterization of Two Aromatic Aminotransferases. *Arch. Microbiol.* **1982**, *133* (3), 242–248. https://doi.org/10.1007/BF00415010.

[149] Urrestarazu, A.; Vissers, S.; Iraqui, I.; Grenson, M. Phenylalanine- and Tyrosine-Auxotrophic Mutants of Saccharomyces Cerevisiae Impaired in Transamination. *Mol Gen Genet* **1998**, *257* (2), 230–237. https://doi.org/10.1007/s004380050643.

[150] *Saccharomyces cerevisiae tyrosine biosynthesis*. https://pathway.yeastgenome.org/YEAST/NEW-IMAGE?type=PATHWAY&object=PWY3O-4120 (accessed 2023-10-01).

[151] Rodriguez, A.; Kildegaard, K. R.; Li, M.; Borodina, I.; Nielsen, J. Establishment of a Yeast Platform Strain for Production of P-Coumaric Acid through Metabolic Engineering of Aromatic Amino Acid Biosynthesis. *Metab Eng* **2015**, *31*, 181–188. https://doi.org/10.1016/j.ymben.2015.08.003.

[152] Mao, J.; Liu, Q.; Song, X.; Wang, H.; Feng, H.; Xu, H.; Qiao, M. Combinatorial Analysis of Enzymatic Bottlenecks of L-Tyrosine Pathway by p-Coumaric Acid Production in Saccharomyces Cerevisiae. *Biotechnol Lett* **2017**, *39* (7), 977–982. https://doi.org/10.1007/s10529-017-2322-5.

[153] Liu, Q.; Yu, T.; Li, X.; Chen, Y.; Campbell, K.; Nielsen, J.; Chen, Y. Rewiring Carbon Metabolism in Yeast for High Level Production of Aromatic Chemicals. *Nat Commun* **2019**, *10* (1), 4976. https://doi.org/10.1038/s41467-019-12961-5.

[154] Li, Y.; Mao, J.; Song, X.; Wu, Y.; Cai, M.; Wang, H.; Liu, Q.; Zhang, X.; Bai, Y.; Xu, H.; Qiao, M. Optimization of the L-Tyrosine Metabolic Pathway in Saccharomyces Cerevisiae by

Analyzing p-Coumaric Acid Production. *3 Biotech* **2020**, *10* (6), 258. https://doi.org/10.1007/s13205-020-02223-3.

[155] Zhou, P.; Yue, C.; Shen, B.; Du, Y.; Xu, N.; Ye, L. Metabolic Engineering of Saccharomyces Cerevisiae for Enhanced Production of Caffeic Acid. *Appl Microbiol Biotechnol* **2021**, *105* (14–15), 5809–5819. https://doi.org/10.1007/s00253-021-11445-1.

[156] Li, Y.; Mao, J.; Liu, Q.; Song, X.; Wu, Y.; Cai, M.; Xu, H.; Qiao, M. De Novo Biosynthesis of Caffeic Acid from Glucose by Engineered Saccharomyces Cerevisiae. *ACS Synth Biol* **2020**, *9* (4), 756–765. https://doi.org/10.1021/acssynbio.9b00431.

[157] Babaei, M.; Borja Zamfir, G. M.; Chen, X.; Christensen, H. B.; Kristensen, M.; Nielsen, J.; Borodina, I. Metabolic Engineering of Saccharomyces Cerevisiae for Rosmarinic Acid Production. *ACS Synth Biol* **2020**, *9* (8), 1978–1988. https://doi.org/10.1021/acssynbio.0c00048.

[158] DeLoache, W. C.; Russ, Z. N.; Narcross, L.; Gonzales, A. M.; Martin, V. J. J.; Dueber, J. E. An Enzyme-Coupled Biosensor Enables (S)-Reticuline Production in Yeast from Glucose. *Nat Chem Biol* **2015**, *11* (7), 465–471. https://doi.org/10.1038/nchembio.1816.

[159] Trenchard, I. J.; Siddiqui, M. S.; Thodey, K.; Smolke, C. D. De Novo Production of the Key Branch Point Benzylisoquinoline Alkaloid Reticuline in Yeast. *Metab Eng* **2015**, *31*, 74–83. https://doi.org/10.1016/j.ymben.2015.06.010.

[160] Koopman, F.; Beekwilder, J.; Crimi, B.; van Houwelingen, A.; Hall, R. D.; Bosch, D.; van Maris, A. J. A.; Pronk, J. T.; Daran, J.-M. De Novo Production of the Flavonoid Naringenin in Engineered Saccharomyces Cerevisiae. *Microb Cell Fact* **2012**, *11*, 155. https://doi.org/10.1186/1475-2859-11-155.

[161] Guo, X.; Wu, X.; Ma, H.; Liu, H.; Luo, Y. Yeast: A Platform for the Production of L -Tyrosine Derivatives. *Yeast* **2023**, *40* (5–6), 214–230. https://doi.org/10.1002/yea.3850.

[162] Jiang, L.; Huang, L.; Cai, J.; Xu, Z.; Lian, J. Functional Expression of Eukaryotic Cytochrome P450s in Yeast. *Biotechnology and Bioengineering* **2021**, *118* (3), 1050–1065. https://doi.org/10.1002/bit.27630.

[163] Luttik, M. a. H.; Vuralhan, Z.; Suir, E.; Braus, G. H.; Pronk, J. T.; Daran, J. M. Alleviation of Feedback Inhibition in Saccharomyces Cerevisiae Aromatic Amino Acid Biosynthesis: Quantification of Metabolic Impact. *Metab Eng* **2008**, *10* (3–4), 141–153. https://doi.org/10.1016/j.ymben.2008.02.002.

[164] Bisquert, R.; Planells-Cárcel, A.; Valera-García, E.; Guillamón, J. M.; Muñiz-Calvo, S. Metabolic Engineering of Saccharomyces Cerevisiae for Hydroxytyrosol Overproduction Directly from Glucose. *Microb Biotechnol* **2022**, *15* (5), 1499–1510. https://doi.org/10.1111/1751-7915.13957.

[165] Liu, Y.; Liu, H.; Hu, H.; Ng, K. R.; Yang, R.; Lyu, X. De Novo Production of Hydroxytyrosol by Metabolic Engineering of Saccharomyces Cerevisiae. *J Agric Food Chem* **2022**, *70* (24), 7490–7499. https://doi.org/10.1021/acs.jafc.2c02137.

[166] Suástegui, M.; Yu Ng, C.; Chowdhury, A.; Sun, W.; Cao, M.; House, E.; Maranas, C. D.; Shao, Z. Multilevel Engineering of the Upstream Module of Aromatic Amino Acid Biosynthesis in Saccharomyces Cerevisiae for High Production of Polymer and Drug Precursors. *Metabolic Engineering* **2017**, *42*, 134–144. https://doi.org/10.1016/j.ymben.2017.06.008.

[167] Leavitt, J. M.; Wagner, J. M.; Tu, C. C.; Tong, A.; Liu, Y.; Alper, H. S. Biosensor-Enabled Directed Evolution to Improve Muconic Acid Production in Saccharomyces Cerevisiae. *Biotechnol J* **2017**, *12* (10). https://doi.org/10.1002/biot.201600687.

[168] Averesch, N. J. H.; Prima, A.; Krömer, J. O. Enhanced Production of Para-Hydroxybenzoic Acid by Genetically Engineered Saccharomyces Cerevisiae. *Bioprocess Biosyst Eng* **2017**, *40* (8), 1283–1289. https://doi.org/10.1007/s00449-017-1785-z.

[169] Sun, X.; Shen, X.; Jain, R.; Lin, Y.; Wang, J.; Sun, J.; Wang, J.; Yan, Y.; Yuan, Q. Synthesis of Chemicals by Metabolic Engineering of Microbes. *Chem. Soc. Rev.* **2015**, *44* (11), 3760–3785. https://doi.org/10.1039/C5CS00159E.

[170] Dias, D. A.; Urban, S.; Roessner, U. A Historical Overview of Natural Products in Drug Discovery. *Metabolites* **2012**, *2* (2), 303–336. https://doi.org/10.3390/metabo2020303.

[171] Schwartz, R. E.; Hirsch, C. F.; Sesin, D. F.; Flor, J. E.; Chartrain, M.; Fromtling, R. E.; Harris, G. H.; Salvatore, M. J.; Liesch, J. M.; Yudin, K. Pharmaceuticals from Cultured Algae.

Journal of Industrial Microbiology **1990**, *5* (2–3), 113–123. https://doi.org/10.1007/BF01573860.

[172] Chaganty, S.; Golakoti, T.; Heltzel, C.; Moore, R. E.; Yoshida, W. Y. Isolation and Structure Determination of Cryptophycins 38, 326, and 327 from the Terrestrial Cyanobacterium *Nostoc* Sp. GSV 224. *J. Nat. Prod.* **2004**, *67* (8), 1403–1406. https://doi.org/10.1021/np0499665.

[173] Kobayashi, M.; Aoki, S.; Ohyabu, N.; Kurosu, M.; Wang, W.; Kitagawa, I. Arenastatin A, a Potent Cytotoxic Depsipeptide from the Okinawan Marine Sponge Dysidea Arenaria. **1994**.

[174] Magarvey, N. A.; Beck, Z. Q.; Golakoti, T.; Ding, Y.; Huber, U.; Hemscheidt, T. K.; Abelson, D.; Moore, R. E.; Sherman, D. H. Biosynthetic Characterization and Chemoenzymatic Assembly of the Cryptophycins. Potent Anticancer Agents from *Nostoc* Cyanobionts. *ACS Chem. Biol.* **2006**, *1* (12), 766–779. https://doi.org/10.1021/cb6004307.

[175] Liang, J.; Moore, R. E.; Moher, E. D.; Munroe, J. E.; Al-awar, R. S.; Hay, D. A.; Varie, D. L.; Zhang, T. Y.; Aikins, J. A.; Martinelli, M. J.; Shih, C.; Ray, J. E.; Gibson, L. L.; Vasudevan, V.; Polin, L.; White, K.; Kushner, J.; Simpson, C.; Pugh, S.; Corbett, T. H. Cryptophycins-309, 249 and Other Cryptophycin Analogs: Preclinical Efficacy Studies with Mouse and Human Tumors. *Invest New Drugs* **2005**, *23* (3), 213–224. https://doi.org/10.1007/s10637-005-6729-9.

[176] Borbély, A.; Figueras, E.; Martins, A.; Esposito, S.; Auciello, G.; Monteagudo, E.; Di Marco, A.; Summa, V.; Cordella, P.; Perego, R.; Kemker, I.; Frese, M.; Gallinari, P.; Steinkühler, C.; Sewald, N. Synthesis and Biological Evaluation of RGD–Cryptophycin Conjugates for Targeted Drug Delivery. *Pharmaceutics* **2019**, *11* (4), 151. https://doi.org/10.3390/pharmaceutics11040151.

[177] Borbély, A.; Thoreau, F.; Figueras, E.; Kadri, M.; Coll, J.; Boturyn, D.; Sewald, N. Synthesis and Biological Characterization of Monomeric and Tetrameric RGD-Cryptophycin Conjugates. *Chemistry* **2020**, *26* (12), 2602–2605. https://doi.org/10.1002/chem.201905437.

[178] Weiss, C.; Figueras, E.; Borbely, A. N.; Sewald, N. Cryptophycins: Cytotoxic Cyclodepsipeptides with Potential for Tumor Targeting. *Journal of Peptide Science* **2017**, *23* (7–8), 514–531. https://doi.org/10.1002/psc.3015.

[179] Mofid, M. R.; Finking, R.; Essen, L. O.; Marahiel, M. A. Structure-Based Mutational Analysis of the 4'-Phosphopantetheinyl Transferases Sfp from Bacillus Subtilis: Carrier Protein Recognition and Reaction Mechanism,. *Biochemistry* **2004**, *43* (14), 4128–4136. https://doi.org/10.1021/bi036013h.

[180] Mootz, H. D.; Schörgendorfer, K.; Marahiel, M. A. Functional Characterization of 4'-Phosphopantetheinyl Transferase Genes of Bacterial and Fungal Origin by Complementation of Saccharomyces Cerevisiae Lys5. *FEMS Microbiol Lett* **2002**, *213* (1), 51–57. https://doi.org/10.1111/j.1574-6968.2002.tb11285.x.

[181] Jiang, F.; Doudna, J. A. CRISPR–Cas9 Structures and Mechanisms. *Annual Review of Biophysics* **2017**, *46* (1), 505–529. https://doi.org/10.1146/annurev-biophys-062215-010822.

[182] Boeke, J. D.; Trueheart, J.; Natsoulis, G.; Fink, G. R. [10] 5-Fluoroorotic Acid as a Selective Agent in Yeast Molecular Genetics. In *Methods in Enzymology*; Elsevier, 1987; Vol. 154, pp 164–175. https://doi.org/10.1016/0076-6879(87)54076-9.

[183] Trumbly, R. J. Glucose Repression in the Yeast Saccharomyces Cerevisiae. *Mol Microbiol* **1992**, *6* (1), 15–21. https://doi.org/10.1111/j.1365-2958.1992.tb00832.x.

[184] Nehlin, J. O.; Carlberg, M.; Ronne, H. Control of Yeast GAL Genes by MIG1 Repressor: A Transcriptional Cascade in the Glucose Response. *The EMBO Journal* **1991**, *10* (11), 3373–3377. https://doi.org/10.1002/j.1460-2075.1991.tb04901.x.

[185] Griggs, D. W.; Johnston, M. Promoter Elements Determining Weak Expression of the GAL4 Regulatory Gene of Saccharomyces Cerevisiae. *Mol Cell Biol* **1993**, *13* (8), 4999–5009.

[186] Ehmann, D. E.; Gehring, A. M.; Walsh, C. T. Lysine Biosynthesis in Saccharomyces Cerevisiae: Mechanism of α-Aminoadipate Reductase (Lys2) Involves Posttranslational Phosphopantetheinylation by Lys5. *Biochemistry* **1999**, *38* (19), 6171–6177. https://doi.org/10.1021/bi9829940.

[187] Chen, W. N.; Tan, K. Y. "Malonate Uptake and Metabolism in Saccharomyces Cerevisiae." *Appl Biochem Biotechnol* **2013**, *171* (1), 44–62. https://doi.org/10.1007/s12010-013-0334-8.

[188] Hunkeler, M.; Stuttfeld, E.; Hagmann, A.; Imseng, S.; Maier, T. The Dynamic Organization of Fungal Acetyl-CoA Carboxylase. *Nat Commun* **2016**, *7* (1), 11196. https://doi.org/10.1038/ncomms11196.

[189] *gcua – graphical codon usage analyser*. https://gcua.schoedl.de/ (accessed 2023-11-22).

[190] Curran, K. A.; Karim, A. S.; Gupta, A.; Alper, H. S. Use of High Capacity Terminators in Saccharomyces Cerevisiae to Increase mRNA Half-Life and Improve Gene Expression Control for Metabolic Engineering Applications. *Metab Eng* **2013**, *19*, 88–97. https://doi.org/10.1016/j.ymben.2013.07.001.

[191] Curran, K. A.; Morse, N. J.; Markham, K. A.; Wagman, A. M.; Gupta, A.; Alper, H. S. Short Synthetic Terminators for Improved Heterologous Gene Expression in Yeast. *ACS Synth Biol* **2015**, *4* (7), 824–832. https://doi.org/10.1021/sb5003357.

[192] David, F.; Nielsen, J.; Siewers, V. Flux Control at the Malonyl-CoA Node through Hierarchical Dynamic Pathway Regulation in Saccharomyces Cerevisiae. *ACS Synth. Biol.* **2016**, *5* (3), 224–233. https://doi.org/10.1021/acssynbio.5b00161.

[193] Joska, T. M.; Mashruwala, A.; Boyd, J. M.; Belden, W. J. A Universal Cloning Method Based on Yeast Homologous Recombination That Is Simple, Efficient, and Versatile. *Journal of Microbiological Methods* **2014**, *100*, 46–51. https://doi.org/10.1016/j.mimet.2013.11.013.

[194] Borodina, I.; Kildegaard, K. R.; Jensen, N. B.; Blicher, T. H.; Maury, J.; Sherstyk, S.; Schneider, K.; Lamosa, P.; Herrgård, M. J.; Rosenstand, I.; Öberg, F.; Forster, J.; Nielsen, J. Establishing a Synthetic Pathway for High-Level Production of 3-Hydroxypropionic Acid in Saccharomyces Cerevisiae via β-Alanine. *Metabolic Engineering* **2015**, *27*, 57–64. https://doi.org/10.1016/j.ymben.2014.10.003.

[195] Hügler, M.; Menendez, C.; Schägger, H.; Fuchs, G. Malonyl-Coenzyme A Reductase from Chloroflexus Aurantiacus, a Key Enzyme of the 3-Hydroxypropionate Cycle for Autotrophic CO2 Fixation. *J Bacteriol* **2002**, *184* (9), 2404–2410. https://doi.org/10.1128/JB.184.9.2404-2410.2002.

[196] Manual Metab AAC Columns, Isera Innovation and Service in Analytics.Pdf.

[197] *Aminex HPX-87H Column #1250140 | Bio-Rad*. https://www.bio-rad.com/de-de/sku/1250140-aminex-hpx-87h-column?ID=1250140 (accessed 2023-12-16).

[198] Bleykasten-Grosshans, C.; Neuvéglise, C. Transposable Elements in Yeasts. *Comptes Rendus Biologies* **2011**, *334* (8), 679–686. https://doi.org/10.1016/j.crvi.2011.05.017.

[199] Boeke, J. D.; Garfinkel, D. J.; Styles, C. A.; Fink, G. R. Ty Elements Transpose through an RNA Intermediate. *Cell* **1985**, *40* (3), 491–500. https://doi.org/10.1016/0092-8674(85)90197-7.

[200] Wicker, T.; Sabot, F.; Hua-Van, A.; Bennetzen, J. L.; Capy, P.; Chalhoub, B.; Flavell, A.; Leroy, P.; Morgante, M.; Panaud, O.; Paux, E.; SanMiguel, P.; Schulman, A. H. A Unified Classification System for Eukaryotic Transposable Elements. *Nat Rev Genet* **2007**, *8* (12), 973–982. https://doi.org/10.1038/nrg2165.

[201] Maury, J.; Germann, S. M.; Jacobsen, S. A. B.; Jensen, N. B.; Kildegaard, K. R.; Herrgård, M. J.; Schneider, K.; Koza, A.; Forster, J.; Nielsen, J.; Borodina, I. EasyCloneMulti: A Set of Vectors for Simultaneous and Multiple Genomic Integrations in Saccharomyces Cerevisiae. *PLOS ONE* **2016**, *11* (3), e0150394. https://doi.org/10.1371/journal.pone.0150394.

[202] Liu, D.; Hwang, H. J.; Otoupal, P. B.; Geiselman, G. M.; Kim, J.; Pomraning, K. R.; Kim, Y.-M.; Munoz, N.; Nicora, C. D.; Gao, Y.; Burnum-Johnson, K. E.; Jacobson, O.; Coradetti, S.; Kim, J.; Deng, S.; Dai, Z.; Prahl, J.-P.; Tanjore, D.; Lee, T. S.; Magnuson, J. K.; Gladden, J. M. Engineering Rhodosporidium Toruloides for Production of 3-Hydroxypropionic Acid from Lignocellulosic Hydrolysate. *Metabolic Engineering* **2023**, *78*, 72–83. https://doi.org/10.1016/j.ymben.2023.05.001.

[203] Liu, S.; Sun, Y.; Wei, T.; Gong, D.; Wang, Q.; Zhan, Z.; Song, J. Engineering 3-Hydroxypropionic Acid Production from Glucose in Yarrowia Lipolytica through Malonyl-CoA Pathway. *Journal of Fungi* **2023**, *9* (5), 573. https://doi.org/10.3390/jof9050573.

[204] Yang, Y.-M.; Chen, W.-J.; Yang, J.; Zhou, Y.-M.; Hu, B.; Zhang, M.; Zhu, L.-P.; Wang, G.-Y.; Yang, S. Production of 3-Hydroxypropionic Acid in Engineered Methylobacterium Extorquens AM1 and Its Reassimilation through a Reductive Route. *Microb Cell Fact* **2017**, *16* (1), 179. https://doi.org/10.1186/s12934-017-0798-2.

[205] Bianchi, F.; van't Klooster, J. S.; Ruiz, S. J.; Poolman, B. Regulation of Amino Acid Transport in Saccharomyces Cerevisiae. *Microbiology and Molecular Biology Reviews* **2019**, *83* (4), 10.1128/mmbr.00024-19. https://doi.org/10.1128/mmbr.00024-19.

[206] Liu, Z.; Qin, N.; Li, L.; Wan, X.; Ji, X.; Chen, Y.; Li, C.; Liu, P.; Zhang, Y.; Yang, W.; Jang, J.; Xia, J.; Shi, S.; Tan, T.; Nielsen, J.; Chen, Y. *Increased CO2 Fixation Enables High Carbon-Yield Production of the Acrylic Acid Precursor 3-Hydroxypropionic Acid in Yeast*; preprint; In Review, 2023. https://doi.org/10.21203/rs.3.rs-3278694/v1.

[207] Chun, A. Y.; Yunxiao, L.; Ashok, S.; Seol, E.; Park, S. Elucidation of Toxicity of Organic Acids Inhibiting Growth of Escherichia Coli W. *Biotechnol Bioproc E* **2014**, *19* (5), 858–865. https://doi.org/10.1007/s12257-014-0420-y.

[208] Peetermans, A.; Foulquié-Moreno, M. R.; Thevelein, J. M. Mechanisms Underlying Lactic Acid Tolerance and Its Influence on Lactic Acid Production in Saccharomyces Cerevisiae. *Microb Cell* **2021**, *8* (6), 111–130. https://doi.org/10.15698/mic2021.06.751.

[209] Suyama, A.; Higuchi, Y.; Urushihara, M.; Maeda, Y.; Takegawa, K. Production of 3-Hydroxypropionic Acid via the Malonyl-CoA Pathway Using Recombinant Fission Yeast Strains. *Journal of Bioscience and Bioengineering* **2017**, *124* (4), 392–399. https://doi.org/10.1016/j.jbiosc.2017.04.015.

[210] De Smidt, O.; Du Preez, J. C.; Albertyn, J. The Alcohol Dehydrogenases of *Saccharomyces Cerevisiae* : A Comprehensive Review. *FEMS Yeast Research* **2008**, *8* (7), 967–978. https://doi.org/10.1111/j.1567-1364.2008.00387.x.

[211] Shen, L.; Nishimura, Y.; Matsuda, F.; Ishii, J.; Kondo, A. Overexpressing Enzymes of the Ehrlich Pathway and Deleting Genes of the Competing Pathway in Saccharomyces Cerevisiae for Increasing 2-Phenylethanol Production from Glucose. *Journal of Bioscience and Bioengineering* **2016**, *122* (1), 34–39. https://doi.org/10.1016/j.jbiosc.2015.12.022.

[212] Yu, S.; Yao, P.; Li, J.; Ren, J.; Yuan, J.; Feng, J.; Wang, M.; Wu, Q.; Zhu, D. Enzymatic Synthesis of 3-Hydroxypropionic Acid at High Productivity by Using Free or Immobilized Cells of Recombinant Escherichia Coli. *Journal of Molecular Catalysis B: Enzymatic* **2016**, *129*, 37–42. https://doi.org/10.1016/j.molcatb.2016.03.011.

[213] Lin, X.-C.; Wang, Y.-M.; Chen, X.; You, P.-Y.; Mo, K.-M.; Ning, G.-H.; Li, D. A Photosensitizing Metal–Organic Framework as a Tandem Reaction Catalyst for Primary Alcohols from Terminal Alkenes and Alkynes. *Angewandte Chemie International Edition* **2023**, *62* (35), e202306497. https://doi.org/10.1002/anie.202306497.

[214] Berman, P.; De Haro, L. A.; Jozwiak, A.; Panda, S.; Pinkas, Z.; Dong, Y.; Cveticanin, J.; Barbole, R.; Livne, R.; Scherf, T.; Shimoni, E.; Levin-Zaidman, S.; Dezorella, N.; Petrovich-Kopitman, E.; Meir, S.; Rogachev, I.; Sonawane, P. D.; Aharoni, A. Parallel Evolution of Cannabinoid Biosynthesis. *Nat. Plants* **2023**, *9* (5), 817–831. https://doi.org/10.1038/s41477-023-01402-3.

[215] Gottardi, M.; Reifenrath, M.; Boles, E.; Tripp, J. Pathway Engineering for the Production of Heterologous Aromatic Chemicals and Their Derivatives in Saccharomyces Cerevisiae: Bioconversion from Glucose. *FEMS Yeast Res* **2017**, *17* (4). https://doi.org/10.1093/femsyr/fox035.

[216] Steinmann, A.; Schullehner, K.; Kohl, A.; Dickmeis, C.; Finger, M.; Hubmann, G.; Jach, G.; Commandeur, U.; Girhard, M.; Urlacher, V. B.; Lütz, S. A Targeted Metabolomics Method for Extra- and Intracellular Metabolite Quantification Covering the Complete Monolignol and Lignan Synthesis Pathway. *Metabolic Engineering Communications* **2022**, *15*, e00205. https://doi.org/10.1016/j.mec.2022.e00205.

[217] Lampropoulos, A.; Sutikovic, Z.; Wenzl, C.; Maegele, I.; Lohmann, J. U.; Forner, J. GreenGate - A Novel, Versatile, and Efficient Cloning System for Plant Transgenesis. *PLoS ONE* **2013**, *8* (12), e83043. https://doi.org/10.1371/journal.pone.0083043.

[218] Szybalski, W.; Kim, S. C.; Hasan, N.; Podhajska, A. J. Class-IIS Restriction Enzymes — a Review. *Gene* **1991**, *100*, 13–26. https://doi.org/10.1016/0378-1119(91)90345-C.

[219] Jendresen, C. B.; Stahlhut, S. G.; Li, M.; Gaspar, P.; Siedler, S.; Förster, J.; Maury, J.; Borodina, I.; Nielsen, A. T. Highly Active and Specific Tyrosine Ammonia-Lyases from Diverse Origins Enable Enhanced Production of Aromatic Compounds in Bacteria and Saccharomyces Cerevisiae. *Appl Environ Microbiol* **2015**, *81* (13), 4458–4476. https://doi.org/10.1128/AEM.00405-15.

[220] Hazelwood, L. A.; Daran, J.-M.; van Maris, A. J. A.; Pronk, J. T.; Dickinson, J. R. The Ehrlich Pathway for Fusel Alcohol Production: A Century of Research on Saccharomyces Cerevisiae Metabolism. *Appl Environ Microbiol* **2008**, *74* (8), 2259–2266. https://doi.org/10.1128/AEM.02625-07.

[221] Ehrlich, F. Über Die Bedingungen Der Fuselölbildung Und Über Ihren Zusammenhang Mit Dem Eiweißaufbau Der Hefe. *Berichte der deutschen chemischen Gesellschaft* **1907**, *40* (1), 1027–1047. https://doi.org/10.1002/cber.190704001156.

[222] Vuralhan, Z.; Morais, M. A.; Tai, S.-L.; Piper, M. D. W.; Pronk, J. T. Identification and Characterization of Phenylpyruvate Decarboxylase Genes in Saccharomyces Cerevisiae. *Appl Environ Microbiol* **2003**, *69* (8), 4534–4541. https://doi.org/10.1128/AEM.69.8.4534-4541.2003.

[223] Sentheshanmuganathan, S. The Mechanism of the Formation of Higher Alcohols from Amino Acids by Saccharomyces Cerevisiae. *Biochem J* **1960**, *74* (3), 568–576.

[224] Combes, J.; Imatoukene, N.; Couvreur, J.; Godon, B.; Brunissen, F.; Fojcik, C.; Allais, F.; Lopez, M. Intensification of P-Coumaric Acid Heterologous Production Using Extractive Biphasic Fermentation. *Bioresource Technology* **2021**, *337*, 125436. https://doi.org/10.1016/j.biortech.2021.125436.

[225] Canelas, A. B.; ten Pierick, A.; Ras, C.; Seifar, R. M.; van Dam, J. C.; van Gulik, W. M.; Heijnen, J. J. Quantitative Evaluation of Intracellular Metabolite Extraction Techniques for Yeast Metabolomics. *Anal. Chem.* **2009**, *81* (17), 7379–7389. https://doi.org/10.1021/ac900999t.

[226] Canelas, A. B.; Harrison, N.; Fazio, A.; Zhang, J.; Pitkänen, J.-P.; van den Brink, J.; Bakker, B. M.; Bogner, L.; Bouwman, J.; Castrillo, J. I.; Cankorur, A.; Chumnanpuen, P.; Daran-Lapujade, P.; Dikicioglu, D.; van Eunen, K.; Ewald, J. C.; Heijnen, J. J.; Kirdar, B.; Mattila, I.; Mensonides, F. I. C.; Niebel, A.; Penttilä, M.; Pronk, J. T.; Reuss, M.; Salusjärvi, L.; Sauer, U.; Sherman, D.; Siemann-Herzberg, M.; Westerhoff, H.; de Winde, J.; Petranovic, D.; Oliver, S. G.; Workman, C. T.; Zamboni, N.; Nielsen, J. Integrated Multilaboratory Systems Biology Reveals Differences in Protein Metabolism between Two Reference Yeast Strains. *Nat Commun* **2010**, *1* (1), 145. https://doi.org/10.1038/ncomms1150.

[227] Mukai, N.; Masaki, K.; Fujii, T.; Kawamukai, M.; Iefuji, H. PAD1 and FDC1 Are Essential for the Decarboxylation of Phenylacrylic Acids in Saccharomyces Cerevisiae. *Journal of Bioscience and Bioengineering* **2010**, *109* (6), 564–569. https://doi.org/10.1016/j.jbiosc.2009.11.011.

[228] Demir, O.; Aksan Kurnaz, I. An Integrated Model of Glucose and Galactose Metabolism Regulated by the GAL Genetic Switch. *Computational Biology and Chemistry* **2006**, *30* (3), 179–192. https://doi.org/10.1016/j.compbiolchem.2006.02.004.

[229] Abdulrehman, D.; Monteiro, P. T.; Teixeira, M. C.; Mira, N. P.; Lourenço, A. B.; dos Santos, S. C.; Cabrito, T. R.; Francisco, A. P.; Madeira, S. C.; Aires, R. S.; Oliveira, A. L.; Sá-Correia, I.; Freitas, A. T. YEASTRACT: Providing a Programmatic Access to Curated Transcriptional Regulatory Associations in Saccharomyces Cerevisiae through a Web Services Interface. *Nucleic Acids Res* **2011**, *39* (Database issue), D136-140. https://doi.org/10.1093/nar/gkq964.

[230] Teixeira, M. C.; Monteiro, P. T.; Guerreiro, J. F.; Gonçalves, J. P.; Mira, N. P.; dos Santos, S. C.; Cabrito, T. R.; Palma, M.; Costa, C.; Francisco, A. P.; Madeira, S. C.; Oliveira, A. L.; Freitas, A. T.; Sá-Correia, I. The YEASTRACT Database: An Upgraded Information System for the Analysis of Gene and Genomic Transcription Regulation in Saccharomyces Cerevisiae. *Nucleic Acids Res* **2014**, *42* (Database issue), D161-166. https://doi.org/10.1093/nar/gkt1015.

[231] Wang, Y.; Halls, C.; Zhang, J.; Matsuno, M.; Zhang, Y.; Yu, O. Stepwise Increase of Resveratrol Biosynthesis in Yeast Saccharomyces Cerevisiae by Metabolic Engineering. *Metab Eng* **2011**, *13* (5), 455–463. https://doi.org/10.1016/j.ymben.2011.04.005.

[232] Sun, Z.-J.; Lian, J.-Z.; Zhu, L.; Jiang, Y.-Q.; Li, G.-S.; Xue, H.-L.; Wu, M.-B.; Yang, L.-R.; Lin, J.-P. Combined Biosynthetic Pathway Engineering and Storage Pool Expansion for High-Level Production of Ergosterol in Industrial Saccharomyces Cerevisiae. *Front Bioeng Biotechnol* **2021**, *9*, 681666. https://doi.org/10.3389/fbioe.2021.681666.

[233] Zhang, H.; Cao, M.; Jiang, X.; Zou, H.; Wang, C.; Xu, X.; Xian, M. De-Novo Synthesis of 2-Phenylethanol by Enterobactersp. CGMCC 5087. *BMC Biotechnology* **2014**, *14* (1), 30. https://doi.org/10.1186/1472-6750-14-30.

[234] Ahmadi, M. K.; Fang, L.; Moscatello, N.; Pfeifer, B. A. E. Coli Metabolic Engineering for Gram Scale Production of a Plant-Based Anti-Inflammatory Agent. *Metabolic Engineering* **2016**, *38*, 382–388. https://doi.org/10.1016/j.ymben.2016.10.001.

[235] Hansen, E. H.; Møller, B. L.; Kock, G. R.; Bünner, C. M.; Kristensen, C.; Jensen, O. R.; Okkels, F. T.; Olsen, C. E.; Motawia, M. S.; Hansen, J. De Novo Biosynthesis of Vanillin in Fission Yeast (*Schizosaccharomyces Pombe*) and Baker's Yeast (*Saccharomyces Cerevisiae*). *Appl Environ Microbiol* **2009**, *75* (9), 2765–2774. https://doi.org/10.1128/AEM.02681-08.

[236] Niu, H.; Li, R.; Liang, Q.; Qi, Q.; Li, Q.; Gu, P. Metabolic Engineering for Improving L-Tryptophan Production in Escherichia Coli. *Journal of Industrial Microbiology and Biotechnology* **2019**, *46* (1), 55–65. https://doi.org/10.1007/s10295-018-2106-5.

[237] Liu, X.; Niu, H.; Li, Q.; Gu, P. Metabolic Engineering for the Production of L-Phenylalanine in Escherichia Coli. *3 Biotech* **2019**, *9* (3), 85. https://doi.org/10.1007/s13205-019-1619-6.

[238] Samel, S. A.; Marahiel, M. A.; Essen, L.-O. How to Tailor Non-Ribosomal Peptide Products—New Clues about the Structures and Mechanisms of Modifying Enzymes. *Mol. BioSyst.* **2008**, *4* (5), 387. https://doi.org/10.1039/b717538h.

[239] Smith, C. D.; Zhang, X.; Mooberry, S. L.; Patterson, G. M. L.; Moore, R. E. Cryptophycin: A New Antimicrotubule Agent Active against Drug-Resistant Cells1. *Cancer Research* **1994**, *54* (14), 3779–3784.

[240] Saint-Prix, F.; Bönquist, L.; Dequin, S. Functional Analysis of the ALD Gene Family of Saccharomyces Cerevisiae during Anaerobic Growth on Glucose: The NADP+-Dependent Ald6p and Ald5p Isoforms Play a Major Role in Acetate Formation. *Microbiology* **2004**, *150* (7), 2209–2220. https://doi.org/10.1099/mic.0.26999-0.

[241] Yu, W.; Cao, X.; Gao, J.; Zhou, Y. J. Overproduction of 3-Hydroxypropionate in a Super Yeast Chassis. *Bioresource Technology* **2022**, *361*, 127690. https://doi.org/10.1016/j.biortech.2022.127690.

[242] Hussain, T.; Espley, R. V.; Gertsch, J.; Whare, T.; Stehle, F.; Kayser, O. Demystifying the Liverwort Radula Marginata, a Critical Review on Its Taxonomy, Genetics, Cannabinoid Phytochemistry and Pharmacology. *Phytochem Rev* **2019**, *18* (3), 953–965. https://doi.org/10.1007/s11101-019-09638-8.

[243] Hussain, T.; Plunkett, B.; Ejaz, M.; Espley, R. V.; Kayser, O. Identification of Putative Precursor Genes for the Biosynthesis of Cannabinoid-Like Compound in Radula Marginata. *Frontiers in Plant Science* **2018**, *9*.

[244] Gülck, T.; Møller, B. L. Phytocannabinoids: Origins and Biosynthesis. *Trends in Plant Science* **2020**, *25* (10), 985–1004. https://doi.org/10.1016/j.tplants.2020.05.005.

[245] Merck. *Yeast SD-Drop Out Composition*. https://www.sigmaaldrich.com/DE/de/technical-documents/protocol/microbiological-testing/microbial-culture-media-preparation/yeast-drop-out (accessed 2023-11-28).

[246] Mullis, K.; Faloona, F.; Scharf, S.; Saiki, R.; Horn, G.; Erlich, H. Specific Enzymatic Amplification of DNA In Vitro: The Polymerase Chain Reaction. *Cold Spring Harbor Symposia on Quantitative Biology* **1986**, *51* (0), 263–273. https://doi.org/10.1101/SQB.1986.051.01.032.

[247] *NEB Tm Calculator*. https://tmcalculator.neb.com/#!/main (accessed 2023-12-11).

[248] Hamilton', R.; Watanabe, C. K.; de Boer, H. A. Compilation and Comparison of the Sequence Context around the AUG Startcodons in Saccharomyces Cerevisiae mRNAs. *Nucleic Acids Research* **1987**.

[249] Liu, H.; Naismith, J. H. An Efficient One-Step Site-Directed Deletion, Insertion, Single and Multiple-Site Plasmid Mutagenesis Protocol. *BMC Biotechnology* **2008**, *8* (1), 91. https://doi.org/10.1186/1472-6750-8-91.

[250] Zou, Y.; Mason, M. G.; Wang, Y.; Wee, E.; Turni, C.; Blackall, P. J.; Trau, M.; Botella, J. R. Nucleic Acid Purification from Plants, Animals and Microbes in under 30 Seconds. *PLoS Biol* **2017**, *15* (11), e2003916. https://doi.org/10.1371/journal.pbio.2003916.

[251] Meselson, M.; Yuan, R. DNA Restriction Enzyme from E. Coli. **1968**, *217*.

[252] Loenen, W. A. M.; Dryden, D. T. F.; Raleigh, E. A.; Wilson, G. G.; Murray, N. E. Highlights of the DNA Cutters: A Short History of the Restriction Enzymes. *Nucleic Acids Research* **2014**, *42* (1), 3–19. https://doi.org/10.1093/nar/gkt990.
[253] Pingoud, A. Structure and Function of Type II Restriction Endonucleases. *Nucleic Acids Research* **2001**, *29* (18), 3705–3727. https://doi.org/10.1093/nar/29.18.3705.
[254] Zeugin, J. A.; Hartley, J. L. Ethanol Precipitation of DNA. *focus* **1985**, *7* (4), 1–2.
[255] *NEBioCalculator*. https://nebiocalculator.neb.com/#!/ligation (accessed 2023-12-11).
[256] Im, H. The Inoue Method for Preparation and Transformation of Competent E. Coli:" Ultra Competent" Cells. *Bio-protocol* **2011**, e143–e143.
[257] Hanahan, D. Studies on Transformation of Escherichia Coli with Plasmids. *Journal of Molecular Biology* **1983**, *166* (4), 557–580. https://doi.org/10.1016/S0022-2836(83)80284-8.
[258] Gietz, R. D.; Schiestl, R. H. High-Efficiency Yeast Transformation Using the LiAc/SS Carrier DNA/PEG Method. *Nat Protoc* **2007**, *2* (1), 31–34. https://doi.org/10.1038/nprot.2007.13.
[259] Schiestl, R. H.; Gietz, R. D. High Efficiency Transformation of Intact Yeast Cells Using Single Stranded Nucleic Acids as a Carrier. *Curr Genet* **1989**, *16* (5), 339–346. https://doi.org/10.1007/BF00340712.
[260] Ito, H.; Fukuda, Y.; Murata, K.; Kimura, A. Transformation of Intact Yeast Cells Treated with Alkali Cations. *J Bacteriol* **1983**, *153* (1), 163–168. https://doi.org/10.1128/jb.153.1.163-168.1983.